UNIVERSITY OF OKLAHOMA

GRADUATE COLLEGE

APPLICATION OF TIAB'S DIRECT SYNTHESIS TECHNIQUE TO MULTI-LAYER NATURALLY FRACTURED RESERVOIRS

A Dissertation

SUBMITTED TO THE GRADUATE FACULTY

in partial fulfillment of the requirements for the

degree of

Doctor of Philosophy

By

Jalal Farhan Owayed
Norman, Oklahoma
2000

UMI Number: 9988309

UMI®

UMI Microform 9988309

Bell & Howell Information and Learning Company
300 North Zeeb Road
P.O. Box 1346
Ann Arbor, MI 48106-1346

APPLICATION OF TIAB'S DIRECT SYNTHESIS TECHNIQUE TO
MULTI-LAYER NATURALLY FRACTURED RESERVOIRS

A Dissertation APPROVED FOR THE
SCHOOL OF PETROLEUM AND GEOLOGICAL ENGINEERING

BY

Djebbar Tiab

S. Osisanya

Subhash N. Shah

Michael L. Wiggins

Md. Musharrafuzzaman

DEDICATION

I dedicate this work to:

H. H. Sheikh Jaber Al-Ahmad Al-Jaber Al-Sabah,

Amir of the State of Kuwait

H. H. Sheikh Saad Al-Abdullah Al-Salem Al-Sabah,

Crown Prince and Prime Minister

and the Government of Kuwait.

Dr. Jalal Farhan Owayed

ACKNOWLEDGMENTS

I would like to express sincere gratitude to my major advisor Dr. Djebbar Tiab for the excellent technical guidance, encouragement, and supervision in conducting this study. Sincere appreciation is extended to Dr. Samuel Osisanya, Dr. Subhash Shah, Dr. Michael Wiggins, and Dr. Musharraf Zaman for serving as members in the supervision committee.

My appreciation is also directed to staff members, and friends who care for me and my study in the Mewbourne School of Petroleum and Geological Engineering of the University of Oklahoma.

I would like to thank the Government of Kuwait, represented by Kuwait University, for their financial support given during this study. The financial support has made my graduate studies possible.

I am grateful to my loving and affectionate parents and my family members for their encouragement, understanding, and prayers.

TABLE OF CONTENTS

LIST OF TABLES

LIST OF FIGURES

ABSTRACT

From fluid loss during drilling to simulation and completion design to reservoir characterization; understanding of the unique reservoir behavior of multi-layered systems is required in both homogeneous and double-porosity reservoirs. Pressure analysis theory becomes complicated in a multi-layer reservoir where several layers are communicating through the wellbore only.

The development of the Tiab's Direct Synthesis procedure for a commingled multi-layer infinite-acting, naturally fracture reservoir is examined. In this work, a new set of type curves are developed for both transient and pseudo-steady state flow including wellbore storage and skin. It is important to note that the shapes of either pressure or pressure derivative curves for the layered reservoir are similar to those of a single-layer reservoir. New empirical correlations are developed to solve for the flow capacity in each layer. A very important observation is that for $\frac{\lambda_1}{\lambda_2} > 100$, the derivative curve has two depressions. It is concluded from this study that the peak points on pressure derivative curves are more affected by wellbore storage than by skin.

Next, the problem of the pressure behavior of a well crossed by a uniform-flux and infinite-conductivity vertical fracture and located in a single-layer and multi-layered bounded square reservoir with a double porosity system is studied. The type curves obtained for the infinite-conductivity fracture are qualitatively the same as the

uniform-flux solutions. Only the shape is slightly different at intermediate times. For the case of uniform-flux vertical fracture, type curves show the existence of three flow regimes: (1) the linear flow line of slope 0.5, (2) infinite-acting radial flow line of a horizontal straight line, and (3) pseudo-steady state flow line of slope unity, in addition to the transition region. The infinite-conductivity vertical fracture case reveals a fourth dominated flow regime which can be identified by a straight line of slope 0.36. This flow period is called the bi-radial flow. Unfortunately, the infinite-acting flow period is dominant only if $\left(\frac{x_e}{x_f}\right)$ >8. It was found that the effect of flow capacity ratio is the major factor on the pressure derivative curves during the late time pseudo-steady state.

CHAPTER 1

INTRODUCTION

1.1 Overview

The selection of well site as well as the drilling technique depends on the following factors: reservoir geometry, reservoir characteristics (heterogeneities), drilling technique, productive length, type of well completion, risk, and cost. In order to analyze well test data properly, it is necessary to consider the common heterogeneities and the resulting interpretation problems.

Most of the current studies have been dealing with the semi-analytical and numerical solutions of transient behavior in vertically fractured wells of which infinite and finite conductivity fractures are a subset. In addition, studies on pressure transient behavior in dual-porosity and type-curve matching techniques have been well documented.

No reservoir in its entirety is perfectly homogeneous. Most reservoir rocks, if not all, are heterogeneous in properties from one location to another. The variation in these properties may result from deposition, sequential sedimentation of interbeded fine grain sandstone and shale, folding, and faulting. All the above heterogeneities produce stratification of reservoir.

Naturally fractured reservoirs can be composed virtually of any lithology including carbonates, clastics (sand or shale), and even basement rocks. Theory predicts that homogeneous reservoirs and different types of heterogeneous reservoirs including naturally fractured should display a variety of pressure response depending on the flow model used and the reservoir conditions. Figure (1.1) shows the commonly used configurations to develop reservoir flow models for different matrix/fractures configurations. They are:

(a) homogeneous reservoir heavily fractured with fine matrix voids in communication with each other and with the fractures.

(b) homogeneous reservoir consisting mainly of interconnecting fractures (no matrix voids).

(c) Multiple regions or composite reservoir usually having a high transmissibility fractured region and a lower transmissibility matrix with fine voids region.

(d) Anisotropic reservoir exhibiting parallel fracture planes. Permeability in the direction of fractures is much higher than permeability in the direction normal to them.

(e) Single fracture reservoir where there is a main permeable fault acting as a channel to drain regions away from the well.

(f) Double-porosity reservoir consisting of two media, fracture network and rock matrix acting independently but in communication.

In general, there will be fractured reservoirs that can be described by more than one of the above models or even as a combination of them. As stated by Cinco-ley[1], the ideal pressure behavior of a single well test in each of the above models can be summarized below:

(a&b) The Homogeneous Reservoir Model

Figure 1.1-a and b represent this model. Reservoir properties are considered to be constant throughout the formation. Fluid production is a result of simultaneous expansion of both the fractures and the rock matrix which act as a single medium. Pressure behavior of a buildup or drawdown test for a single well in a homogeneous reservoir can be seen in Figure 1.2. The pressure derivative plot shows a unit slope straight line reflecting welbore-storage effect followed by a transition zone and, then, a horizontal straight line representing a radial flow behavior. Formation flow capacity, kh, and the skin factor, S, can be calculated from this straight line.

(C) The Multiple Region or Composite Reservoir Model

Figure 1.1-c illustrates this model which behaves as a composite radial system. In this case, the system will exhibit two flow capacities: $(kh)_1$ and $(kh)_2$. Wells producing from the fractured region usually have higher productivity than those in the unfractured region. Pressure behavior of a single well drilled in the fractured region of the reservoir is shown in Figure 1.3. This Figure exhibits two straight lines on a semilog plot reflecting two radial flow periods from the fractured and unfractured regions, respectively. The flow capacity of both regions can be calculated from the slope of these straight lines. A log-log plot of the pressure derivative shows the typical behavior for welbore storage effect at early time followed by two horizontal straight lines reflecting the two radial flow periods with a transition period in between. The magnitude of this transition period

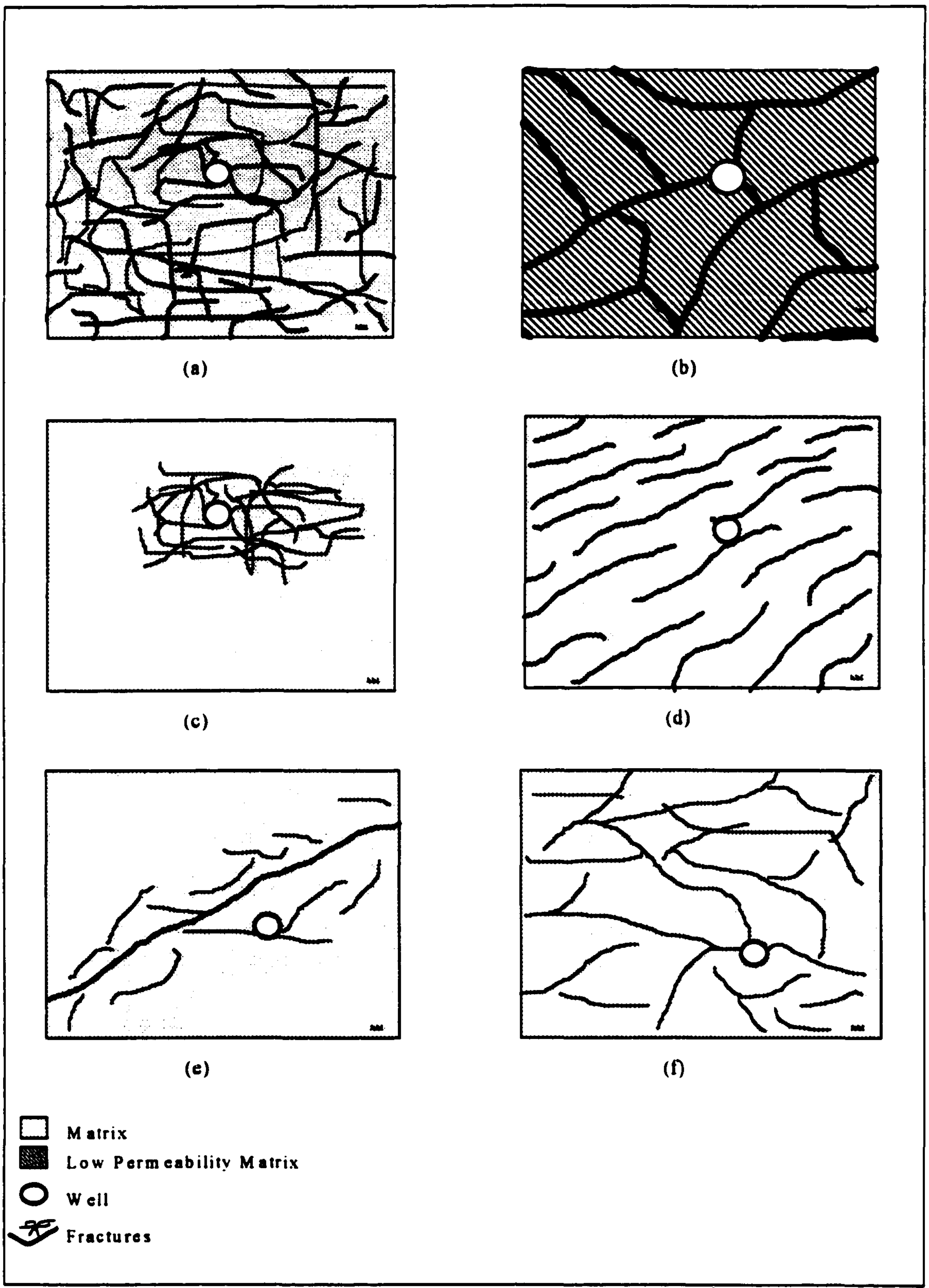

Figure 1.1 Types of naturally fractured reservoirs[1].

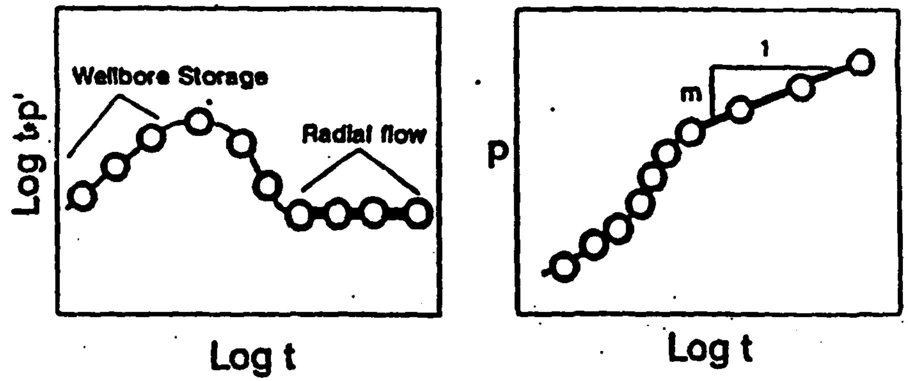

Figure 1.2 Derivative and semilog graph for radial flow in homogeneous reservoirs[1]

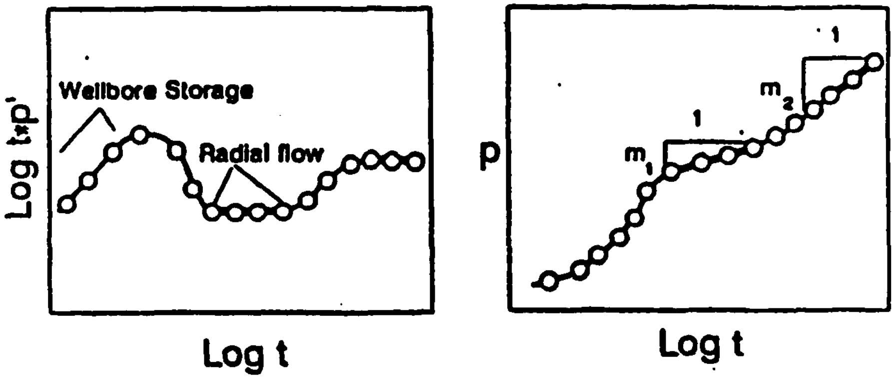

Figure 1.3 Derivative and semilog graph for radial flow in a two region reservoirs[1].

depends on the degree of contrast between the two regions. A transition period with a unit-slope straight line would suggest the presence of a psedosteady-state flow.

(d) The Anisotrophic Reservoir Model

Figure 1.1-d represents this model. This kind exhibits a maximum permeability, k_{max}, along the fractures direction and a minimum permeability, k_{min}, in the direction normal to the fractures. A single well test in this model of a reservoir will provide the geometric average permeability, $\bar{k}$, where:

$$\bar{k} = \sqrt{k_{max} k_{min}} \tag{1.1}$$

Pressure interference test is the best method to characterize this model. This method can be used to characterize K_{max} and K_{min} along with the orientation of the principal permeability axis. For a meaningful interference test, a minimum of three observation wells, not aligned on a straight line, are required. Figure 1.4 shows the pressure responses of these observation wells which look similar on a log-log crossplot, only displaced in time. Interpretation of such tests is usually performed through the application of type curve matching for the radial flow model using the line-source solution.

(e) The Single-Fracture Model

Figure 1.1-e illustrates this model. In this kind, a major fracture in the form of a permeable fault will act as a channel through which most of the reservoir fluid flows. The

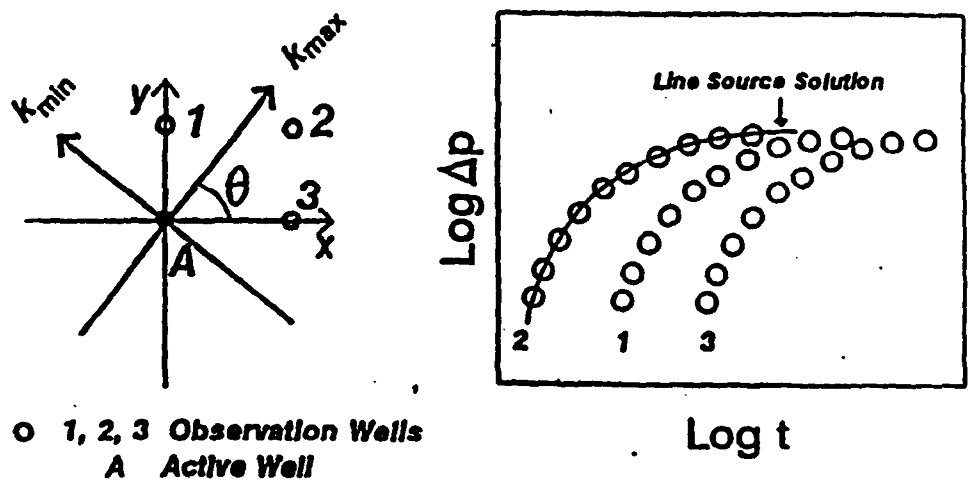

Figure 1.4 Log-log graph for observation pressures from interference tests in an anisotropic reservoirs[1].

system can be characterized by fracture half length, x_f; fracture conductivity, $k_f w_f$; distance between the well and the fracture, d_f; and the formation flow capacity, kh. Detecting and evaluating the fault can be achieved as shown in Figure 1.5. The derivative log-log graph of a single well test will show a well bore storage effect followed by a radial-flow period reflected as a horizontal straight line. Then, after a transition period, the well behaves as if it was located near a constant pressure boundary exhibiting a straight line with a -1.0 slope. At the end of the flow behavior, the system reaches a bilinear-flow period reflected by a one-quarter slope straight line. The semilog plot can be used to calculate formation flow capacity, kh, and skin factor, S. Whereas, the distance between the well and the fracture, d_f, can be determined from the slope of the straight portion in the specialized constant pressure boundary graph of p vs. t. The fracture conductivity, $k_f w_f$, can be determined from the slope of the straight line portion in the bilinear-flow graph of p vs. $t^{1/4}$

(f) The Classic Double-Porosity Model

Figure 1.1-f illustrates this kind of naturally fractured reservoir. This kind is the widely used model which considers the formation to be composed of fracture network and matrix voids. Fluid production is a result of the independent expansion of each element at different times. Figure 1.6 shows pressure behavior of a single well of this kind. The semilog graph of p vs. log t predicts two parallel straight lines representing the fracture dominated flow period and the total system (fracture/matrix) dominated flow period, respectively. The flow capacity, kh, and skin factor, S, can be calculated from

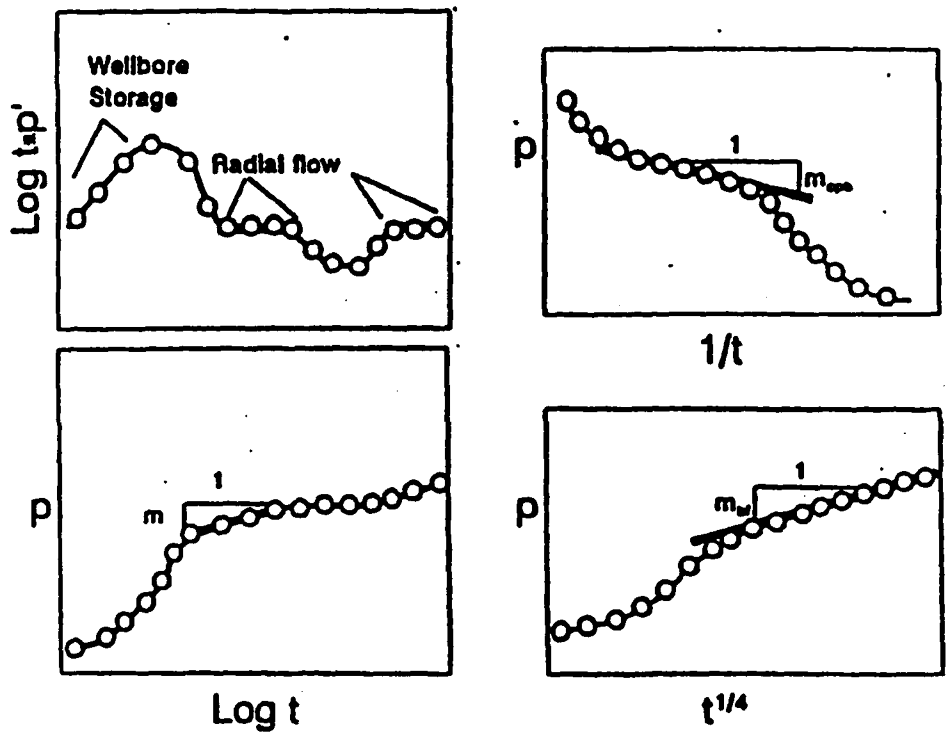

Figure 1.5 Derivative and specialized graph for a well near a conductive fault[1].

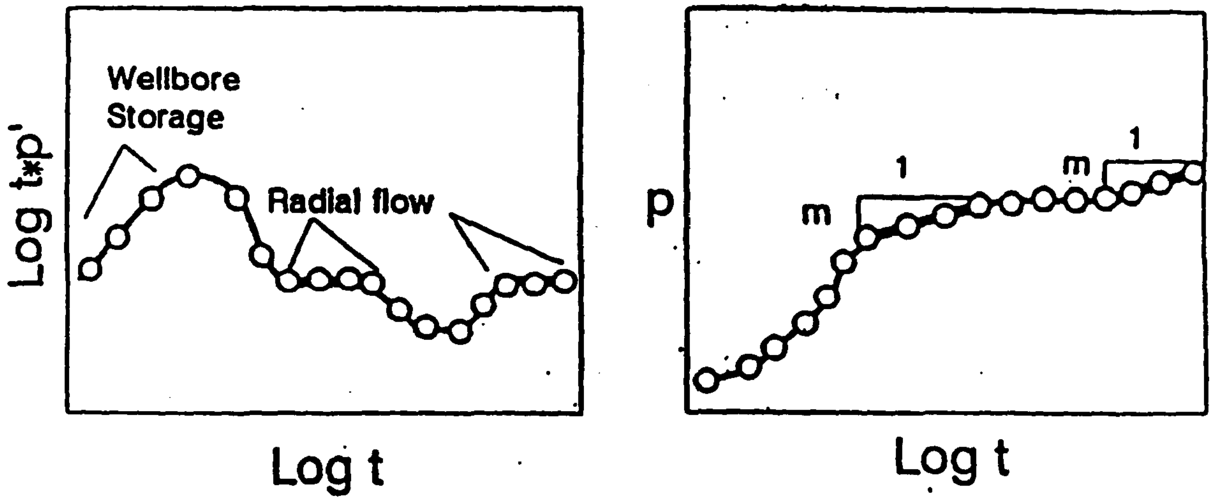

Figure 1.6 Derivative and semilog graph for radial flow in a double-porosity reservoirs[1].

either the first or second straight line. Figure 1.6 illustrates a log-log plot of (t*p') versus t, and demonstrates the wellbore storage effect at an early time followed by a radial-flow period reflected as a horizontal straight line, representing the fracture dominated flow period. Then, a transition period of matrix interacts with the fracture network, producing a V-shaped curve followed by another horizontal line reflecting the total system (fracture/matrix) dominated flow period.

Most models proposed to date in this category consider the regularly shaped matrix blocks (sugar cube model) and assume that fluid is transfered between matrix and fractures under a pseudosteady state condition as first introduced by Warren and Root (1963)[2]. The matrix blocks may be represented by cubes, parallelepipeds, cylinders, or spheres. Warren and Root concluded that fracture storativity ratio, ω; and matrix/fractures permeability ratio, λ, are enough parameters to describe naturally fractured reservoirs. λ is a measure of the mass transfer rate from the matrix to the fracture network.

Table 1.1 lists the required parameters to characterize fluid flow behavior in each reservoir model which is described above.

An actual naturally fractured formation is a heterogeneous system of vugs, fractures, and matrix which are random in nature as seen in Figure 1.7. Also shown is the sugar-cube model which was presented by Warren and Root[2]; it consists of discrete matrix block elements separated by an orthogonal system of continuous, uniform fracture. Another model was presented by Kazemi (1969)[3] and is known as the layer, stratum, or

Model	*Parameters*	*Applications*
Homogeneous	kh, and S	Highly fractured reservoir or low-permeability matrix.
Multiple Region or Composite	$(kh)_1$, $(kh)_2$, and S	Regionally fractured reservoir.
Anisotropic	K_{max} and k_{min}	Oriented fractures.
Single Fracture	F_{CD}, S_f, d_f, k_f, and S	Reservoir with dominant fracture or well near a permeable fault.
Double Porosity	$(kh)_f$, S, λ, and ω	Heavily fractured reservoir with intermediate matrix permeability.

Table 1.1 Parameters and applications of flow models for naturally fractured reservoirs[1]

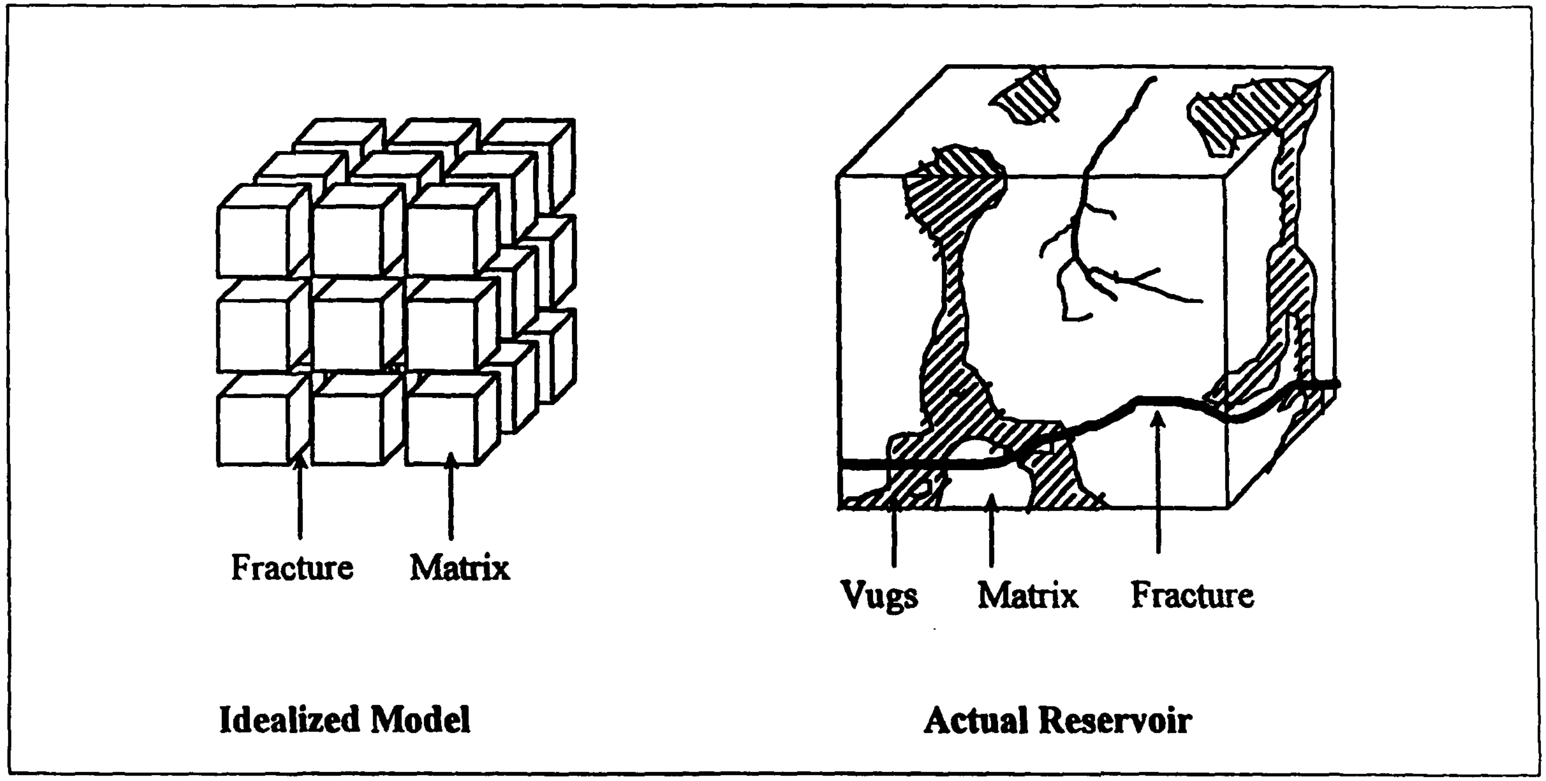

Figure 1.7 The sugar cube model of naturally fractured reservoirs[2].

slab model. It represents a set of uniformly, spaced horizontal matrix layers, alternating with horizontal fracture layers. Both models, in essence, were developed to simplify the mathematical computations and, subsequently, derive an analytical solution.

Pressure transient testing has been used to identify dual porosity, naturally fractured reservoirs. The fractures are assumed to have limited storage capacity but high flow capability while the matrix has low flow capacity but high storage capacity. The fissures produce to the well while the matrix feeds the fluid to the fissures. The corresponding pressure response consists of two parallel straight lines separated by a transitional curve. The straight lines represent depletion of the fracture network and equivalent homogenous flow of the fractures and matrix, respectively. The crossflow from matrix to fractures is reflected in the transitional curve.

Due to the complexity of the environment in which sediments were deposited, and as a result of subsequent physical and chemical changes, many types of heterogeneities are present in all reservoir behavior. The presence of impermeable shale separate the reservoir into two or more layers of differing physical characteristics in the producing formation. Therefore, the pressure behavior of naturally fractured multilayer reservoir is the subject matter of this study.

1.2 Objectives

Geological and engineering understanding of reservoirs has increased steadily through in-fill drilling. One of the most frequently discussed heterogeneous systems, the layered reservoir, is one of the essential parts of this work. Although this work presents and concentrates on the application to a two-layered system, it can be extended to an n-layered reservoir system. This study utilized a layered reservoir without crossflow and also assumed each layer is a naturally fractured and isotropic porous medium, that it contained a slightly compressible fluid of constant viscosity. Flow towards the wellbore is via the fracture.

During the last two decades, the pressure derivative technique has been used widely. The pressure derivative is a powerful diagnostic tool for analyzing pressure transient data. The most versatile plot for identification and diagnosis of reservoir heterogeneities is the combined pressure and pressure derivative format. The high accuracy attainable in modern pressure gauges makes this approach both plausible and reliable. The pressure derivative has been used extensively in the present study.

Type curve matching is more of a trial and error procedure with non-unique results. Therefore, this study used an alternative method referred to as "Tiab's Direct Synthesis." Development of the application of direct synthesis to multi-layer double-porosity reservoirs, with and without hydraulic (vertical) fracturing, will determine the characteristic points and lines necessary for the analysis. Both single and multi-layer reservoirs are examined. It is the focus of this work to use pressure and pressure derivative curves in transient testing as a tool to better understand and describe these types of reservoirs. The ultimate goal is to correctly characterize the reservoir properties; e.g., permeability, fracture half-length, dimensionless storage coefficient, ω, interporosity flow parameter, λ, skin factor, and wellbore storage (if applicable). To achieve this goal, a new technique known as "Tiab's Direct Synthesis" is applied to pressure tests, increasing the accuracy and reliability of the information. Thus, the primary objectives of the study are the following:

1. Examine the pressure behavior of commingled multi-layer double-porosity reservoirs, with and without hydraulic (vertical) fracturing.
2. Develop the application of Tiab's Direct Synthesis Technique to commingled multi-layer double-porosity reservoirs, with and without hydraulic (vertical) fracturing.

The technique developed in this study is reasonably general and useful. For the purpose of discussion only selective plots are included. To the best of my knowledge, the results presented are not available in the literature. It is believed that while the developed models are a result of theoretical development they still can be used for practical purposes.

1.3 Organization

The pressure transient behavior of naturally fractured reservoirs has been analyzed using mathematical models that assume a single layer. Recently, these models extended to infinite-conductivity fractured reservoirs. In this work, pressure analysis theory is extended to a muliti-layer reservoir where several layers are communicating through the wellbore only. However, applying the Tiab's Direct Synthesis technique on such systems has not been discussed. New analytical and empirical expressions were developed as a result of this study.

This work examines the pressure behavior of multi-layer naturally fractured reservoirs and applies the Tiab's Direct Synthesis technique. Development of the application of direct synthesis to double porosity systems with and without hydraulic fracturing will determine the characteristic points and lines necessary for the analysis. This dissertation organized into the following topics:

Chapter 1: introduction,

Chapter 2: literature review,

Chapter 3: will emphasize the development of the direct synthesis procedure for a commingled multi-layer infinite-acting, naturally fractured reservoir. Also, this Chapter will show that it is possible to isolate the properties of a single layer if the flow rate from the layer is known,

Chapter 4: applies the Direct Synthesis technique to a vertically fractured reservoir with double porosity. Both uniform-flux and infinite-conductivity vertical fractures are considered,

Chapter 5: extends the work presented in Chapter 4 to multi-layer systems. Also, it presents an analysis procedure for multi-layer vertically-fractured systems with double porosity. This procedure will show later that it is possible to estimate the individual properties of a single layer if the flow rate from the layer is known,

Chapter 6: shows applications from published literature. Either drawdown or buildup real test data will be analyzed to estimate reservoir properties, and

Chapter 7: discussion, conclusions and recommendations.

The results derived from this study have a major impact on improving the interpretation of pressure behaviors of multi-layer systems.

1.4 Computer Models

In this work, the numerical inversion method was used to evaluate the analytical solutions of the layered system problems in Laplace space. Computer codes were developed to generate P_D vs t_D data. The real space solution for the reservoir pressure behavior as a function of time was obtained by evaluating the inverse transformation to the Laplace space solution. This was accomplished with a numerical inversion scheme presented by Stehfest[6]. The scheme is based upon the following equation:

$$p_D(t_D) = \frac{\ln 2}{t_D} \sum_{i=1}^{N} V_i * \bar{p}_D(s_i) \tag{1.2}$$

where,

$$s_i = \frac{\ln 2}{t_D} * i \tag{1.3}$$

The value of N determines the accuracy of the approximation. The V_i's are constants dependent upon N in the following manner:

$$V_i = (-1)^{\frac{N}{2}+i} \sum_{k=(\frac{i+1}{2})}^{\max(\frac{N}{2},i)} \frac{k^{\frac{N}{2}}(2k)!}{(\frac{N}{2}-k)!\,k!\,(k-1)!\,(i-k)!\,(2k-i)!} \tag{1.4}$$

In order to generate a new set of log-log plots of P_D and $t_D*P'_D$, FORTRAN language was used to write computer codes which will aid the development of the curves.

The optimum value of N and the accuracy of the inversion scheme can be determined by comparing the results to known functions. For N=8, in double precision arithmetic, inversion scheme solutions are presented in Tables 1.2. The solutions compare extremely well. The difference between the computation methods is very small at all times. Appendix A presents the computer code of the numerical inversion

Infinite-acting reservoir, Pseudosteady state flow in matrix blocks.
Dimensionless storage coefficient, ω=0.1
Interporosity flow parameter, $\lambda=1\times10^{-6}$
Wellbore storage, C_D=0.0

T_D	P_D*	P_D**	Error %
1.0000E+00	1.650695	1.651	0.02
2.0000E+00	1.958927	1.959	0.00
4.0000E+00	2.281516	2.282	0.02
8.0000E+00	2.613744	2.614	0.01
1.0000E+01	2.722795	2.723	0.01
2.0000E+01	3.063423	3.062	0.05
4.0000E+01	3.405077	3.405	0.00
8.0000E+01	3.748744	3.749	0.01
1.0000E+02	3.859209	3.860	0.02
2.0500E+02	4.216728	4.217	0.01
8.0500E+02	4.897237	4.898	0.02
1.0050E+03	5.006655	5.007	0.01
2.0550E+03	5.360431	5.360	0.01
8.0550E+03	6.013672	6.014	0.01
1.0050E+03	6.115026	6.115	0.00

** Developed Numerical Model.*
*** Engler[63].*

Table 1.2 Comparing inversion scheme solutions.

CHAPTER 2

LITERATURE REVIEW

Drilling through a producing formation should be considered a completion operation, as well as a drilling operation. In order to maximize hydrocarbon production rates and recoveries, the interaction of drilling fluids, various formation damage mechanisms, and reservoir heterogeneities must be considered. No reservoir in its entirety is perfectly homogeneous. Most reservoir rocks, if not all, are heterogeneous in properties from one location to another. Some of these reservoirs exhibit a dual porosity pressure behavior.

A brief literature review relevant to the present study is presented in this chapter. The literature review emphasizes the discussion of flow models developed for well testing in vertical fracture homogeneous and double-porosity reservoirs for both single and multilayer systems. This will be followed by a very brief discussion on the direct synthesis technique. The following sections will highlight the most important models and briefly describe their assumptions and applications.

2.1 Naturally Fractured Reservoir

Many studies have been introduced for analysis of transient pressure behavior of naturally fractured reservoirs. Several flow models have been developed to describe this pressure behavior. Numerous analytical and numerical models have been published in the petroleum literatures concerning pressure response in dual-porosity systems. Pollard (1959)[7] developed one of the early theories through the evaluation of acid treatment in fractured limestone reservoir. His theory takes into account (1) existence of a finite void system, (2) difference between the rate of flow from the well and the rate of flow between matrix voids and fissures, (3) pressure gradient in the fissures, and (4) existence of resistance to flow (skin) between the fissures system and the well. The pressure differential in the well was assumed to be in response to three distinct flow regions The first region is the damaged or improved region in the fractures near the well. The second region considers the pressure loss due to the flow resistance within the fractures, and the last region is the pressure response between the matrix and the fracture system. Pollard[7] suggested that flow was taking place from the matrix blocks into the fracture which simultaneously delivered this fluid into the wellbore. Also, the effect of matrix blocks was felt at the wellbore during the later stages of production; therefore, the total pressure drop in the wellbore can be represented by a series of time exponential terms such as:

$$p_i - p_w = Ce^{-a_1 t} + De^{-a_2 t} + Ee^{-a_3 t} \tag{2.1}$$

where, the parameters C, D, E, a_1, a_2, a_3, and B are empirical constants determined from graphical analysis given by:

$$C = \frac{a_3(p_i - (p_f)_{t=0})}{a_3 - a_1} \tag{2.2}$$

$$D = \frac{a_3 B}{a_3 - a_2} \tag{2.3}$$

$$E = p_i - (p_w)_{t=0} - C - D \tag{2.4}$$

and,

P_i = initial pressure in the reservoir

P_w = bottom hole pressure

t = time

$(P_f)_{t=0}$ = initial pressure in fracture system, at t = 0

B = constant

$(P_w)_{t=0}$ = initial bottom hole pressure, at t = 0

In Equation (2.1), the first exponential term $Ce^{-a_1 t}$, which approximates pressure in the fissures, depends on the rate of flow from the matrix fine voids into the fissures. This change in pressure will continue until the reservoir pressure stabilizes. The second term, $De^{-a_2 t}$, approximates pressure differential due to fluid flow across the fissures system in the vicinity of the well and will last for another time period. Finally, the third exponential term, $Ee^{-a_3 t}$, approximates pressure differential across the skin regime that may exist between the fissures surrounding the well and the borehole.

Figure (2.1) illustrates a schematic of log (p_i-p_w) versus time, t, for naturally fractured reservoirs. The straight line segment, RS, reflects the process of repressurizing fissures voids with fluid from the matrix pores after Δp within fissures voids and Δp between the fissures and the wellbore across the skin area have become negligible. The extrapolated C value is approximately the difference between static reservoir pressure, P, and the initial fracture, $(P_f)_{t=0}$. The slope is equal to a_1.

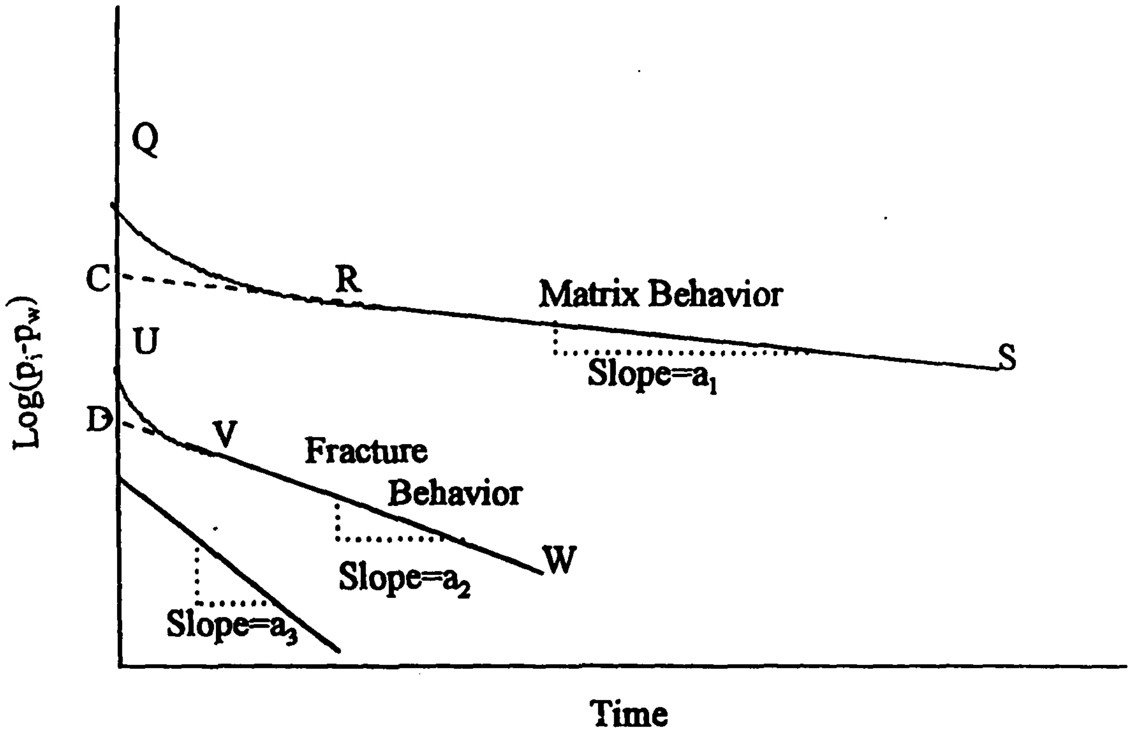

Figure 2.1 Schematic representation of the Pollard Plot.

inversion scheme solutions?

Conversely, a curve which is a resultant of adding several transients may be broken down into its various single transients by extrapolating the longest lived transient back to time zero and plotting a "difference" curve between the original curve and the extrapolated straight line. This procedure should be carried out once again if the "first difference" is a curve. In the case of a formation having a skin area, fractures, and matrix porosity, there will be a first difference curve (curve QR–line CR) and a second difference (curve UV–line DV) straight line. The extrapolated D value is approximately the difference between initial fracture pressure and the pressure in fractures near the wellbore. Segment UD represents the pressure drop due to skin.

The fracture, matrix, and skin pore volumes can be estimated from the respective straight line segments as developed by Pollard[7]:

$$V_f = \frac{0.234qB}{a_2 D c_f} \tag{2.5}$$

$$V_m = \frac{0.234qB}{a_1 (C+D) c_m} \tag{2.6}$$

$$V_s = \frac{0.234qB}{a_3 E c_t} \tag{2.7}$$

where, q = flow rate, standard conditions, BBL/day

B = oil formation volume factor, RBBL/STB

The total volume of fluid, V_t, affected by pressure build-up or drawdown may be expressed by:

$$V_t = V_f + V_m = \pi r_e^2 h \phi_t (1 - S_w) \tag{2.8}$$

where,

r_e = drainage radius of the reservoir

h = effective pay thickness of the reservoir

Also, volume of the fluid involved in the skin area may be expressed as:

$$V_s = \pi r_s^2 h \phi_t (1 - S_{xo}) \tag{2.9}$$

where,

r_s = radius of the skin zone

S_{xo} = water saturation in the invaded zone.

Since pressure loss across the skin area, Δp_s, can be estimated from segment UD, the skin factor, S, may be determined from:

$$S = \frac{kh\Delta p_s}{141.2qB\mu} \tag{2.10}$$

Furthermore, the dimensionless matrix/fracture permeability ratio, which is called the interporosity flow parameter, λ, is defined by Warren and Root (1963)[2] as:

$$\lambda = \alpha r_w^2 \frac{k_m}{k_f} \tag{2.11}$$

which has been used by several other investigators to describe the degree of reservoir heterogeneity. Where α is the interporosity flow shape factor, ft^{-2}.

The basic equations for flow in fractured reservoirs of double porosity were formulated by Barenblant et al.,[8,9]. They considered that the two media, fracture and matrix block, are an overlapping continuum such where the mathematical definition of flow and medium parameters are defined at each point. Barenblant et al.,[8,9] suggested that the flow fluid within the matrix blocks occurs under pseudo-steady state conditions. Waren and Root[2] modified Barenblatt et al.'s solution to account for fracture compressibility. Waren and Root[2] present a more comprehensive and applicable solution to the double porosity, naturally fractured problem. Waren and Root[2] introduced their model which presented two new parameters for the purpose of reservoir characterization of flow in the naturally fractured formations. These parameters are: (1) relative storativity: it is the ratio of porosity-compressibility product of the fractures to the total system porosity-compressibility product, given as follows:

$$\omega = \frac{(\phi c_t)_f}{(\phi c_t)_f + (\phi c_t)_m} \tag{2.12}$$

and (2) the interporosity flow parameter is defined in Equation 2.11. Where $\alpha = \frac{12}{h_m^2}$ and $\alpha = \frac{15}{r_m^2}$ for horizontal slab and spherical matrix blocks, respectively. α is defined as:

$$\alpha = \frac{4j(j+2)}{L^2} \tag{2.13}$$

for slab model j=1 and if L = h_m, then for the slab-shaped matrix system (Figure 2.2):

$$\alpha = \frac{(4 \times 1)(1+2)}{h_m^2} = \frac{12}{h_m^2} \tag{2.14}$$

Therefore;

$$\lambda = 12\, r_w^2 \frac{k_m}{k_f h_m^2} \tag{2.15}$$

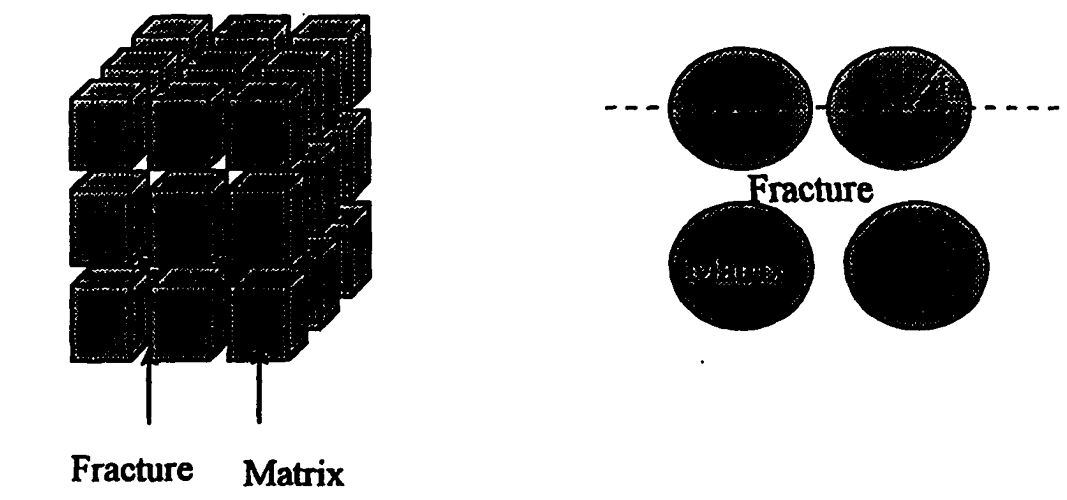

(a) Slab Matrix Blocks **(b) Spherical Matrix Blocks**

Figure 2.2 Matrix fractured geometry.

and for sphere-shaped matrix system (Figure 2.2):

$$\lambda = 15\, r_w^2 \frac{k_m}{k_f r_m^2} \tag{2.16}$$

The Warren and Root[2] model is also well known as sugar cube model and considered by many researchers as an idealized representation of the fractured formation. The model is based on the following assumptions: (1) the rock matrix is homogeneous and isotropic, and is contained within a systematic array of identical, rectangular parallelopipes; (2) all of the secondary porosity is contained within an orthogonal system of continuous, uniform fractures; and (3) the complex of primary and secondary porosities is homogeneous albeit anisotropic. Warren and Root[2] derived an approximate equation which is valid for all time ranges for the dimensionless pressure drop under pseudosteady-state flow assumption between matrix and fracture:

$$p_{wD} = \frac{1}{2}\left[\ln(t_D) + 0.80907\right] + \frac{1}{2}\,\mathrm{Ei}\left(-\frac{\lambda t_D}{\omega(1-\omega)}\right) - \frac{1}{2}\,\mathrm{Ei}\left(-\frac{\lambda t_D}{(1-\omega)}\right) + s \tag{2.17}$$

The above equation assumes wellbore storage effects are negligible and holds for $t_D > 100\omega$ if $\lambda << 1$ and for $t_D > (100\lambda - 1)/\lambda$ if $\omega << 1$. Taking the derivative of the above equation, then the pressure derivative is given by:

$$P'_{wD} = \frac{1}{2}\left\{1 + \exp\left(\frac{-\lambda t_D}{\omega(1-\omega)}\right) - \exp\left(\frac{-\lambda t_D}{(1-\omega)}\right)\right\} \tag{2.18}$$

Figures 2.3 and 2.4 show type curves for different values of dimensionless fracture storativity, ω, and interporosity flow coefficient, λ, parameters. ω is the ratio of porosity-compressibility product of the fractures to the total system porosity-compressibility

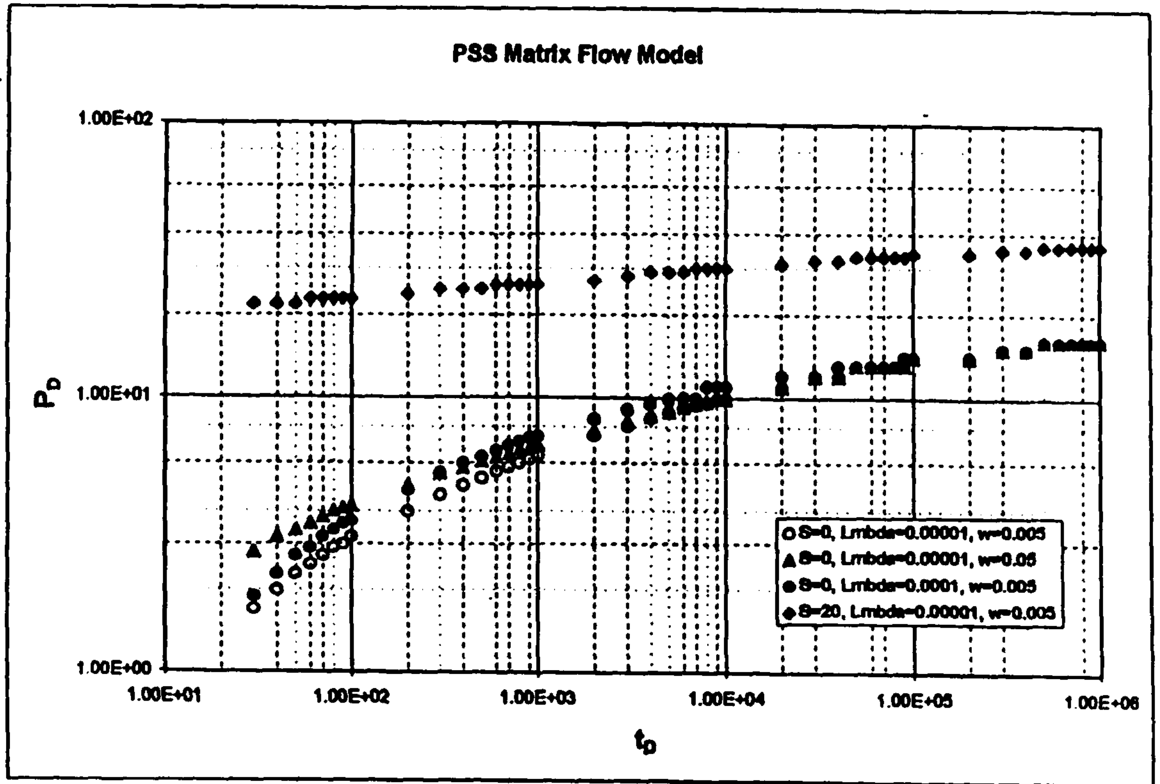

Figure 2.3 Dimensionless pressure curves.

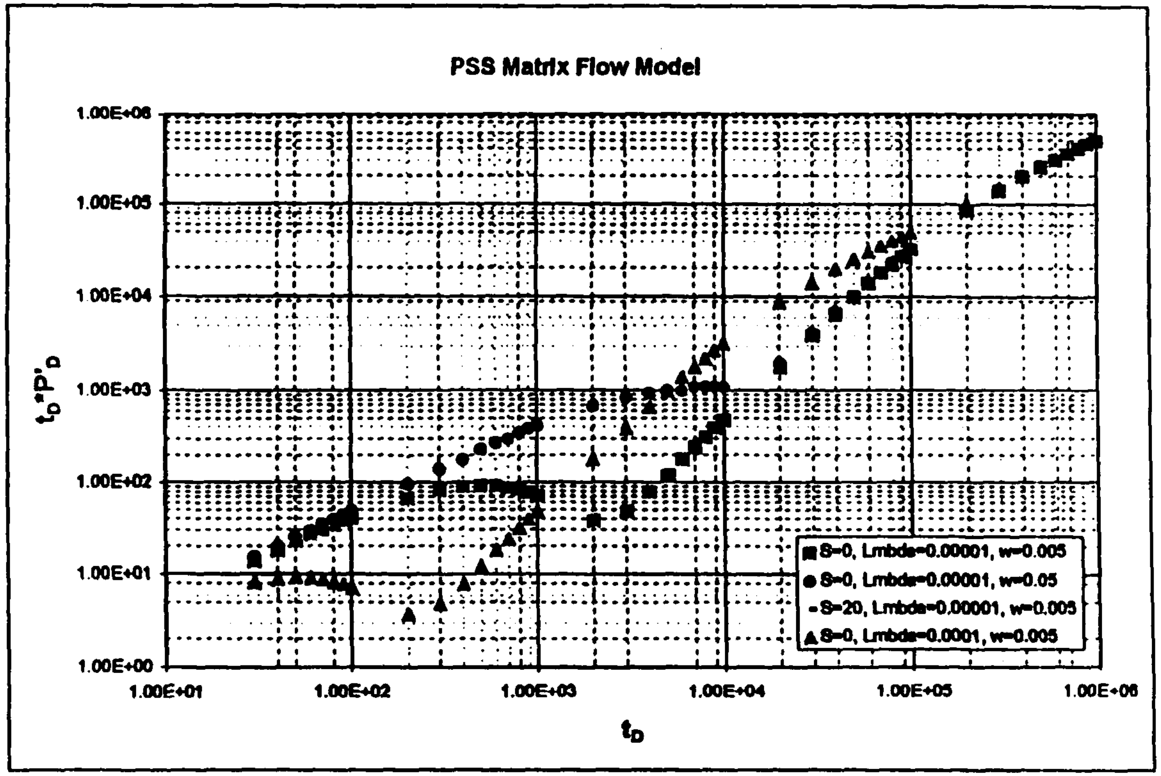

Figure 2.4 Dimensionless pressure derivative curves.

product, and λ is a measure of the mass transfer rate from the matrix to the fracture network. The Figures illustrate the effect of varying ω and λ. A decrease in the fracture storage capacity corresponds to faster depletion and a decrease in λ means the transfer of fluid is limited and thus a delay in the pressure plateau and subsequent increase in fracture pressure drop occurs.

During early times, when the pressure response is dominated totally by the fracture system, Equation 2.17 reduces to:

$$p_{wD} = \frac{k_f h \Delta p}{141.2 q B \mu} = \frac{1}{2}\left[\ln(t_D) + 0.80907 + \ln\left(\frac{1}{\omega}\right)\right] + s \tag{2.19}$$

Once the dimensionless storage coefficient ω is known from well testing, the pressure response during the initial flow period can be calculated be:

$$p_{wD} = \frac{1}{2}\left[\ln(t_D) + 0.80907 + \ln\left(\frac{1}{\omega}\right)\right] + s \tag{2.20}$$

Now the values of P_D can be calculated using the above equation corresponding to the values of t_D. An approximate equation for the region where the entire reservoir produces as an equivalent homogeneous reservoir equal to the fracture permeability is:

$$p_{wD} = \frac{1}{2}\left[\ln(t_D) + 0.80907\right] + s \tag{2.21}$$

The dimensional form of Equation 2.17 can be given as:

$$\Delta p = m\left\{\log(t_D) + 0.351 + 0.435\left[\mathrm{Ei}\left(-\frac{\lambda t_D}{\omega(1-\omega)}\right) - \mathrm{Ei}\left(-\frac{\lambda t_D}{(1-\omega)}\right)\right] + 0.87s\right\} \tag{2.22}$$

where

$$m = \frac{162.6qB\mu}{k_f h} \tag{2.23}$$

Figure 2.5 shows a plot of Δp versus the log of time where m is the of the two parallel straight lines. The fracture permeability can be estimated from the slope equation. Skin factor can be calculated from the early time straight line:

$$S = 1.151\left\{\frac{p_i - (p_{wf})_{t=0}}{m} - \log\left(\frac{k_f}{(\phi c)_t \mu r_w^2}\right) + 3.23 + \log\left(\frac{1}{\omega}\right)\right\} \tag{2.24}$$

or from the late time straight line where $\log\left(\frac{1}{\omega}\right)$ is eliminated:

$$S = 1.151\left\{\frac{p_i - (p_{wf})_{t=0}}{m} - \log\left(\frac{k_f}{(\phi c)_t \mu r_w^2}\right) + 3.23\right\} \tag{2.25}$$

If both straight lines are present, the displacement can be used to calculate the reservoir storage coefficient:

$$\omega = e^{-2.3025\frac{D_p}{m}} \tag{2.26}$$

Odeh (1965)[10], in his analysis of data from various fractured reservoirs, concluded that there is no distinction between homogeneous and fractured reservoirs based on pressure drawdown and/or buildup data, and no two parallel semi-log straight lines, as theoretically expected by Warren and Root[2], were over observed.

Kazemi (1969)[3] developed a numerical model to analyze pressure transient of a well centrally located in a naturally fractured reservoir with a layered matrix and fracture system distribution. His model was based on the work of Warren and Root. Kazemi[3]

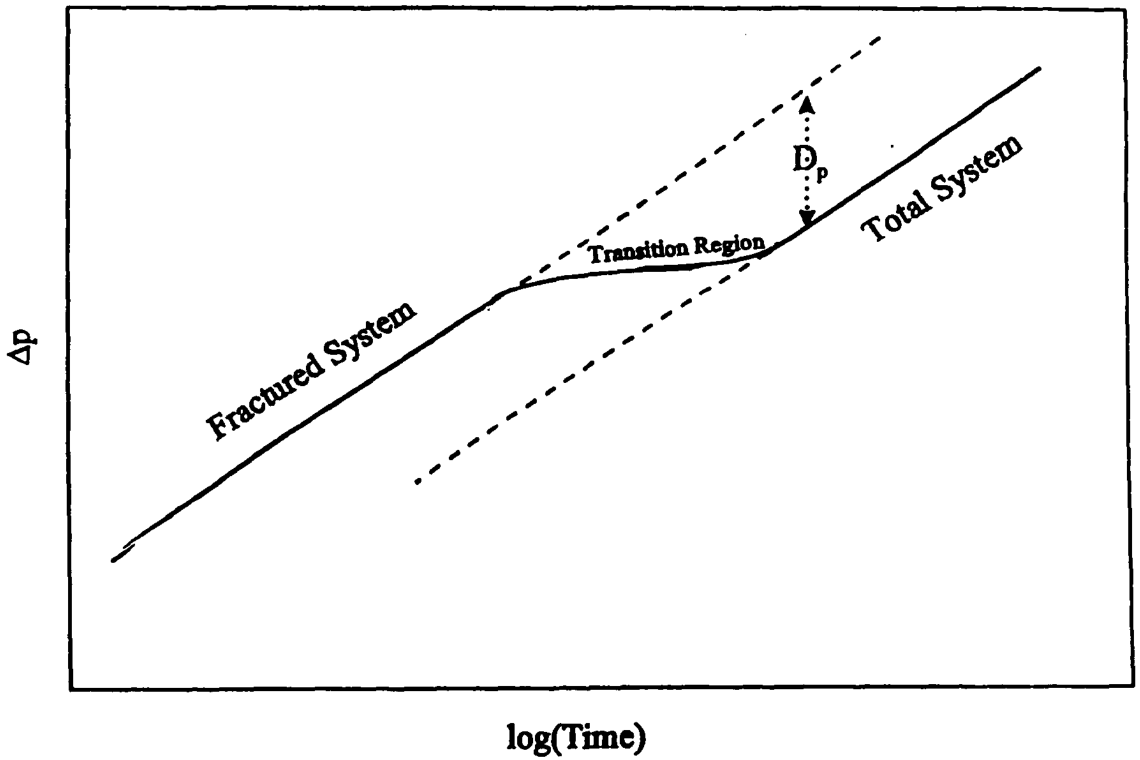

Figure 2.5 Estimation of storage coefficient from dimensionless pressure.[2]

approximated the naturally fractured reservoir as a layered system composed of thin but highly conductive layers, which represent the fractures and alternate with thick, low conductive, high storage capacity layers, which represent the matrix. Transient flow was assumed in the matrix layers and the solution was obtained by numerical simulation. The results of the previously mentioned studies confirmed that naturally fractured reservoir can be represented by two parallel semilog straight line portions. The first semilog straight portion occurs at very short shut-in time. Therefore, this straight line may be obscured by the wellbore storage effect. Kazemi[3] suggested that the degree of precision of result obtained through the analysis of pressure transient data of a dual-porosity reservoir depends on the degree and type of heterogeneity of the system.

De Swaan (1976)[11] developed the analytical equations for the asymptotes (two parallel straight lines) considering transient flow and either matrix block or layer geometries, i.e. both layer and sugar-cube geometries are considered. The fracture diffusivity equation is similar to Warren an Root's except in terms of intrinsic rather than bulk properties. He assumed that the reservoir is composed of two regions: namely, highly permeable fractures and tight matrix blocks.

Earlougher (1977)[12] described the elliptical flow regime resulting from anisotropic permeability. He proposed that it is impossible to recognize rock anisotropy from a single well test.

Mavor and Cinco Ley (1979)[13] extended Warren and Root model to improve analysis of wellbore and reservoir conditions. The study considered finite reservoirs to identify pseudo-steady state and long time reservoir behavior. The model was used to calculate rock matrix and fracture storativity using a single well test data. In addition, the study concluded that constant pressure tests in naturally fractured reservoirs were analogous to those in unfractured formations. Mavor and Cinco Ley[13] derived a solution for pseodosteady state interporosity flow, including wellbore storage and skin in Laplace space. They obtained an approximation to the real space solution by taking a weighted average of values of the Laplace space result.

Bourdet and Gringarten (1980)[14] presented type curves to obtain several reservoir parameters including: permeability, skin factor, wellbore storage constant, and fissure volume. Their type curves also applied damaged, acidized, and fractured wells in fissured reservoirs. The type curves were based on log-log analysis of double porosity systems to provide mainly two parameters: ω the ratio of the fissure storativity to the total storativity, and λ the interporosity flow coefficient, which depends upon the shape, the size, and the permeability of the matrix blocks.

Lai. et al., (1983)[15] derived new governing equations for transient matrix flow maintaining the sugar-cube geometry and considering the fractures and matrix as an overlapping continuum. They obtained an equation similar to Kazemi's fracture equation with the exception of the source term evaluated at one-half the fracture spacing instead of one-half the fracture thickness. Their solution includes both skin and wellbore storage and is expressed as a series of Bessel functions which must be numerically inverted.

Streltsova (1983)[16] developed a pressure for transient behavior in a layered, naturally fractures reservoir and is known as the "gradient-flow" model. Assuming only vertical flow in the matrix to the fracture. The matrix pressure was found to be dependent on both the time and spatial location within the matrix layer, subsequently forming pressure gradients. These gradients are highly nonlinear and affect the flux at the interface.

Bourdet et al., (1983)[17] developed a set of type curves that aided the analysis of data obtained from well testing fractured formations. Bourdet et al[18] (1984) added another set of type curves for the use in evaluating build-up and drawdown tests.

Blasingame and Lee (1985)[19] used decline curve analysis to propose analysis techniques for post-transient flow assuming constant bottom-hole pressure. This study considered homogeneous reservoirs, vertically fractured reservoirs, and naturally fractured formations. The methods provided useful tools for obtaining drainage area, reservoir shape factor, and reservoir fracture factor for homogeneous and vertically fractured reservoirs.

Onur and Staman (1991)[20] introduced type curves based on derivative of dimensionless pressure, its integral, and a new dimensionless group. The type curves were based on double-porosity model and valid for both pseudo-steady state and transient flow conditions. The authors showed field data and used it to determine many key parameters of naturally fractured reservoirs.

Hyes and Vaughan (1991)[21] showed that Earlougher's[12] thought is valid when the anisotropy occurs as a result of very small scale permeability variations. These authors described the flow regime resulting from large scale anisotropy. The model used was assumed to contain a regular series of parallel partial baffles in an isotropic permeability field. Hyes and Vaughan[21] presented a dimensionless type curves which can be used to quantify permeability anisotropy from the pressure response at the disturbing well only considering the effects of wellbore storage.

Engler and Tiab (1996)[22] developed direct synthesis method for interpreting pressure transient tests in naturally fractured reservoirs without type curve matching. The method offers several advantages including: (1) accurate results using exact analytical solutions to calculate reservoir parameters; (2) independent verification of the obtained parameters; and (3) obtaining useful information when not all flow regimes are observed. One of the main advantages of this method is that it also considered wellbore storage effect.

Engler and Tiab[22] developed a smooth empirical relationship between the pressure derivative ratio and ω. It is valid form $0 \leq \omega \leq 0.10$ with less than $\pm 1.5\%$ error:

$$\omega = 0.15866\left(\frac{(t*\Delta p'_w)_{min}}{(t*\Delta p'_w)_R}\right) + 0.54653\left(\frac{(t*\Delta p'_w)_{min}}{(t*\Delta p'_w)_R}\right)^2 \tag{2.27}$$

where $(t*\Delta p'_w)_R$ is the pressure derivative at some convenient time, t, during the infinite-acting radial flow line. $(t*\Delta p'_w)_{min}$ is the minimum value of the pressure derivative curve. An alternative relationship to determine ω is possible from the characteristics times defined from the pressure derivative curve.

$$\frac{50t_{E1}}{\omega(1-\omega)} = \frac{t_{B2}}{5(1-\omega)} = \frac{t_{min}}{\omega \ln(1/\omega)} \tag{2.28}$$

where t_{E1} is the end of the first horizontal straight line, t_{B2} is the beginning of the second horizontal straight line, and t_{min} is the minimum pressure derivative time. Two more empirical correlations were developed for solving for ω using t_{E1}, and t_{B2}.

Engler and Tiab[22] provided an empirical correlation for estimating the interporosity flow parameter, λ:

$$\lambda = \frac{42.5h(\phi c_t)_t r_w^2}{qB}\left(\frac{(t*\Delta p'_w)_{min}}{t_{min}}\right) \tag{2.29}$$

An alternative method of determining λ were achieved by observing a characteristic unit slope, straight line during the late transition period.

$$\lambda = \frac{(\phi c_t)_t \mu r_w^2}{0.0002637k_{fb}}\left(\frac{1}{t_{USRi}}\right) = \frac{1}{\alpha t_{USRi}} \tag{2.30}$$

where t_{USRi} is the intersection of the transition period unit slope line with the infinite acting, radial flow derivative line and α represents the inverse of the group of constants in parentheses in the above equation. Engler presented a general relationship from which the interporosity flow parameter can be calculated from any of the characteristic time values by the following relationships:

$$\lambda = \frac{1}{\alpha t_{USRi}} = \frac{\omega(1-\omega)}{50\alpha t_{E1}} = \frac{\omega \ln(1/\omega)}{\alpha t_{min}} = \frac{5(1-\omega)}{\alpha t_{B2}} \tag{2.31}$$

Engler and Tiab[22] extended the work to include the effect of wellbore storage. He used the pressure and pressure derivative curves solve for the wellbore storage constant. Detailed investigations have shown the minimum point is unaffected by wellbore storage for all ω and λ. Subsequently, the procedures described previously are valid for the range:

$$\frac{(t_{wD})_{min}}{(t_{wD})_x} \geq 10.0 \tag{2.32}$$

Otherwise, An alternative method to determine λ and ω. An empirical correlations presented to estimate λ. The wellbore storage constant, skin factor, and interporosity flow parameter must be known to coupled with the minimum to infinite-acting radial flow pressure derivative ratio, to provide a means of determining ω.

2.2 Hydraulic Fracturing

Some reservoirs have low effective permeability and required some types of stimulation treatment to improve the performance and achieve commercial production rates. Creating a hydraulic fracture in the reservoir by pumping fluid and proppant into the formation at high pressure is a commonly applied stimulation method. Accurate characterization of the fractured well is needed for performance forecasting and optimal reservoir development. The use of large hydraulic fracture treatments for simulation of tight formations has become a common practice. Tight formations are characterized by permeabilities less than 10 md. The permeability is usually less than 1 md and is often less than 0.1 md. Hydraulic fracturing is a process by which a large surface area of the low-permeability formation is exposed to flow of fluid to the wellbore. Furthermore, it is evident that if this process is performed effectively it might drastically increase productivity.

Numerous semi-analytical, asymptotic analytical, numerical models, and type curves have been presented to describe the pressure behavior of vertically fractured reservoirs.

Solutions for the pressure transient behavior of vertically fractured wells as presented by several authors hinges on three basic types of vertical fractures:

(1) Infinite conductivity fracture: (fracture conductivity, $\kappa_f b_f/\kappa x_f > 300$) is defined as a condition at which the fracture conductivity is high enough that there is no pressure drop along the fracture plane at any instant in time.

(2) Finite conductivity: the pressure drop along the fracture is significant because finite conductivity vertical fractures have finite low flow capacities. This type of fracture exists for fracture conductivity, $\kappa_f b_f/\kappa x_f < 300$.

(3) Uniform-flux: The flow capacity in this flow type of fracture is high but not infinite as in the infinite conductivity case. This type implies that there is a definite pressure drop along the fracture plane and it varies.

Several papers have been published on the behavior of wells intercepting vertical fractures. Type curve matching has been proposed as an analysis method under this condition. Russel and Truitt (1964)[23] presented a mathematical model along with a set of simulated pressure buildup curves to predict transient behavior in vertically fractured wells. They presented their study to consider a single-plane vertical fracture. The results of this study were presented as tables of the dimensionless pressure drop as a function of time and fracture penetration.

Then, Cinco-Ley et al., (1976)[24] modified the work of Russe and Truitt[23] and developed a semi-analytical model and type-curves or interpreting pressure response of a well crossed by a finite conductivity vertical fracture in an infinite slab reservoir. Cinco-Ley et al.,[24] assumed an isotropic, homogeneous, and horizontal infinite reservoir bounded by an upper and lower impermeable strata. They found the semi-logarithmic techniques may be applied to interpret pressure data in vertically fractured wells intercepted by finite conductivity fractures. Cinco-Ley et al.,[24] concluded that two parameters: fracture storage capacity, $w\phi_f c_{fl}/\pi L_f$, and ratio of the diffusivities of the fracture and formation, $\kappa_f\phi c_t/\kappa\phi_f c_{fl}$, are sufficient to correlate pressure response.

In 1977, Cinco-Ley et al.,[25] extended their previous work to include the effect of wellbore storage and fracture damage in which the skin was defined as an infinitesimal zone surrounding the fracture. They concluded that the effect of skin or fracture damage is an important phenomenon that must be seriously considered in order to analyze pressure transient data in fractured wells effectively.

Baker and Ramy (1978)[26] published a finite element model to study the behavior of well intersecting a finite conductivity vertical fracture at the center of a closed square reservoir. They stated that graphs of log P_{WD} against log t_{Dxf} for various values of fracture conductivities, F_{CD}, have a few distinguishing characteristics to aid type-curve matching. Baker and Ramy[26] emphasized the fact that data from pseudoradial flow period gave a good estimate of formation permeability and wellbore skin effect when matched with any of several curves.

Cinco-Ley and Samaniego-V (1978)[27] presented a new semi-analytical method for analyzing pressure transient data intercepted by a finite conductivity vertical fracture based on the bilinear flow theory. This flow period considers transient linear flow in both fracture and formation. Their purpose was to present a new interpretation technique for early time pressure data including the criteria to determine the end of wellbore storage effects. Cinco-Ley and Samaniego-V[27] assumed an infinite, isotropic, and homogeneous, horizontal reservoir that contains a slightly compressible fluid of constant compressibility and viscosity. The well is intercepted by a fully penetrating vertical fracture and the porous media has a uniform thickness and constant porosity and permeability. In addition, they assumed gravity effects are negligible, and flow entering the wellbore comes only through the fracture. Furthermore, although the flow path in the fracture flow region is two dimensional in x- and y-direction, it was assumed as being one dimensional in x-direction using the principle of pseudo-function which indicates that velocities within the fracture independent of the vertical direction coordinate. Cinco-Ley and Samaniego-V[27] have shown that the early time response of a finite conductivity fracture is also influenced by the storage capacity of the fracture. The dimensionless storage capacity is defined by:

$$C_{fD} = \frac{w_f \phi_f c_{ft}}{x_f \bar{\phi} c_t} \tag{2.33}$$

Hanley and Bandyopadhyay (1979)[28] presented a simple semi-analytical model for a well in a square with a fully penetrating fracture of uniform flux and finite fracture capacity. They investigated the effect of wellbore storage, fracture length, fracture capacity, formation properties, and reservoir boundaries. They assumed the fluid flow pattern in the fracture is linear because the ratio of fracture length to the fracture width is very small such that the influx of fluid through the fracture tip can be neglected. Based on their work, three basic flow periods exist such as; fracture linear flow, bilinear flow and formation linear flow. Also, Hanley and Bandyopadhyay[28] suggest that the effect of wellbore storage should be taken into account in the pressure transient response of a fractured well in tight reservoir.

Ahmed (1982)[29] presented a comprehensive study on all the available techniques used to analyze transient pressure data from hydraulically fractures wells. He stated that there are five basic methods used to interpret transient pressure behavior of hydraulically fractured wells. These methods are fracture linear flow, bilinear flow (fourth-root time analysis), formation linear flow (square-root time analysis), modified pseudoradial flow(semi-log analysis), type curve matching, and reservoir history matching analysis. These techniques are applied to evaluate the following parameters: formation permeability, fracture half length, and fracture conductivity. Based on his studies, Ahmed[29] indicated that due to the fact that the duration of fracture linear flow is very short and the estimated of fracture properties such as fracture porosity and fracture permeability are not available for this period in most cases, the significance and usage of this flow period are very minimal or non-existing.

Puthigai and Tiab (1982)[30] extended the application of pressure derivative type curves to interpret pressure behavior of a well located in an infinite reservoir. Both uniform influx and infinite conductivity fractures were considered. Puthigai and Tiab[30] assumed the reservoir to be isotropic, horizontal, homogeneous, uniform in thickness and has constant permeability and porosity. They found that dimensionless pressure derivative, P_{WD}, was expressed as:

$$p'_{wD} = \sqrt{\frac{\pi}{2t_{xfD}}}\left[\operatorname{erf}\left(\frac{1-x_D}{2\sqrt{t_{xfD}}}\right)+\operatorname{erf}\left(\frac{1+x_D}{2\sqrt{t_{xfD}}}\right)\right] \tag{2.34}$$

The dimensionless pressure derivative for a uniform flux vertical fracture in an infinite-acting system was obtained from the above equation by letting $x_D=0$. For the case of an infinite conductivity fracture $x_D=0.732$.

In 1989, Tiab[31] applied the direct synthesis method to uniform flux and infinite conductivity vertical fracture models in closed system. Then in 1994[32], Tiab extended the work to vertically fractured wells in closed system. He presented a procedure to calculate permeability, half fracture length, skin, drainage area, and shape factor without using type curve matching.

Some dual-porosity reservoirs have low effective permeability and required some types of stimulation treatment, such as creating a hydraulic fracture in the reservoir, to achieve commercial production rates. Houze et al., (1984)[33] developed a set of type curves for the pressure transient behavior of hydraulically fractured wells in dual-porosity systems. The type curves are specifically developed for the behavior of a well produced at constant rate with an infinite conductivity vertical hydraulic fracture in an infinite-acting dual-porosity system. Houze et al.,[33] models are semi-analytical and consider the pseudo-steady state type of matrix/fracture fluid transfer and both the uniform flux fracture and the infinite conductivity fracture.

In 1986, Lancaster and Gatens[34] applied the available analytical techniques in their post-fracture well tests for hydraulically fractured wells in a dual-porosity reservoir. They used the techniques which have been presented for analyzing post-fracture well test data from hydraulically fractured wells in single-porosity reservoirs. Also, Lancaster and Gatens[34] used Houze et al.[33] type curves which were presented for the behavior of a well intercept an infinite conductivity vertical hydraulic fracture in an infinite-acting dual-porosity system. Lancaster and Gatens[34] analyzed post-fracture well test data from a number of wells for the purpose of estimating fracture conductivity and length. They concluded that the post-fracture well test data can be analyzed using type curves developed for single-porosity reservoirs, if the data do not exhibit complete dual-porosity behavior.

Cinco-Ley and Meng (1988)[35] developed an analytical solution for the behavior of a well intercepted by a finite conductivity vertical fracture in a double-porosity system. Two models for the matrix/fracture fluid transfer are considered: the pseudo-steady state matrix flow model and the transient matrix flow model. Their model demonstrated that these systems exhibit the basic behavior of a well with a finite conductivity fracture: that is bilinear flow, pseudolinear flow, and pseudoradial flow in addition to the transition flow periods. Cinco-Ley and Meng presented type curves to analyze data falling in the bilinear and pseudolinear flow regions. Also, they presented a general semi analytical model for the behavior of the system including the effect of wellbore storage.

Liu Ci-Qun and Yang-Jim (1989)[36] presented approximate analytical solutions of transient pressure for a finite-conductivity vertical fracture in a reservoir with double-porosity by using the concept of disturbed extent for elliptical flow. They found that the log-log diagnosis plot of the pressure calculated by the approximated formula may be divided into early bilinear flow stage, middle inter-porosity flow stage, and late pseudoradial flow stage. The equation of transient pressure behavior for a finite conductivity vertical fracture in a reservoir with double porosity media for late pseudo-radial flow stage as presented by Liu and Yang as:

$$p_{wD} = 0.5\,\mathrm{Ln}(t_{Dxf} + \frac{(1-\omega)^2}{\lambda}) + 1.39 \tag{2.35}$$

2.3 Multi-layer Reservoirs

Due to the complexity of the environment in which sediments were deposited, and as a result of subsequent physical and chemical changes, many types of heterogeneities are present in all reservoir behavior. The presence of impermeable shale separate the reservoir into two or more layers of differing physical characteristics in the producing formation. The pressure behavior of such a reservoir is the subject matter of this study.

Although a number of studies on the pressure behavior of layered systems have been undertaken during the past two decades, the state of knowledge is not complete for well test analysis. The problem lies in the evaluation of complex mathematical expressions that describe the analytical solution of such systems and in the large number of possible solutions.

The behavior of pressure transients for layered systems has been studied and can be separated into two categories: (1) layers which are separated by impermeable barriers (no formation crossflow); and (2) layers which communicate in the reservoir. Based on published studies, layered systems can be of two types:

1- Different layers of the system communicate only by means of the wellbore. This type of reservoir is known as a commingled reservoir. The behavior of such a reservoir is significantly different from that of a single-layered reservoir. A commingled reservoir system can have large differences between the average pressure of each layer.

2- A significant amount of inter-layer cross-flow occurs in the system. Crossflow reservoirs do not have a large difference in pressure between the layers and tend to act as though the reservoir properties are more uniforms than the commingled situation. Russell and Prats[37] studied such systems and concluded that the reservoir behavior is analogous to that of a single-layer reservoir with the average properties of the layered system.

Formation crossflow has been modeled mainly by two methods: pseudosteady state crossflow and transient crossflow. Pseudosteady state crossflow assumes that the resistance to crossflow is confined to the interlayer boundary and the flow is horizontal within each layer. This assumption reduces a two-dimensional problem to a one-dimensional problem. Transient crossflow utilizes the two-dimensional diffusivity equation for each layer.

Lefkovits et al., (1961)[38] developed the first comprehensive study of commingles reservoirs. They presented analytical solutions of pressure behavior in commingled reservoirs. They assumed that each layer is homogeneous, isotropic, and bounded. They used Laplace transformation techniques to handle n-layer problems. Lefkovits et al.,[38] concluded that the more permeable layer depletes faster than the less permeable layer until the steady state condition in reached.

Tariq (1978)[39] studied the effects of wellbore storage and skin on the pressure response of commingled bounded reservoirs. The diffusivity equations were solved using the Laplace transformation techniques. Then, results were inverted numerically by using the Stehfest algorithm[6]. Tariq[39] presented general type curves for commingled reservoirs with wellbore storage and skin factor. He found that for two layer cases, two straight lines may exist. The first line represents the transmissibility, kh, from the more permeable layer, and the second line is that from the total system of the reservoir.

In 1981, Raghavan et al.,[40] extended Tariq's study by large contrast in the skin factor on the pressure behavior of two layer reservoir. He also investigated the effects of skin factor on the layer rate. Raghavan et al.,[40] solved the diffusivity equations using finite difference techniques. He concluded that, if the skin factor contrast is high, the use of conventional procedures to estimate the flow capacity and skin factor will be erroneous.

Satman (1981)[41] presented drawdown and buildup behaviors for a commingled, multi-layered composite reservoir. He considered different discontinuity boundary radii for different layers. In his model, Satman used the concept of a tilted front for layered composite reservoirs, because the fluid front would propagate at different rates in different layers.

Gao and Chan-Qing (1984)[42] studied the single-phase unsteady flow in a multilayer reservoir with cross-flow when each layer produces under a constant wellbore pressure. Approximate theoretical expressions for the total flow rate and the crossflow between layers were given. They concluded that the constant pressure flow test can be used to determine the total transmissibility, kh value, of the multilayer reservoir.

Ehlig-Economides et al., (1985)[43], studied the general problem of n-homogeneous layers, in which any two adjacent flowing layers may or may not be crossflowing in the formation. Furthermore, a method is provided using simultaneously acquired pressure and flowrate transient data for several layers during the course of one well test. They presented a model and solved analytically for the n-layer system. Properties, including permeability, porosity, layer thickness, the wellbore skin factor, and the vertical permeability between crossflowing layers, were distinct for each flowing layer. Wellbore storage effects were also included, and solutions were provided for infinite-acting and bounded systems. Ehlig-Economides et al.,[43] compared the general characteristics of two different multi-layer reservoir models. The first model consisted of two commingled zones. Each zone was divided into several inter-communicating layers. The second model was a five-layer commingled reservoir. They found that in the early time, the pressure behavior of the first model exhibits as if it were a commingled reservoir, and thus, commingled reservoir approaches are adequate to analyze it. Ehlig-Economides et al.,[43] concluded that the combination of wellbore pressure and layer flowrates provides sufficient information for determination of the complete layered reservoir description. Also, the solution technique can be extended to other applications in multi-layered testing such as vertical fractures, dual porosity, interference analysis, etc.

Ehlig-Economides et al., (1986)[44] presented a procedure for acquiring the transient flowrate and pressure response of any single layer in a commingled system. They referred to the test as the Commingled Single Layer Transient (CSLT) test, to emphasize the multi-layered aspect of the test configuration. The following information describes an example of how the CSLT test works. If two flowrate sensors are positioned such that one is just above the layer perforations and the other just below, the sensors can be spaced further apart, provided first that no flow from the layer adjacent and above the layer tested reaches the upper flowmeter, and second, that the lower flowmeter is above the level of the perforation for the next lower layer. In this way, the difference between the flowmeter readings is equal to the layer flowrate. The CSLT may be conducted as follows: (a) position the sensors as described above while the well is flowing at a constant surface rate; (b) record flowrates and pressure; and (c) determine the stabilized trend in flowrate and pressure at the end of the flow period; and (d) change the surface rate and record flowrates and pressure versus time elapsed, Δt, since the surface rate change. The interpretation procedure which was listed in the paper suggested that the rate normalized pressure, $\Delta p_{wf} / \Delta q_L$, and time be calculated. q_L is defined as the layer flow rate. Then, for the equivalent log-log analysis, the derivative of the rate normalized pressure with respect to the time can be calculated and the log of the result versus log Δt may be plotted. Ehlig-Economides et al.,[44] stated that the transient behavior observed in the plot was virtually identical to that of the single layer pressure transient which would result if the layers were isolated in the wellbore by packers. They used the log-log presentation to diagnose the model for the layer transient response and for type curve matching. Ehlig-Economides et al.,[44] concluded that the properties of a dual porosity zone can be determined by analyzing the rate normalized pressure response or by type curve matching with the rate normalized pressure derivative. Both approaches are considerably easier when the wellbore storage effect is minimized.

Joseph et al., (1986)[45] discussed the interpretation of well pressure data in bounded reservoirs in general and in the Shengli Field in China in particular. An analytical model of the two-layer bounded system was utilized. It is capable of treating skin, wellbore storage, and both crossflow and commingling of the reservoir fluids. Finally, field data sets displaying layering (supported by geologic evidence) were analyzed. Joseph et al.,[45] noted that the cases which were studied can be reduced to the equivalent homogeneous single layer problem by keeping the storativity ratio, ω, equal to the fractional flow capacity, k. They found the Laplace transformation of the dimensionless well pressure drop inclusive of storage and skin to be:

$$\overline{P}_{wD} = \frac{1}{C_D s^2 + \dfrac{1}{\overline{P}_{wDC_D=0}}} \tag{2.36}$$

where s is the Laplace variable of time t_D. The above equation is entirely general and allows one to pass from a pressure transform exclusive of wellbore storage (i.e., $\overline{P}_{wDC_D=0}$) to one inclusive of the storage effect (i.e., $\overline{P}_{wD}$).

Kucuk et al., (1986)[46] presented analysis techniques to obtain individual-layer properties such as permeabilities and skin factors for layer reservoirs. Two different analysis techniques were presented to estimate layer parameters. The first technique, which is the logarithmic convolution method, estimates the approximate values of parameters. The second technique, which is the nonlinear least-squares estimation method, improves the first estimates. Kucuk et al.,[46] showed that layer permeabilities and skin factors can be estimated uniquely from simultaneously measured wellbore pressure and flow-rate data that is acquired from all layers sequentially.

Mavor and Walkup Jr. (1982)[47] developed a new mathematical model of a commingled multi-layered reservoir for both single and double porosity systems. Through the use of the Laplace Transformation, they treated the behavior of a multi-layered reservoir system as an equivalent resistance network in which the total resistance to fluid flow can be obtained by adding the resistance to fluid flow in each layer. For this purpose, they applied the elementary concept of resistances in parallel. Mavor and Walkup Jr.[47] applied the parallel resistance concept based upon both pressure and flow rate data to determine individual layer properties. The resistance terms for each layer depend upon the reservoir model selected for each layer. For example, if one layer is assumed to be an infinite-acting dual porosity reservoir, the corresponding resistance function is as follows.

$$R_i = \frac{K_0(R_{wi}\sqrt{f_i s})}{(R_{wi}\sqrt{f_i s})K_1(R_{wi}\sqrt{f_i s})} + S_i \tag{2.37}$$

where K_0 and K_1 represent modified Bessel functions of the second kind, zeroth and first order respectively, the function f_i converts the single porosity solution into the corresponding dual porosity reservoir solution, and S is skin factor. R_{wi} is dimensionless wellbore radius which is defined as:

$$R_{wi} = \frac{r_w}{r_b}. \tag{2.38}$$

They[47] listed the f_i function required to simulate three types of double porosity response: restricted interporosity flow, unrestricted interporosity flow (often referred to as transient interporosity flow), and partially restricted interporosity flow which considers a skin factor between the primary and secondary porosity systems. They came to two major conclusions. First, the log-log plot of pressure change and derivative group versus time is sufficient to define the various flow periods. Second, it is possible to isolate the properties of each layer if the flow rate from the layer is known. Mavor and Walkup Jr.[47] stated that "during the infinite-acting period individual properties can be determined from a semi-log plot of $(\Delta P)/(\Delta q_{ri})$ versus time." q_{ri} is the relative rate of each layer, which is defined as the ratio of the flow rate from the layer of interest to the surface flow rate:

$$q_{ri} = \frac{q_i}{q_T} \tag{2.39}$$

Then, they presented equations to calculate the layer permeabilities and skin factor from either the drawdown or the buildup as follows:

$$k_i = \frac{162.6(q_T B)\mu_i}{|m_i| h_i} \tag{2.40}$$

The skin factor from the drawdown test is:

$$s_i = 1.151\left\{\frac{\left(\frac{\Delta P}{\Delta q_{ri}}\right)_{1HR}}{|m_i|} - \log\left(\frac{k_i}{\phi_i \mu_i c_{ti} r_{wi}^{\ 2}}\right) + 3.2274\right\} \tag{2.41}$$

and from the buildup test is:

$$s_i = 1.151\left\{\frac{\left(\dfrac{\Delta P}{\Delta q_{ri}}\right)_{1HR}}{|m_i|} - \log\left(\frac{t_p k_i}{(t_{pt}+1)\phi_i \mu_i c_{ti} r_{wi}^{\ 2}}\right) + 3.2274\right\} \tag{2.42}$$

Mavor and Walkup Jr.[47] used rates relative to the total surface rate as an approximation of the total downhole rate.

Hatzignatiou et al., (1987)[48], showed a solution for interference pressure transient response in a two-layered reservoir having pseudosteady state formation crossflow. With this solution, They described a type-curve matching technique to estimate the reservoir properties.

Shah et al., (1988)[49] described the problem of estimating horizontal and vertical permeabilities, skin factor, and average pressure within the drainage area in each layer in a multilayered reservoir in the presence of formation crossflow between the layers. Shah et al.,[49] proposed a multistep testing procedure that involves simultaneous analysis of downhole measurement of the pressure and the fluid flow rate. An approach for the entire data set gathered during the test has been proposed. This approach is based on history-matching the test data using a numerical single-well model.

Anbarci et al., (1989)[50] developed an analytical solution for a two-layer, composite reservoir. They considered pseudosteady state crossflow between the layers. Wellbore storage and skin effects were included. Anbarci et al.,[50] used a type-curve matching technique to locate the front location in a particular layer.

Larsen (1989)[51] reformulates the model of Ehlig-Economides and Joseph[43] into an eigenvalue problem and allows for outer boundaries that can be generated by image wells. Bidaux et al., (1992)[52] presented a new solution technique for the analysis of multi-layered tests. This technique is based on an analytical conversion of a single-layer response. Formation cross-flow is taken into account and a wide variety of inner and outer boundary conditions are possible. Bidaux et al.,[52] solution technique uses the same eigenvalue formulation as Larsen[51], but applies it in the Laplace domain to perform a direct transformation of any single-layer transient pressure response into a multi-layer response without using unbounded solution or image wells.

Gomes and Ambastha (1993)[53] developed a new analytical solution for multi-layered composite reservoirs with pseudosteady state interlayer crossflow. The developed analytical solution for an n-layered composite reservoir is applicable for any irregularly-shaped discontinuity boundary, as well as for closed, constant-pressure and infinite outer boundary conditions.

Bennett et al.,[54] examined the performance of wells intercepting finite conductivity vertical fractures in a single layer system. They showed the effect of varying fracture conductivity, fracture height, h_f, fracture length and effect of settling of propping agents on the performance of a single-layer reservoir drained by a vertically fractured well. They presented a numerical model using a block-centered finite difference approximation to represent the governing partial differential equation and to validate their analytical solution. They assumed the fractured well is situated at the center of a reservoir consisting of a square drainage region. They found that for a single-layer reservoir, the effect of vertical gradient is significant if $h_f>h$. However, for multilayered reservoirs the effect of vertical gradient is significant if $h_f = h$.

Bennett et al.,[55] extended their earlier work and presented relatively new analytical and numerical solutions to the response of a vertically fractured well intercepting a two-layered reservoir without communication. Bennett et al.,[55] found that the difference between the response of a well in a single layer reservoir and the response of a well in a multilayer reservoir is the dimensionless reservoir conductivity, R_{CD}. Therefore, they suggest that results from commingled reservoirs can be correlated with the solution of a single system if pressure data are plotted in terms of t_{Dxf}/R^2_{CD}. As a consequence, if it is possible to correlate the well response for multilayer reservoirs with single layer systems, then additional type curves will not be needed to analyze fractured wells that drain commingled systems.

Britt and Bennett (1985)[56] extended the previous techniques that can be used to determine fracture conductivity from pressure transient data of hydraulically fractured tight gas wells to wells in moderate permeability reservoirs. They utilized the previous work done by Bennett et al.,[54,55], using the bilinear flow concepts. Britt and Bennett[56] found that applying these techniques in moderate permeability reservoirs can be done, because this type of reservoir exhibits bilinear flow behavior.

Oshinuga (1988)[57] presented a new analytical model for analyzing pressure transient data for wells intercepted by a finite conductivity vertical fracture in a closed square multilayered reservoir. The solution considers the effect of wellbore storage. The primary aim is to estimate fracture half-length and fracture conductivity. He assumed two layers of different flow properties, and each layer consists of a homogeneous and isotropic porous medium. In addition, Oshinuga[57] assumed the flow is a single-phase, slightly compressible fluid of a constant viscosity in both the fracture and the formation. Fluid flow toward the wellbore takes place only through the fracture, and gravity effect is negligible. He developed type curves applicable for analyzing transient pressure data for a square multilayered reservoir intercepted by a finite conductivity vertical fracture. Oshinuga[57] found that pressure transient response in a closed square multilayered reservoir intercepted by a finite conductivity vertical fracture may exhibit four flow regimes: fracture linear flow analysis, bilinear flow analysis, formation linear flow analysis, and pseudosteady state flow analysis. Also, he concluded that results from a multilayered reservoir may be correlated with the solution of a single system if pressure data are plotted in terms of t_{Dxf}/R^2_{CD}.

Okoye et al., (1989)[58] extended Oshinuga's work for a tight gas reservoir in order to determine fracture conductivity and fracture half-length. Okoye et al.,[58] conclude that the results of the analysis are in good agreement with published results. They stated that the model presented in their study may be more appropriate for expressing the pressure transient behavior in multilayer fractured tight gas reservoirs than for the existing model, particularly when the fracture conductivity is finite. Okoye et al.,[58] concluded that the duration of bilinear flow period depends on fracture conductivity, and as the conductivity increases, the duration of the bilinear flow period diminishes.

Okoye et al., (1990)[59] used the type curves they developed earlier[58] to match drawdown and buildup curves to determine fracture conductivity, fracture half-length, and reservoir permeability. They also correlated a two-layered solution with the single-layer solution. Okoye et al.,[59] emphasized that their study of the two-layered reservoir solution can be extended to an n-layered system. Based on their results, they concluded that for practical values, the solution can be correlated in terms of only fracture conductivity, F_{CD}, and reservoir conductivity, R_{CD}.

2.4 Tiab's Direct Synthesis Technique

The Interpretation of pressure data recorded during a well test has been used for many years to evaluate reservoir characteristics. Transient pressure analysis provides a description of the reservoir flowing behavior.

Many methods are proposed for interpretation of transient well tests. Horner build up and drawdown tests are considered to be the most widely used and well known methods for using transient well testing for reservoir evaluation.

Recently, type curves have been used to indicate the pressure response of flowing wells under a variety of well and reservoir configurations. Type curves are considered by many well test analysts as overly simplified or overly difficult to distinguish, and/or cumbersome to use. Many authors have used the Stehfest algorithm[6] to solve complex transient flow behavior. As a direct consequence of numerical inversion, type curves were developed for both transient and pseodosteady state flow including wellbore storage and skin[14].

Early techniques for interpreting pressure transient tests included conventional semilog and log-log type curve methods. Both methods are accurate provided that certain criteria are established. That is, all flow regimes must be observed in the pressure and pressure derivative curve over a sufficient period of time. If not present, semilog analysis will be incomplete and unfortunately, type matching is a trial-and-error method which frequently provides nonunique answers.

During the last two decades, the pressure derivative technique has been widely used. This technique provides a description of the flow behavior in the reservoir. It also emphasizes the infinite radial flow regime. The pressure derivative is a powerful diagnostic tool for analyzing pressure transient data. The most versatile plot for identification and diagnosis of reservoir heterogeneities is the combined pressure and pressure derivative format. The high accuracy attainable in modern pressure gauges makes this approach both plausible and reliable. The use of pressure derivative versus time is mathematically satisfactory because the derivative is directly represented in one term of the diffusivity equation. Therefore, the pressure derivative is more sensitive to small phenomena of interest and also diminished by the pressure versus time solutions. The collection of differential pressure transient data creates difficulty for using the pressure derivative analysis. In addition, accurate and frequent pressure measurements are required. However, the availability of accurate pressure measurements (from electronic pressure gauges) and the development of computer processing software aides this kind of analysis.

Therefore, it is proposed to use an alternative method referred to as "Direct Synthesis". This method utilizes the characteristic intersection points, slopes, and times of various straight lines from a log-log plot of pressure and pressure derivative data.

Values of these points are linked directly to the exact, analytical solutions to obtain reservoir and well parameters. The direct synthesis method offers the following advantages:

(1) Accurate results from using the exact, analytical equations to calculate reservoir parameters.

(2) Independent verification is frequently possible from a third unique point.

(3) Useful information is obtained when not all flow regimes are observed, as a direct result of the additional characteristic values developed by the method.

The use of the pressure derivative for interpretation of well test data, which was first introduced by Tiab and Colleagues,[60] has gained wide acceptance over the past several years. Type curves based on the pressure derivative display more character than conventional type curves and make it easier to identify various flow regimes.

In 1989, Tiab[31] applied the Direct Synthesis method to uniform flux and infinite conductivity vertical fracture models in closed systems[32]. He presented a procedure to calculate permeability, half-fracture length, skin, drainage area, and shape factor without using type curve matching.

Tiab (1994)[61] said that "Horn (1990)[62] showed that log-log curve matching is not as accurate as conventional semilog methods, because log-log axes tend to mask inaccuracies at late time, where 1 mm deviation of a pressure point may mean an actual error of 200 psia". Therefore, Tiab applied the Direct Synthesis Technique to homogeneous reservoirs with skin and wellbore storage. Several unique features of the pressure derivative plot have been identified, including the point of intersection of the unit slope line with the infinite-acting line as well as the maximum pint and the starting time of the infinite acting line. Equations corresponding to these unique features have been developed. For example, an empirical equation has been derived to estimate the wellbore storage coefficient or the reservoir permeability from the coordinates of the peak point:

$$k = \left(\frac{59.3q\mu B}{h}\right)\frac{1}{\left(0.015\frac{qB}{C}\right)t_x - \left(t * \Delta p'\right)_x} \tag{2.43}$$

where t_x is the time of the maximum point (peak), and $\left(t * \Delta p'\right)_x$ is the pressure derivative of the maximum point (peak). Also, the coordinates of the maximum point of the pressure derivative have been used to present two empirical equations which can be used to determine skin factor:

$$S = 0.171\left(\frac{t_x}{t_i}\right)^{1.24} - 0.5Ln\left(C_D\right) \tag{2.44}$$

$$S = 0.921\left(\frac{(t * \Delta p')_x}{(t * \Delta p')_i}\right)^{1.1} - 0.5Ln\left(C_D\right) \tag{2.45}$$

where,

$$C_D = \left(\frac{0.8935}{\phi c_t h r_w^2}\right)C \tag{2.46}$$

where t_i and $\left(t * \Delta p'\right)_i$ are the time the pressure derivative respectively of the intersection between the unit slope line and the late time infinite acting line of the pressure derivative.

Engler[63] extended this technique to naturally fractured reservoirs for infinite-acting and bounded outer boundaries. Both pseudosteady state vs. transient matrix flow, with or without skin, and storage were examined.

In this work, the development of the application of Tiab's Direct Synthesis Technique to multi-layer naturally fractured reservoirs with and without hydraulic (vertical) fracture is studied. The technique determines the characteristic points and lines necessary for the analysis.

The application chapter describes the procedures for analyzing real transient test data, either drawdown or buildup, from the published literature.

CHAPTER 3

APPLICATION OF TIAB'S DIRECT SYNTHESIS TO MULTI-LAYER DOUBLE POROSITY RESERVOIRS

Pressure buildup analysis of wells in a multi-layer reservoir, with several layers communicating through the wellbore only, is very complicated. Various authors[37,38,64,69-71] have presented results of theoretical studies of pressure buildup performance for a well completed in a multi-layer reservoir. The conventional buildup tests from layered reservoirs usually suffer from cross-flow between layers, especially if the layers communicate through the wellbore only and the permeability contrast between these layers is high. The major problem for layered systems is the estimation of individual layer permeabilities and skin factors from the conventional well tests. Conventional drawdown and build up tests, if interpretable, reveal the behavior of the total system.

Despite the large number of publications on the behavior of pressure analysis, the combined effects of layered and double porosity system on the pressure behavior needed to be examined. Mathematical formulation is presented and type curves for wellbore pressure and its derivative are generated. Therefore, this chapter will emphasize the development of Tiab's Direct Synthesis procedure for a commingled multi-layer infinite-acting, naturally fractured reservoir. Mathematical formulation is presented and type curves for wellbore pressure and its derivative are generated. Analytical expressions and correlations from characteristic points and lines will be developed. These characteristic values or combinations of these values will determine the necessary reservoir parameters of each layer in multi-layer naturally fractured reservoirs. In order to simplify the mathematical model, only a two-layer reservoir without cross-flow is considered. However, results provided here can be generalized to muli-layer systems. The interpretation presented here utilizes a new version of pressure and pressure derivative type curves including the dimensionless storage coefficient, ω, the interporosity flow parameter, λ, and permeability-thickness product (flow capacity) of each layer, kh. Based on observations of the sensitivity of the response of these parameters, new correlations have been developed. However, to make these correlations universal in real units, normalized forms are derived. The most important conclusion obtained from this chapter is that the significant transient event in interpreting a production data from an infinite, multi-layer reservoir is the initial flow period.

3.1 Theory and Laplace Space Solution

Many studies have been introduced for analysis of transient pressure analysis of naturally fractured reservoirs. Several flow models have been developed to describe this pressure behavior. Numerous analytical and numerical models have been published in the petroleum literatures concerning pressure response in dual-porosity systems. Two key parameters were derived by Warren and Root[2] to characterize naturally fractured reservoirs: the dimensionless storage coefficient, ω; and the interporosity flow parameter, λ. The ω provides an estimate of the magnitude and distribution of matrix and fracture storage. The interporosity flow parameter is a measure of the mass transfer rate from the matrix to the fractures.

Due to the complexity of the environment in which sediments were deposited, and as a result of subsequent physical and chemical changes, many types of heterogeneities are present in all reservoir behavior. The presence of impermeable shale separates the reservoir into two or more layers of differing physical characteristics in the producing formation. The pressure behavior of such a reservoir is the subject matter of this study.

Although a number of studies on the pressure behavior of layered systems have been undertaken during the past two decades, the state of knowledge is not complete for well test analysis. The problem lies in the evaluation of complex mathematical expressions that describe the analytical solution of such systems and in the large number of possible solutions. Russell and Prats[37] studied the inter-layer cross-flow systems and concluded that the reservoir behavior is analogous to that of a single-layer reservoir with the average properties of the layered system. The present study focuses on the behavior of a commingled reservoir system because the behavior of such a reservoir is significantly different from that of a single-layered reservoir.

Many authors have used the Stehfest algorithm to solve complex transient flow source functions and/or to include skin and wellbore storage with transient matrix flow[14-16,67,68]. Mavor and Cinco Ley[13] (1979) derived a solution for pseodosteady state interporosity flow by using the Laplace space numerical inversion technique proposed by Stehfest. For the case of a single layer, infinite, naturally fractured reservoir, the dimensionless pressure at the wellbore is given as:

$$\bar{p}_D = \frac{K_0(\sqrt{f(s)s})}{s(\sqrt{f(s)s})K_1(\sqrt{f(s)s})} \tag{3.1.1}$$

where, K_0, and K_1 modified Bessel functions of the second kind, zeroth and first order respectively, and the function $f(s)$ converts the single porosity solution into the corresponding dual porosity reservoir solution. It is a function of the matrix geometry and flow regime in Laplace space. In the above equation, wellbore storage and skin are negligible.

Also, Mavor and Cinco's[13] presented their solution in the Laplace space for infinite outer boundary, including wellbore storage and skin as follows:

$$\bar{P}_D = \frac{\left[K_o(\sqrt{sf(s)}) + S\sqrt{sf(s)}K_1(\sqrt{sf(s)})\right]}{s\left\{\sqrt{sf(s)}K_1(\sqrt{sf(s)}) + sC_D\left[K_o(\sqrt{s'(s)}) + S\sqrt{sf(s)}K_1(\sqrt{sf(s)})\right]\right\}} \tag{3.1.2}$$

Because four parameters had to be adjusted (C_D, S, ω, λ), the number of type curves required for log-log analysis would be more complicated. Using wellbore storage and skin solution for Mavor and Cinco[13], Bourdet and Gringarten[14] found an appropriate combination of parameters which allows the construction of a new type-curve suitable for practical interpretation. Bourdet and Gringarten[14] showed that Equation (3.2) can be approximated in all practical cases by:

$$\overline{P}_D = \frac{1}{s\left\{ s + \left[\ln\left(\frac{2}{\gamma\sqrt{\frac{sf(s)}{C_D e^{2S}}}} \right) \right]^{-1} \right\}} \tag{3.1.3}$$

where, $\gamma = 1.78$ is the exponential of Euler's constant.

This Section presents the solution for the layered reservoir model that was obtained through the use of the Laplace transformation. The geometry of the solution is schematically illustrated in Figure 3.1.1. A detailed derivation for the general solution of an infinite acting double porosity reservoir is obtained and demonstrated in Appendix B. For an n-layer double porosity system, each layer is considered an isotropic property. Small and constant compressibility, single phase, radial flow, and small pressure gradients are assumed in each layer. The actual solution with the above assumptions is:

$$\frac{\partial^2 \overline{p}_{fDi}}{\partial r_D^2} + \frac{1}{r_D}\frac{\partial \overline{p}_{fDi}}{\partial r_D} = sf(s)_i\,\overline{p}_{fDi} \tag{3.1.4}$$

The terms and their corresponding units used in all equations are presented in the nomenclature, and the definitions for the dimensionless variables are listed in Appendix B. In Appendix B, $\overline{k}$ and $\overline{\phi c_t}$ refer to base properties used to define the dimensionless terms. These base properties are values that set to thickness-weighted average values, where:

$$\overline{k}h = \sum_{i=1}^{n} k_{fi} h_i \tag{3.1.5}$$

$\overline{k}$ represents the thickness-averaged value of layer permeabilities. k_{fi} and h_i refer to the permeability and thickness of layer i, and n is the total number of layers. The thickness-averaged value of the layer porosity-compressibility product is defined by:

$$\overline{\phi c_t} h = \sum_{i=1}^{n} \phi_i c_{ti} h_i \tag{3.1.6}$$

where ϕ_i and c_{ti} are the porosity and compressibility of layer i.

For the case of multi-layer systems, derivations for $f(s)_i$ function to simulate three types of double porosity response are presented in Appendices (C, D, and E). The types are: (1) pseudosteady state matrix flow; (2) transient matrix flow of a slab geometry; and (3) transient matrix flow of a sugar-cube geometry. The derived functions of both the pseudosteady state matrix flow, and the transient matrix flow of a slab geometry agreed with the ones presented by Mavor and Walkup Jr.[47], where the function of the transient matrix flow of a sugar-cube geometry is new.

If the permeability units extend laterally hundreds of feet around the well, flow within the strata may be treated as if it is parallel and thickness-weighted arithmetic averaging should be used in the calculations of horizontal flow[102]. Therefore, this chapter treats the behavior of a multi-layered reservoir system based on arithmetic averaging in which the general description of the layered commingled model can be obtained by using the derived $f(s)_i$ functions. For example, the solution in Laplace space for a two layer system where both layers are an infinite double porosity is simply:

$$\bar{p}_D = \frac{\bar{p}_{D1} + \bar{p}_{D2}}{2} \tag{3.1.7}$$

Ignoring wellbore storage and skin:

$$\bar{p}_{D1} = \frac{K_0(\sqrt{f(s)_1 s})}{s(\sqrt{f(s)_1 s})K_1(\sqrt{f(s)_1 s})} \tag{3.1.8}$$

and

$$\bar{p}_{D2} = \frac{K_0(\sqrt{f(s)_2 s})}{s(\sqrt{f(s)_2 s})K_1(\sqrt{f(s)_2 s})} \tag{3.1.9}$$

Including wellbore storage and skin:

$$\bar{p}_{D1} = \frac{1}{s\left\{s + \left[\ln\left(\dfrac{2}{\gamma\sqrt{\dfrac{s\,f(s)_1}{C_D e^{2S}}}}\right)\right]^{-1}\right\}} \tag{3.1.10}$$

and

$$\bar{p}_{D2} = \frac{1}{s\left\{s + \left[\ln\left(\dfrac{2}{\gamma\sqrt{\dfrac{s\,f(s)_2}{C_D e^{2S}}}}\right)\right]^{-1}\right\}} \tag{3.1.11}$$

The derived f_i functions convert the single porosity solution into the corresponding multi-layer dual porosity reservoir solution. Equation 3.1.7 is used to study the pressure behavior for a naturally fractured multi-layer reservoir. Subsequently, the system of two layers will be examined in detail, and the dimensionless type curves will be obtained for this system. Before going into details, the validity of the Equation is examined. The proposed model was validated by comparing its response against the response of an equivalent single-layer model. For verification, the assumption in which these two-layer reservoirs have the same physical properties is made. Thus:

$(k_f h)_1 = (k_f h)_2$

$\omega_1 = \omega_2$

$\lambda_1 = \lambda_2$

From Figures 3.1.2-8, it is clear that the solution obtained from Equation 3.1.7 is similar to the one which was obtained by Mavor and Cinco Ley[13] (1979) for single layer naturally fractured reservoirs. Figure 3.1.2 shows a comparison of pressure and derivative responses provided by both models, multi-layer and single-layer. These curves are identical and validate the use of the proposed multi-layer model. The type-curves, in Figure 3.1.2, were constructed for various values of wellbore storage and skin combination as suggested by Bourdet and Gringarten[14]. Figures 3.1.3-6 illustrate the characteristics of pressure behavior response in both single and multiple layer infinite-acting, naturally fractured reservoirs with pseudosteady state interporosity flow. Both wellbore storage and skin are ignored. Figures 3.1.3 and 3.1.4 show the effect of the storage coefficient on the pressure response where the interporosity flow parameter is held constant while the storage coefficient is variable. Figures 3.1.5 and 3.1.6 show the effect of the variation in the interporosity flow parameter at constant storage coefficient on the pressure response. Figures 3.1.7 and 3.1.8 compare the pressure and pressure derivative responses for pseudosteady state, transient matrix flow in a slab system, and transient matrix flow in a sugar-cube system. It is evident from these Figures that the derived $f(s)_i$ functions to simulate the three types of double porosity response are correct. An important observation obtained from these figures is that the pseudosteady state response produces a sharper image and therefore parameters are more easily identifiable.

As a direct consequence of numerical inversion, new type curves were developed for two-layer model. These curves are presented in Figure 3.1.9 including wellbore storage and skin effects. The developed type curves show that wellbore storage dominate the early time pressure behavior. Figure 3.1.10 illustrates the characteristics of pressure and pressure derivative type curves in a two-layer infinite-acting, naturally fractured reservoir. Figure 3.1.11 shows the characteristics of pressure derivative response in a two-layer infinite-acting, naturally fracture reservoir with pseudosteady state interporosity flow. This Figure illustrates the effect of C_De^{2s} group; flow capacity ratio, $\frac{(k_fh)_1}{(k_fh)_2}$; dimensionless storage coefficient, ω; and interporosity flow parameter, λ on the pressure derivative response. The interporosity flow parameter which is defined in Equation 2.11 varies as the flow capacity varies because λ depends on fracture permeability, k_f. The Figure shows that for $\frac{\lambda_1}{\lambda_2} > 100$, the derivative curve has two depressions. Figure 3.1.11 also shows a unit slope, straight line on the pressure derivative curve during the late transition period. The intersection of the transition period unit slope line with the infinite-acting, radial flow line gives an expression to determine λ as will be shown later. This figure shows that wellbore storage can dominate the early time pressure behavior, hence masking the fracture flow straight line and even the transition region.

Unfortunately type matching is a trial-and-error method, which frequently provides non-unique answers. Therefore it is proposed to use an alternative method referred to as "Tiab's Direct Synthesis." This method utilizes the characteristic intersection points, slopes, and times of various straight lines from a log-log plot of pressure and pressure derivative data. Values of these points are linked directly to the exact, analytical solutions to obtain reservoir and well parameters. The following sections will discuss the characteristic points and lines from pressure behavior of a layered naturally fractured reservoir. These characteristic values will determine the necessary reservoir parameters in such systems.

3.2 Multi-Layer Infinite Reservoir without Wellbore Storage and Skin

During the last two decades, the pressure derivative technique has been used widely. The use of the pressure derivative for interpretation of well test data, which was first introduced by Tiab and Colleagues,[60] has gained wide acceptance over the past several years. Tiab used the pressure and the pressure derivative to introduce a new technique called direct synthesis. This technique is based on the log-log plot of pressure and pressure derivative data. It combines the characteristic points and lines from the field data with the exact analytical reservoir solutions, and provides accurate calculation of the reservoir parameters.

In Figure 3.2.1, the characteristic points and lines available for evaluating the pressure test can be identified. This figure illustrates the characteristic pressure derivative response in a two layer infinite-acting, naturally fractured reservoir with pseudosteady state interporosity flow. Both wellbore storage and skin are ignored. The figure shows the effect of flow capacity ratio on the pressure response where the permeability-thickness product ratio (flow capacity ratio) is variable. Both wellbore storage and skin are ignored.

The infinite acting radial flow portion of the pressure derivative is a horizontal straight line. At small values of time (early time), the fluid production is due to the expansion of the fracture network. During this flow period, the effect of the matrix is negligible. This flow period in double porosity system has been called "fracture storage dominated flow period." At large values of time (late time), the compressibility of the total system dominates the pressure derivative behavior of the reservoir. This flow period corresponds to an equivalent homogeneous reservoir. For this case, an equation for the pressure derivative during these times is:

$$t_D * p'_{wD} = 0.5 \tag{3.2.1}$$

The dimensionless pressure and dimensionless time respectively are expressed as follows:

$$p_{wD} = \frac{2\pi \bar{k} h (p_i - p_w)}{q_t B \mu} \tag{3.2.2}$$

$$t_D = \frac{\bar{k}t}{\overline{\phi c_t}\mu r_w^2} \tag{3.2.3}$$

where $\bar{k}$ is defined in Equation 3.5 and $\overline{\phi c_t}$ is defined in Equation 3.6. Substituting Equation 3.2.2 and 3.2.3 into Equation 3.2.1, then:

$$(t * \Delta p'_w)_R = \frac{70.6 q_t B\mu}{\bar{k}h} \tag{3.2.4}$$

The infinite acting radial flow at early and late times corresponds to all layers; therefore $\bar{k}h$ represents the total thickness-averaged value of layer permeabilities. Then, the total flow capacity of the well can be calculated by:

$$\bar{k}h = \frac{70.6 q_t B\mu}{(t * \Delta p'_w)_{R1}} \tag{3.2.5}$$

where the subscript R1 stands for radial flow line at time=1 hour.

The flow capacity of each layer is an important parameter for characterization of multi-layer naturally fractured reservoirs and therefore must be quantified by direct synthesis. From Figure 3.2.1, an important observation that will be used to develop a correlation for calculating the flow capacity of each layer is that the time of the beginning of the first horizontal straight line, $(t_D)_{b1}$, increases as the flow capacity ratio of the two layers increases. That is because under practical operating conditions, the larger rate will come from the larger permeability. Therefore, the early time pressure response of high flow capacity ratio, $\frac{(k_f h)_1}{(k_f h)_2}$, is less than the response of low flow capacity ratio. This occurs due to partial penetration effects, even if both layers are perforated and naturally fractured. The partial penetration effects is a result of significant variations in fracture permeability in each layer. Aguilera[101] (July 2000) observed that the problem of multi-layered permeability response may be recognized by a pressure derivative indicating partial completion effects even if the well is perforated in all fractured layers. This observation compares favorably with the above conclusion. Figure 3.2.1 shows that for the case of $\frac{(k_f h)_1}{(k_f h)_2} < 8$, the results are close to the results for an ideal single-layer case. In this figure, almost all curves are coincident for the case of $\frac{(k_f h)_1}{(k_f h)_2} < 8$.

Figure 3.2.2 shows the effect of storage coefficient on the pressure derivative response in a two-layer infinite-acting, naturally fracture reservoir with pseudosteady state interporosity flow. Figure 3.2.3 shows that characteristic time, $(t_D)_{b1}$, is not affected by changing interporosity flow parameter, λ.

In order to determine the flow capacity ratio, a correlation has been obtained from normalizing the characteristic time, $(t_D)_{b1}$, by the time, t_{Dmin}, of the minimum derivative point of the transition region. The empirical equation which fits the correlation with less than 1% error is given by:

$$\frac{(k_f h)_1}{(k_f h)_2} = 2x10^{-5}\left[\frac{(t)_{b1}}{\lambda(t)_{min}}\right]^2 + 0.0004\left[\frac{(t)_{b1}}{\lambda(t)_{min}}\right] \tag{3.2.6}$$

The flow capacity of layer 1 is given by:

$$(k_f h)_1 = (\bar{k}h)\frac{(k_f h)_1}{(\bar{k}h)} \tag{3.2.7}$$

Equation 3.2.7 can be written as:

$$\frac{(k_f h)_1}{(\bar{k}h)} = \frac{(k_f h)_1}{(k_f h)_1 + (k_f h)_2} \tag{3.2.8}$$

The above equation yields:

$$\frac{(k_f h)_1}{(\bar{k}h)} = \frac{\dfrac{(k_f h)_1}{(k_f h)_2}}{\dfrac{(k_f h)_1}{(k_f h)_2} + 1} \tag{3.2.9}$$

Then, the flow capacity of Layer 2 is:

$$(k_f h)_2 = (\bar{k}h)\left[1 - \frac{(k_f h)_1}{(\bar{k}h)}\right] \tag{3.2.10}$$

or,

$$(k_f h)_2 = (\bar{k}h) - (k_f h)_1 \tag{3.2.11}$$

Independent verification is frequently possible. Therefore, an alternative relationship can be developed by dividing the time of the beginning of the first horizontal straight line by the beginning of the second straight line, $(t_D)_{b2}$. With less than 1% error, the empirical equation is given by:

$$\frac{(k_f h)_1}{(k_f h)_2} = 0.003\left[\frac{(t)_{b1}}{\lambda(t)_{b2}}\right]^2 + 0.0439\left[\frac{(t)_{b1}}{\lambda(t)_{b2}}\right] \tag{3.2.12}$$

3.3 Multi-Layer Infinite Reservoir with Wellbore Storage and no Skin

This section investigates the effect of wellbore storage upon the pressure and pressure derivative behavior of a constant surface flow rate well in an infinite naturally fractured reservoir. Under practical operating conditions, the initial production from a shut-in well originates from the volume of fluid stored in the wellbore. After wellbore storage effects have ended, the production response is equal to that of a well with no wellbore storage from time zero. Figure 3.3.1 illustrates the characteristics of pressure and pressure derivative response in an infinite-acting, naturally fractured reservoir with pseudosteady state interporosity flow using the developed two layer model, where $\omega_1=\omega_2=0.1$ and $\lambda_1=\lambda_2=10^{-5}$, and wellbore storage effect is considered.

As discussed above, the first typical regime observed on the log-log plot of pressure and pressure derivative versus time is wellbore storage effect. At early time, all the curves merge to a line of slope equal to unity, corresponding to pure wellbore storage effect. The equation of this straight line given by:

$$p_D = \frac{t_D}{C_D} \tag{3.3.1}$$

where, C_D is well storage and defined as:

$$C_D = \frac{0.8935\,C}{h\overline{\phi c_t} r_w^2} \tag{3.3.2}$$

Combining Equation 3.2.3 and Equation 3.3.2, yields:

$$\frac{t_D}{C_D} = 2.95\text{x}10^{-4}\,\frac{h\bar{k}}{\mu}\left(\frac{t}{C}\right) \tag{3.3.3}$$

To solve for the wellbore storage, substitute Equation 3.2.2 and Equation 3.3.3 into Equation 3.3.1:

$$C = \left(\frac{q_t B}{24}\right)\frac{t}{\Delta p} \tag{3.3.4}$$

where t and Δp are any convenient point on the unit slope line.

The dimensionless pressure derivative is actually a better way to analyze data and powerful for diagnosis. It starts out increasing, then towards the end of the wellbore storage distortion displays a classical bell-shape much more pronounced than that of the usual pressure curves. As for pressure, all the pressure derivative responses are identical at early time, and the curves merge on a single unit slope line. The equation of this line is:

$$\left(\frac{t_D}{C_D}\right)p'_D = \frac{t_D}{C_D} \tag{3.3.5}$$

where the dimensionless pressure derivative is:

$$p'_D = \left(\frac{26.856h\overline{\phi c_t}r_w^2}{q_t B}\right)\Delta p'_w \tag{3.3.6}$$

Then, the equation from the unit slope pressure derivative line can be expressed in real units as follows:

$$C = \left(\frac{q_t B}{24}\right)\frac{t}{(t * \Delta p'_w)} \tag{3.3.7}$$

The following expression can be obtained from the intersection point of the unit slope line with the infinite-acting radial flow line:

$$\left(\frac{t_{D_{USRi}}}{C_D}\right) = 0.5 \tag{3.3.8}$$

Then, the wellbore storage in real units becomes:

$$C = \frac{h\bar{k}\, t_{USRi}}{1695\mu} \tag{3.3.9}$$

As a direct observation of the developed type curves, when the late time period of infinite-acting radial flow is reached, the effect of flow capacity ratio is no longer present on the pressure derivative behaviors. As a result, flow capacity of each layer can be obtained from a peak (maximum) pressure derivative value during the transition between the two asymptotic regimes (unit slope and infinite-acting flow regimes). Relationships are developed by observing the peak pressure derivative value during this period for various values of dimensionless wellbore storage, C_D, as shown in Figures 3.3.2-6. These figures show that for the case of $\frac{(k_f h)_1}{(k_f h)_2} < 8$, the results are close to the results for an ideal single-layer case. Figures 3.3.7 and 3.3.8 illustrate the relationships of $\frac{(k_f h)_1}{(k_f h)_2}$ versus $\frac{(t * \Delta p'_w)_{max}}{(t * \Delta p'_w)_R}$. Taking the best fit of each curve gives the following empirical correlation:

$$\frac{(k_f h)_1}{(k_f h)_2} = Exp\left\{-\frac{1}{A}\left[\frac{(t * \Delta p'_w)_{max}}{(t * \Delta p'_w)_R} - B\right]\right\} \tag{3.3.10}$$

where

$$A = 0.15 \tag{3.3.11}$$

and

$$B = 0.3921\,\mathrm{Ln}(C_D) + 1.6649 \tag{3.3.12}$$

An alternative method to determine production capacity of each layer, $k_f h$, is possible from the total production capacity. Figures 3.3.10 and 3.3.11 show normalized correlations between total flow capacity ratio, $\frac{(k_f h)_1}{(\bar{k}h)}$, and pressure derivative ratio, $\frac{(t*\Delta p'_w)_{max}}{(t*\Delta p'_w)_R}$, for various values of wellbore storage.

3.4 Multi-Layer Infinite Reservoir with Wellbore Storage and Skin

To study the effect of wellbore storage and skin, the combination of parameters presented by Bourdet and Gringarten[14] has been used. New type-curves suitable for practical interpretation of two-layer systems have been constructed for various values of C_De^{2S} group. As a direct observation of the constructed type curves, the flow capacity of each layer can be obtained from a peak (maximum) pressure derivative value during the transition between the two asymptotic regimes (unit slope and infinite-acting flow regimes). Relationships are developed by observing the peak pressure derivative value during this period for various values of C_De^{2S} group, as shown in Figures 3.4.1-10. These figures show that for the case of $\frac{(k_f h)_1}{(k_f h)_2} < 8$, the results are close to the results for an ideal single-layer case. In these figures, almost all curves are coincident for the case of $\frac{(k_f h)_1}{(k_f h)_2} < 8$. For various values of C_De^{2S} group, the following empirical correlation of $\frac{(k_f h)_1}{(k_f h)_2}$ versus $\frac{(t*\Delta p'_w)_{max}}{(t*\Delta p'_w)_R}$ has been derived:

$$\frac{(k_f h)_1}{(k_f h)_2} = Exp\left\{-\frac{1}{D}\left[\frac{(t*\Delta p'_w)_{max}}{(t*\Delta p'_w)_R} - E\right]\right\} \tag{3.4.1}$$

where

$$D = 0.15 \tag{3.4.2}$$

and

$$E = 0.3945\,\mathrm{Ln}(C_D e^{2S}) + 1.6386 \tag{3.4.3}$$

Comparing Equation 3.3.17 with Equation 3.4.3 results in an important observation, which is that the peak points on pressure derivative curves are more affected by wellbore storage than by skin.

The $C_D e^{2S}$ group in Equation 3.4.3 can be estimated by type curve matching using the type curves which are presented in Figure 3.1.9, or by calculating wellbore storage from the early time unit slope line and skin from well testing using Equation 3.4.5. Appendix F shows an alternative way of calculating skin from drilling data.

The radial flow period is only influenced by the mechanical skin attributed to drilling and completion operations. Dividing the dimensionless pressure equation by the dimensionless pressure derivative equation results in an expression for skin. From early time:

$$S = 0.5\left[\frac{(\Delta p_w)_R}{(t * \Delta p'_w)_R} - \ln\left(\frac{\bar{k} t_R}{\phi c_t \mu r_w^2}\frac{1}{\omega}\right) + 7.43\right] \tag{3.4.4}$$

where t_R is any convenient time during the infinite acting radial flow line and $(\Delta p_w)_R$ is the value of (Δp_w) corresponding to t_R. Note that the calculated skin is an average value, because the average reservoir parameters are used. Similarly for the late time period, the average skin can be calculated by:

$$S = 0.5\left[\frac{(\Delta p_w)_R}{(t * \Delta p'_w)_R} - \ln\left(\frac{\bar{k}t_R}{\phi c_t \mu r_w^2}\right) + 7.43\right] \tag{3.4.5}$$

Skin factor of each layer can be determined from either Equation 3.4.4 or Equation 3.4.5 by substituting layer parameters instead of average parameters. Therefore, Equation 3.4.4 becomes:

$$S_i = 0.5\left[\frac{(\Delta p_w)_R}{(t * \Delta p'_w)_R} - \ln\left(\frac{k_{fi} t_R}{(\phi c_t)_{ti} \mu_i r_w^2}\frac{1}{\omega_i}\right) + 7.43\right] \tag{3.4.6}$$

where subscripts i refer to layer number, (i=1 or 2 in a two layer reservoir). Subsequently, Equation 3.4.5 becomes:

$$S_i = 0.5\left[\frac{(\Delta p_w)_R}{(t * \Delta p'_w)_R} - \ln\left(\frac{k_{fi} t_R}{(\phi c_t)_{ti} \mu_i r_w^2}\right) + 7.43\right] \tag{3.4.7}$$

As mentioned earlier, for simplification only a two-layer reservoir without cross-flow is considered. However, results provided in this study can be generalized to muli-layer systems. For example, in the case of three-layer reservoir:

$$(\bar{k}h) = (k_f h)_{Layer1} + (k_f h)_{Layer2} + (k_f h)_{Layer3} \tag{3.4.8}$$

$$(kh)_1 = (k_f h)_{Layer1} \tag{3.4.9}$$

and

$$(kh)_2 = (k_f h)_{Layer2} + (k_f h)_{Layer3} \tag{3.4.10}$$

3.5 Transition Period:

In modeling the pressure transient data from naturally fractured reservoirs, the dual porosity models which are commonly used in analyzing well tests from naturally fractured reservoirs is considered. The pseudo-steady state interporosity flow model as well as the transient state interporosity flow model are considered. Many studies[2,11,13,14,69,72-77] deal with the estimation of parameters determining the interporosity flow. These are largely based on the classical model of Warren and Root[2] where matrix blocks were idealized as identical rectangular blocks which flowed only into the fracture system. The fracture system was also idealized as an orthogonal set of regular fractures parallel to the principal permeability axes. Based on model, the semi-log plot of dimensionless pressure drop versus time gives straight lines at early and late times corresponding to the fracture system and total system respectively. As only the fracture system is conductive to fluid, these lines have identical slope. The transition between the two lines represents the interaction of the two parameters used to define the dual porosity system. The two key parameters derived by Warren and Root[2] to characterize naturally fractured reservoirs are: the dimensionless storage coefficient, ω, and the interporosity flow parameter, λ. The dimensionless storage coefficient provides an estimate of the magnitude and distribution of matrix and fracture storage. The interporosity flow parameter is a measure of the mass transfer rate from the matrix to the fractures.

In practical applications, the form of the transition between the initial and final system depends on whether the interporosity flow is described by pseudo-steady state or transient flow. Early techniques for interpreting pressure transient tests included conventional semi-log and log-log type curve methods used to determine the dimensionless storage coefficient, ω, and the interporosity flow parameter, λ. In 1995, Engler[63] developed the direct synthesis method for interpreting pressure transient tests in single-layer naturally fractured reservoirs for both pseudosteady state and transient matrix flow. He provided empirical correlations for estimating the dimensionless storage coefficient, ω, and the interporosity flow parameter, λ.

In this Section, the dimensionless storage coefficient, ω, and the interporosity flow parameter, λ, are investigated by observing the pressure and pressure derivative response from a multi-layer infinite-acting naturally fractured reservoir, i.e this section extends Engler's work. An extensive study of the developed type curves for pseudosteady state, transient matrix flow in a slab system and transient matrix flow in a sugar-cube system has been made.

Figure 3.5.1 compares the pressure and pressure derivative responses for the pseudosteady state, transient matrix flow in a slab system, and transient matrix flow in a sugar-cube system. An important observation obtained from these figures is that the pseudosteady state response produces a sharper image and therefore parameters are more easily identifiable. Figures 3.5.2 through 3.5.7 illustrate the effect of the dimensionless storage coefficient, ω, in both single and multiple layered infinite-acting, naturally fractured reservoirs with pseudosteady state interporosity flow and transient matrix flow. A higher value of the dimensionless storage coefficient, ω, will increase the transition dip.

Many attempts in this work to determine an equivalent single layer dimensionless storage coefficient, ω_i, from the response of a layered system have been made. The most important result from this study is that the pressure response alone does not contain sufficient information to determine the individual layer dimensionless storage coefficient, ω_i. This is due to the large number of parameters that needed to be estimated in such systems, i.e. multi-layer systems. Therefore, estimating the individual layer dimensionless storage coefficient, ω_i, from multi-layer naturally fractured reservoirs by the pressure response alone is often difficult if not impossible. This observation agrees with the studies[43,46,47,64] which have been made to determine an equivalent single layer system from the response of a layered system. The result from these studies is that the pressure response alone does not contain sufficient information to determine individual properties.

This study concluded that the dimensionless storage coefficient, ω, calculated here is analogous to that of a single-layer reservoir with the average properties of the layered system. As a direct consequence, the average value of the dimensionless storage coefficient, ω, for pseudosteady state, transient matrix flow in a slab system and transient matrix flow in a sugar-cube system can be estimated by several methods previously developed by Engler[63].

Figure 3.5.3 shows the effect of the storage coefficient on the pressure response in a two layer infinite-acting, naturally fractured reservoir with pseudosteady state interporosity flow. This figure also shows the transition period which occurs during the infinite-acting radial flow period illustrating the unit slope derivative line. The analytic equation for this late transition time is:

$$\ln(t_D * p'_{wD})_{US} = \ln\left(\frac{\lambda(t_D)_{US}}{2}\right) \tag{3.5.1}$$

where the subscript US stands for unit slope derivative line. The late transition period unit slope line is a unique method of determining interporosity flow parameter, λ. The intersection point between the unit slope line with the infinite-acting line is:

$$\lambda = \frac{(\phi c_t)_n \mu r_w^2}{0.0002637 k_{fi} t_{USRi}} \tag{3.5.2}$$

where the subscript USRi stands for the intersection point between the unit slope line with the infinite-acting line. k_{fi} is the fracture permeability of layer i and $(\phi c_t)_n$ is the layer storage capacity. The above equation is independent of the dimensionless storage coefficient, ω.

Figure 3.5.5 shows the effect of the storage coefficient on the pressure response in a two-layer infinite-acting, naturally fractured reservoir with transient matrix flow in a slab system. A straight line of $(t_D * p'_D) = 0.25$ is observed during the transition period. An alternative method of calculating total flow capacity of the well can be achieved by observing this characteristic line. Substituting for the dimensionless terms yields the following expression:

$$\bar{k}h = \frac{35.3 q_t B \mu}{(t * \Delta p'_w)_{L1}} \tag{3.2.3}$$

Figures 3.5.8 through 3.5.13 illustrate the effect of the interporosity flow parameter, λ, on the pressure derivative response in both single and multiple layered infinite-acting, naturally fractured reservoirs with pseudosteady state interporosity flow and transient matrix flow. In summary, the procedures in Engler[63] are valid for estimating the individual layer interporosity flow parameter, λ_i, of multi-layer naturally fractured reservoirs. This parameter can be calculated using correlations developed by Engler[63] with a minor exception. The basic procedure is the same but individual layer parameters must be used in the correlations instead of average reservoir parameters.

Figures 3.1.10 and 3.5.14 through 3.5.16 yield a very important observation. They show that for $\frac{\lambda_1}{\lambda_2} > 100$, the derivative curve has two depressions. A higher value of the interporosity flow parameter, λ, corresponds to a higher ability of the matrix to feed the fractures and therefore results in an earlier transition. Hence, the first depression is caused by the layer which has a higher value of $\frac{k_m}{k_f}$ ratio, while the second is caused by the layer which has a lower value of $\frac{k_m}{k_f}$ ratio, where the subscripts m and f refer to matrix and fracture respectively. As a direct consequence, individual values of λ and ω can be estimated. The first depression gives values of λ and ω for one layer, and the second depression gives values of λ and ω for the other layer. Care must be taken here to avoid misinterpretation of the test data with the pressure distortion caused by phase segregation. A complication arises from the similarity between the effect of the phase segregation and transition flow of multi-layer fractured reservoirs on the derivative curve. Olarewaju and Lee[79] indicated that phase segregation causes a pressure hump which appears in the pressure derivative curve as a depression similar to the transition flow of layer reservoir with crossflow. Wellbore phase segregation occurs in a well that is shut in with gas and liquid flowing simultaneously in the tubing.

Figures 3.5.14 through 3.5.17 illustrate the characteristic pressure and pressure derivative response in a two-layer infinite-acting, naturally fractured reservoir with pseudosteady state interporosity flow taking in consideration the effect of wellbore storage. These Figures show that wellbore storage can be dominate the early time pressure behavior, hence masking the fracture flow straight line and even the transition region.

Engler[63] extended his work to include the effect of wellbore storage. Alternative methods to determine λ and ω have been presented. The wellbore storage constant, skin factor, and interporosity flow parameter must be known, in addition to the minimum to infinite-acting radial flow pressure derivative ratio, to provide a means of determining ω. It is evident from Figures 3.5.14-17, the procedures described by Engler[63] are valid for a multi-layer fractured reservoir.

All in all, this Section shows that the shape of the transition period depends on the assumed matrix flow geometry. One aspect in which studies differ is the way they model the flow between the matrix and fractures in a double porosity reservoir. Matrix flow has been modeled mainly by two methods: pseudosteady state matrix flow and transient matrix flow. However, this study presents both models. One of the main contributions in this work is the derivation of $f(s)_i$ functions to simulate: (1) the transient matrix flow of a sugar-cube geometry; (2) the pseudosteady state matrix flow; and (3) the transient matrix flow of a slab geometry.

The solutions developed in this study are efficient. The pressure derivative was shown to be a useful tool for diagnosing, understanding, and interpreting layered reservoir behavior. High resolution pressure gauges can produce data of quality suitable for the analysis.

3.6 Pressure Derivative and Flow Rate Behavior in Infinite-Acting Naturally Fractured Reservoir

In many instances, usually due to economic reasons, wells are completed simultaneously in two or more layers of a reservoir. The major drawback of the multiple completion is that the difficulty of accurately applying reservoir engineering principles to predict the recovery and future performance under primary and enhanced recovery operations of each of the layers. In order to improve the prediction of reservoir behavior, it is necessary to determine the properties of the various layers.

This work presents a new method which describes pressure tests in naturally fractured systems. The new conventional and simple method of analysis is based on observations by several authors[43,46,47,64]. This method is useful for the analysis of simultaneously measured down-hole sand-face rate and pressure. Current methods of analysis of multi-rate tests, in naturally fractured reservoirs, use both conventional and rate-normalized type curve matching. None of the current methods uses a direct approach to analyze the multi-layer double porosity reservoirs. Thus, this section presents an analysis procedure for commingled layered systems that is completely analogous to that used for single layered systems. This new method uses Tiab's direct synthesis technique which is developed from an understanding of the various flow periods described in the previous sections. Analyze infinite acting pressure and flow rate data to determine individual layer properties, such as permeability, dimensionless storage coefficient, ω, interporosity flow parameter, λ, and skin values. An application will be used to demonstrate the technique presented in this chapter.

It is important to note that the shapes of either pressure or pressure derivative curves for the layered reservoir are similar to those of a single layer reservoir. Thus the shape of the well response will not be useful in identifying the layered nature of the formation. Due to the diversity of existing idealized naturally fractured reservoir models, e.g. double porosity models with pseudo-steady or transient interporosity flow, and the large number of parameters needed to be estimated in these models, the analysis of well test data from naturally fractured reservoirs by the well-known conventional graphical techniques is often difficult if not impossible.

Many attempts[43,46,47,64] to determine an equivalent single layer system from the response of a layered system have been made. The most important result from these studies is that the pressure response alone does not contain sufficient information to determine individual properties. Therefore, an alternative procedure has been suggested by different authors[43,46,47]. They show that the rate-normalized pressure of $(\Delta P)/q_{ri}$ from the exact Laplace space solutions gives an equivalent single layer pressure behavior. The consequence of these observations is that during the infinite-acting period, individual properties can be determined from a semi-log or log-log plot of $(\Delta P)/(\Delta q_{ri})$ versus time, where the relative flow rate of each layer is the ratio of the flow rate from the layer of interest to the surface flow rate:

$$q_{ri} = \frac{q_i}{q_t} \tag{3.6.1}$$

Economides[66] stated that it is possible to isolate the properties of a single layer if the flow rate from the layer is known. He confirmed that the influence function gives an equivalent single layer pressure behavior. Economides said that "the simplest form of the influence function is dividing the pressure difference by the corresponding flow rate."[66]

This work addresses the problem of interpretation of layered naturally fractured reservoirs in commingled wells. The approach presented here will allow the reservoir engineers to rigorously interpret the multi-layer data using the existing single-layer analytic models, rather that relying on numerical simulation. This approach will save a great deal of computer time.

The major conclusion from the above discussion is that the log-log plot of pressure change and the derivative group divided by the relative rate change (Δq_{ri}) versus time is sufficient to define the various flow periods. Therefore, it is possible to isolate the properties of a single layer in a multi-layer naturally fractured reservoir. This is important to the overall analysis procedure which is discussed below.

The dimensionless variables for multi-layer naturally fractured reservoir case has been defined and presented in Appendix B. And, Engler[63] developed direct synthesis method for interpreting pressure transient tests in single-layer naturally fractured reservoirs for both pseudosteady state and transient matrix flow. As a conclusion, a log-log plot of $(\Delta P_w)/(\Delta q_{ri})$ and $(t^*\Delta P'_w)/(\Delta q_{ri})$ versus time can be used in developing the analysis procedure that combines the defined dimensionless variables and Engler's work. Subsequently, it is possible to estimate the individual properties of a single layer in a multi-layer naturally fractured reservoir. For example, Equation 2.29 is an empirical correlation which has been presented by Engler to provide a method of estimating the interporosity flow parameter, λ. Based on the procedure described previously, Equation 2.29 becomes:

$$\lambda_i = \frac{42.5 h_i (\phi c_t)_{fi} r_w^2}{q_t B} \left(\frac{\left(\frac{t * \Delta p'_w}{\Delta q_{ri}} \right)_{min}}{t_{min}} \right) \quad (3.6.2)$$

Equation 3.2.5 presented in this study can be used to calculate flow capacity of each layer:

$$k_{fi} = \frac{70.6 q_t B \mu_i}{h_i \left(t * \Delta p'_w / \Delta q_{ri} \right)_{R1}} \quad (3.6.3)$$

3.7 Pressure Derivative and Flow Rate Behavior in Bounded Naturally Fractured Reservoirs

This Section extends the work above to a closed, bounded, and circular naturally fractured reservoir. As a consequence, a pressure response goes through a transitional period and eventually reaches the late time pseudo-steady state flow regime, as shown in Figure 3.7.1. This flow period exhibits a unit slope straight line in the pressure derivative. The corresponding equation of this period is:

$$(t_{DA} * p'_{wD}) = 2\pi t_{DA} \tag{3.7.1}$$

where,

$$t_{DA} = \frac{t_D}{\pi r_{ed}^2} \tag{3.7.2}$$

and

$$r_{edi} = \frac{r_{ei}}{r_w} \tag{3.7.3}$$

The late time pseudo-steady state flow period can give an estimate of the shape and size of each layer. A log-log plot of pressure and pressure derivative versus time can result in an expression to calculate the drainage area. Substituting for the dimensionless variable defined in Appendix B, yields an appropriate equation to determine the drainage area:

$$A_i = \frac{q_t B}{4.27 h_i (\phi c_t)_{ti}} \left(\frac{t}{(t * \Delta p'_w)} \right)_{PSS1} \tag{3.7.4}$$

where PSS1 is the pseudo-steady state line at t=1 hr.

However, a log-log plot of $(\Delta P_w)/(\Delta q_{ri})$ and $(t^*\Delta P'_w)/(\Delta q_{ri})$ versus time yields:

$$A_i = \frac{q_t B}{4.27 h_t (\phi c_t)_n} \left(\frac{t}{\left(t^* \Delta p'_w / \Delta q_n \right)} \right)_{PSSi} \tag{3.7.5}$$

The intersection point of the pseudo-steady state flow period line with the infinite-acting radial flow line in the pressure derivative graph gives the following equation:

$$(t_{DA})_{RPSSi} = \frac{1}{4\pi} \tag{3.7.6}$$

where the subscripts RPSS and i refer to radial-pseudo-steady-state and intersection respectively. Then, by substituting the real units in the above equation yields:

$$A_i = \frac{k_{fi} t_{RPSSi}}{301.77(\phi c_t)_{ti} \mu_i} \tag{3.7.7}$$

where k_{fi} can be estimated as discussed in the previous sections.

Engler[63] extended his work to include the bounded naturally fractured reservoirs. He presented a correlation which couples the start of the pseudo-steady state flow line with the interporosity flow parameter, λ, and the drainage radius, r_{ed}. Figure 3.7.2 can be used to determine either λ_i or r_{edi} of layer i, if the other one is known.

Based on Engler's work, an important conclusion can be made that for $(\lambda\, r_{ed}^2)>500$, the beginning of the pseudo-steady state is approximately 0.134. Then, the dimensionless time can be expressed as:

$$(t_{DA})_{bPSS} = \frac{0.0002637 k_{fi} t_{bPSS}}{(\phi c_t)_{ti} \mu_i A_i} = 0.134 \tag{3.7.8}$$

where the subscript bPSS refers to the beginning of the pseudo-steady state flow period. The above equation can be rearranged to estimate the distance of a circular boundary for each layer:

$$r_{ei} = \left[\frac{0.0006264 k_{fi} t_{bPSS}}{(\phi c_t)_{ti} \mu_i}\right]^{0.5} \tag{3.7.9}$$

3.8 Procedures

The following step-by-step procedures will demonstrate the applicability of Tiab's Direct Synthesis Technique.

Case 1: Multi-Layer Infinite Reservoir without Wellbore Storage and Skin

Step 1: Construct a plot of Δp and $(t^*\Delta p_w')$ versus time on a log-log graph and identify the various characteristic points and lines.

Step 2: Identify either the horizontal, early time, or late time infinite-acting radial flow line. Calculate the total flow capacity of the reservoir, $\bar{kh}$, using Equation 3.2.5.

Step 3: Determine ω and λ as outlined in section 3.1 of Reference 63 for pressure response with no wellbore storage.

Step 4: Calculate $\left[\frac{(t)_{b1}}{\lambda(t)_{min}}\right]$ and $\left[\frac{(t)_{b1}}{\lambda(t)_{b2}}\right]$ ratios.

Step 5: Determine the ratio $\frac{(k_f h)_1}{(k_f h)_2}$ using either Equation 3.2.6 or Equation 3.2.12.

Step 6: Calculate the ratio $\frac{(k_f h)_1}{(\bar{k}h)}$ using Equation 3.2.9.

Step 7: Calculate the flow capacity ratio of Layer 1 using Equation 3.2.7.

Step 8: Calculate the flow capacity ratio of Layer 2 using Equation 3.2.11.

Case 2: Multi-Layer Infinite Reservoir with Wellbore Storage and no Skin

Step 1: Construct a plot of Δp and $(t^*\Delta p_w')$ versus time on a log-log graph and identify the various characteristic points and lines.

Step 2: Identify either the horizontal, early time, or late time infinite-acting radial flow line. Calculate the total flow capacity of the reservoir, $\bar{k}h$, using Equation 3.2.5.

Step 3: Draw the early time unit slope pressure and pressure derivative lines indicative of pure wellbore storage. Calculate the wellbore storage constant from either Equation 3.3.4 or 3.3.7. Identify the intersection point between the unit slope line and infinite-acting radial flow line. Determine or verify wellbore storage constant or the total flow capacity using this point with Equation 3.3.9.

Step 4: Determine ω and λ as outlined in Reference 63.

Step 5: Identify the peak value on the pressure derivative curve. Calculate the ratio $\frac{(t^*\Delta p_w')_{max}}{(t^*\Delta p_w')_R}$.

Step 6: Determine the ratio $\frac{(k_f h)_1}{(k_f h)_2}$ using Equation 3.3.15.

Step 7: Calculate the ratio $\frac{(k_f h)_1}{(\bar{k}h)}$ using Equation 3.2.9.

Step 8: Calculate the flow capacity ratio of Layer 1 using Equation 3.2.7.

Step 9: Calculate the flow capacity ratio of Layer 2 using Equation 3.2.11.

Case 3: Multi-Layer Infinite Reservoir with Wellbore Storage and Skin

Step 1: Construct a plot of Δp and $(t^*\Delta p_w')$ versus time on a log-log graph and identify the various characteristic points and lines.

Step 2: Identify either the horizontal, early time, or late time infinite-acting radial flow line. Calculate the total flow capacity of the reservoir, $\bar{k}h$, using Equation 3.2.5.

Step 3: Draw the early time unit slope pressure and pressure derivative lines indicative of pure wellbore storage. Calculate the wellbore storage constant from either Equation 3.3.4 or 3.3.7. Identify the intersection point between the unit slope line and infinite-acting radial flow line. Determine or verify wellbore storage constant or the total flow capacity using this point with Equation 3.3.9.

Step 4: Determine ω and λ as outlined in Reference 63.

Step 5: Select a Δp and $(t^*\Delta p')$ at a convenient time during the late time, infinite-acting radial flow period. Substitute these values in Equation 3.4.10 and calculate the skin factor.

Step 6: Estimate the C_De^{2S} group using the calculated values of wellbore storage, C_D, and skin, S. Use the developed type curves, for the case of two-layer naturally fractured reservoirs, which are presented in Figure 3.1.9 to match the data and verify the value of C_De^{2S} group.

Step 7: Substitute the value of C_De^{2S} in Equation 3.4.8 and determine the constant E.

Step 8: Identify the peak value on the pressure derivative curve. Calculate the ratio $\frac{(t*\Delta p'_w)_{max}}{(t*\Delta p'_w)_R}$.

Step 9: Determine the ratio $\frac{(k_f h)_1}{(k_f h)_2}$ using Equation 3.4.6.

Step 10: Calculate the ratio $\frac{(k_f h)_1}{(\bar{k}h)}$ using Equation 3.2.9.

Step 11: Calculate the flow capacity ratio of Layer 1 using Equation 3.2.7.

Step 12: Calculate the flow capacity ratio of Layer 2 using Equation 3.2.11.

Step 13: Calculate the skin factor of each layer using Equation 3.4.12.

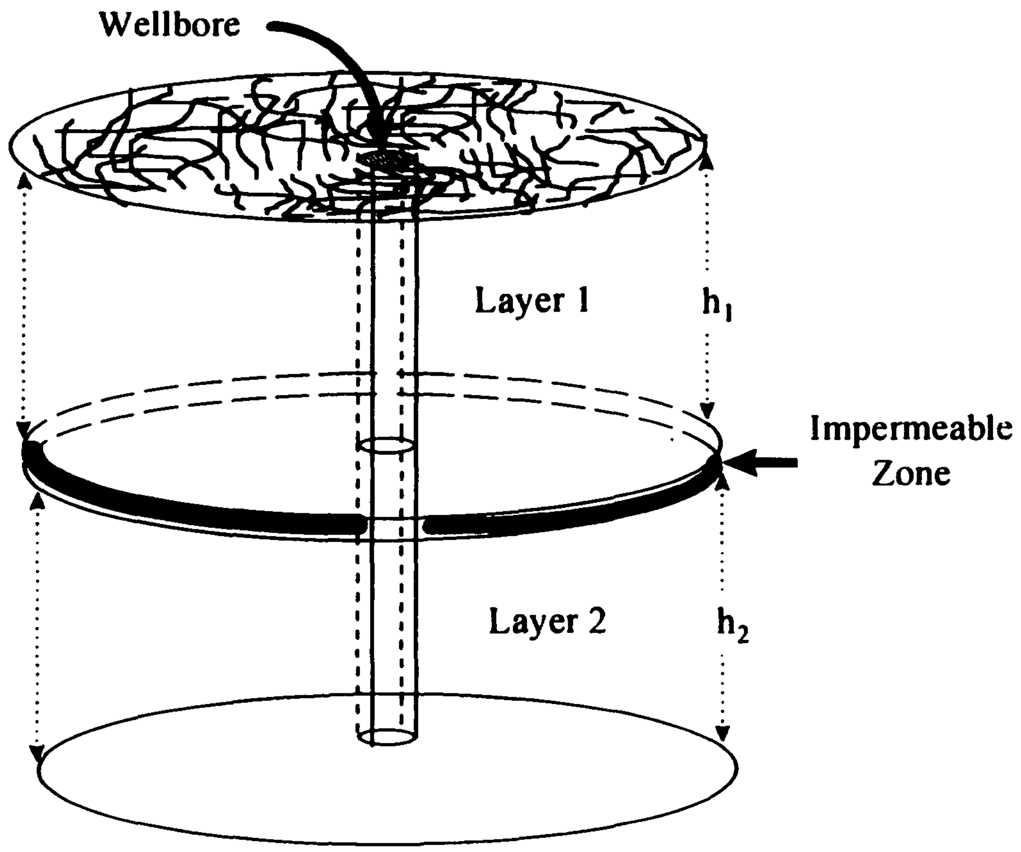

Figure 3.1.1 Two-Layer double porosity Reservoir Model.

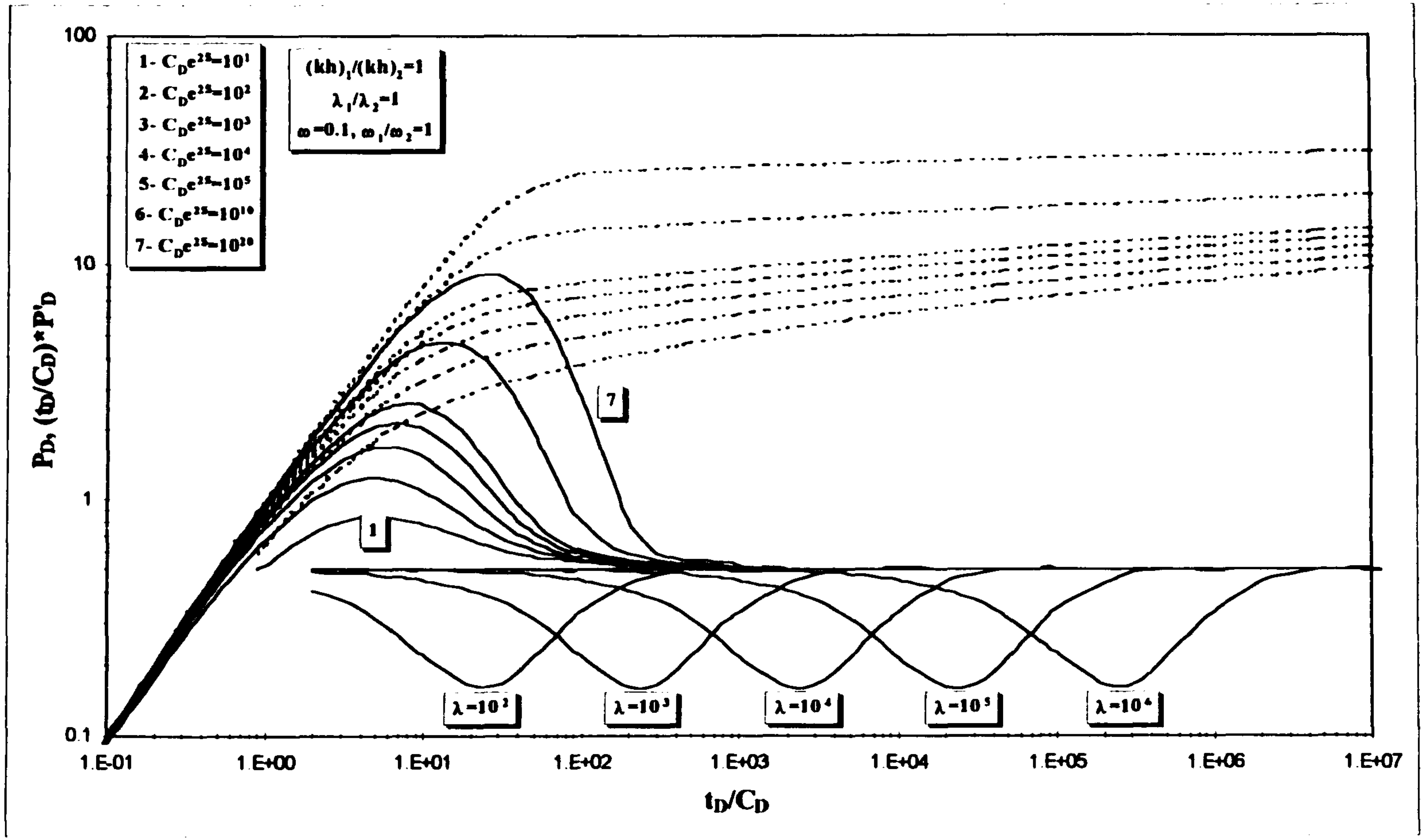

Figure 3.1.2 Multi-layer model response against the response of an equivalent single-layer model.

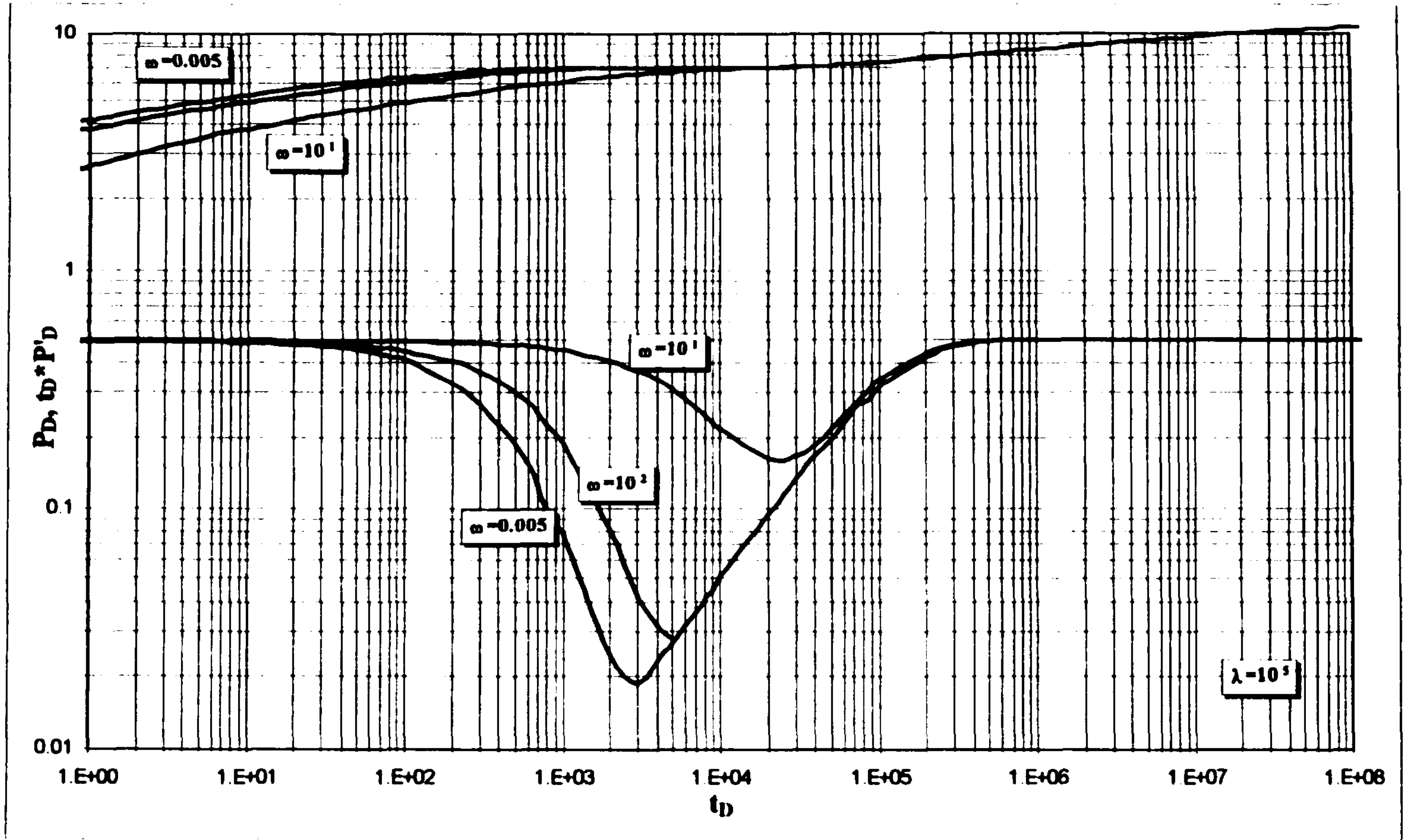

Figure 3.1.3 Effect of storage coefficient on the pressure response in a single-layer infinite-acting, naturally fractured reservoir with pseudosteady state interporosity flow.

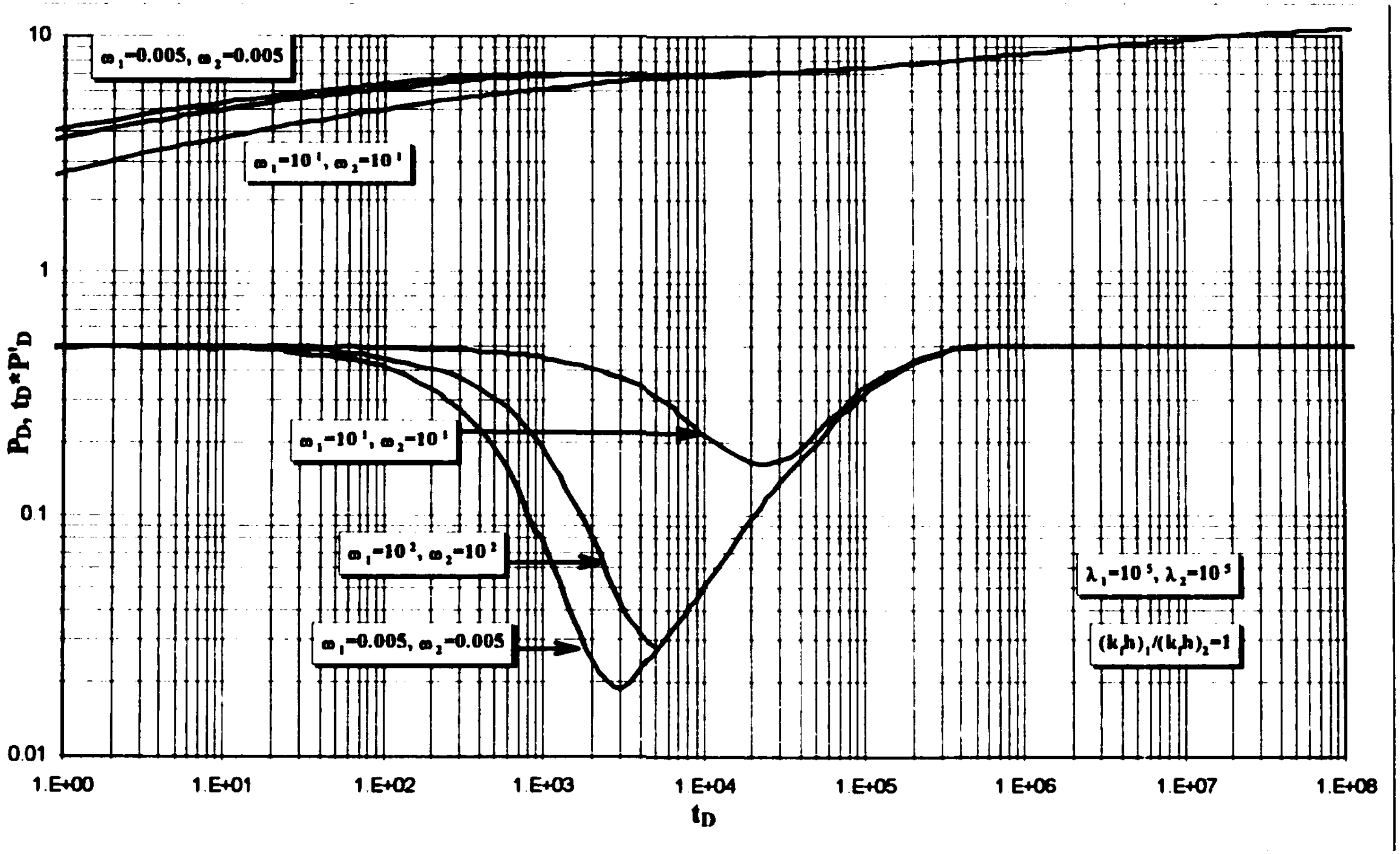

Figure 3.1.4 Effect of storage coefficient on the pressure response in a two-layer infinite-acting, naturally fractured reservoir with pseudosteady state interporosity flow.

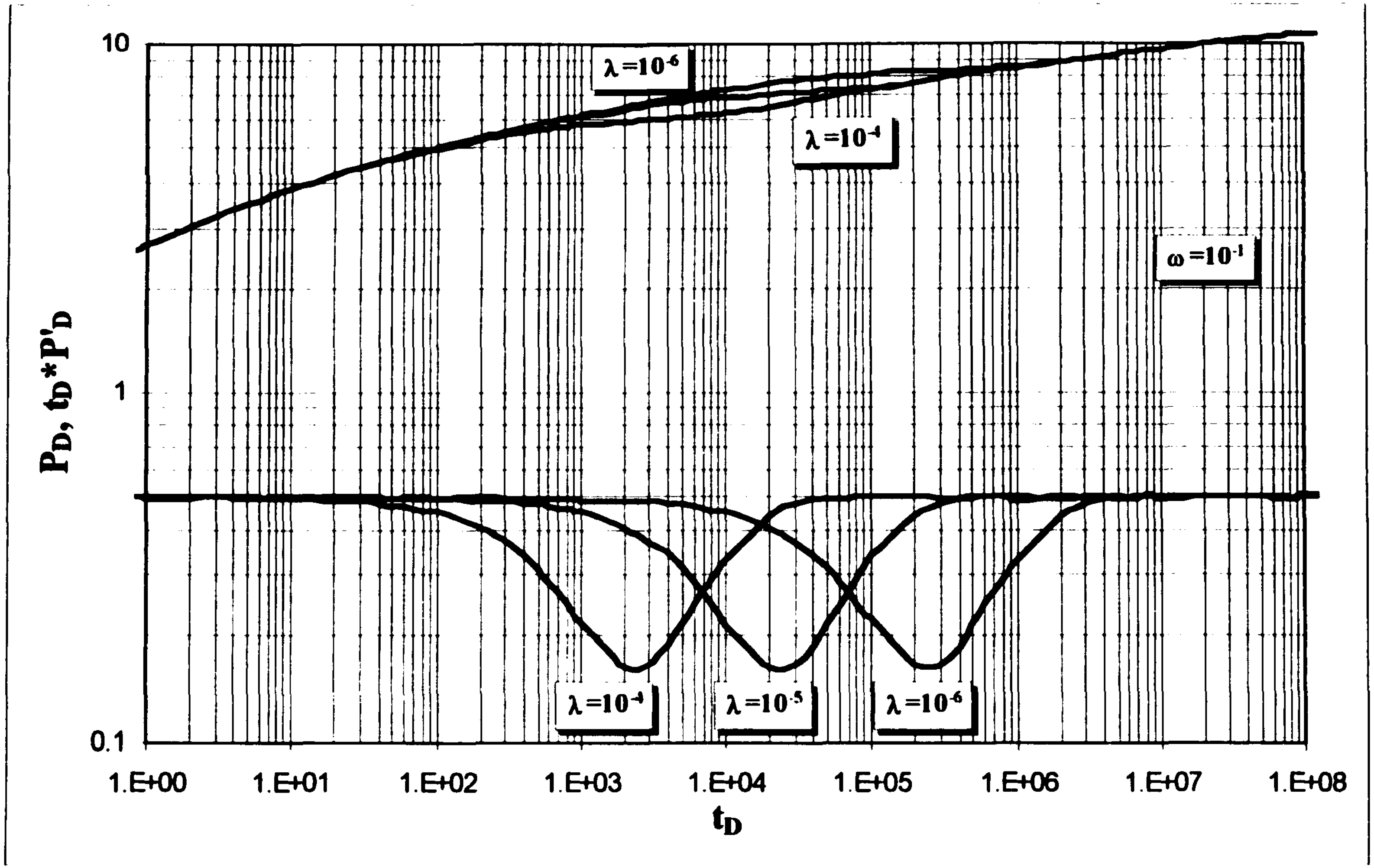

Figure 3.1.5 Effect of interporosity flow parameter on the pressure response in a single-layer infinite-acting, naturally fractured reservoir with pseudosteady state interporosity flow.

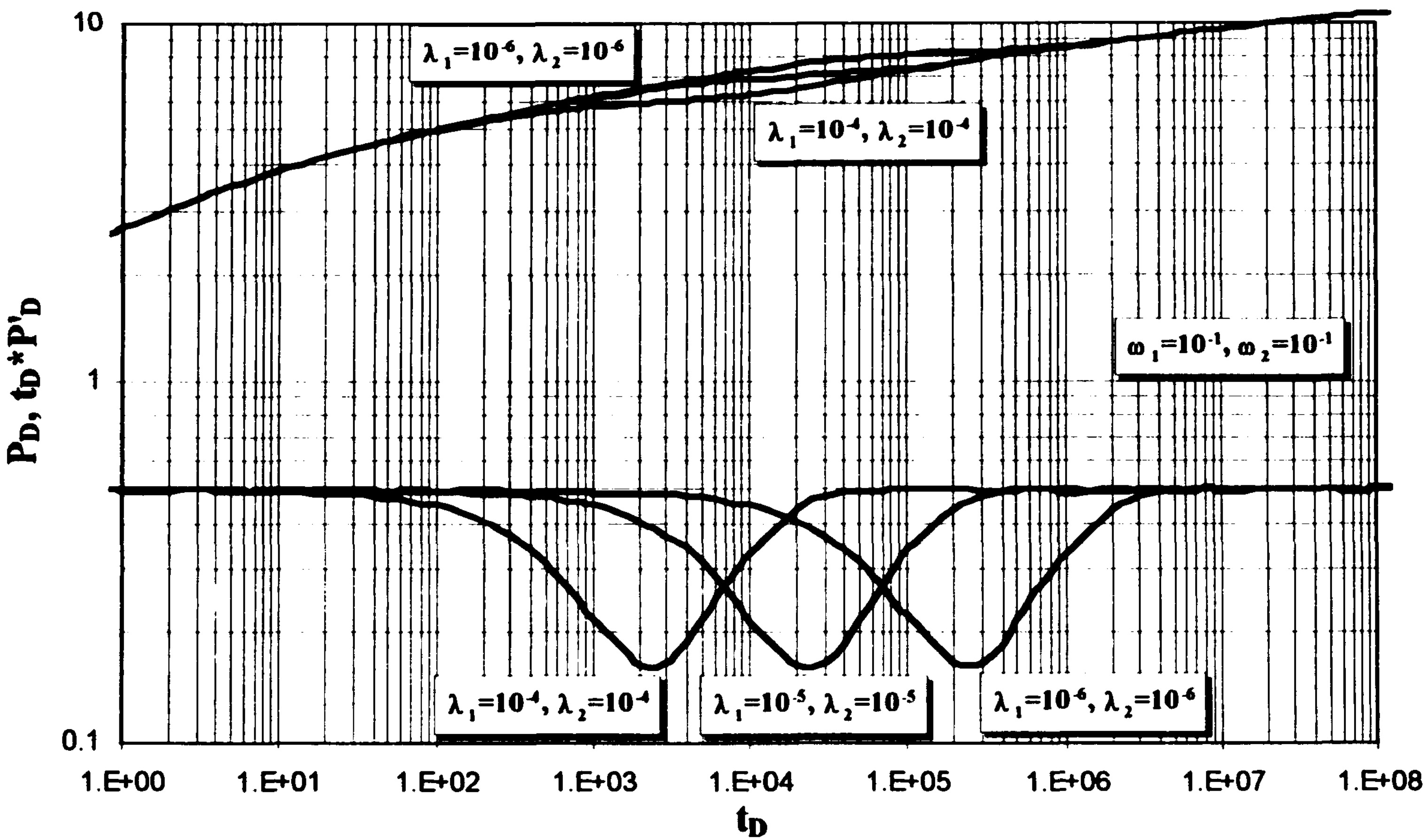

Figure 3.1.6 Effect of interporosity flow parameter on the pressure response in a two-layer infinite-acting, naturally fractured reservoir with pseudosteady state interporosity flow.

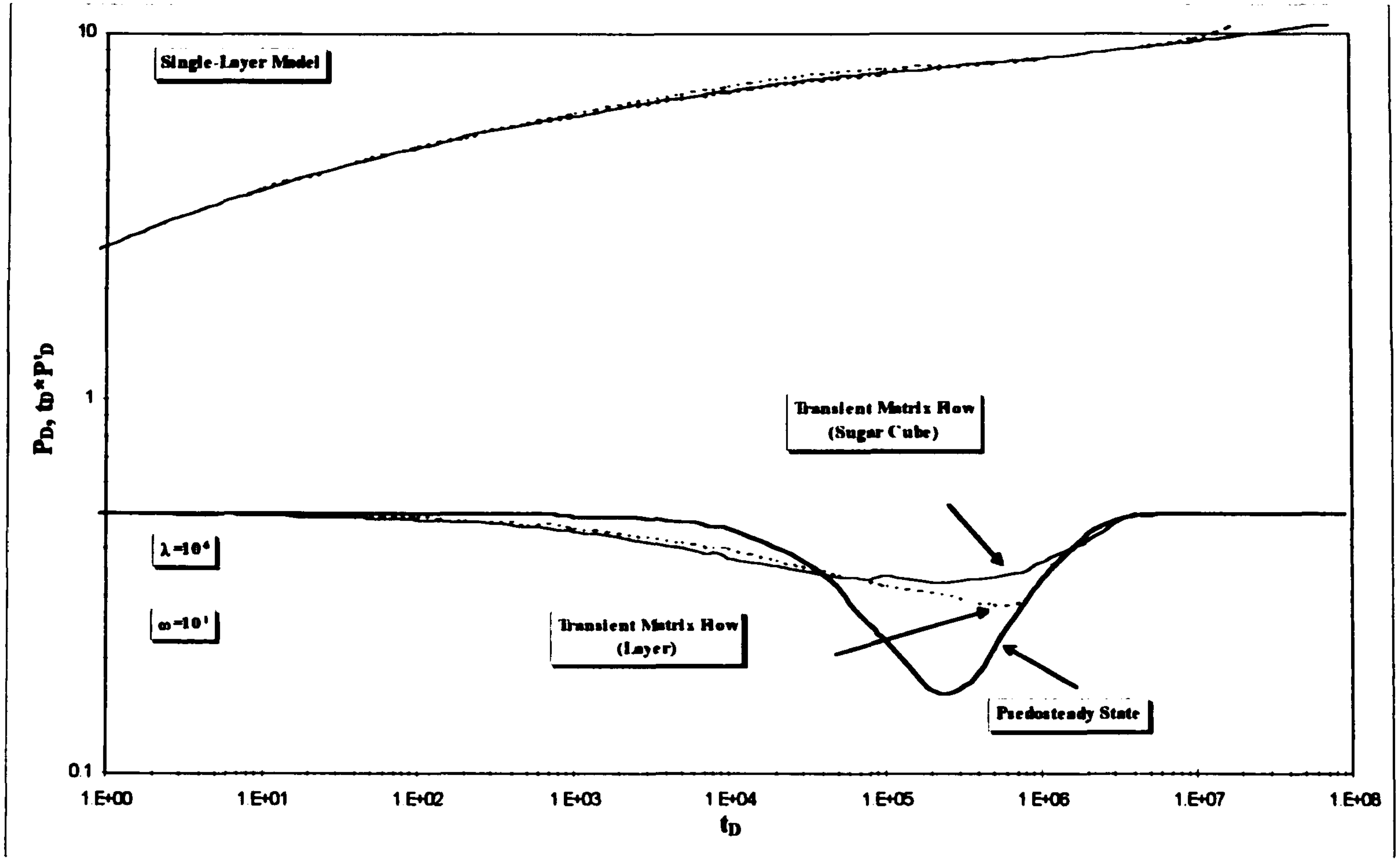

Figure 3.1.7 Comparison of pressure response for various flow regimes and flow geometries in a single-layer infinite-acting, naturally fractured reservoir.

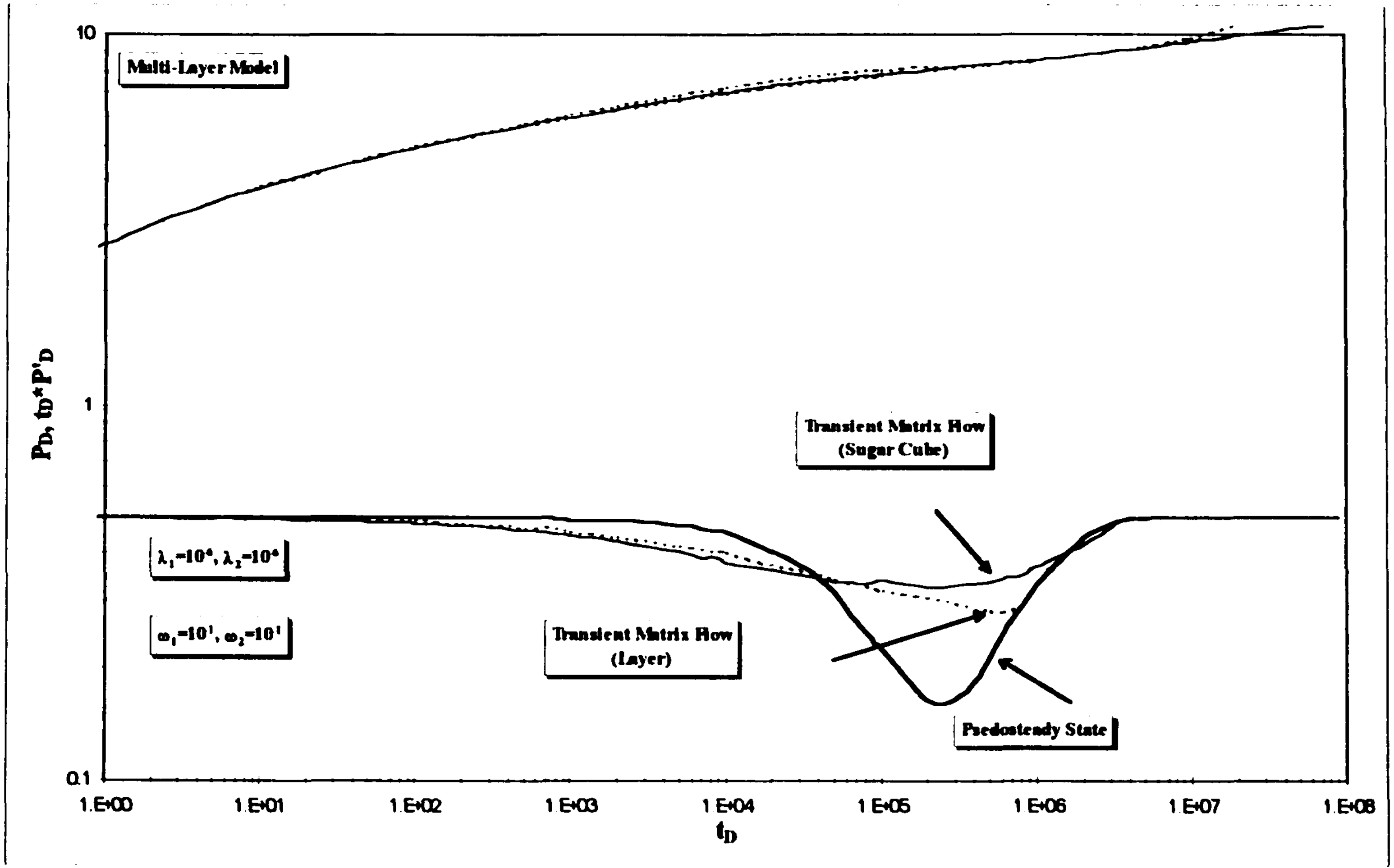

Figure 3.1.8 Comparison of pressure response for various flow regimes and flow geometries in a two-layer infinite-acting, naturally fractured reservoir.

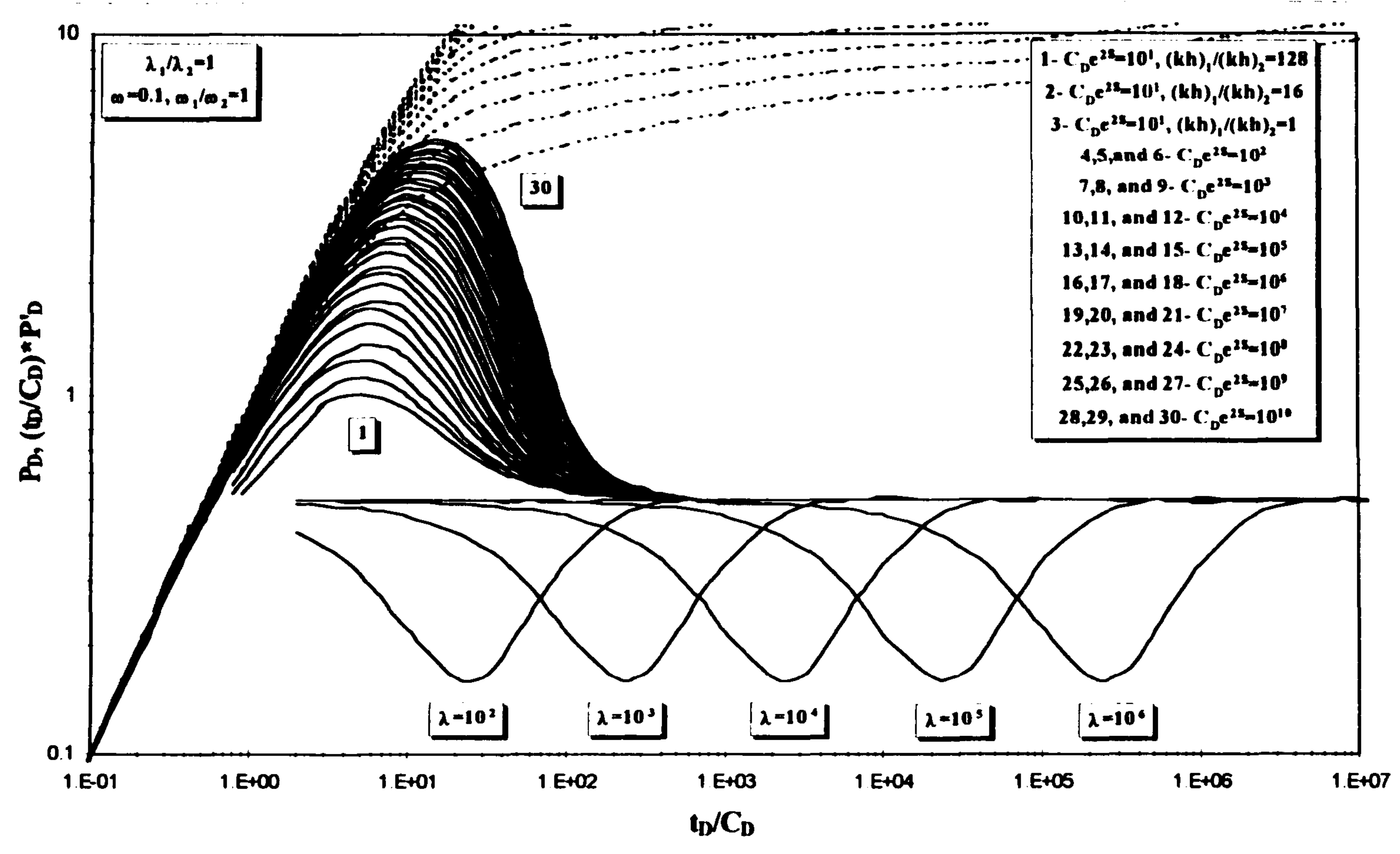

Figure 3.1.9 Pressure and pressure derivative type curves in a two-layer infinite-acting, naturally fractured reservoir with pseudosteady state interporosity flow.

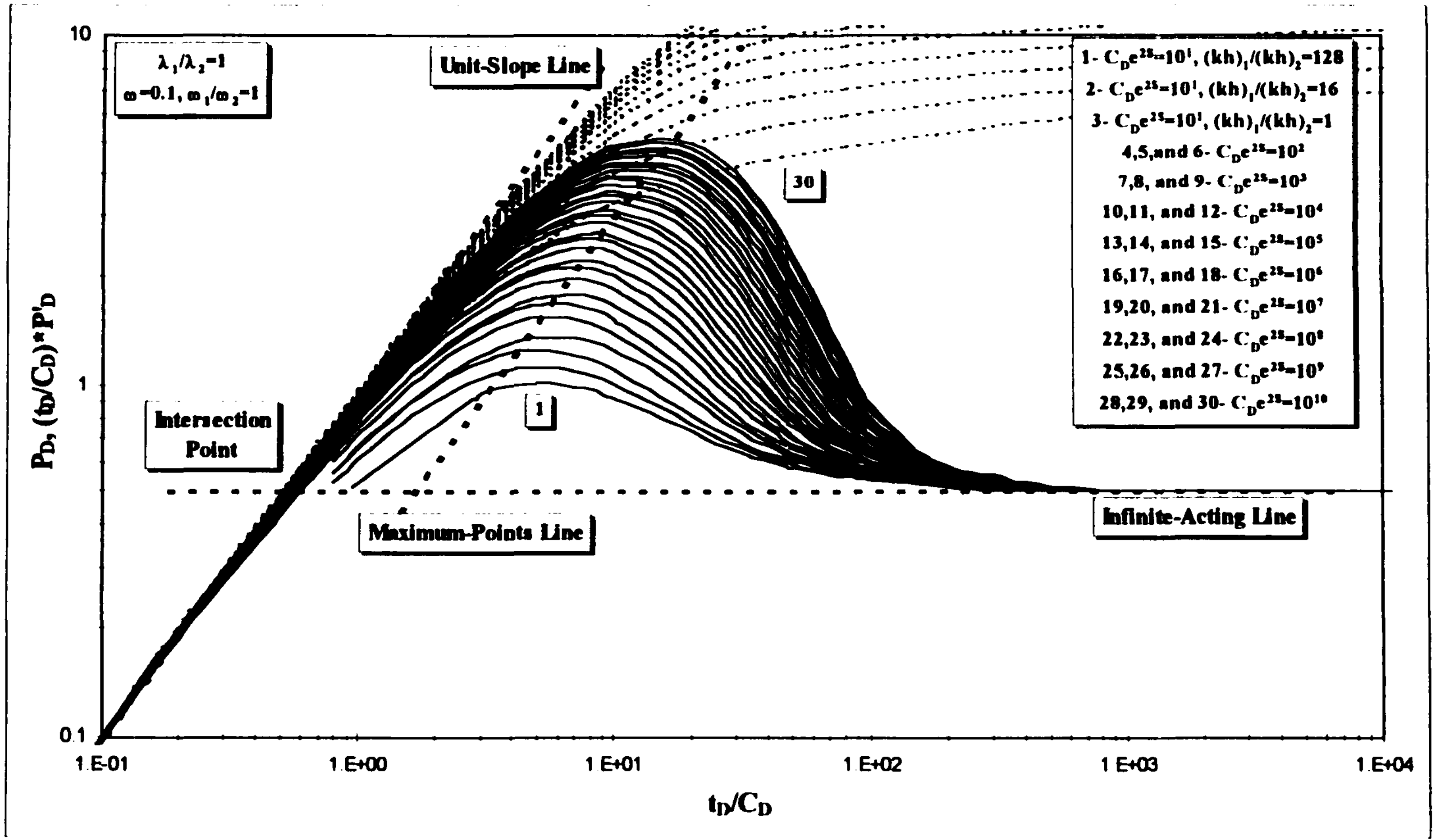

Figure 3.1.10 Characteristics of pressure and pressure derivative type curves in a two-layer infinite-acting, naturally fractured reservoir.

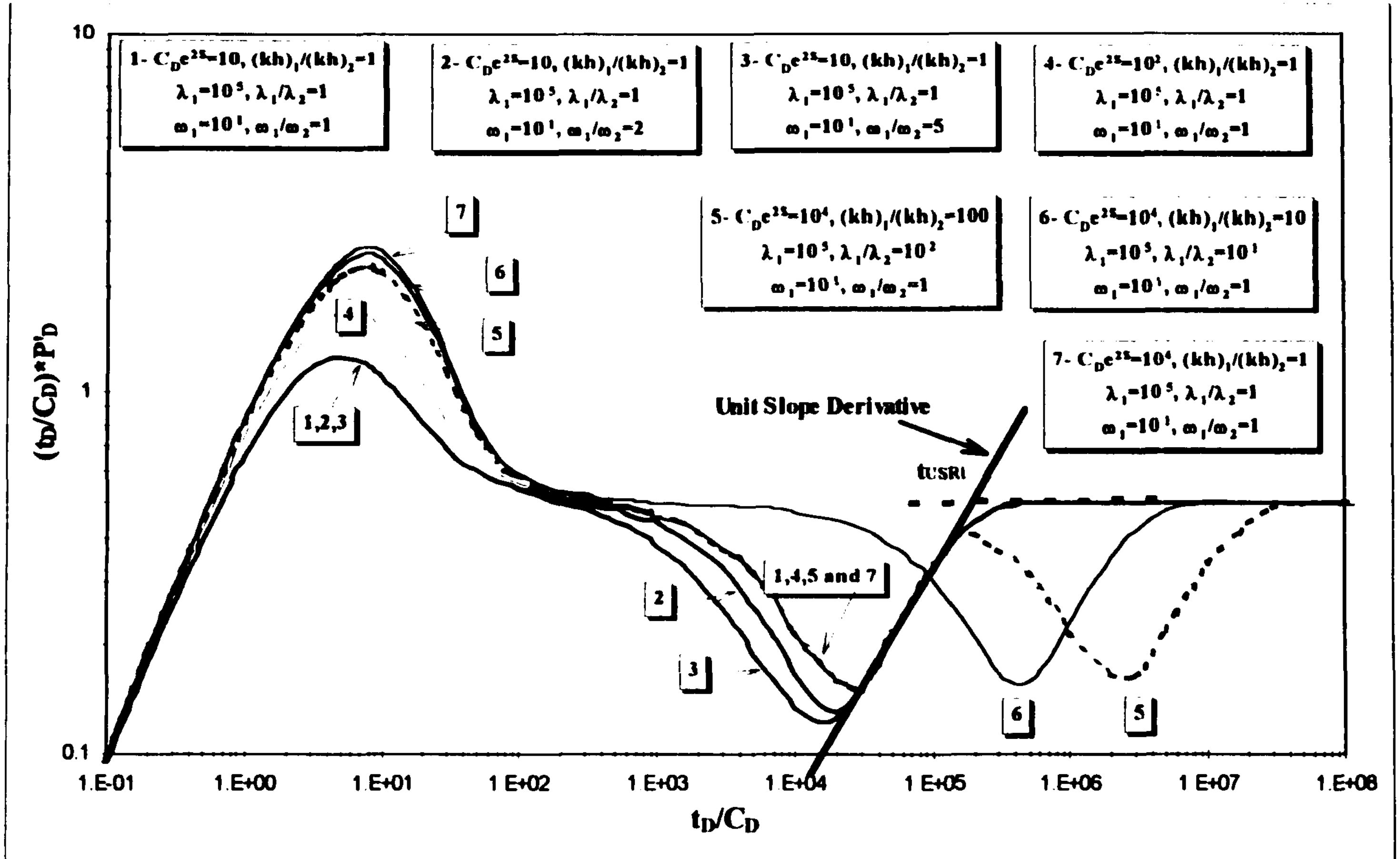

Figure 3.1.11 Characteristics of pressure derivative response in a two-layer infinite-acting, naturally fractured reservoir with pseudosteady state interporosity flow.

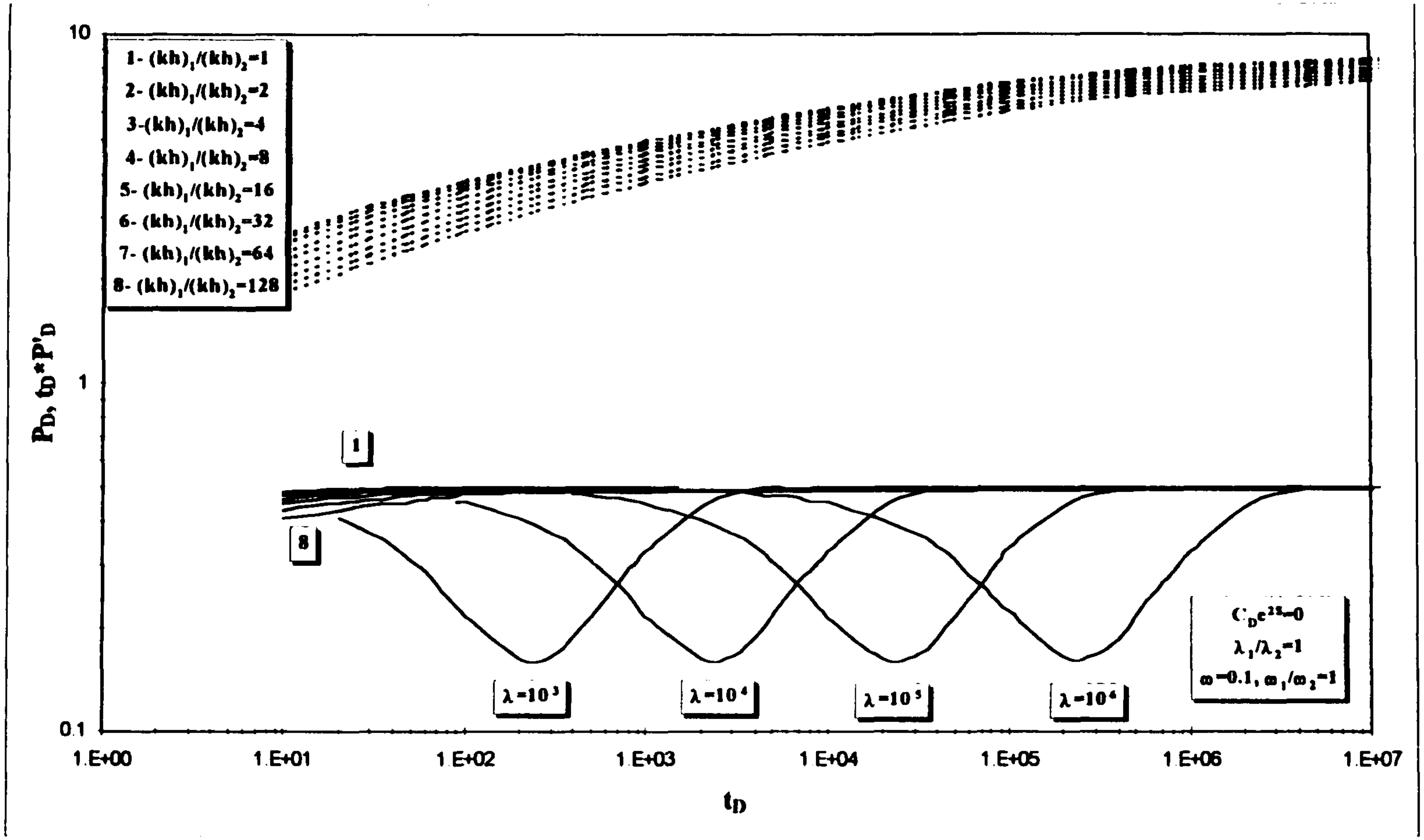

Figure 3.2.1 Pressure derivative response in a two-layer infinite-acting, naturally fractured reservoir with pseudosteady state interporosity flow. Both wellbore storage and skin are ignored.

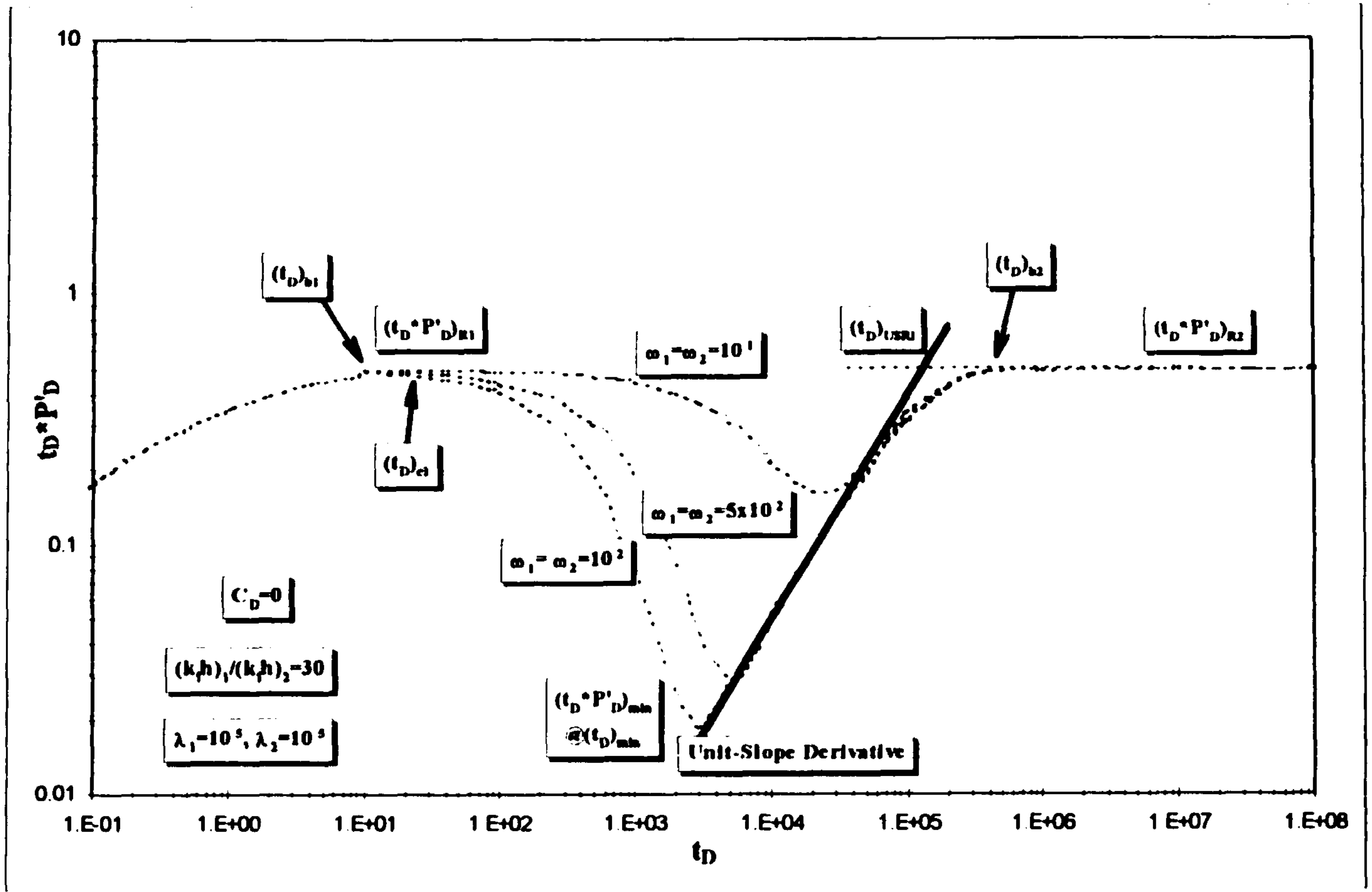

Figure 3.2.2 Characteristic lines and points of pressure derivative in a two-layer infinite-acting, naturally fractured reservoir with pseudosteady state interporosity flow, for $\frac{(k_fh)_1}{(k_fh)_2} = 30$

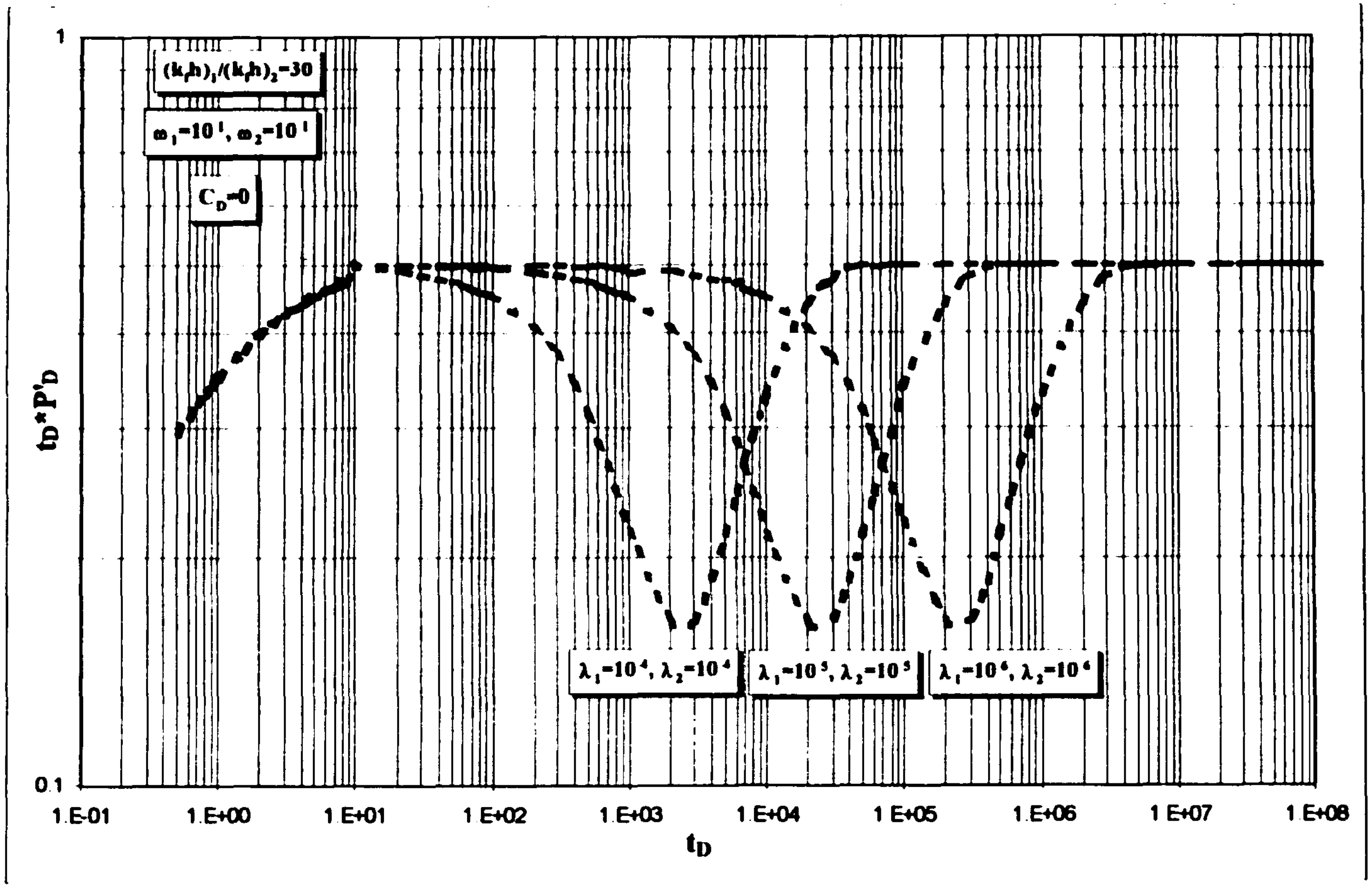

Figure 3.2.3 Effect of interporosity flow parameter on the pressure derivative response in a two-layer infinite-acting, naturally fractured reservoir with pseudosteady state interporosity flow, for $\frac{(k_f h)_1}{(k_f h)_2} = 30$.

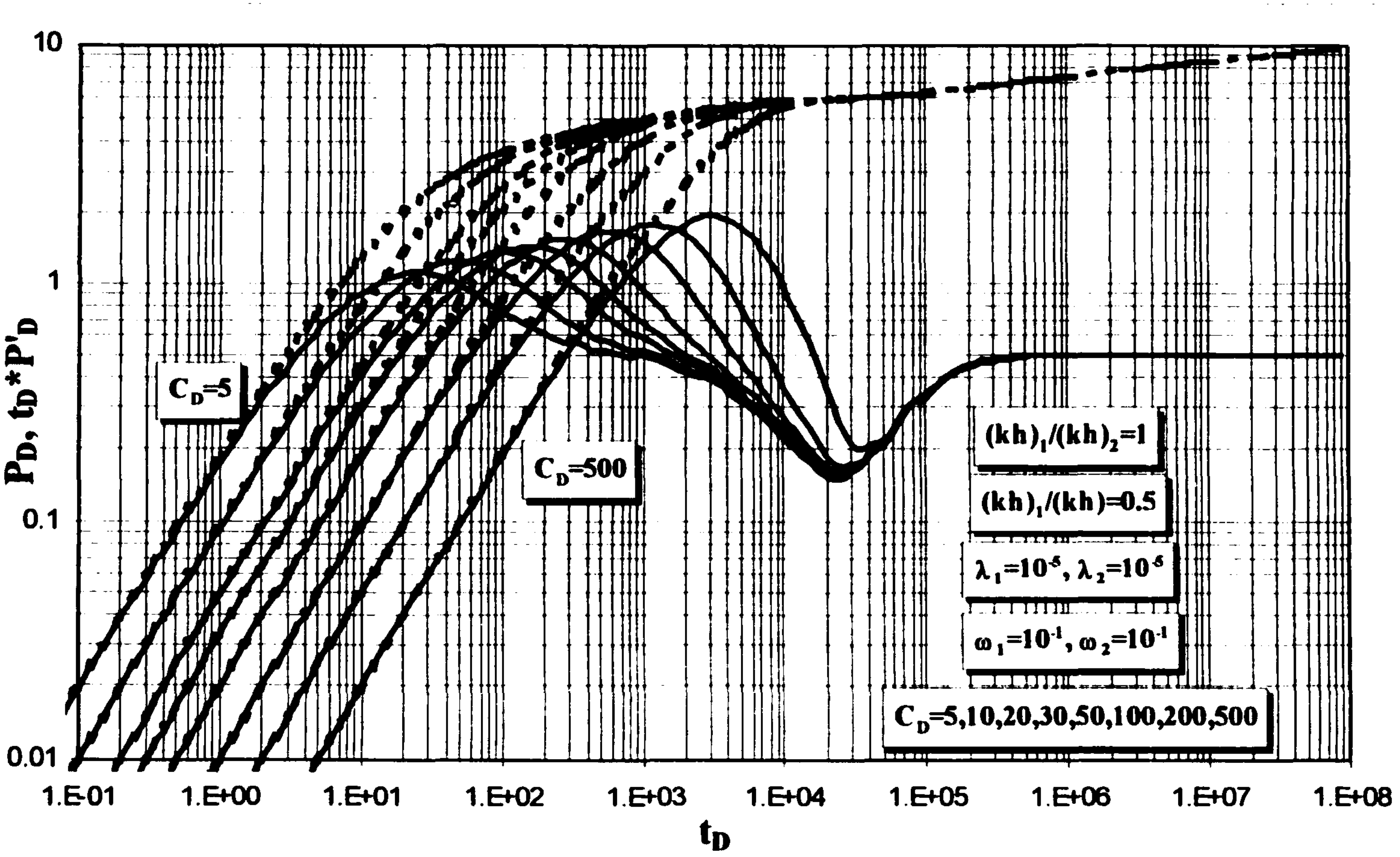

Figure 3.3.1 Characteristics of pressure and pressure derivative response in an infinite-acting, naturally fractured reservoir with pseudosteady state interporosity flow using the developed two layer model, where $\omega_1=\omega_2=0.1$ and $\lambda_1=\lambda_2=10^{-5}$. Wellbore storage effect is considered and no skin

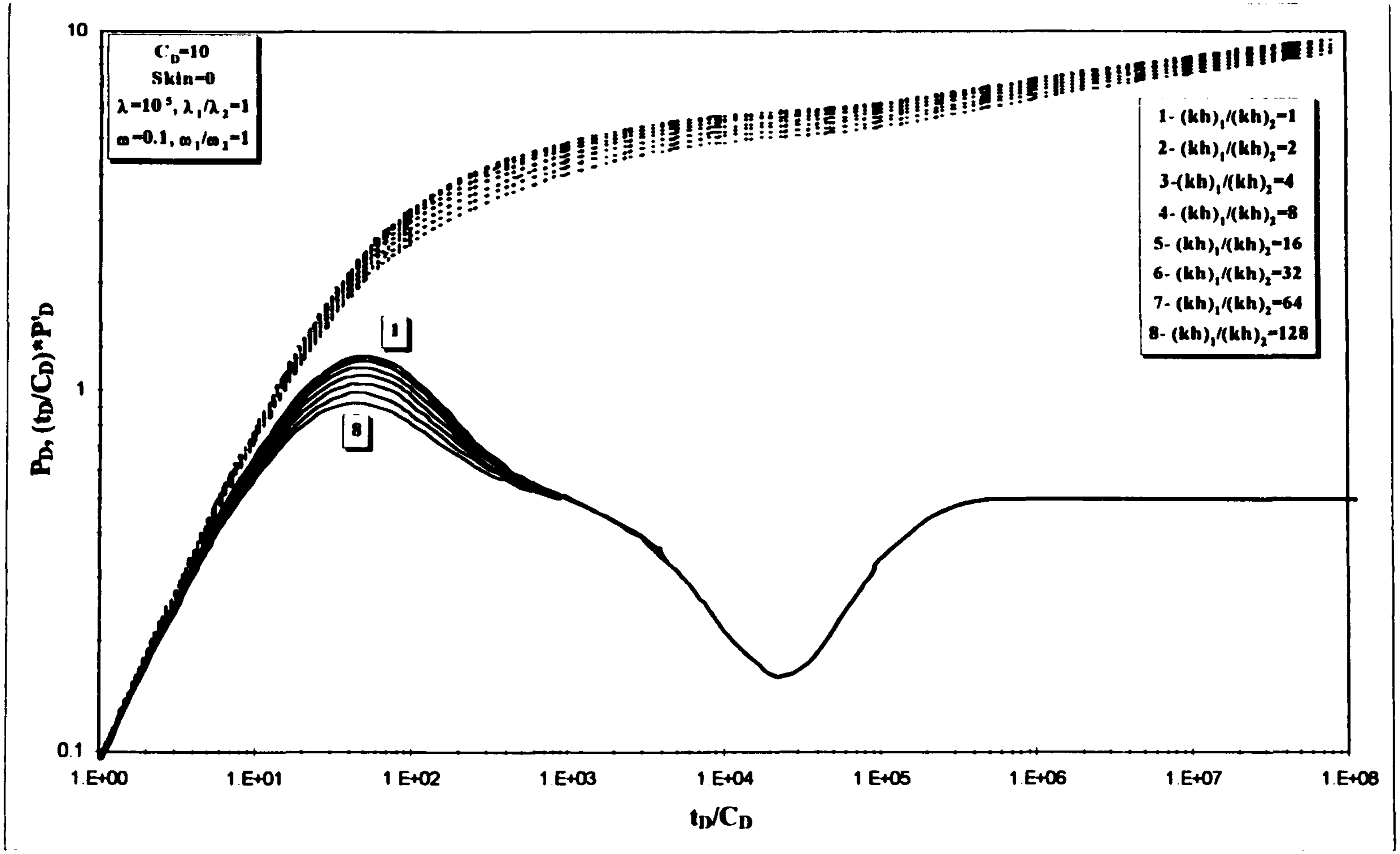

Figure 3.3.2 Characteristics of pressure and pressure derivative response in an infinite-acting, naturally fractured reservoir with pseudosteady state interporosity flow using the developed two layer model, where $\omega_1=\omega_2=0.1$ and $\lambda_1=\lambda_2=10^{-5}$. Wellbore storage=10 and no skin.

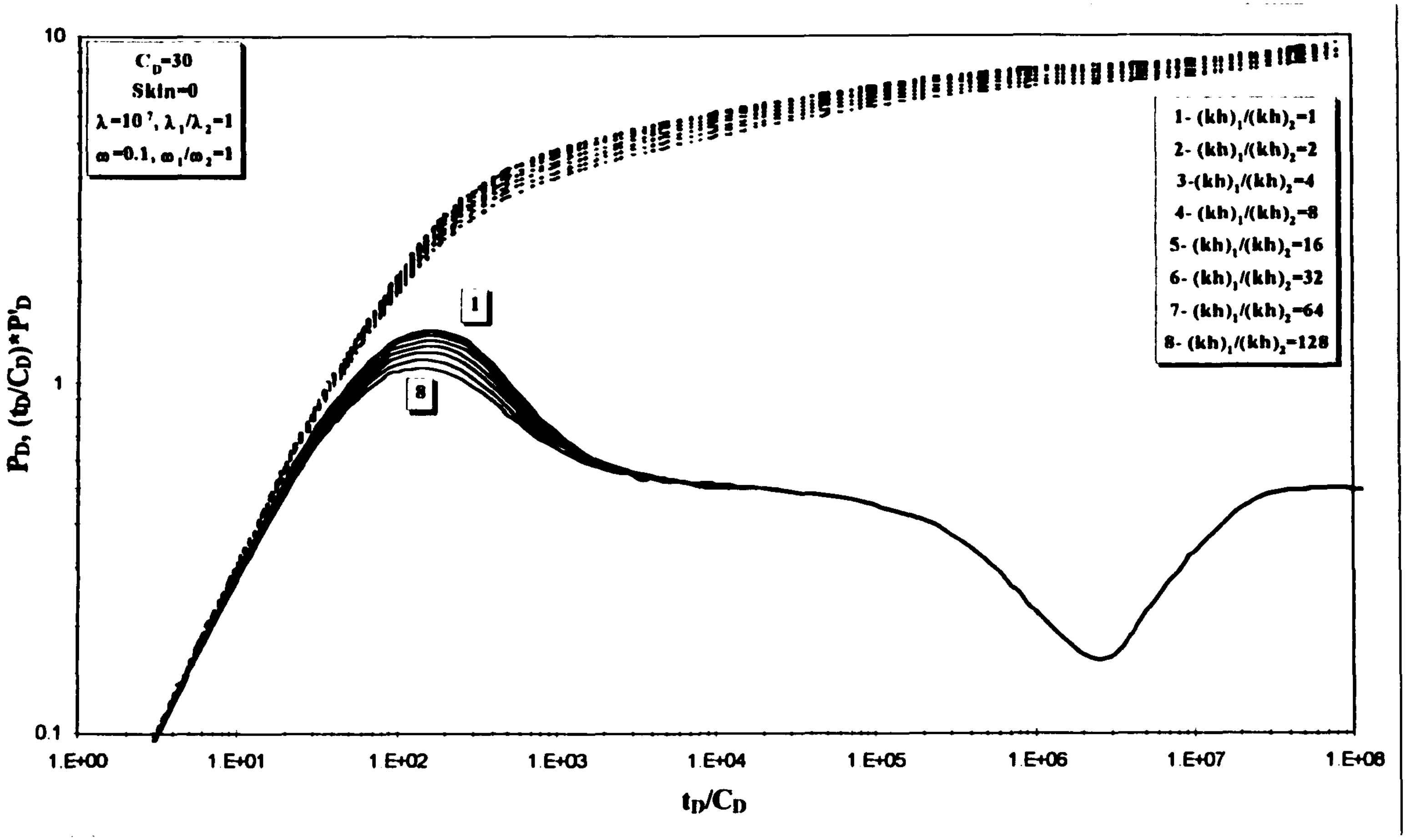

Figure 3.3.3 Characteristics of pressure and pressure derivative response in an infinite-acting, naturally fractured reservoir with pseudosteady state interporosity flow using the developed two layer model, where $\omega_1=\omega_2=0.1$ and $\lambda_1=\lambda_2=10^{-7}$. Wellbore storage=30 and no skin.

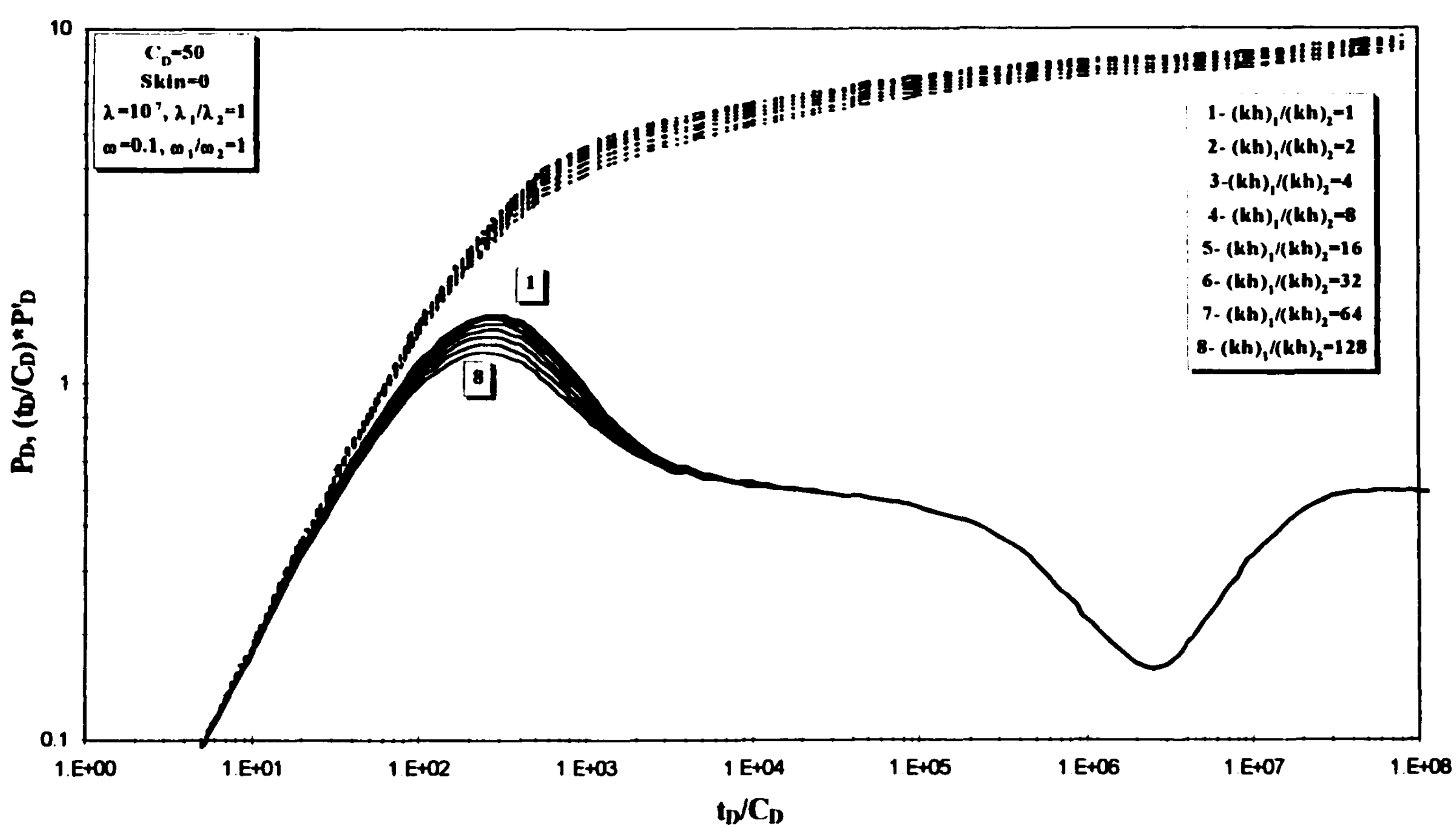

Figure 3.3.4 Characteristics of pressure and pressure derivative response in an infinite-acting, naturally fractured reservoir with pseudosteady state interporosity flow using the developed two layer model, where $\omega_1=\omega_2=0.1$ and $\lambda_1=\lambda_2=10^{-7}$. Wellbore storage=50 and no skin.

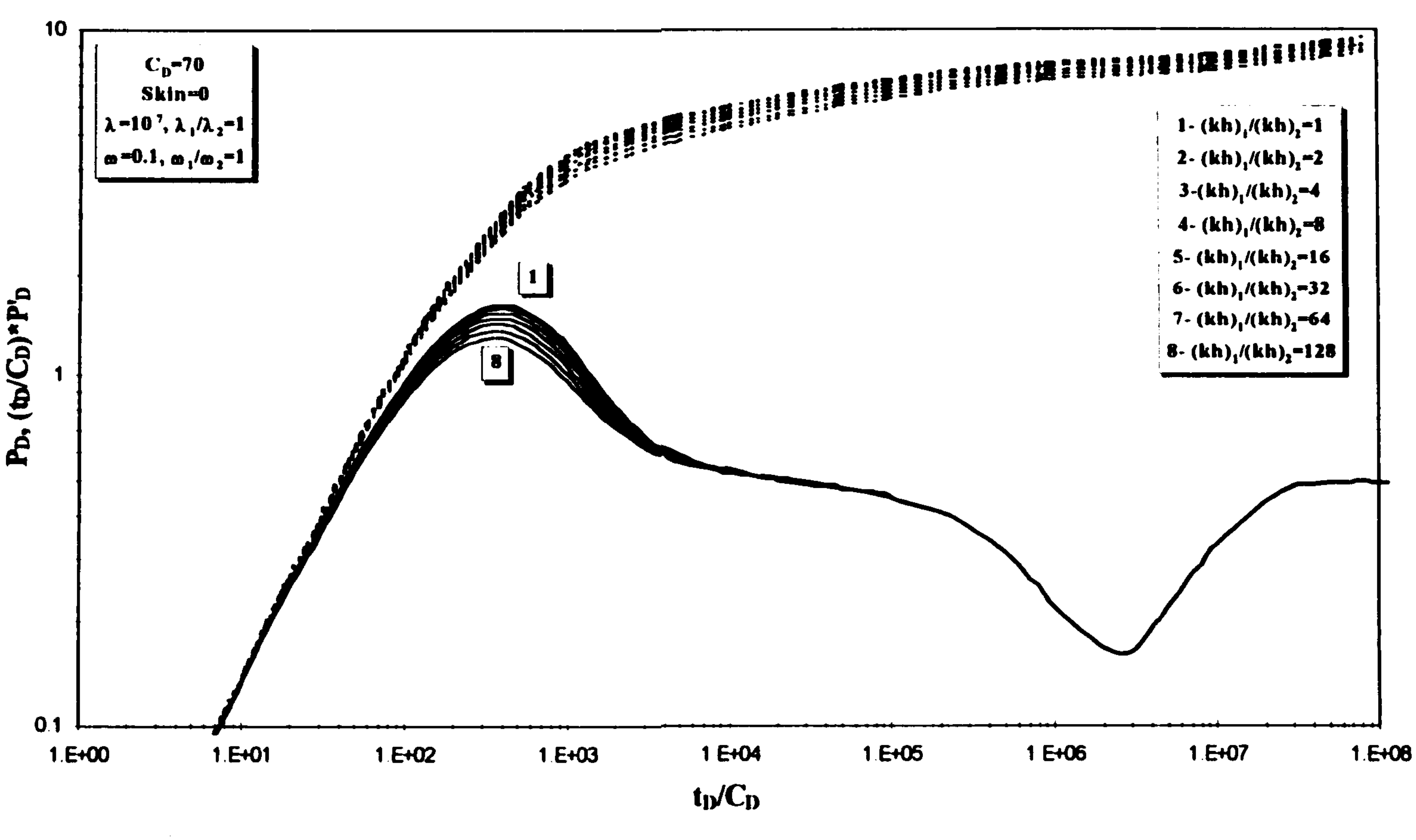

Figure 3.3.5 Characteristics of pressure and pressure derivative response in an infinite-acting, naturally fractured reservoir with pseudosteady state interporosity flow using the developed two layer model, where $\omega_1=\omega_2=0.1$ and $\lambda_1=\lambda_2=10^{-7}$. Wellbore storage=70 and no skin

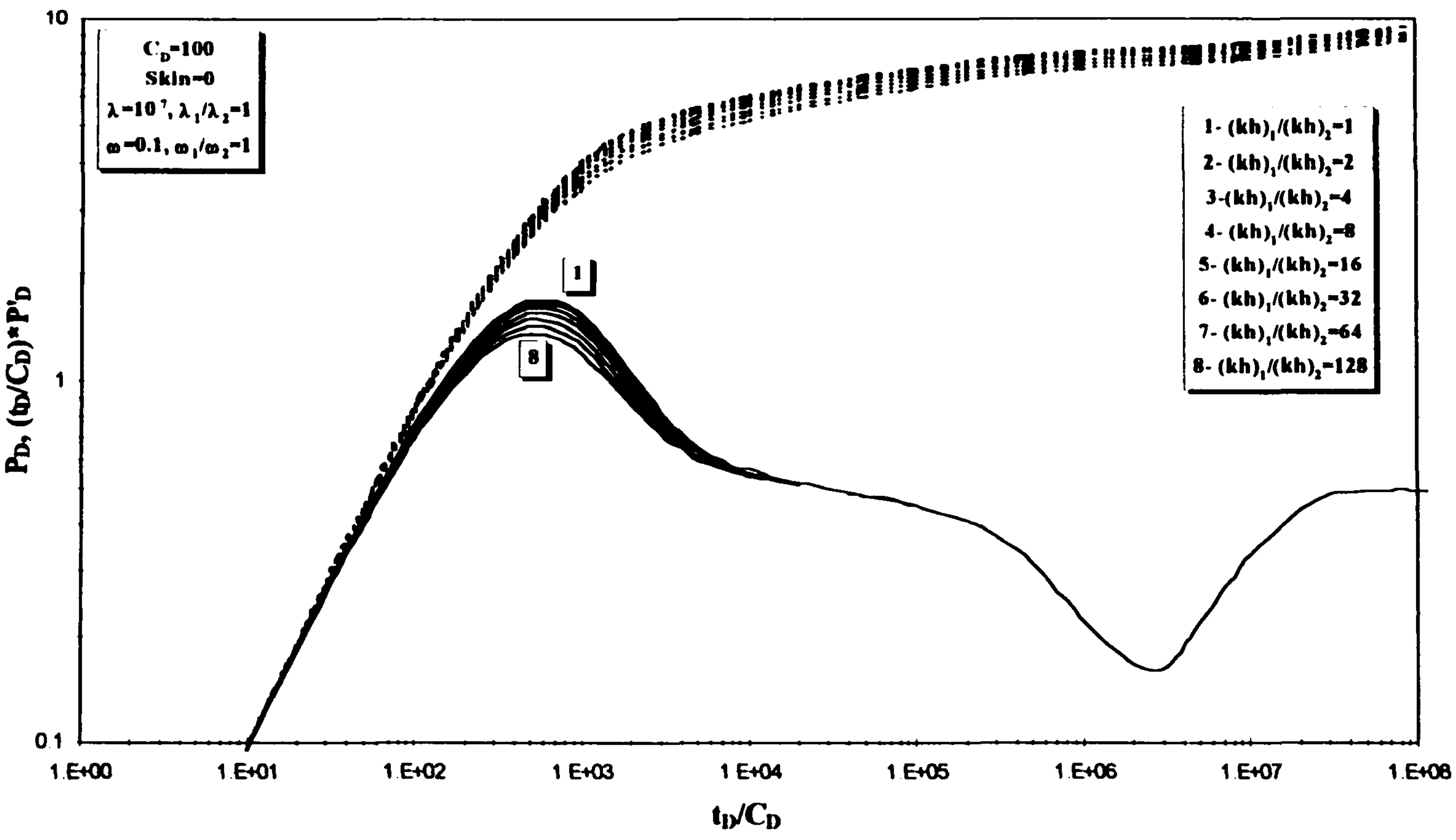

Figure 3.3.6 Characteristics of pressure and pressure derivative response in an infinite-acting, naturally fractured reservoir with pseudosteady state interporosity flow using the developed two layer model, where ω_1=ω_2=0.1 and λ_1=λ_2=10^{-7}. Wellbore storage=100 and no skin.

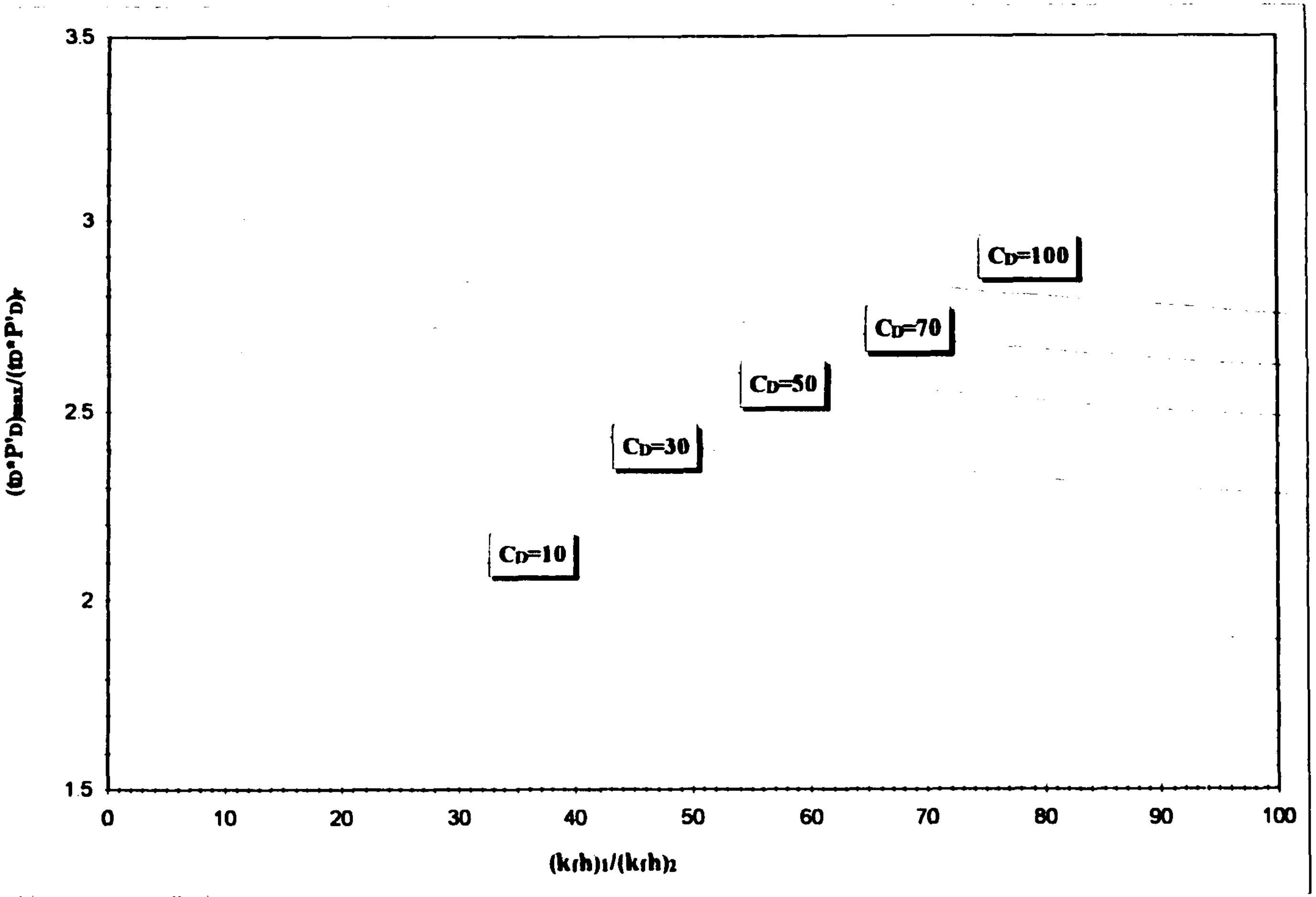

Figure 3.3.7 Normalized correlations between flow capacity ratio and pressure derivative ratio for various values of wellbore storage, for $0 < \frac{(k_f h)_1}{(k_f h)_2} < 100$.

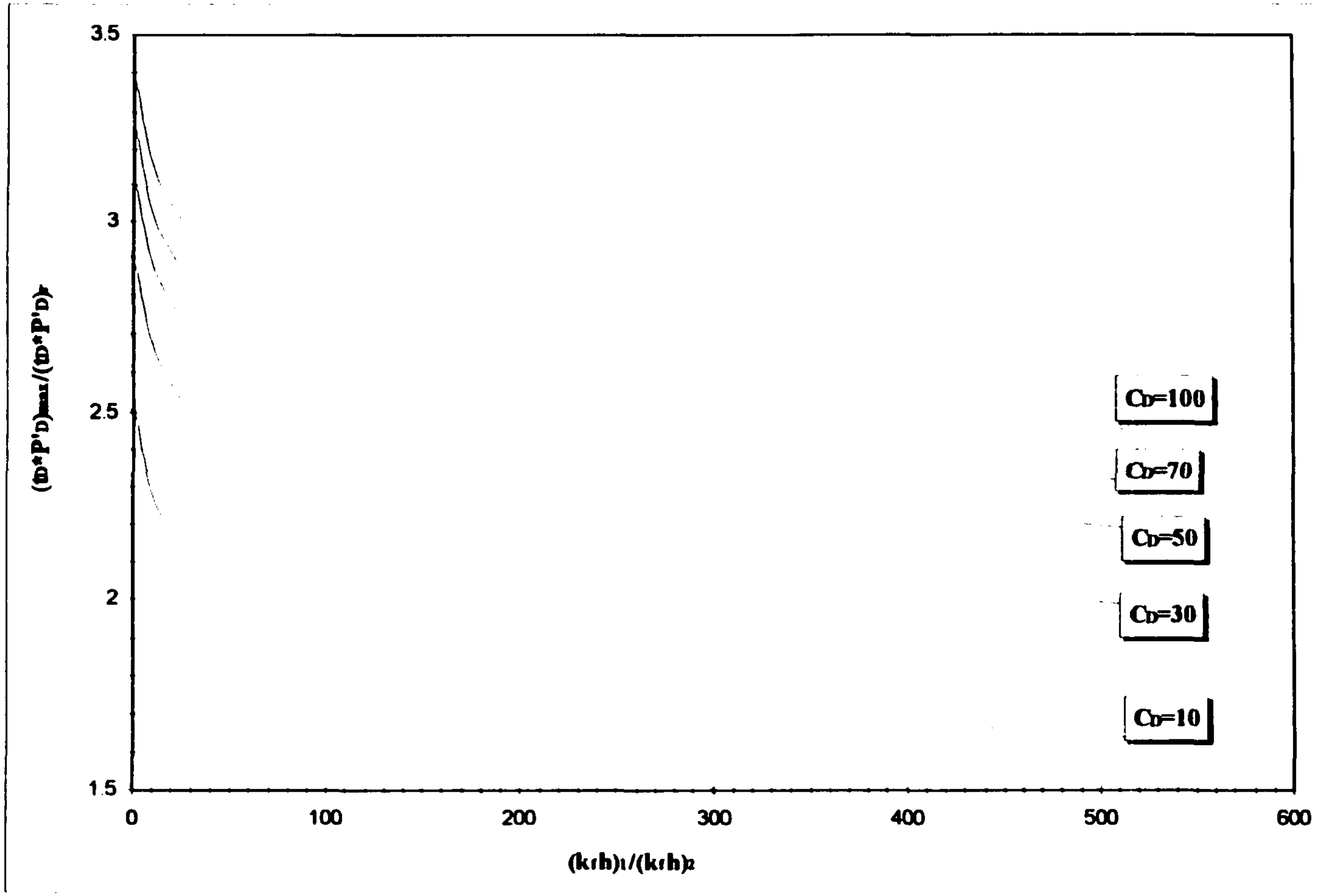

Figure 3.3.8 Normalized correlations between flow capacity ratio and pressure derivative ratio for various values of wellbore storage.

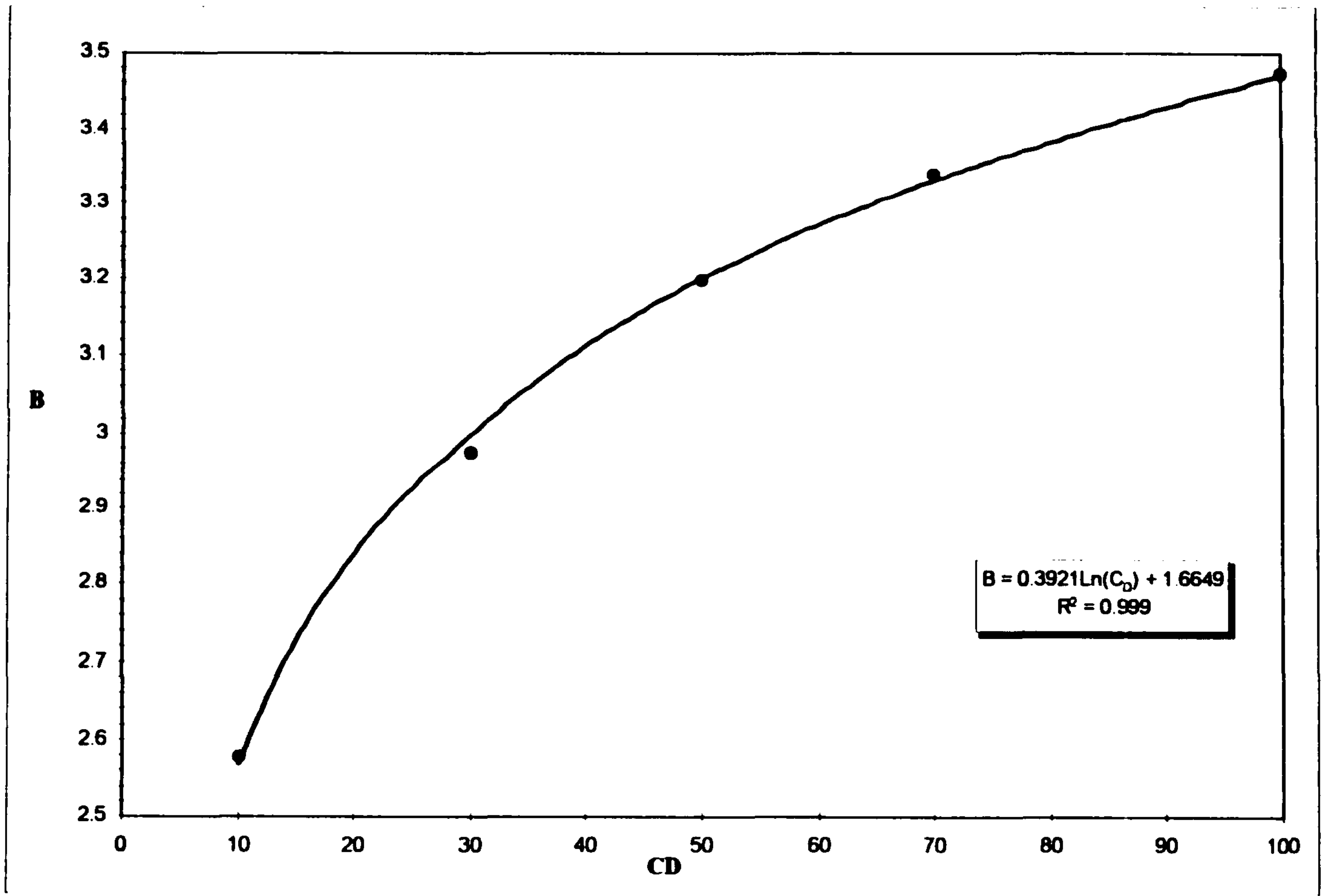

Figure 3.3.9 Correlation between wellbore storage and B values.

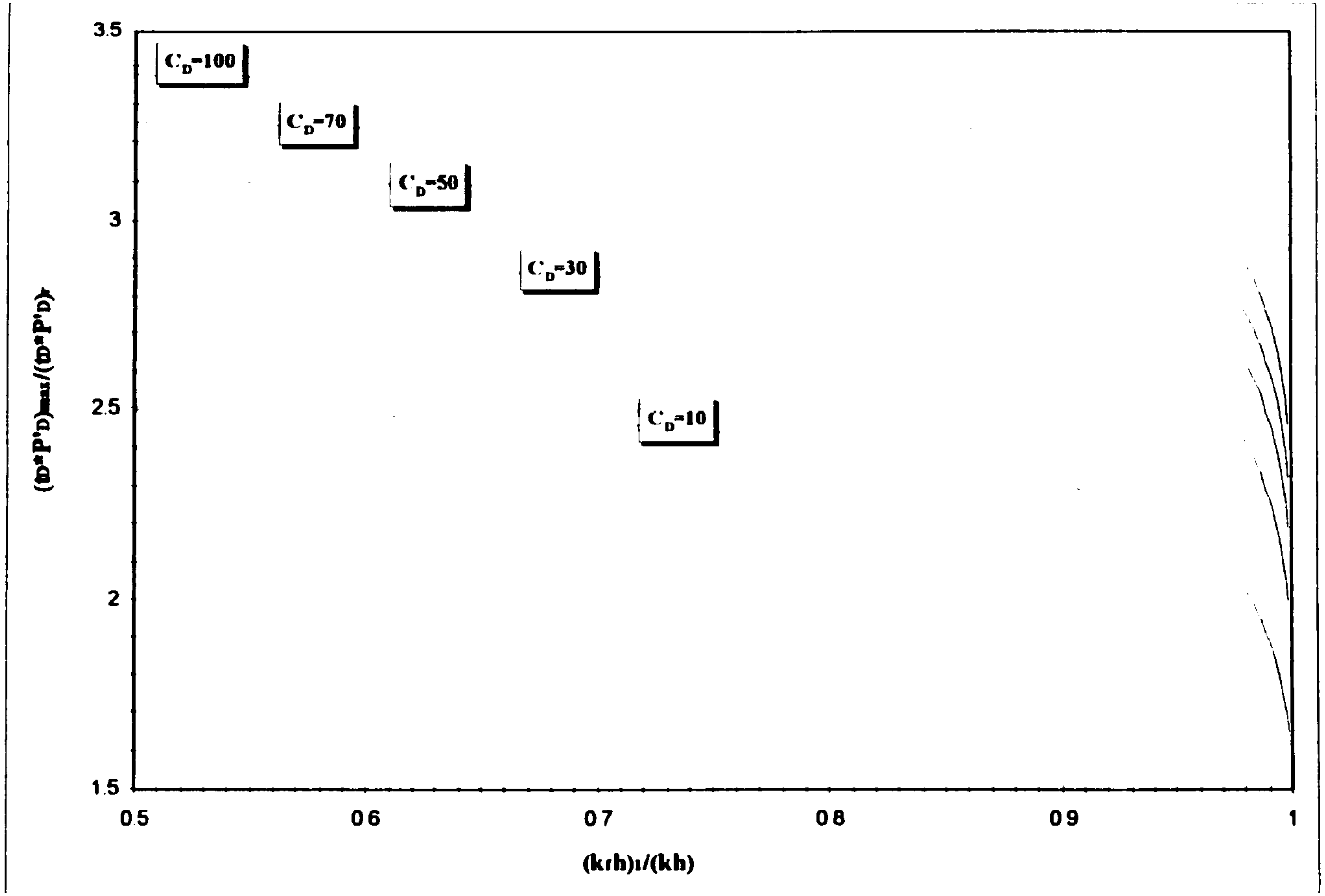

Figure 3.3.10 Normalized correlations between total flow capacity ratio and pressure derivative ratio for various values of wellbore storage, for $0 < \frac{(k_f h)_1}{(\bar{k}h)} < 1$.

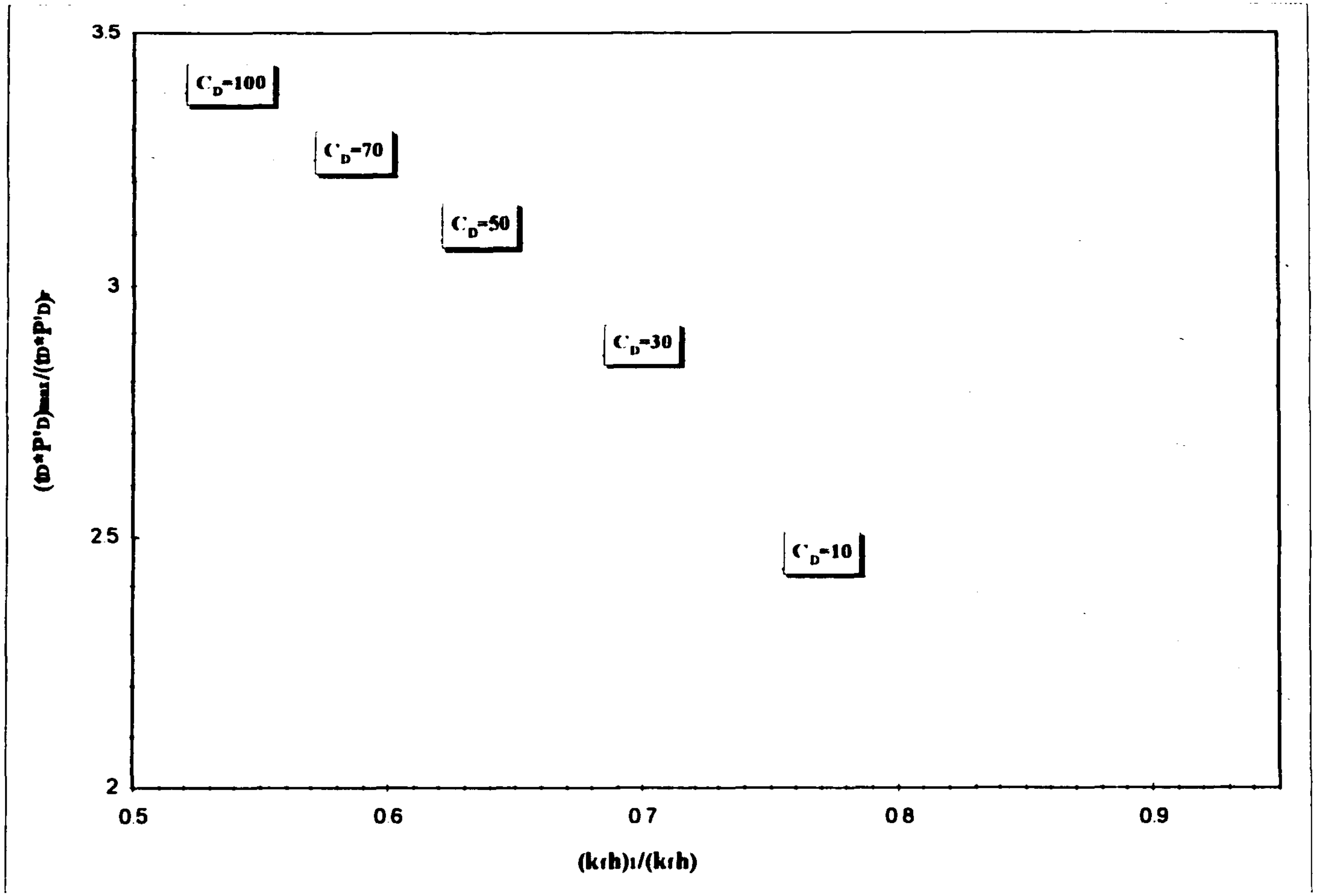

Figure 3.3.11 Normalized correlations between total flow capacity ratio and pressure derivative ratio for various

values of wellbore storage, for $0 < \frac{(k_f h)_1}{(\bar{k}h)} < 0.95$

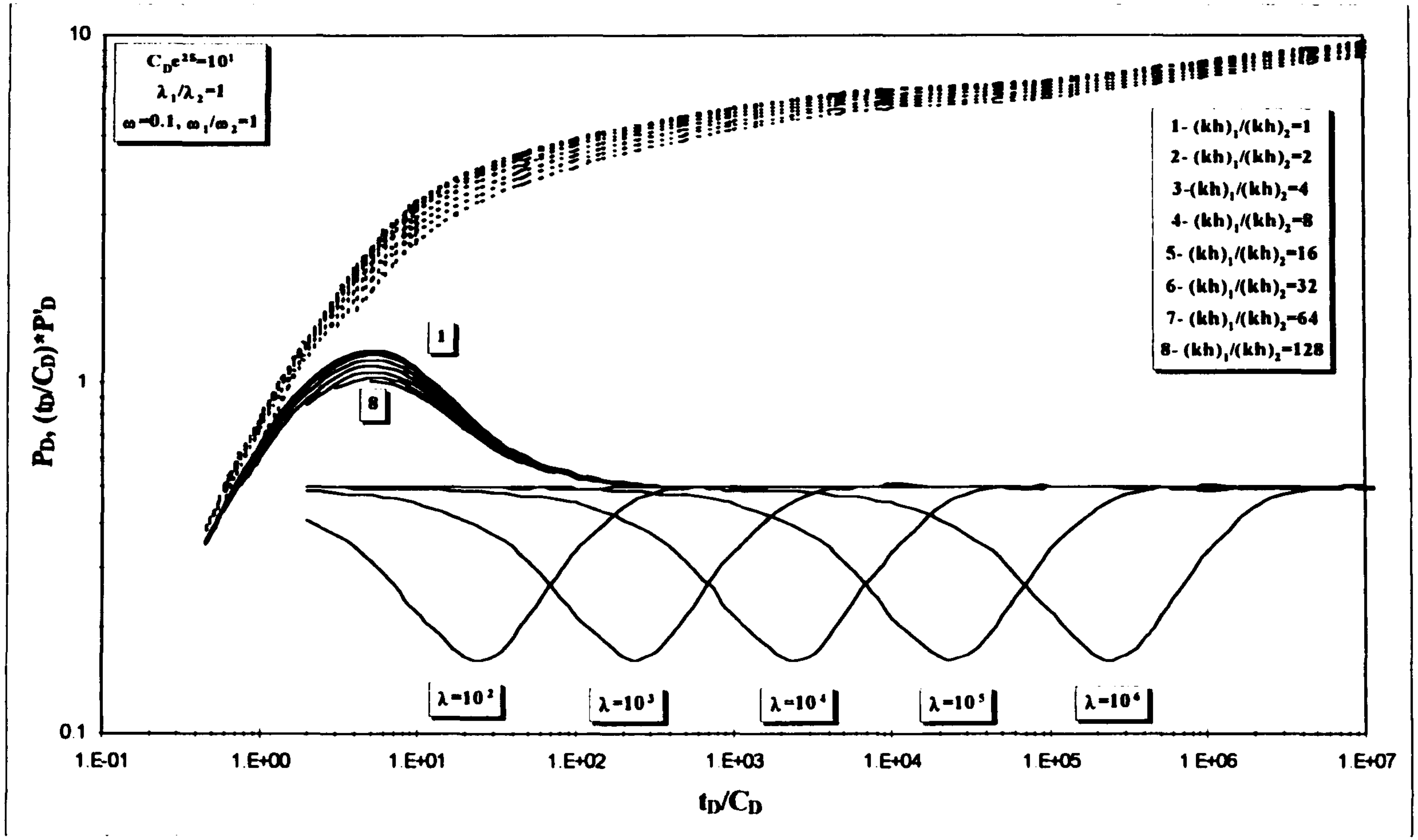

Figure 3.4.1 Pressure and its derivative response in a two-layer infinite-acting, naturally fractured reservoir with pseudosteady state interporosity flow, $C_De^{2S}=10^1$.

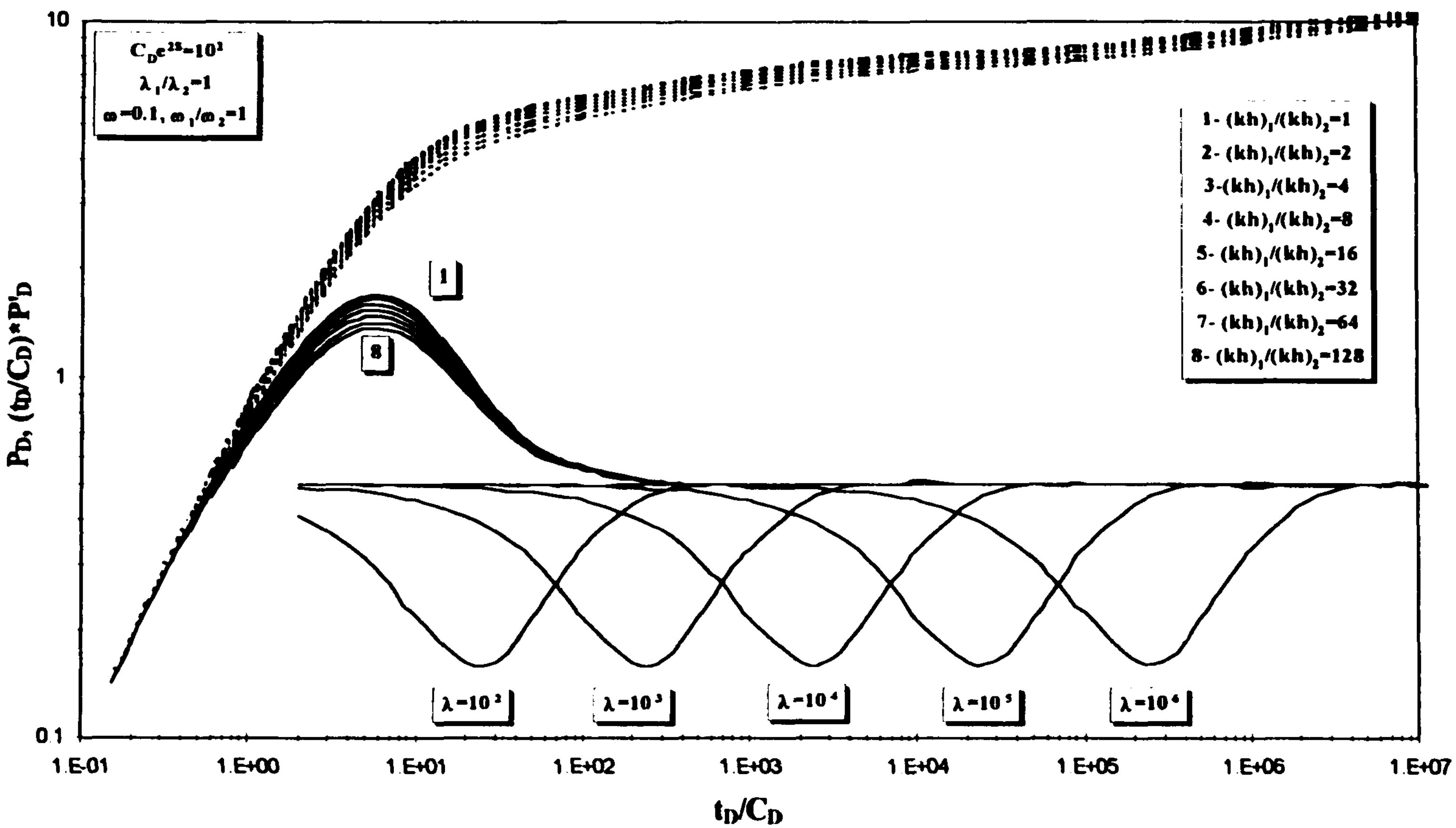

Figure 3.4.2 Pressure and its derivative response in a two-layer infinite-acting, naturally fractured reservoir with pseudosteady state interporosity flow, $C_De^{2S}=10^2$.

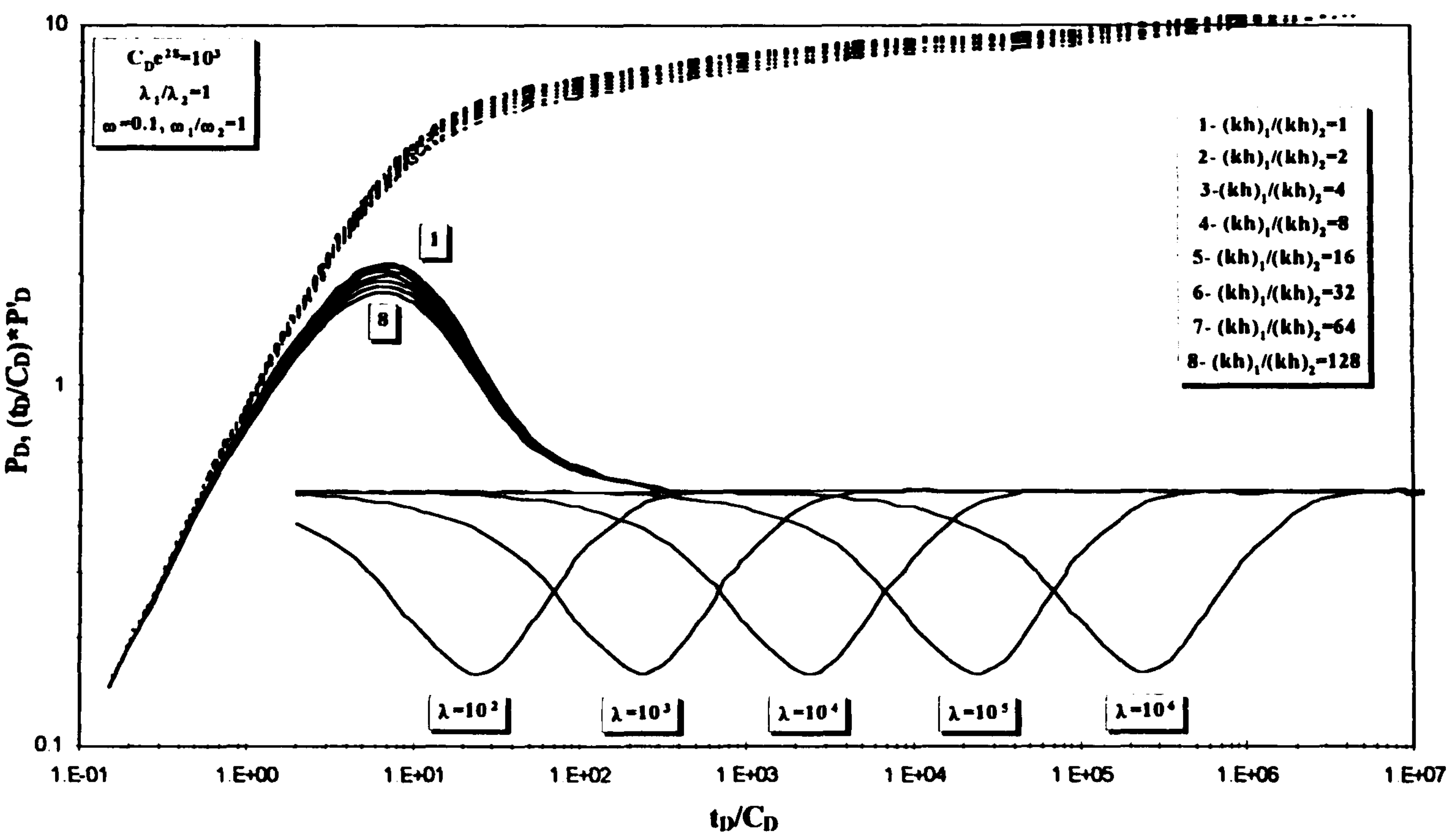

Figure 3.4.3 Pressure and its derivative response in a two-layer infinite-acting, naturally fractured reservoir with pseudosteady state interporosity flow, $C_De^{2S}=10^3$.

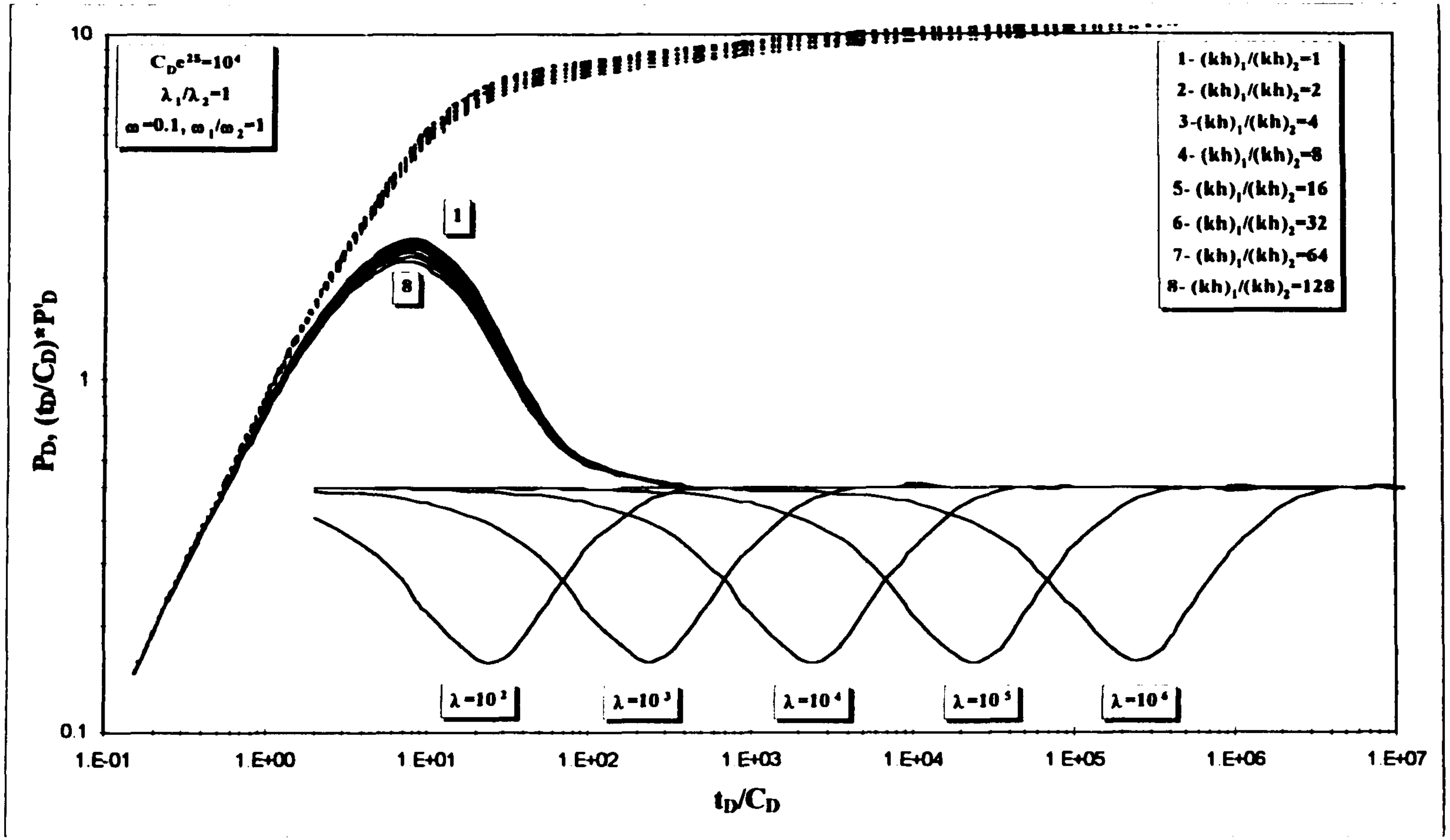

Figure 3.4.4 Pressure and its derivative response in a two-layer infinite-acting, naturally fractured reservoir with pseudosteady state interporosity flow, $C_De^{2S}=10^4$.

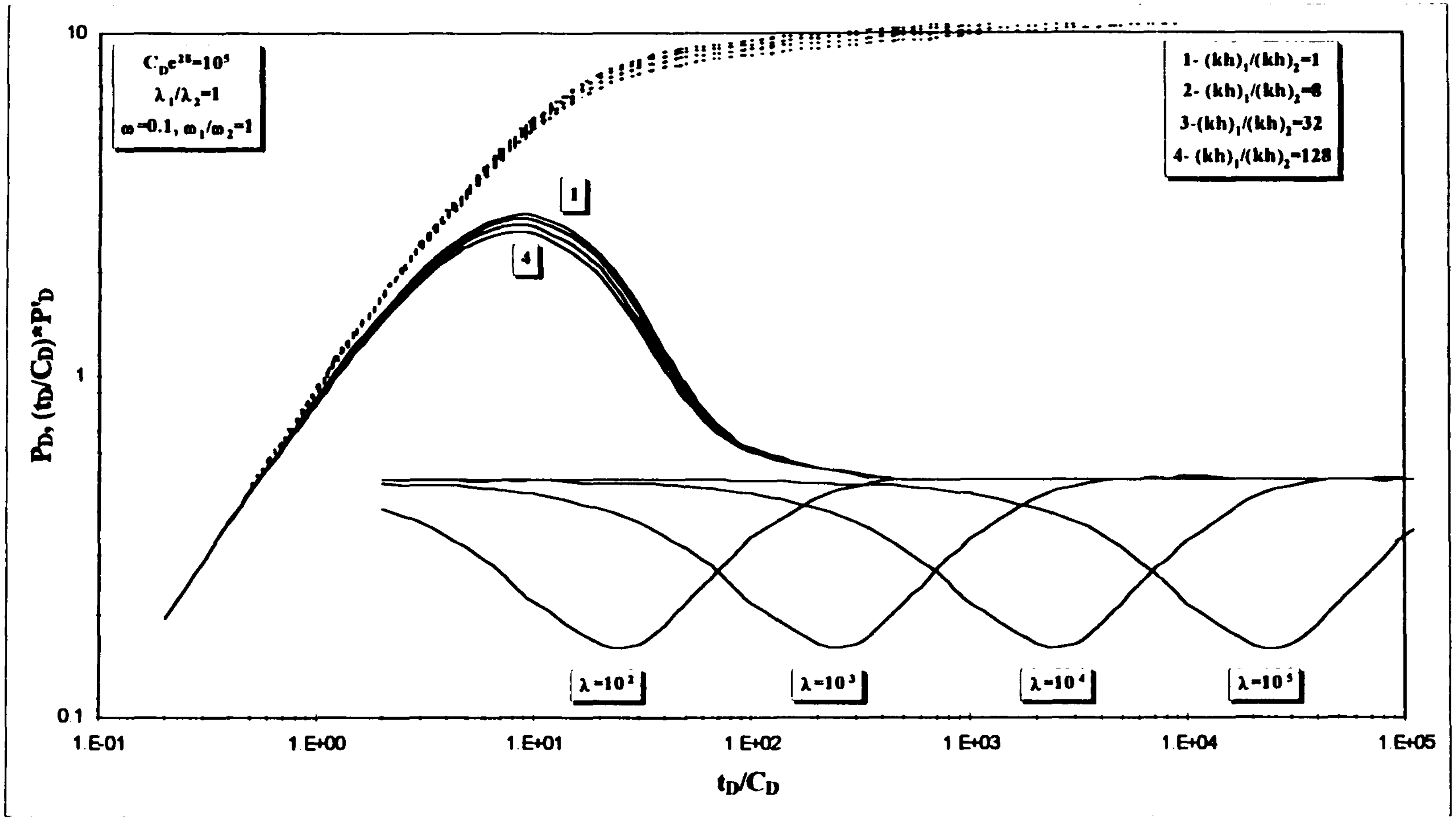

Figure 3.4.5 Pressure and its derivative response in a two-layer infinite-acting, naturally fractured reservoir with pseudosteady state interporosity flow, $C_De^{2S}=10^5$.

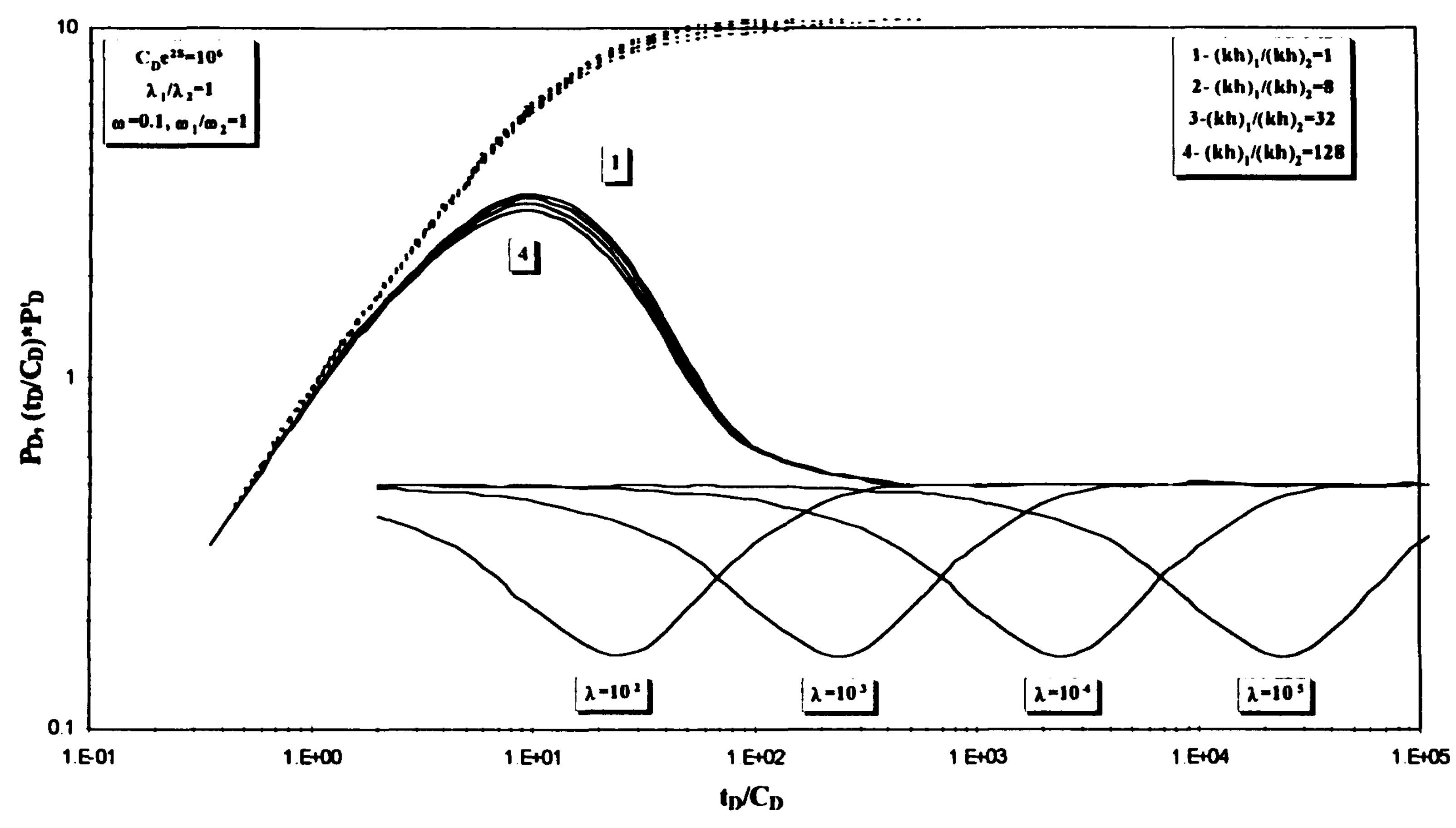

Figure 3.4.6 Pressure and its derivative response in a two-layer infinite-acting, naturally fractured reservoir with pseudosteady state interporosity flow, $C_De^{2S}=10^6$.

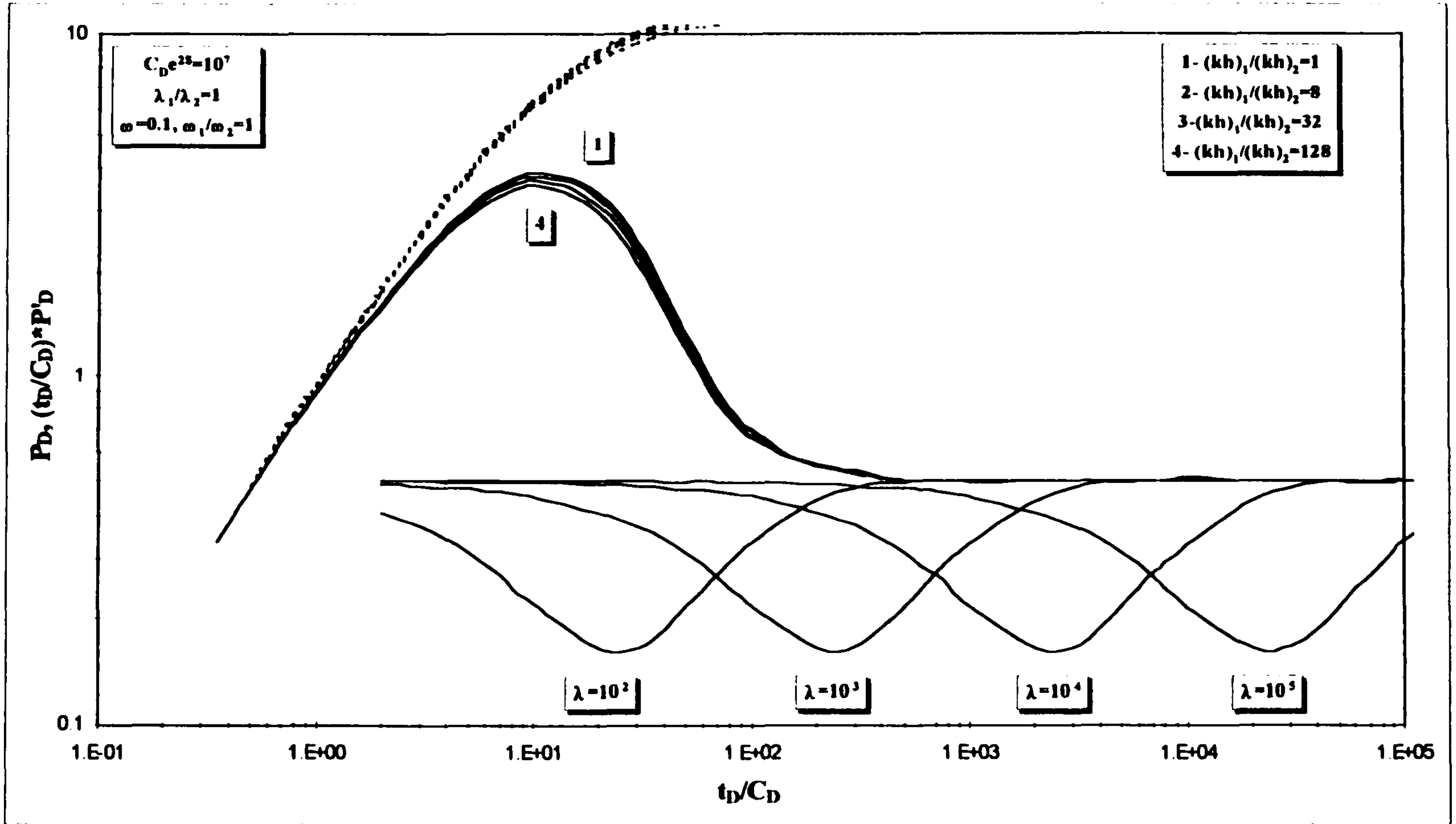

Figure 3.4.7 Pressure and its derivative response in a two-layer infinite-acting, naturally fractured reservoir with pseudosteady state interporosity flow, $C_De^{2S}=10^7$.

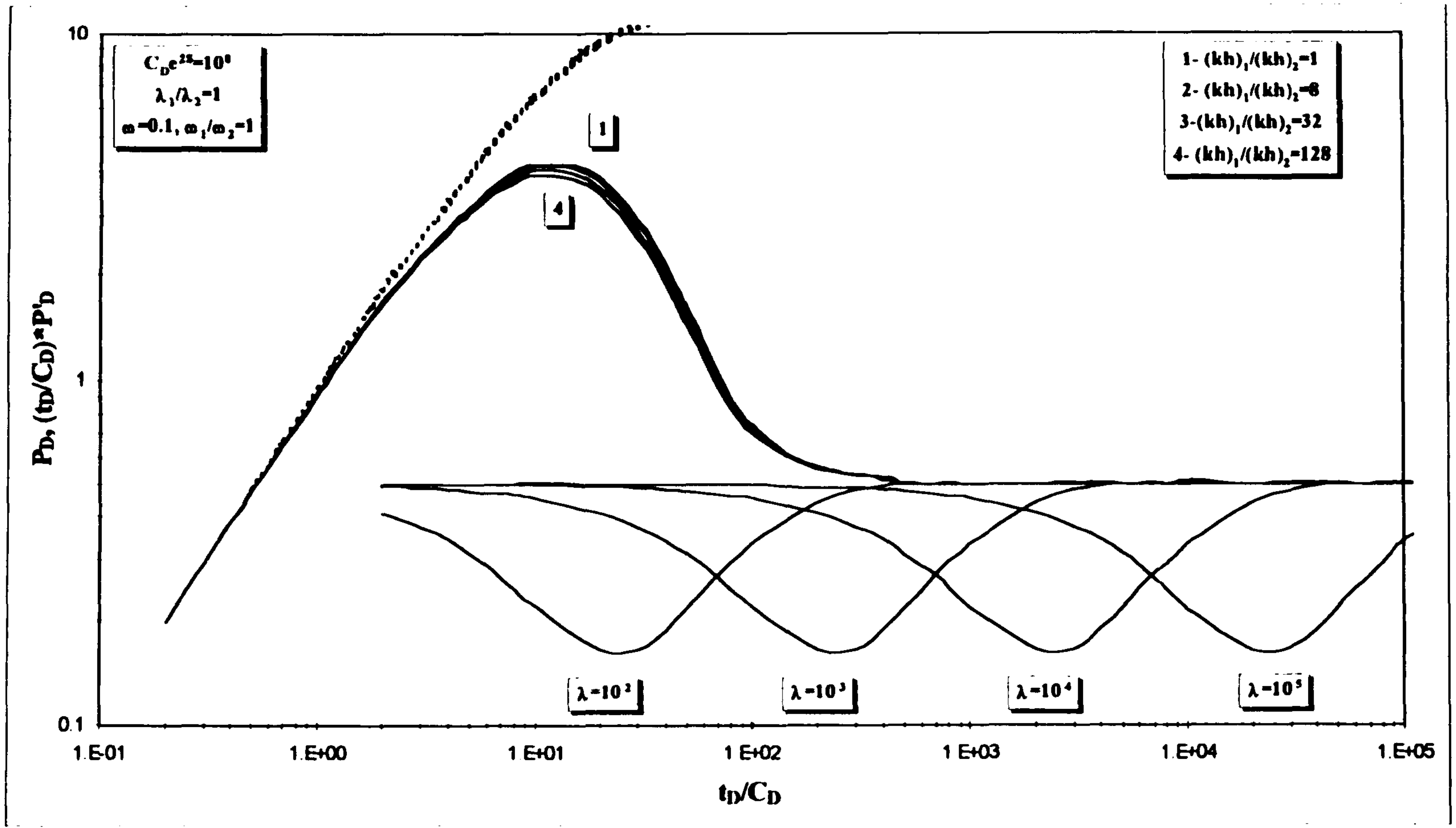

Figure 3.4.8 Pressure and its derivative response in a two-layer infinite-acting, naturally fractured reservoir with pseudosteady state interporosity flow, $C_De^{2S}=10^8$.

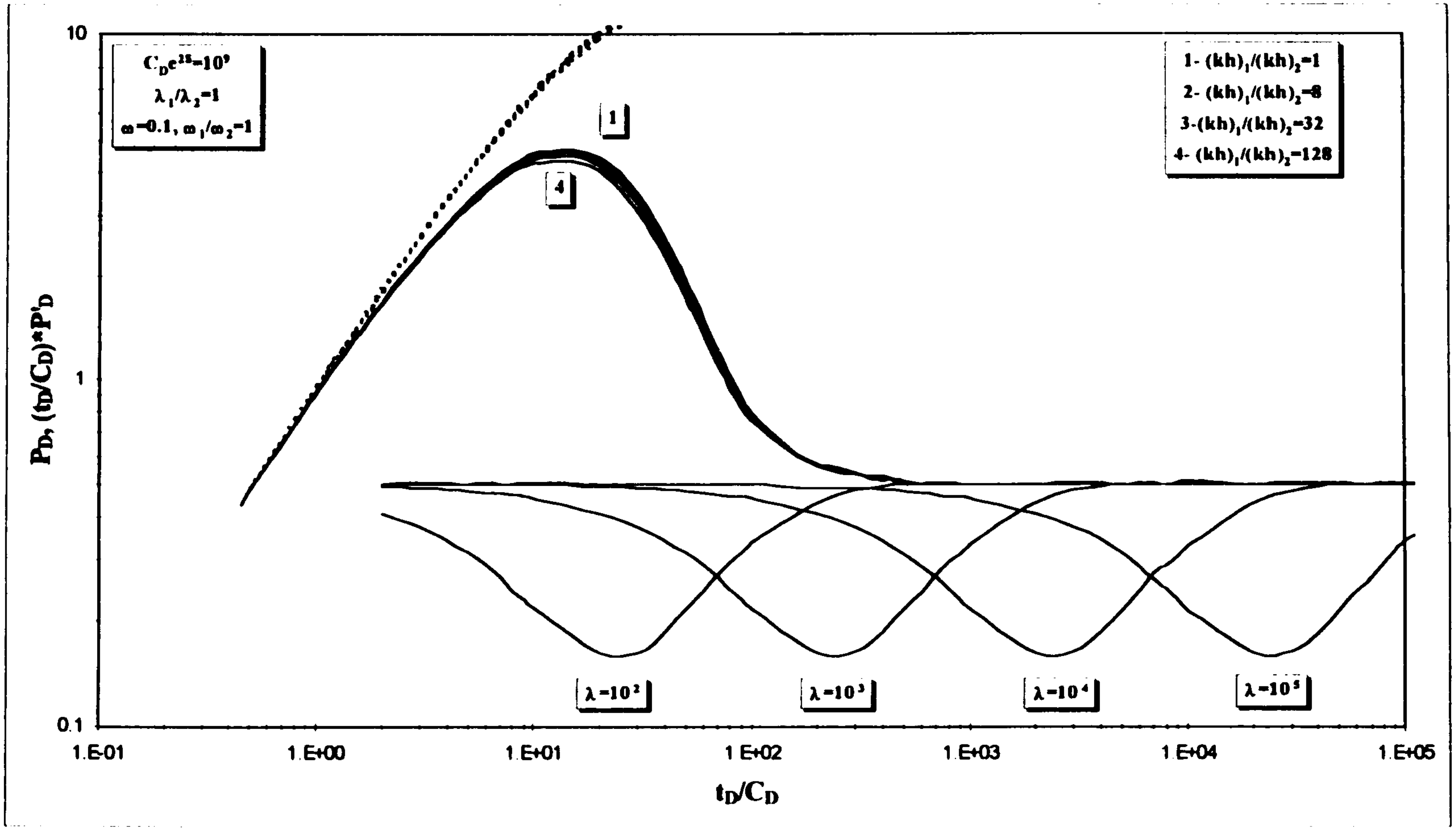

Figure 3.4.9 Pressure and its derivative response in a two-layer infinite-acting, naturally fractured reservoir with pseudosteady state interporosity flow, $C_De^{2S}=10^9$.

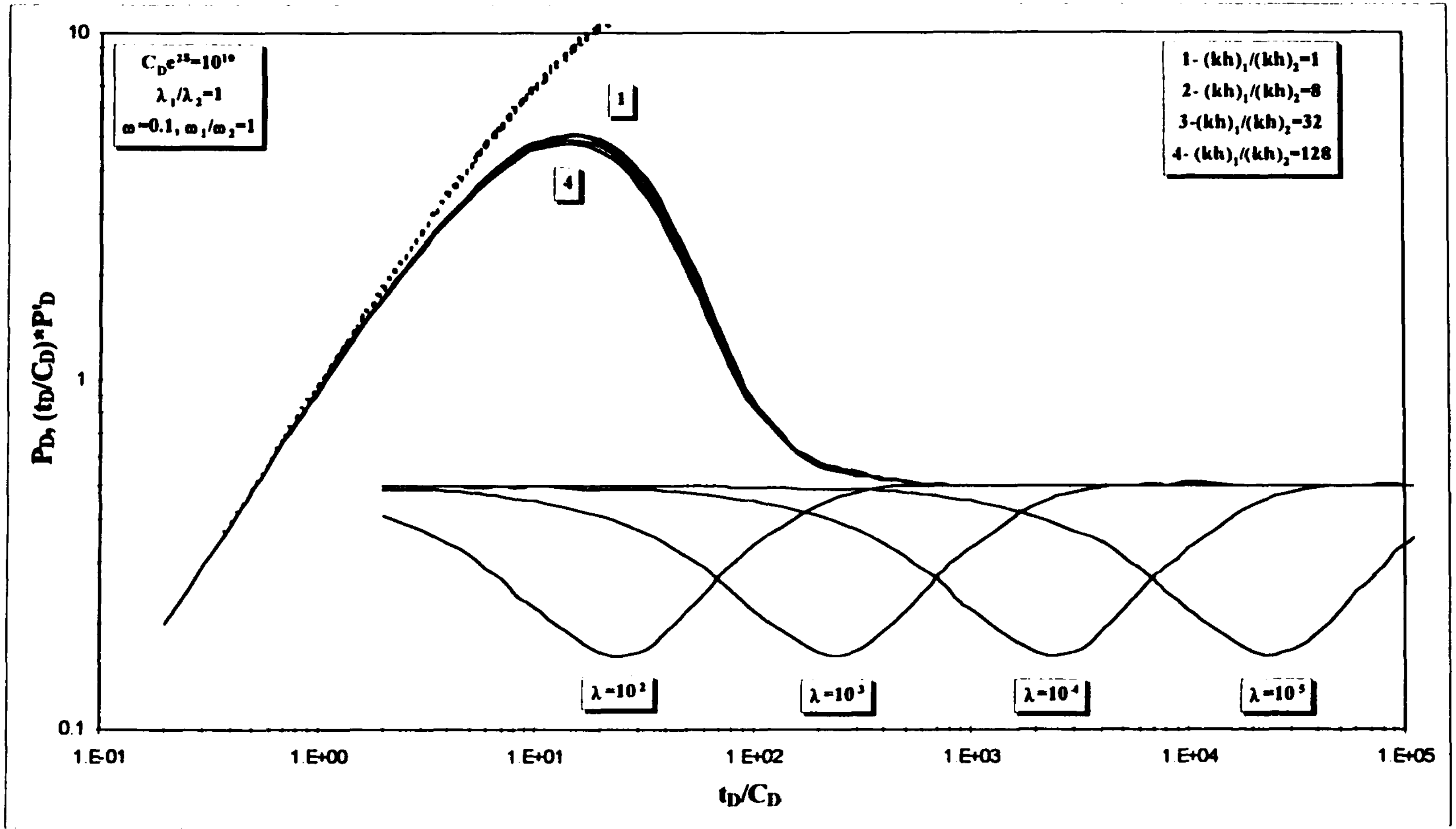

Figure 3.4.10 Pressure and its derivative response in a two-layer infinite-acting, naturally fractured reservoir with pseudosteady state interporosity flow, $C_De^{2S}=10^{10}$

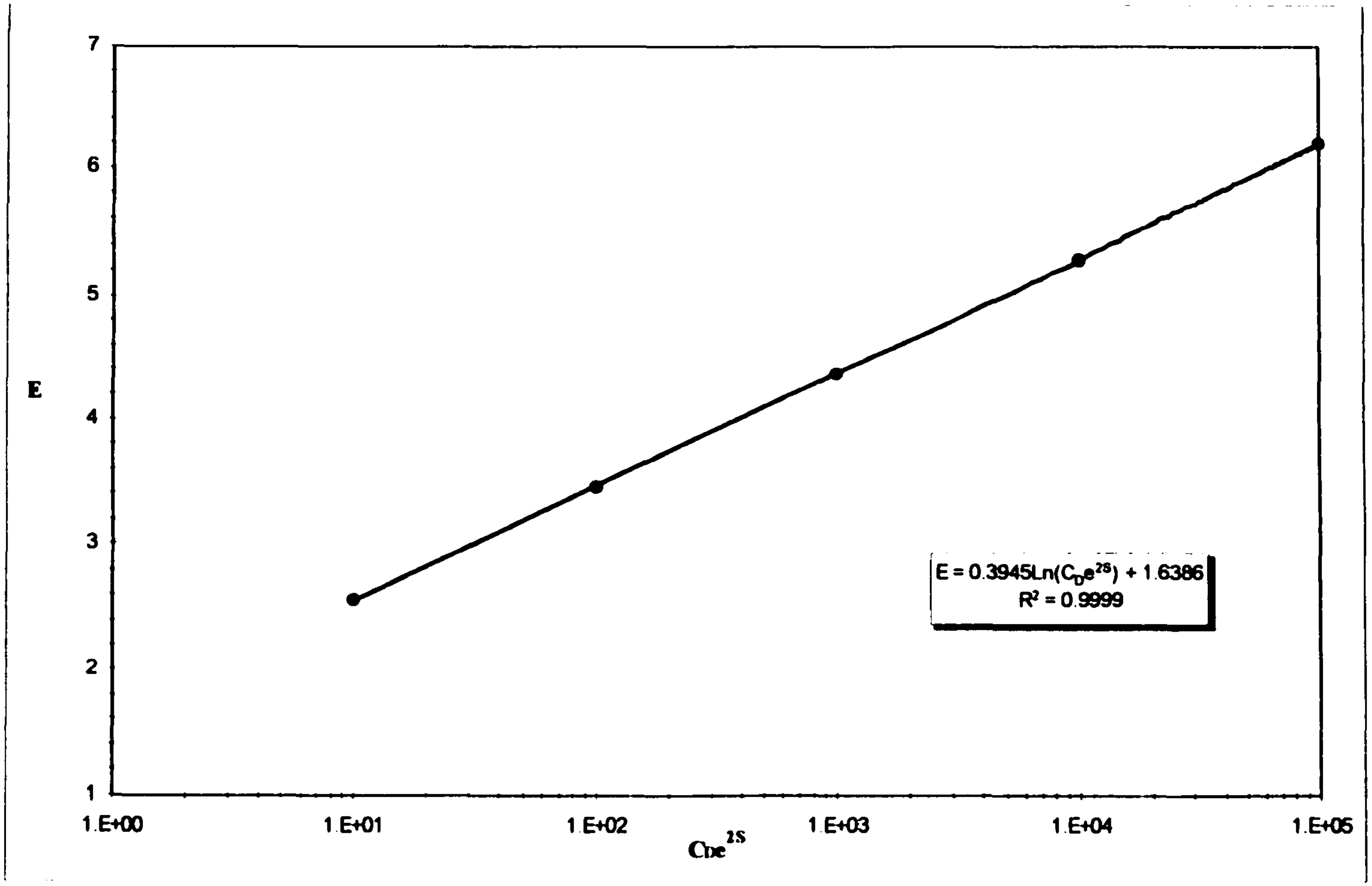

Figure 3.4.11 Correlation between $C_D e^{2S}$ group and E values.

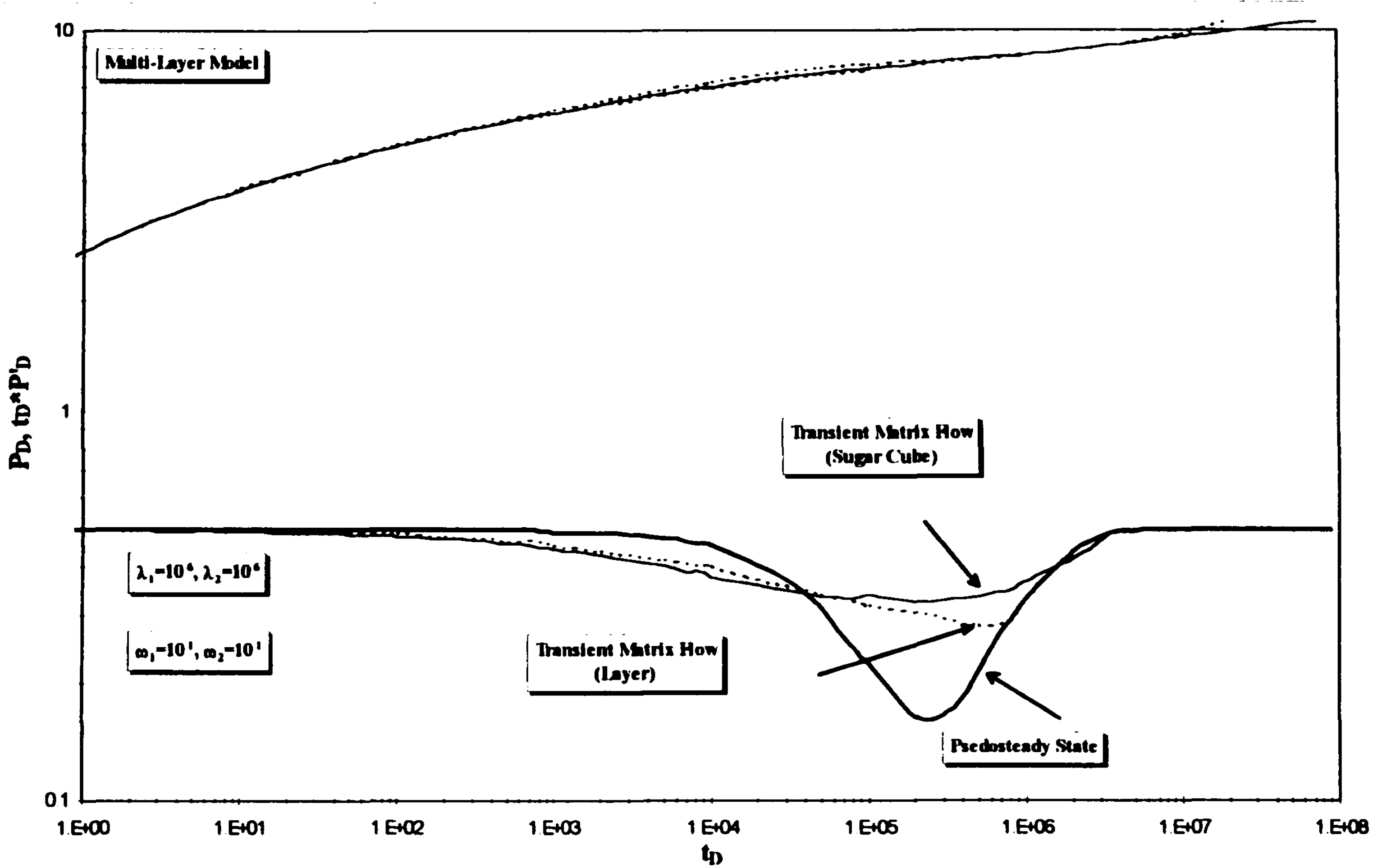

Figure 3.5.1 Comparison of pressure response for various flow regimes and flow geometries in a two-layer infinite-acting, naturally fractured reservoir.

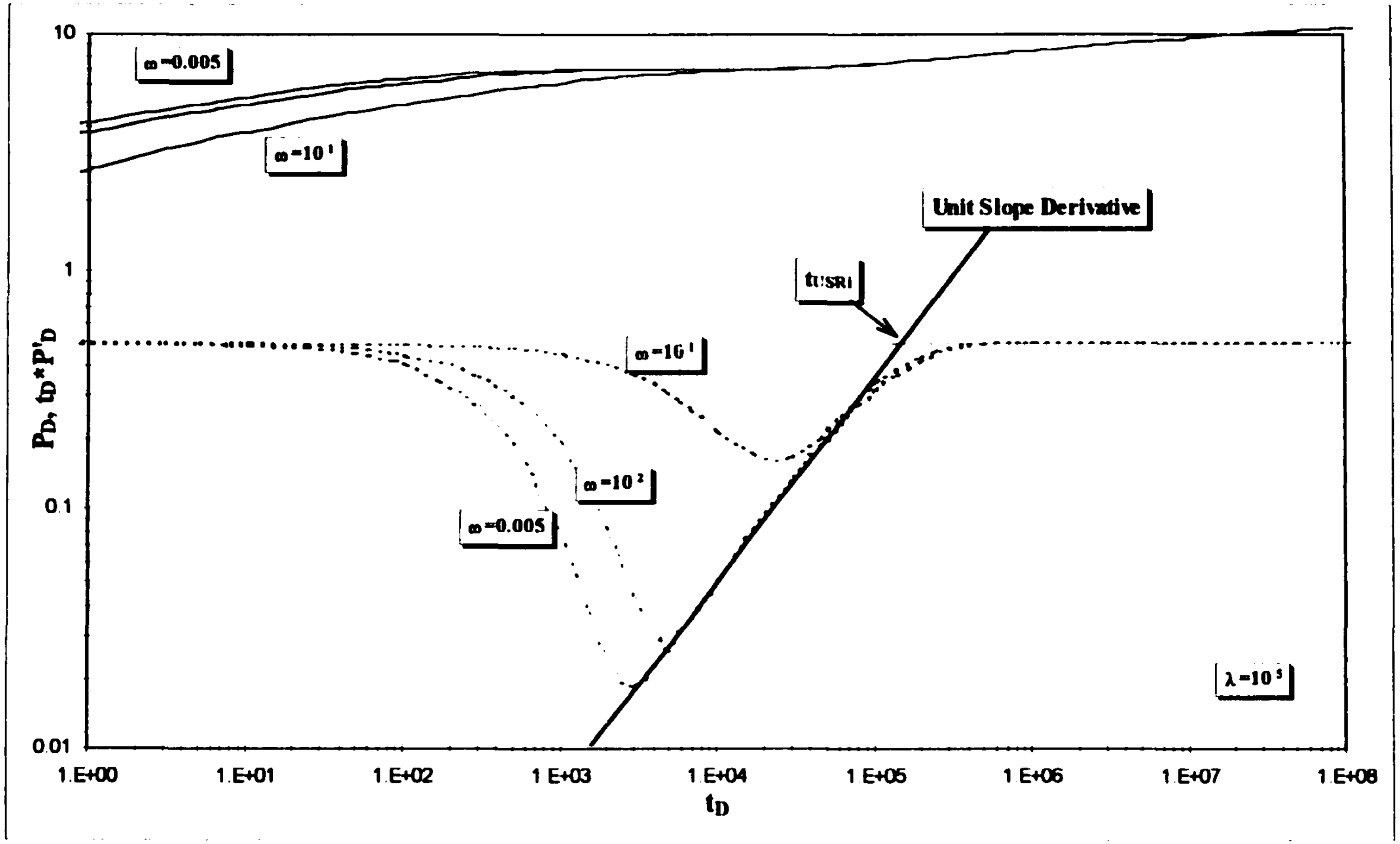

Figure 3.5.2 Effect of storage coefficient on the pressure response in a single-layer infinite-acting, naturally fractured reservoir with pseudosteady state interporosity flow.

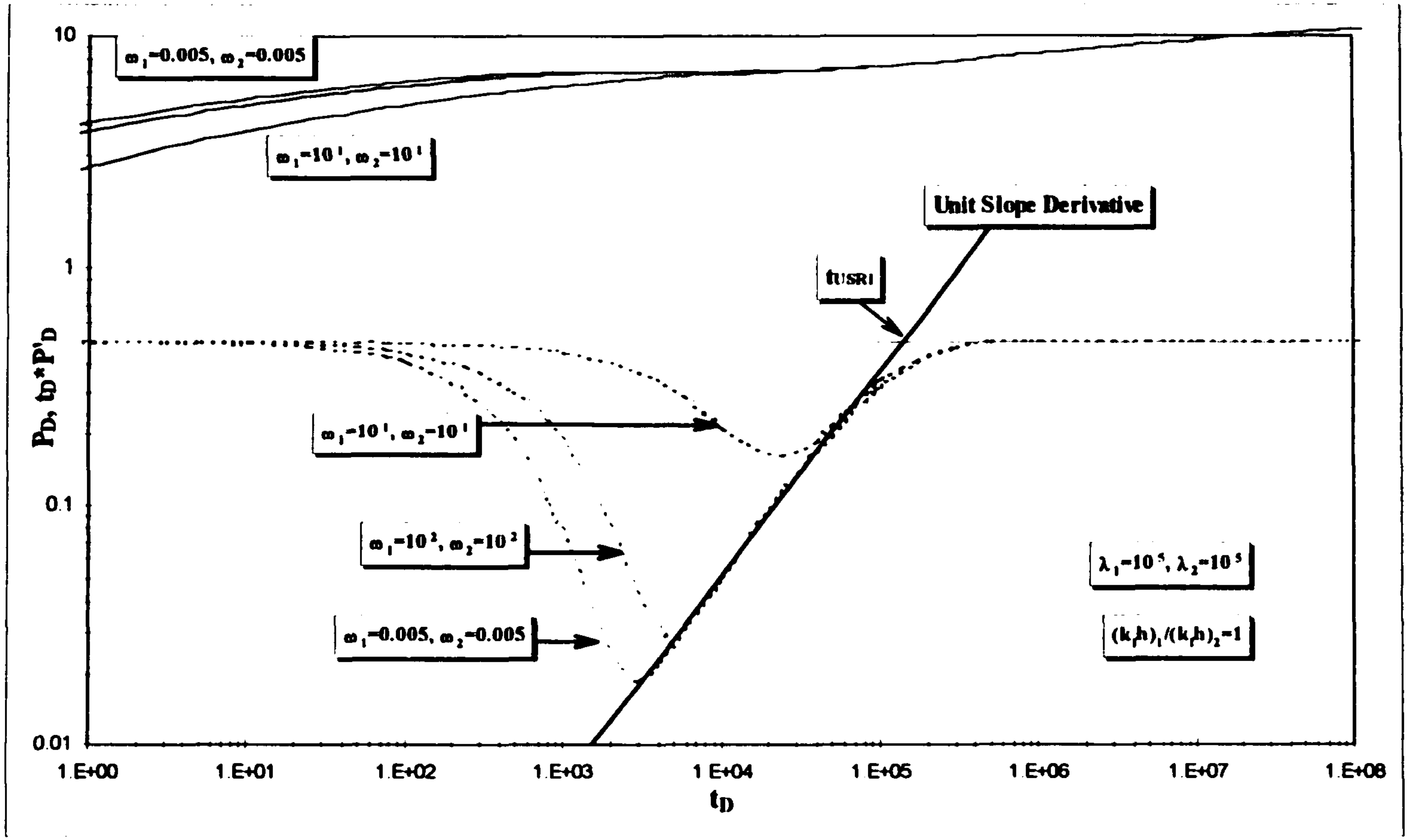

Figure 3.5.3 Effect of storage coefficient on the pressure response in a two-layer infinite-acting, naturally fractured reservoir with pseudosteady state interporosity flow.

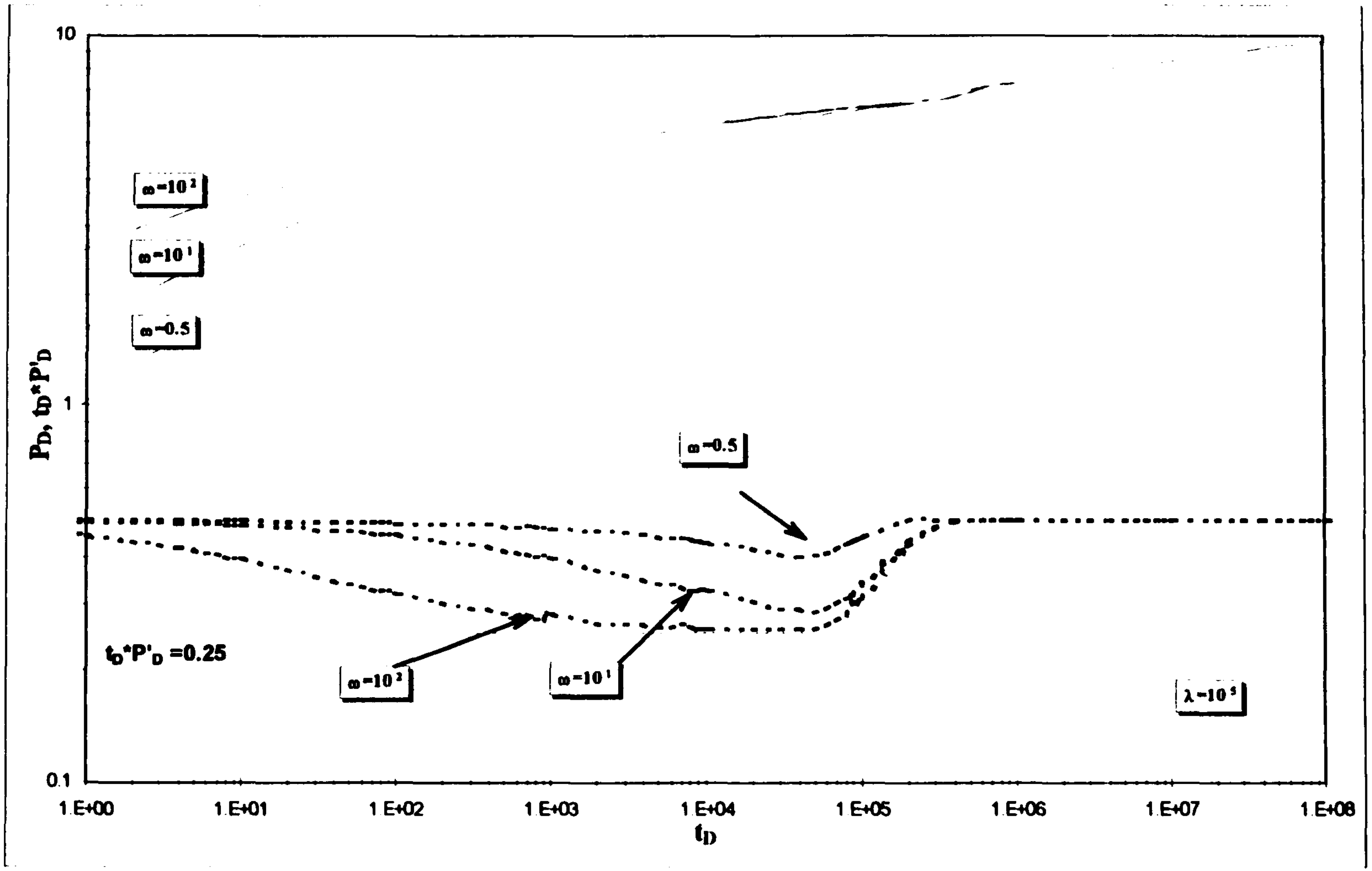

Figure 3.5.4 Effect of storage coefficient on the pressure response in a single-layer infinite-acting, naturally fractured reservoir with transient matrix flow in a slab system.

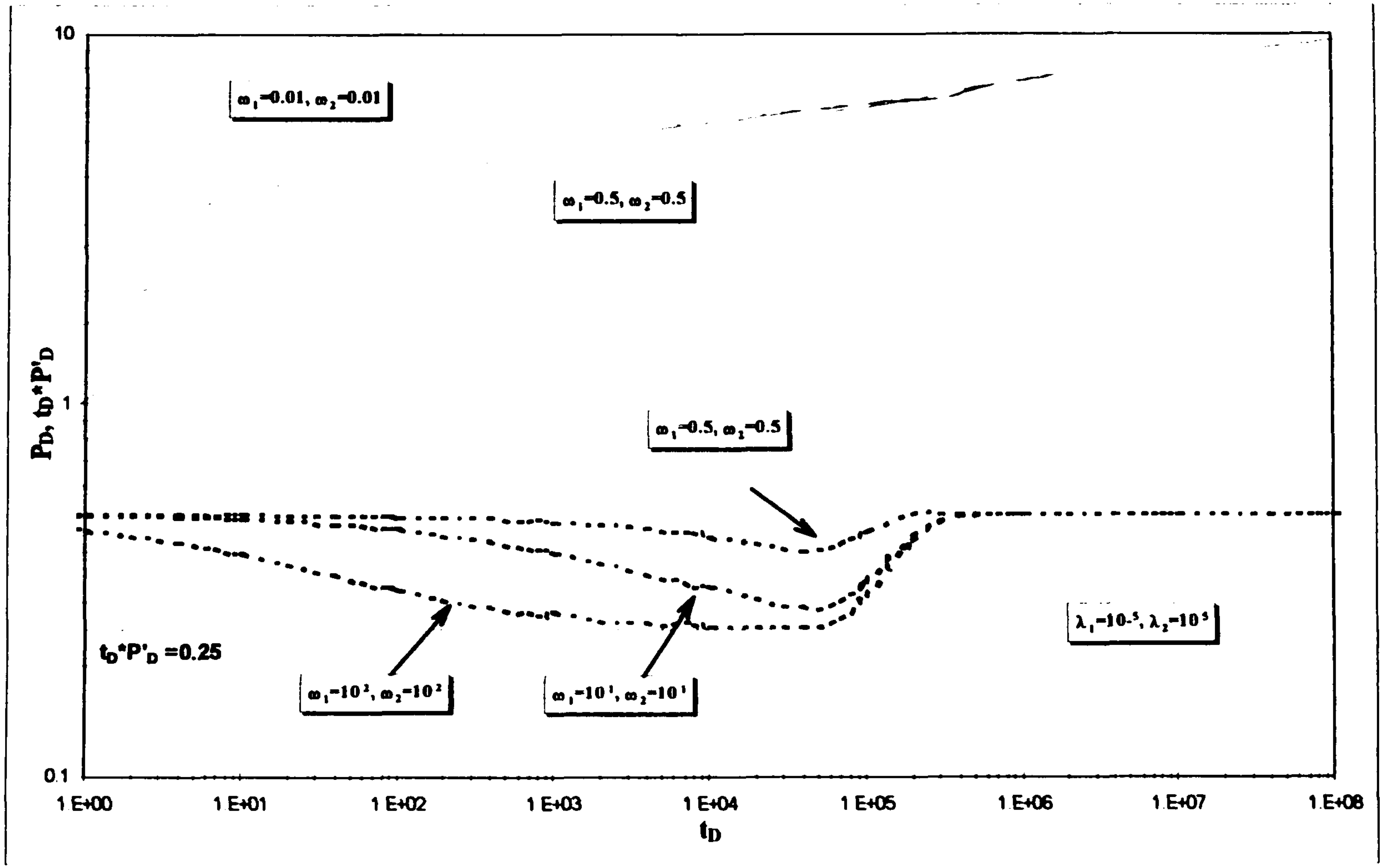

Figure 3.5.5 Effect of storage coefficient on the pressure response in a two-layer infinite-acting, naturally fractured reservoir with transient matrix flow in a slab system.

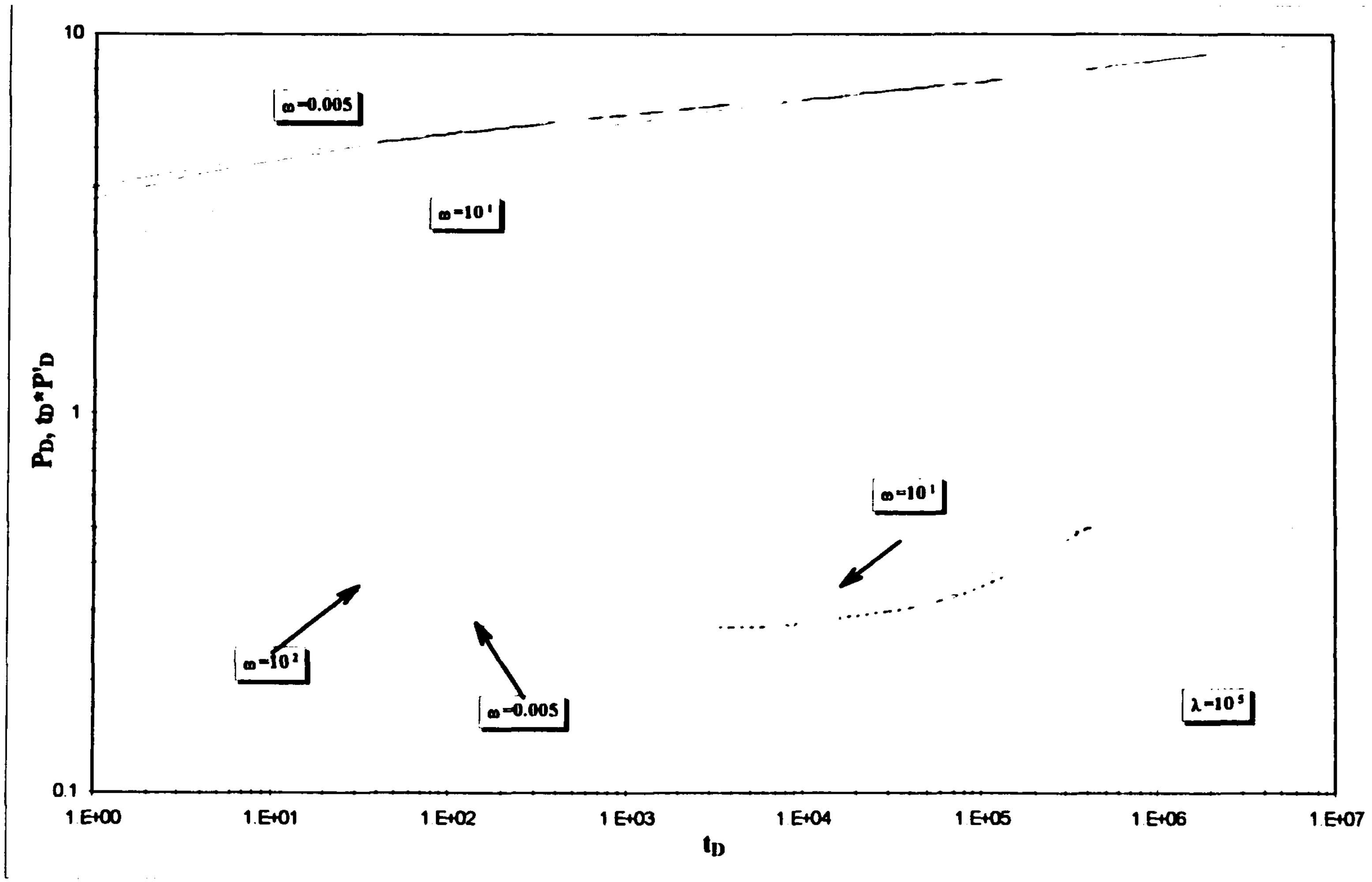

Figure 3.5.6 Effect of storage coefficient on the pressure response in a single-layer infinite-acting, naturally fractured reservoir with transient matrix flow in a sugar-cube system.

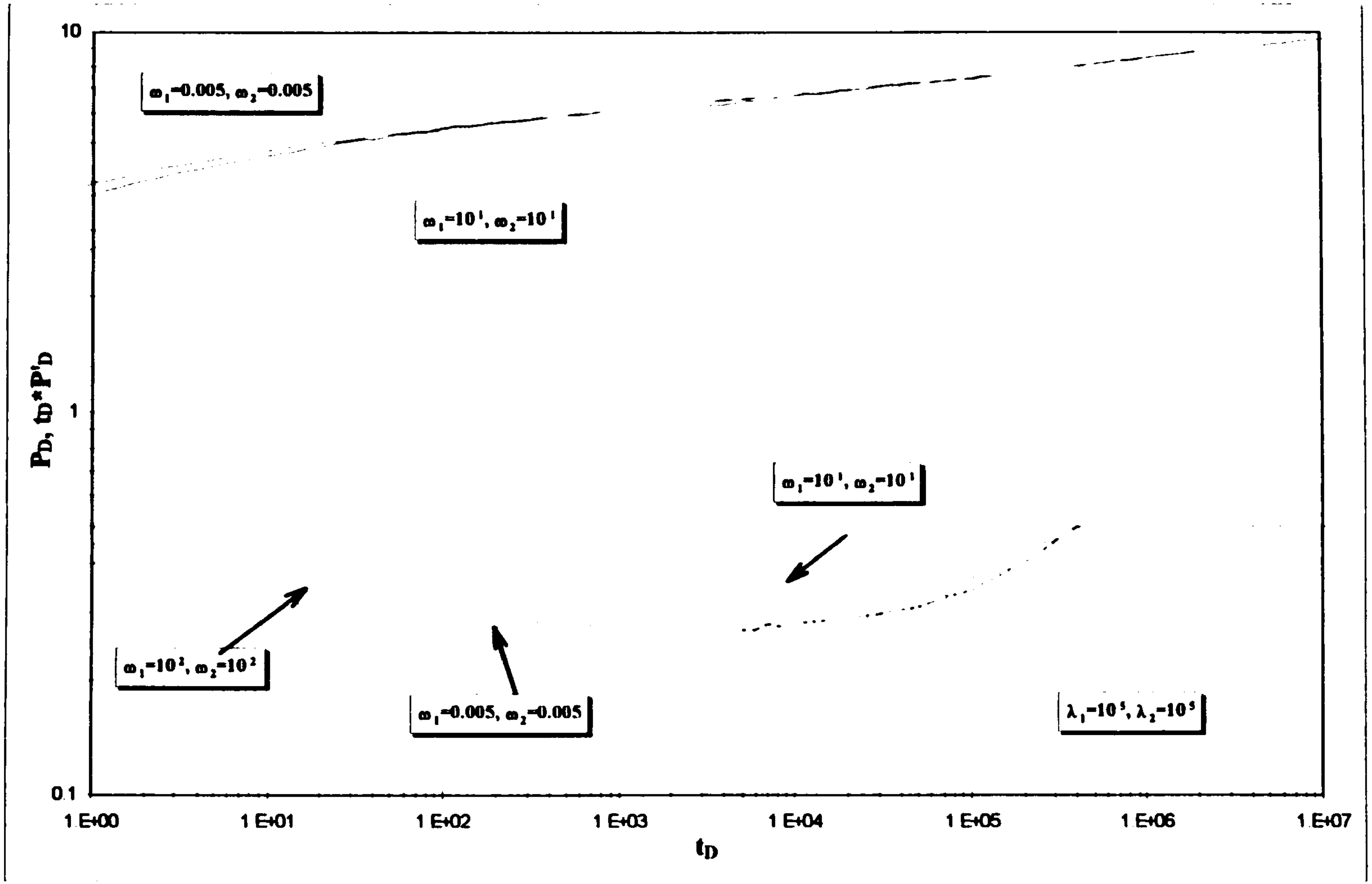

Figure 3.5.7 Effect of storage coefficient on the pressure response in a two-layer infinite-acting, naturally fractured reservoir with transient matrix flow in a sugar-cube system.

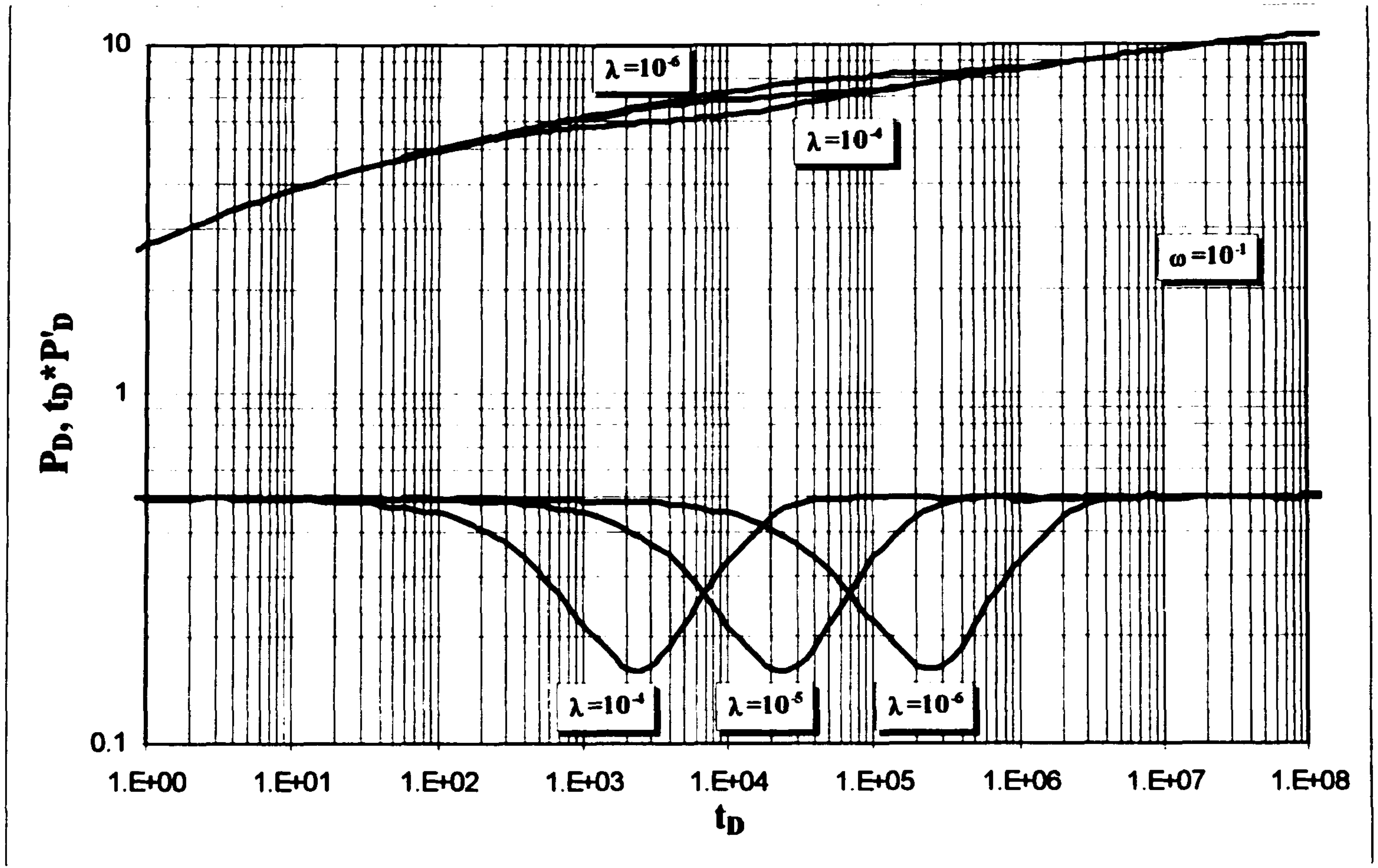

Figure 3.5.8 Effect of interporosity flow parameter on the pressure response in a single-layer infinite-acting, naturally fractured reservoir with pseudosteady state interporosity flow.

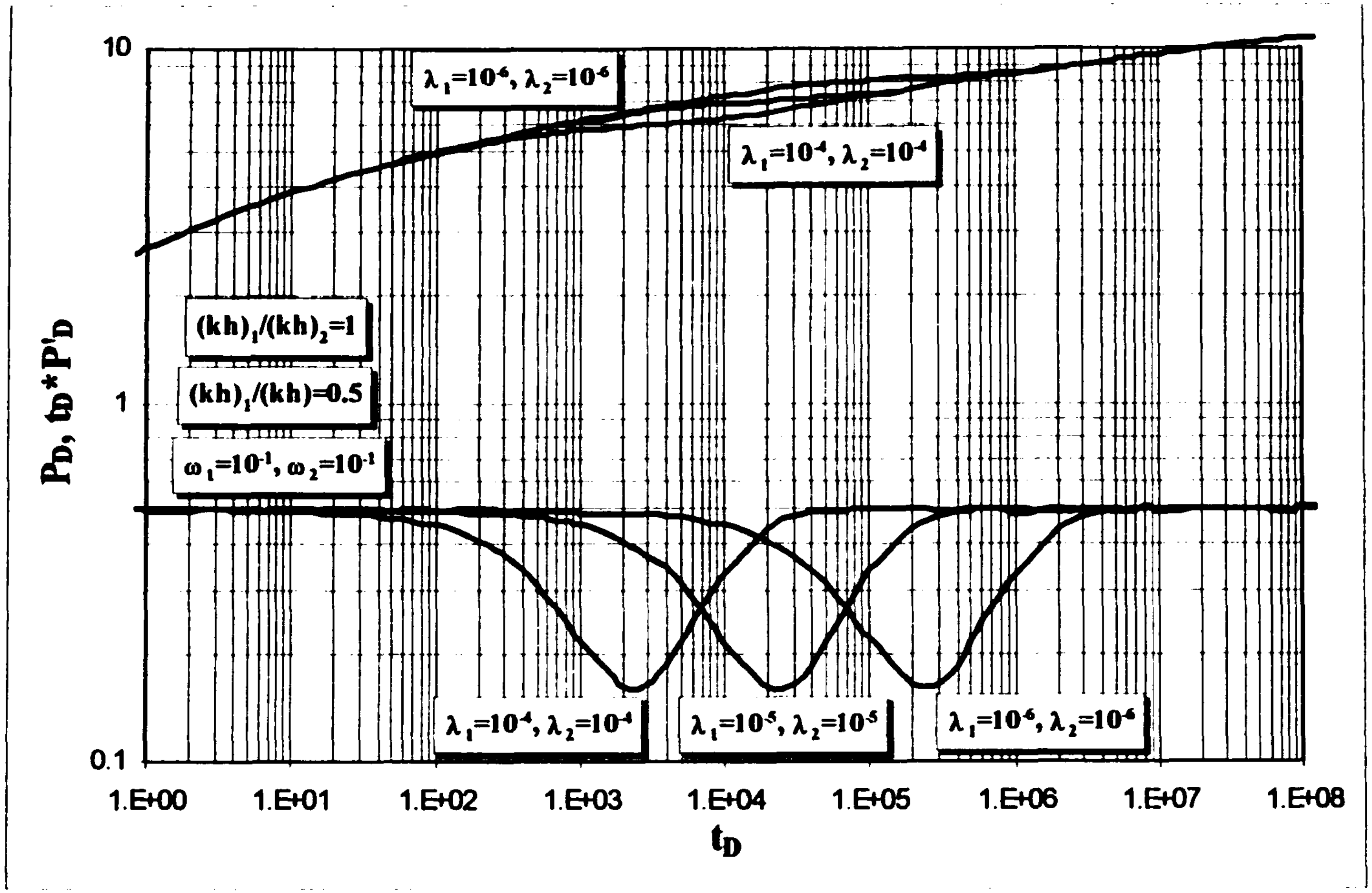

Figure 3.5.9 Effect of interporosity flow parameter on the pressure response in a two-layer infinite-acting, naturally fractured reservoir with pseudosteady state interporosity flow.

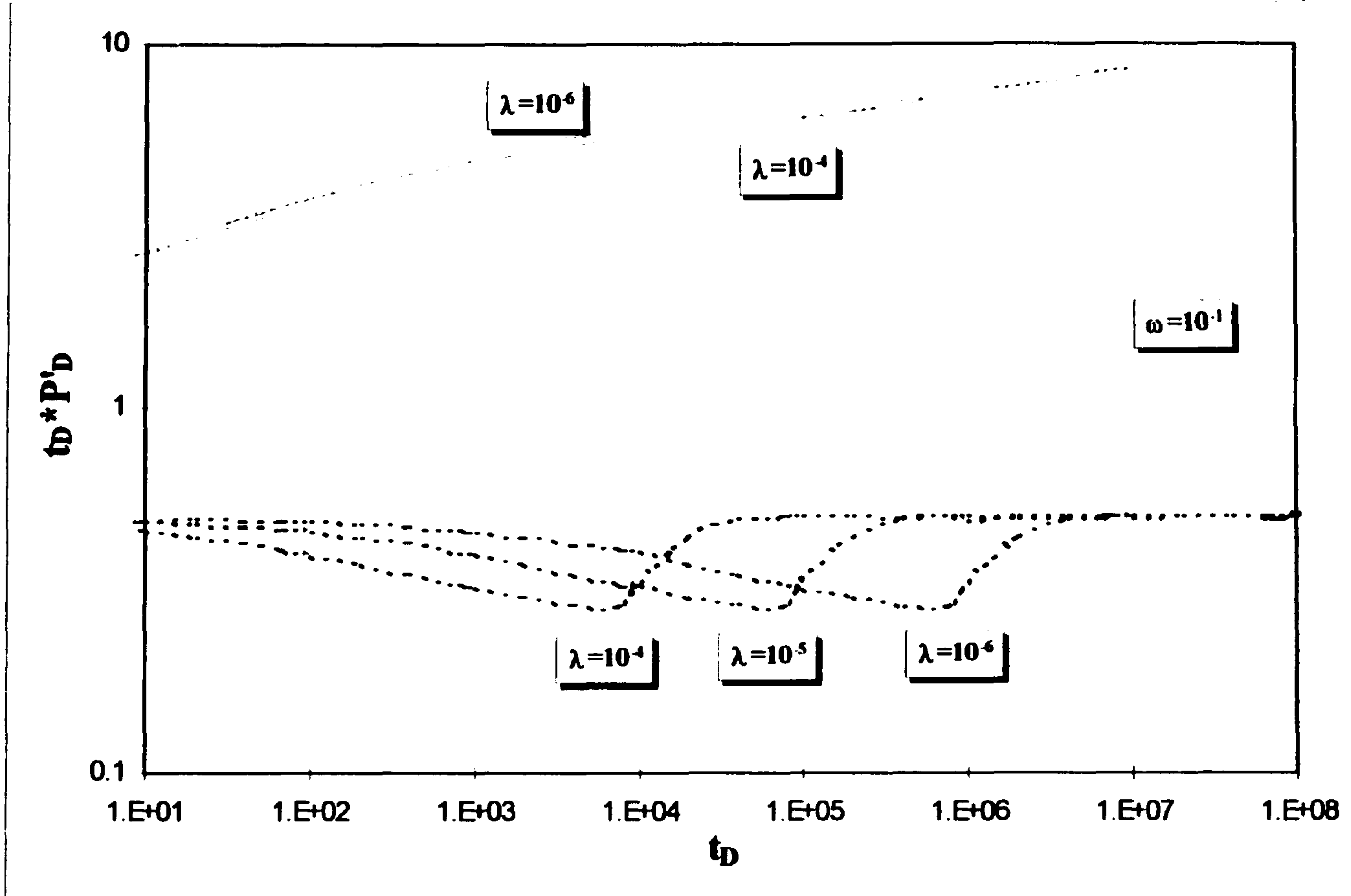

Figure 3.5.10 Effect of interporosity flow parameter on the pressure response in a single-layer infinite-acting, naturally fractured reservoir with transient matrix flow in a slab system.

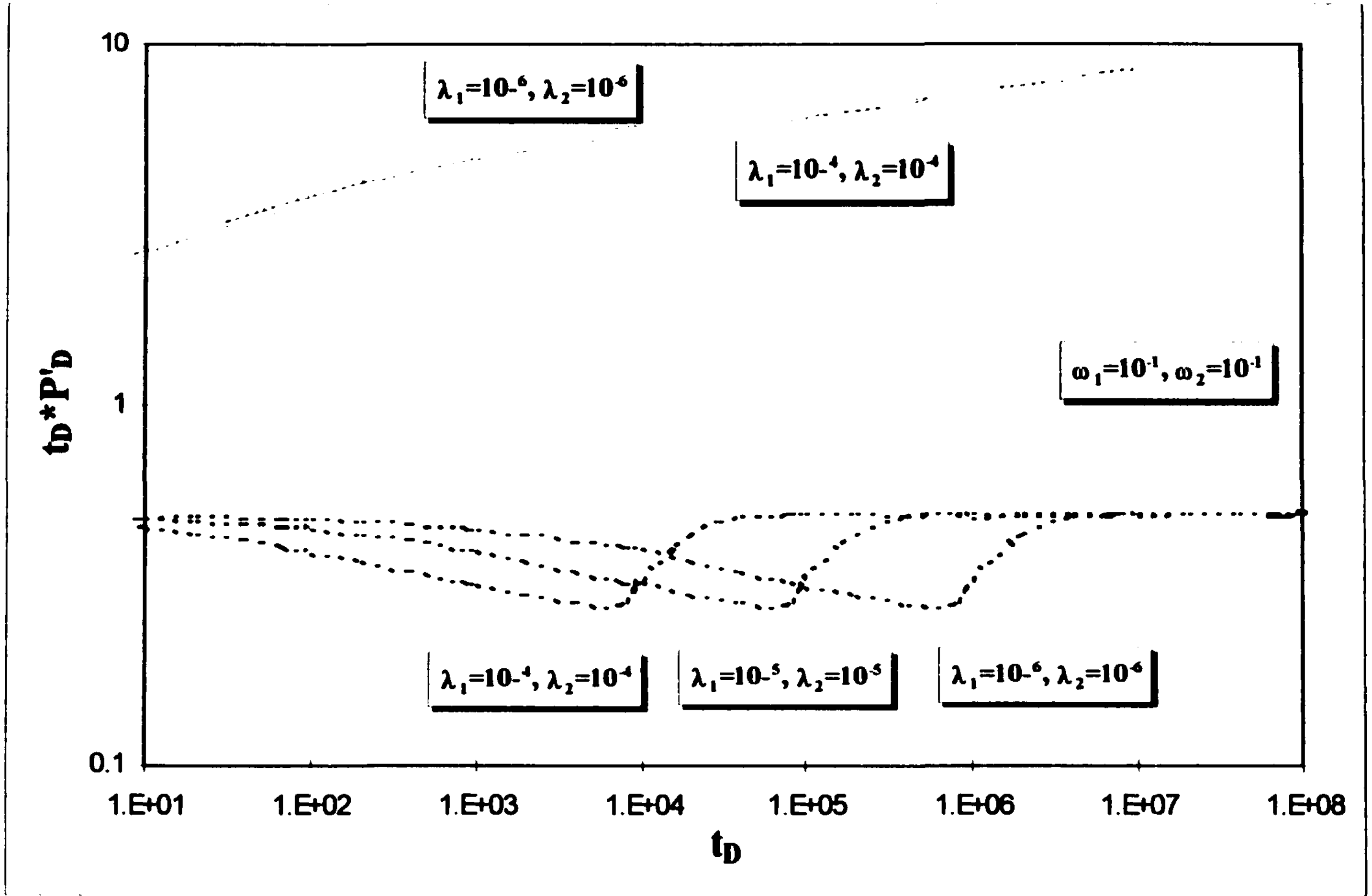

Figure 3.5.11 Effect of interporosity flow parameter on the pressure response in a two-layer infinite-acting, naturally fractured reservoir with transient matrix flow in a slab system.

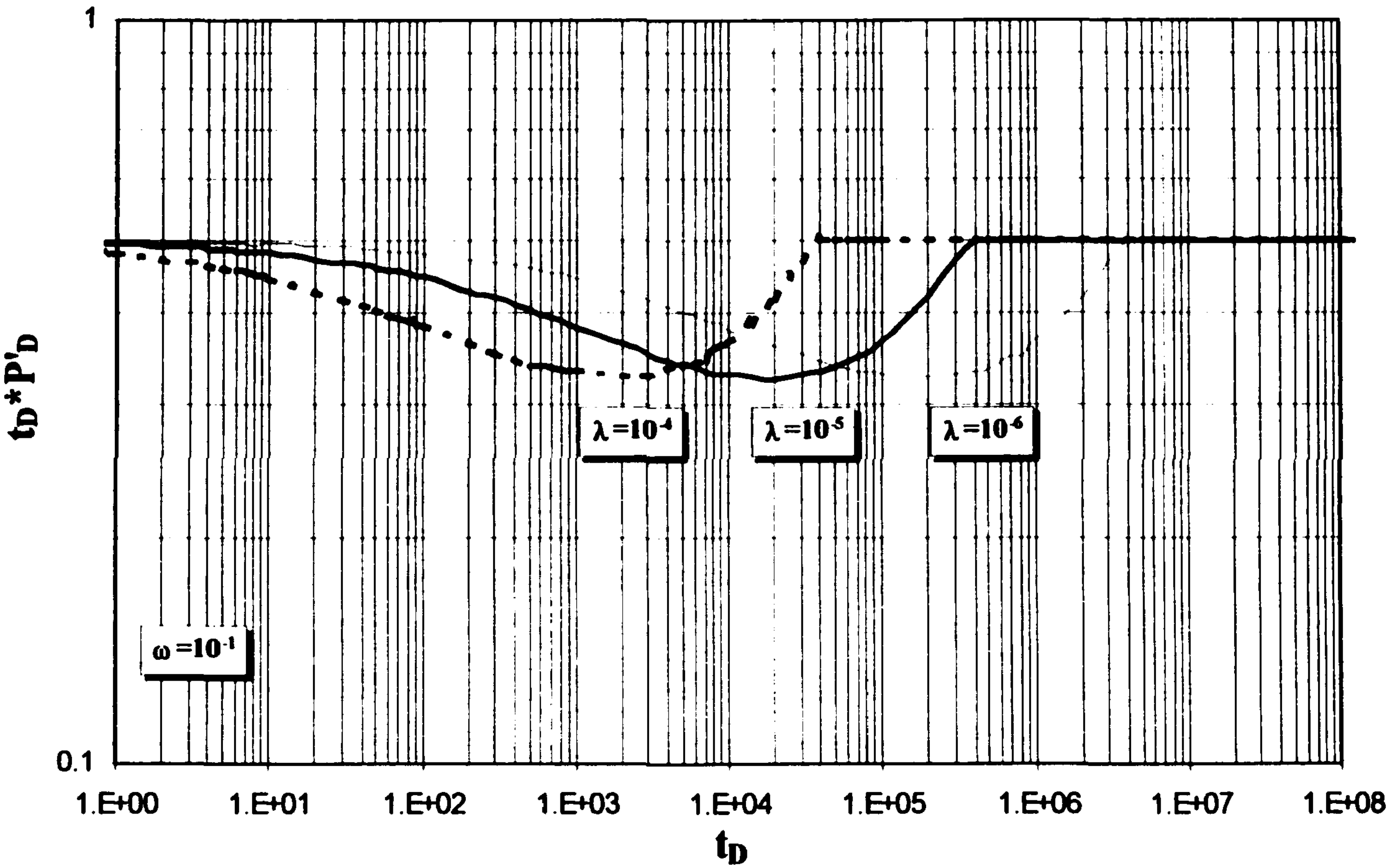

Figure 3.5.12 Effect of interporosity flow parameter on the pressure response in a single-layer infinite-acting, naturally fractured reservoir with transient matrix flow in a sugar-cube system.

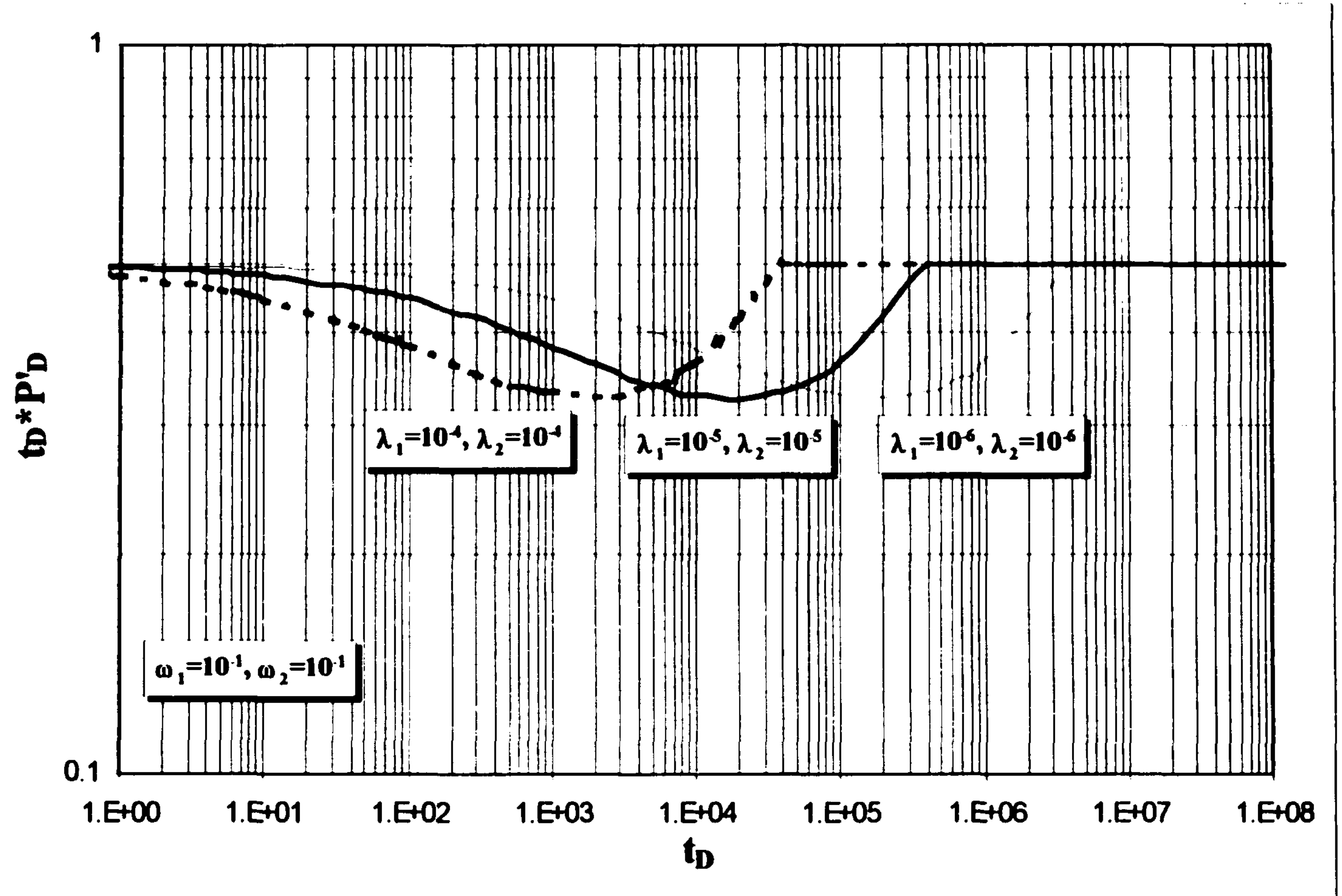

Figure 3.5.13 Effect of interporosity flow parameter on the pressure response in a two-layer infinite-acting, naturally fractured reservoir with transient matrix flow in a sugar-cube system.

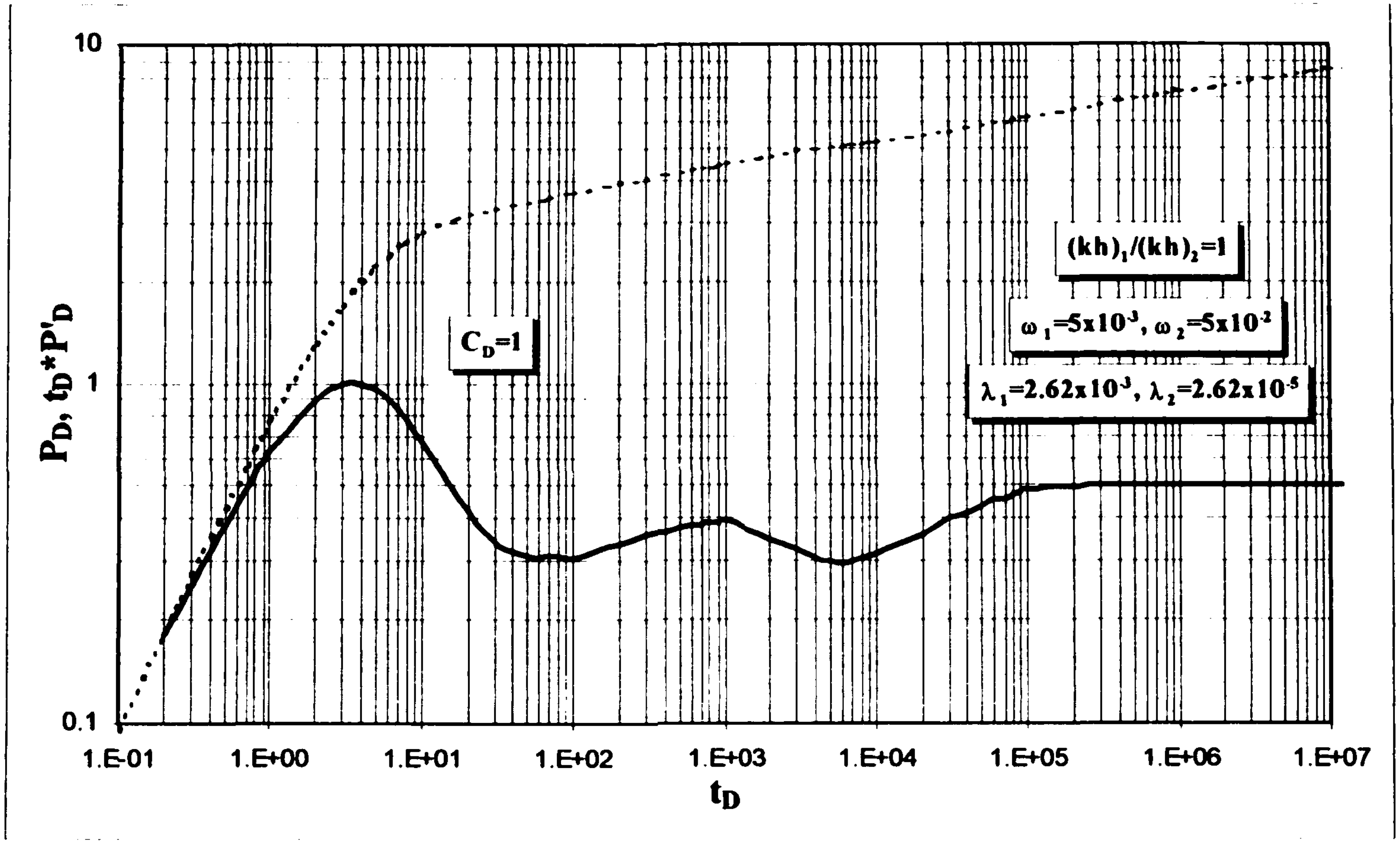

Figure 3.5.14 Characteristics of pressure and pressure derivative response in a two-layer infinite-acting, naturally fractured reservoir with pseudosteady state interporosity flow, $\omega_1=5\times10^{-2}$, $\omega_2=5\times10^{-3}$ and $\lambda_1=2.62\times10^{-3}$ and $\lambda_2=2.62\times10^{-5}$. Wellbore storage=1, $\frac{(kh)_1}{(kh)_2}=1$.

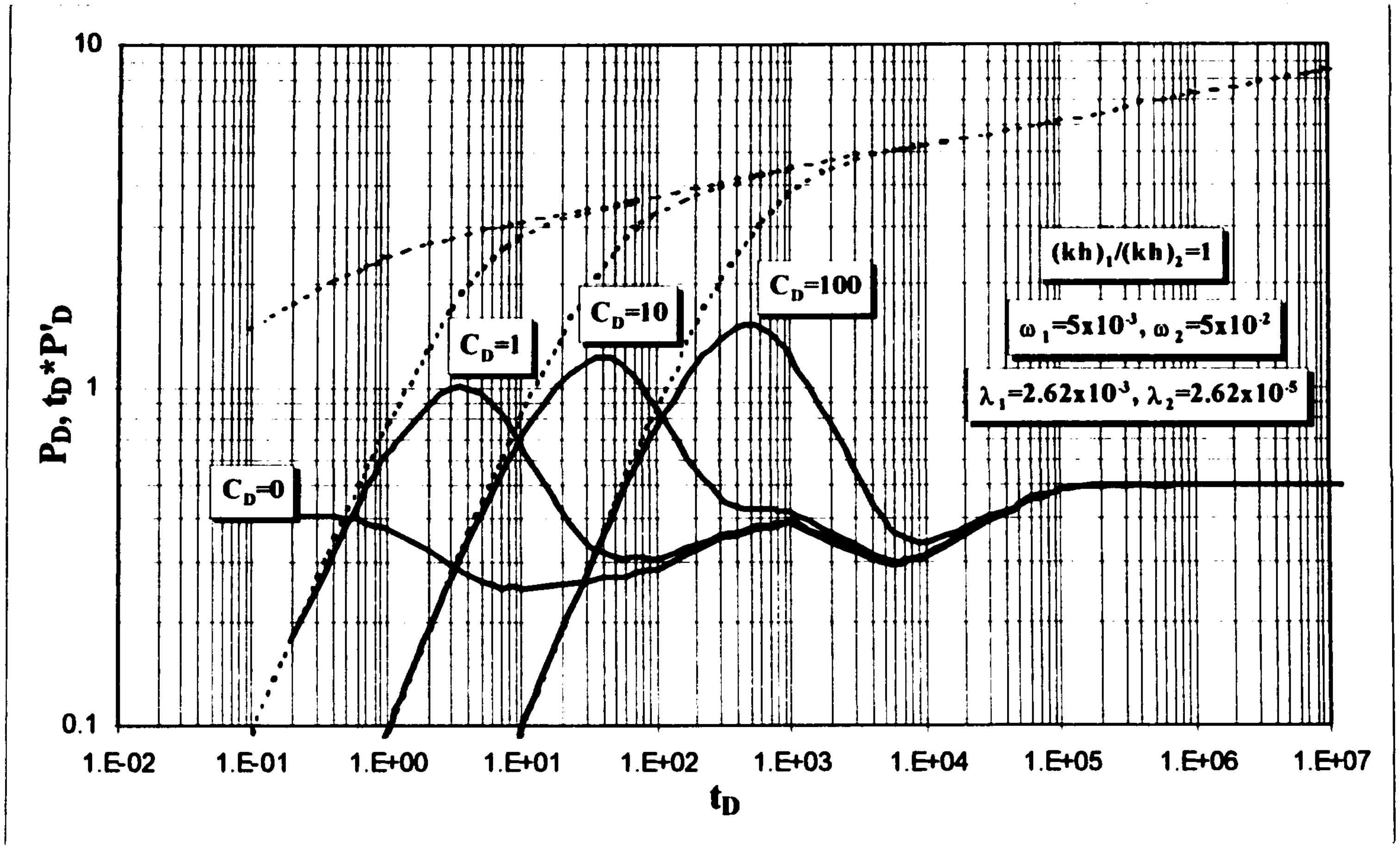

Figure 3.5.15 Characteristics of pressure and pressure derivative response in a two-layer infinite-acting, naturally fractured reservoir with pseudosteady state interporosity flow, $\omega_1=5x10^{-2}$, $\omega_2=5x10^{-3}$ and $\lambda_1=2.62x10^{-3}$ and $\lambda_2=2.62x10^{-5}$, for various values of wellbore storage, $\frac{(kh)_1}{(kh)_2} = 1$

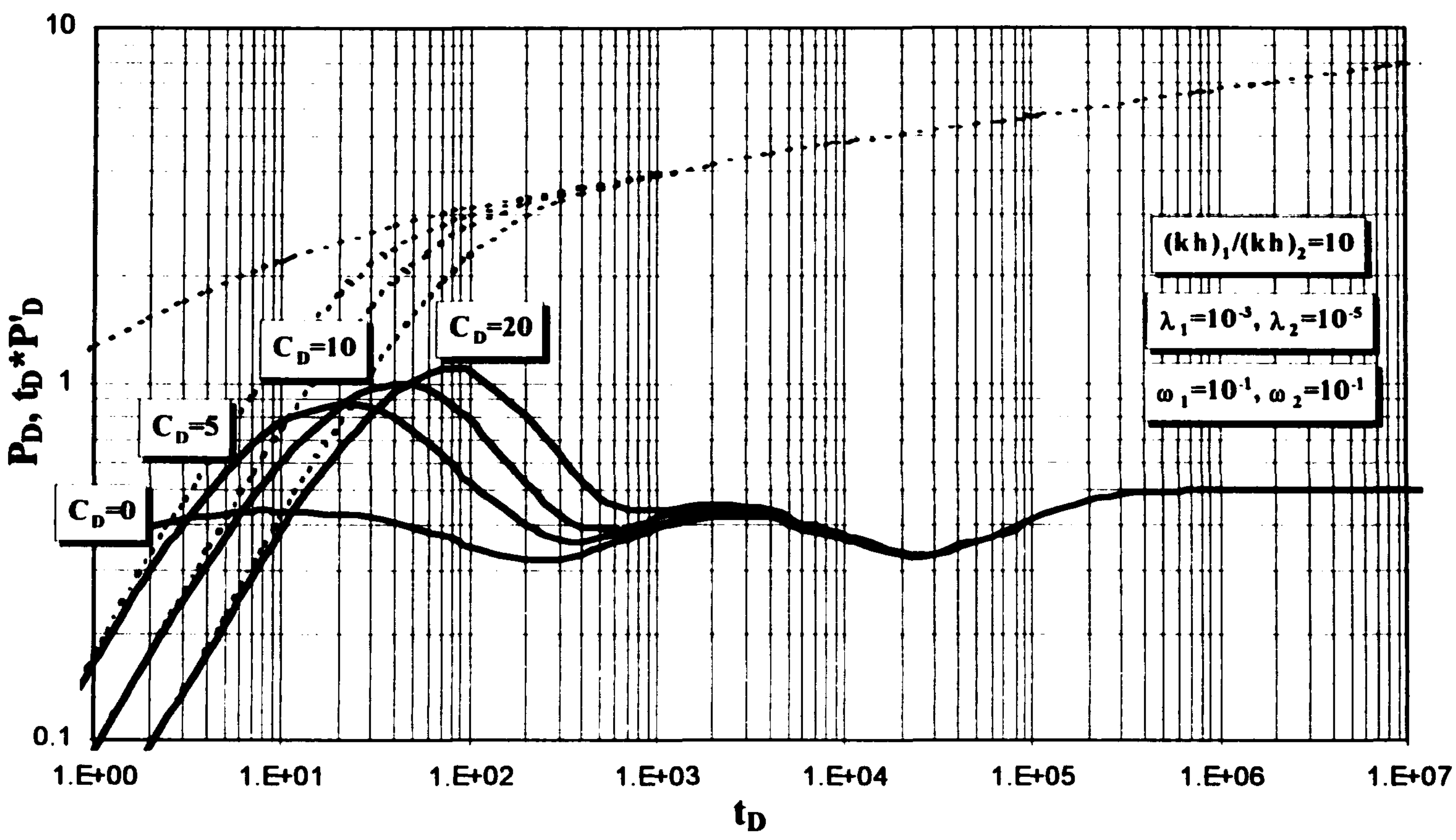

Figure 3.5.16 Characteristics of pressure and pressure derivative response in a two-layer infinite-acting, naturally fractured reservoir with pseudosteady state interporosity flow, $\omega_1=\omega_2=0.1$ and $\lambda_1=10^{-3}$ and $\lambda_2=10^{-5}$, for various values of wellbore storage, $\frac{(kh)_1}{(kh)_2}=10$.

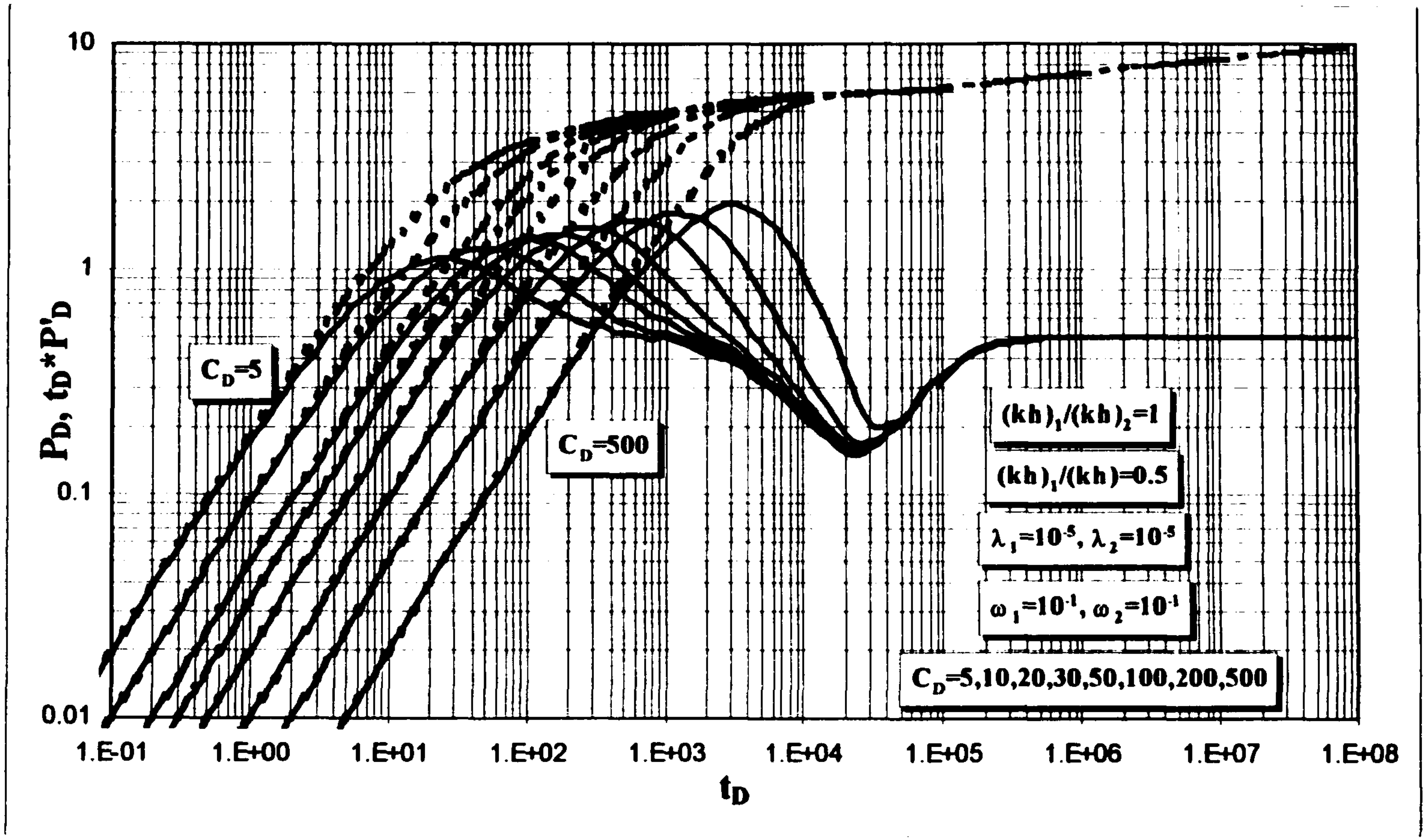

Figure 3.5.17 Characteristics of pressure and pressure derivative response in a two-layer infinite-acting, naturally fractured reservoir with pseudosteady state interporosity flow, $\omega_1=\omega_2=0.1$ and $\lambda_1=\lambda_2=10^{-5}$, for various values of wellbore storage, $\frac{(kh)_1}{(kh)_2} = 1$.

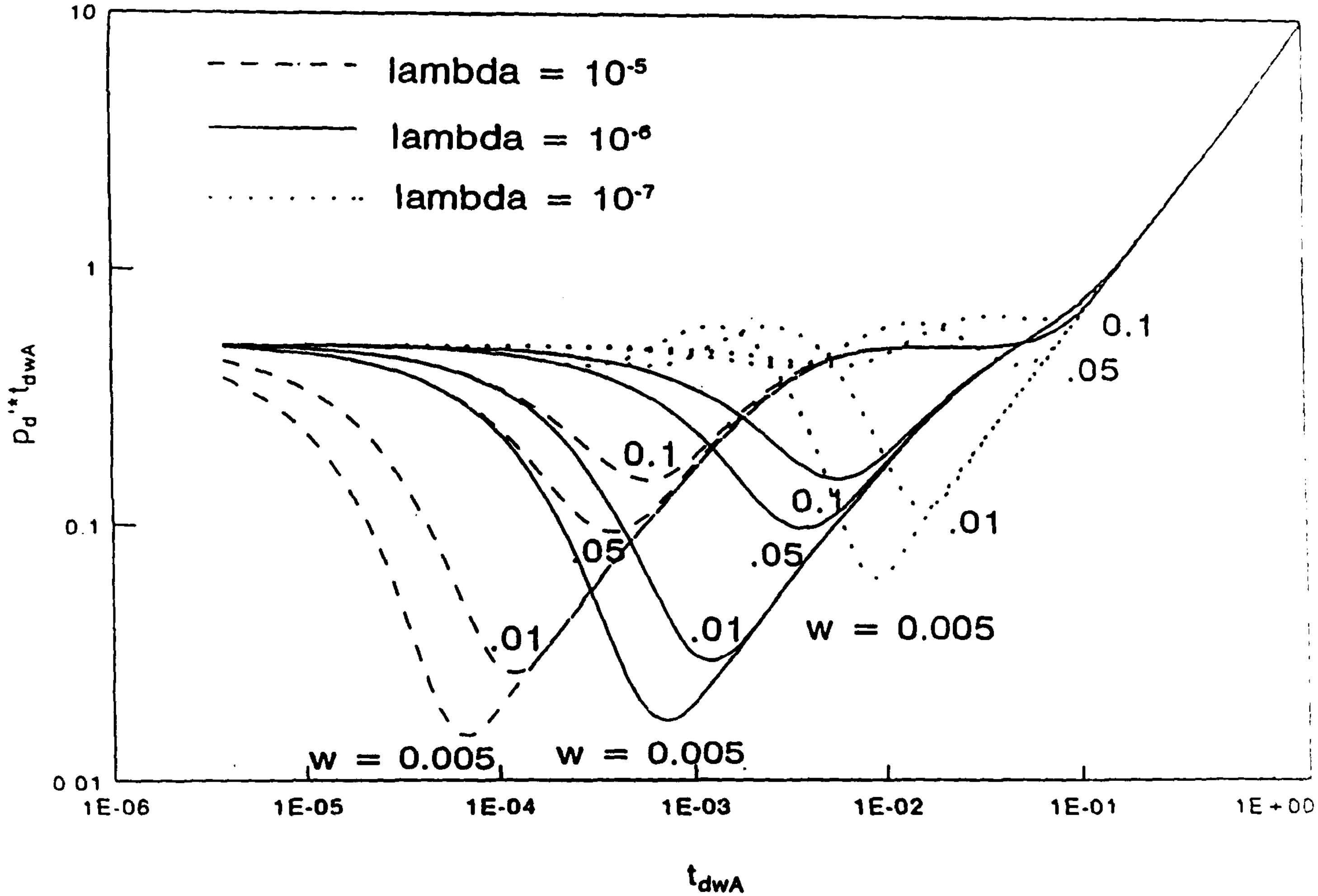

Figure 3.7.1 Effect of storage coefficient and interporosity flow parameter on the pressure response in a bounded reservoir[63], r_{ed}=3520.

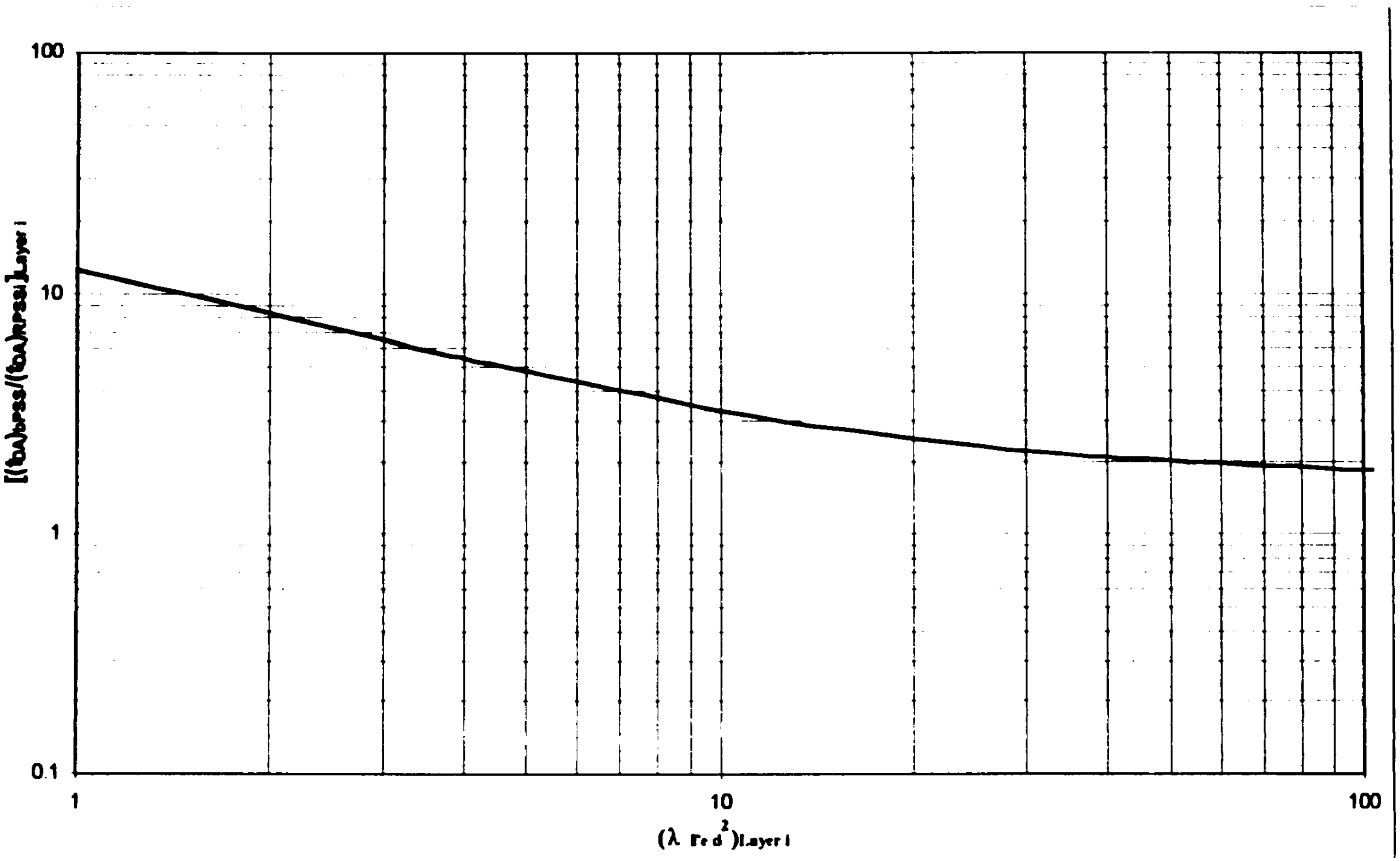

Figure 3.7.2 Correlation of the beginning of Pseudo-steady state flow period with interporosity flow parameter and drainage radius.

CHAPTER 4

APPLICATION OF TIAB'S DIRECT SYNTHESIS TO SINGLE LAYER DOUBLE POROSITY RESERVOIR WITH VERTICAL FRACTURE

Much natural gas and oil cannot be recovered from tight low pressure reservoirs because of formation damage from drilling fluids. Further, some reservoirs have low effective permeability and require some types of stimulation treatment to improve the performance and achieve commercial production rates. Most tight reservoirs are naturally fractured[81]. Tight formations are characterized by permeabilities less than 10 md. The permeability is usually less than 1 md and is often less than 0.1 md[66]. Knowledge of the reservoir permeability is considered essential for the preparation of an appropriate fracture stimulation design. Hydraulic fracturing is one of the stimulation methods which is used to eliminate the damage zone caused by mud filtration and redistribution of stresses during drilling around the wellbore. This method is also used in oil wells which are low in permeability. Hydraulic fracturing is a process by which a large surface area of the low-permeability formation is exposed to flow of fluid towards the wellbore. Furthermore, it is evident that if this process is performed effectively, it might drastically increase productivity. For the purpose of design fracture, damage radius, r_s, is critical. Appendix F presents a method for estimating r_s using drilling data.

The purpose of this chapter is to apply Tiab's Direct Synthesis Technique to a vertically fractured reservoir with double porosity. Below, a mathematical model for the pressure behavior of a well crossed by a uniform-flux or infinite-conductivity vertical fracture located in a bounded square is presented and investigated. This technique dose not require a priori knowledge of the fracture nature (uniform-flux or infinite-conductivity). This method gives direct estimates of fracture and reservoir characteristics without type curve matching. It was found that pressure and pressure derivative are mainly controlled by the fracture extension into the formation. The nature of the fracture has minor effects on pressure derivative. The nature of the fracture affects only the time to the end of the fracture linear flow period. The main applications of the proposed technique in this study are to determine the reservoir properties and fracture-half length.

The vertically fractured well is located at the center of a closed rectangular reservoir. Both uniform-flux and infinite-conductivity vertical fractures will be discussed. The usual assumptions apply; i.e., the porous media is isotropic, horizontal, uniform in thickness, and has constant fractured permeability. Also, it considers that the vertically fractured well is producing at a constant flow rate in a bounded reservoir that contains a slightly compressible fluid of a constant viscosity. The fracture fully penetrates the vertical extent of the formation and is the same length in both sides of the well. In addition, it is convenient to assume gravity effects are negligible, and flow entering the wellbore comes only through the fracture. The unit system is shown schematically in Figure 4.1.1, and Figure 4.1.2 presents the plane view for a hydraulically-fractured well. Under the assumption of pseudo-steady state for inter-porosity flow between the matrix and fracture systems, the dimensionless variables and analytical solution for wells in double porosity reservoirs with hydraulic fractures are discussed in Appendix G. The Laplace transform solution for a fractured well in a closed rectangular double porosity reservoir ignoring wellbore storage and skin as presented by Liu and Yang[80] is:

$$\bar{p}_{wD} = \frac{B}{s} \tag{4.1.1}$$

where,

$$B = \frac{\pi}{2}\left\{\frac{\coth(F_o y_{eD})}{F_o} + 2\sum_{n=1}^{\infty}\frac{1}{(n\pi x_{fD})^2}\sin^2(n\pi x_{fD})\cos(n\pi x_D)\frac{\coth(F_n y_{eD})}{F_n}\right\} \tag{4.1.2}$$

and

$$F_n = \left[s f(s) + (n\pi)^2\right]^{1/2} \tag{4.1.3}$$

This work is restricted to the behavior of a single fractured well in the center of a closed square reservoir; therefore:

$$x_e = y_e \tag{4.1.4}$$

Equation G.43, in Appendix G, is the Laplace transform solution for a fractured well in a closed rectangular double porosity reservoir including skin as given by Liu and Yang[80].

4.1 Uniform-Flux Fracture in Closed Systems

Figures 4.1.3 through 4.1.6 illustrate a log-log plot of the pressure and pressure derivative group versus dimensionless time for various values of $\left(\frac{x_e}{x_f}\right)$ in a single-layer square, naturally fractured reservoir with pseudo-steady state interporosity flow, ω=0.01 and λ=100. Both wellbore storage and skin are ignored. These curves show the characteristic pressure and pressure derivative behaviors. These figures illustrate the existence of three flow regimes: (1) the linear flow line of slope 0.5, (2) infinite-acting radial flow line of a horizontal straight line, and (3) pseudo-steady state flow line of slope unity, in addition to the transition region. The advantage of these analytically produced type curves over the previously published work is the addition of the pressure derivative. These curves of pressure derivative can be used to interpret pressure transient tests in fractured wells without using a type curve matching method. This can be done by applying Tiab's Direct Synthesis Technique to allow the estimation of the fracture-half length, x_f, and fracture permeability, k_f.

4.1.1 Fracture Linear Flow Period: at very small values of dimensionless time, fracture linear flow period behavior occurs and is exhibited in all cases. During this flow period, the effect of the matrix is negligible. The flow is essentially caused by expansion of the fluid within the fracture network, and the flow behavior is linear. The dimensionless pressure equation corresponding to this time as derived by Liu and Yang[80] is:

$$p_{wD} \approx A\sqrt{\frac{\pi t_{DA}}{\omega}} \qquad (4.1.5)$$

where,

$$A = 1 + 2\sum_{n=1}^{\infty} \frac{1}{(n\pi x_{fD})^2} \sin^2(n\pi x_{fD}) \qquad (4.1.6)$$

Equation 4.1.5 can be approximated to:

$$p_{wD} \approx \left(\frac{x_e}{x_f}\right)\sqrt{\frac{\pi t_{DA}}{\omega}} \qquad (4.1.7)$$

Table 4.1.1 compares Equation 4.1.7 with the Laplace solution using the developed computer model. This comparison yields excellent agreement. For homogeneous reservoirs, ω=1.

The derivative of Equation 4.1.5 with respect to dimensionless time is:

$$t_{DA} * p'_{wD} = \frac{\sqrt{\pi}}{2\sqrt{\omega}}\left(\frac{x_e}{x_f}\right)\sqrt{t_{DA}} \qquad (4.1.8)$$

Taking the logarithm of both sides of the above equation and substituting for the dimensionless terms yields:

$$\log(t * \Delta p'_w) = \frac{1}{2}\log(t) + \log[m_L] \qquad (4.1.9)$$

where,

$$m_L = \left[\frac{2.0324 q_t B}{\sqrt{\omega} h}\sqrt{\frac{\mu}{(\phi c_t)_t k_f x_f^2}}\right] \qquad (4.1.10)$$

As expected, a log-log plot of $(t * \Delta p'_w)$ versus time will yield a straight line of slope equal to one half, which is a unique characteristic of the linear flow period. Then, Equation 4.1.9 becomes:

$$(t * \Delta p'_w)_{L1} = \frac{2.032 q_t B}{\sqrt{\omega} h} \sqrt{\frac{\mu}{k_f (\phi c_t)_t x_f^2}} \tag{4.1.11}$$

where $(t * \Delta p'_w)_{L1}$ is the value of $(t * \Delta p'_w)$ at time one hour on the linear flow straight line. Rearranging Equation 4.1.11, then the fracture length, x_f, is:

$$x_f = \frac{2.032 q_t B}{(t * \Delta p'_w)_{L1} \sqrt{\omega} h} \sqrt{\frac{\mu}{k_f (\phi c_t)_t}} \tag{4.1.12}$$

Combining Equations 4.1.7 and 4.1.8, a new expression can be formulated:

$$(\Delta p_w)_{L1} = 2 * (t * \Delta p'_w)_{L1} \tag{4.1.13}$$

where $(\Delta p_w)_{L1}$ is the value of (Δp_w) at time one hour on the fracture linear flow straight line. Unfortunately, some noise will always be present in pressure derivative curves when actual data are being differentiated, because of gauge resolution and vibrations. In such a case, Equation 4.1.13 is a very useful expression, from which $(t * \Delta p'_w)_{L1}$ can be calculated knowing the value of $(\Delta p_w)_{L1}$. Then, draw a straight line of slope 0.5 across the $(t * \Delta p'_w)_{L1}$ point and parallel to the pressure straight line which also has a slope of 0.5. The fracture length, x_f, can be determined from the pressure line as:

$$x_f = \frac{4.064 q_t B}{(\Delta p_w)_{L1} \sqrt{\omega} h} \sqrt{\frac{\mu}{k_f (\phi c_t)_t}} \tag{4.1.14}$$

4.1.2 Pseudoradial Flow Period: The infinite-acting radial flow portion of the pressure derivative is a horizontal straight line. Figure 4.1.4 illustrates the characteristic pressure derivative behavior response in vertically fractured reservoir with double porosity. On this figure, the characteristic points and lines available for evaluating the pressure test can be identified. The figure shows that this flow period is dominant only if $\left(\frac{x_e}{x_f}\right) > 8$. The same condition has been observed by Tiab[32] for the case of vertically fractured wells in closed, homogeneous systems. The equation for the pressure derivative during this flow period is:

$$t_{DA} * p'_{wD} = 0.5 \tag{4.1.15}$$

Substituting the dimensionless pressure and dimensionless time in the above equation yields:

$$(t * \Delta p'_w)_R = \frac{70.6 q_t B \mu}{k_f h} \tag{4.1.16}$$

where the subscript R stands for radial flow line. Rearranging Equation 4.1.16 to solve for the permeability gives:

$$k_f = \frac{70.6 q_t B \mu}{(t * \Delta p'_w)_R h} \tag{4.1.17}$$

The radial flow period is influenced by the skin, which can be calculated using the following equation:

$$S = 0.5\left[\frac{(\Delta p_w)_R}{(t * \Delta p'_w)_R} - \ln\left(\frac{k_f t_R}{(\phi c_t)_t \mu r_w^2}\right) + 7.43\right] \tag{4.1.18}$$

where t_R is any convenient time during the infinite-acting radial flow line and $(\Delta p_w)_R$ is the value of (Δp_w) corresponding to t_R.

4.1.3 Pseudosteady State Flow Period: Applying the direct type curve synthesis technique to a vertically fractured well inside a closed system reveals a unit slope straight line, called the pseudosteady state flow regime.

$$t_{DA} * p'_{wD} = 2\pi t_{DA} \tag{4.1.19}$$

where,

$$t_{DA} = \frac{0.0002637k_f}{(\phi c_t)_t \mu A} \tag{4.1.20}$$

Taking the logarithm of both sides of Equation 4.1.19 and substituting for the dimensionless terms yields:

$$\log(t * \Delta p'_w) = \log(t) + \log\left[\frac{q_t B}{4.27h(\phi c_t)_t A}\right] \tag{4.1.21}$$

At t=1 hr:

$$(t * \Delta p'_w)_{PSS1} = \frac{q_t B}{4.27h(\phi c_t)_t A} \tag{4.1.22}$$

where the subscript PSS1 stands for the pseudosteady state flow regime at t=1 hr. Rearranging Equation 4.1.22 to solve for the drainage area:

$$A = \frac{q_t B}{4.27(t * \Delta p'_w)_{PSS1} h(\phi c_t)_t} \tag{4.1.23}$$

The shape factor, C_A, can be solved using the equation presented by Tiab[32]:

$$C_A = 2.2458\left(\frac{x_e}{x_f}\right)^2 \mathrm{Exp}\left[\left(\frac{0.000527kt_{PSS}}{(\phi c_t)_t \mu A}\right)\left(1-\frac{(\Delta p_w)_{PSS}}{(t*\Delta p'_w)_{PSS}}\right)\right] \tag{4.1.24}$$

where t_{PSS} is any convenient time during the pseudosteady state flow line. $(\Delta p_w)_{PSS}$ and $(t*\Delta p'_w)_{PSS}$ are values of (Δp_w) and $(t*\Delta p'_w)$ corresponding to t_{PSS}, respectively.

4.1.4 The Point of Intersection: The pressure derivative lines for various flow regimes will intersect at specific points. Direct synthetic technique provides a means of using these specific points to identify reservoir parameters.

A- The intersection point between the linear flow line and the infinite-acting radial flow line is described by:

$$(t_{DA})_{LRi} = \frac{\omega}{\pi}\left(\frac{x_f}{x_e}\right)^2 \tag{4.1.25}$$

where the subscripts L, R and i stand for linear flow period, radial flow period, and intersection respectively. Substitution for dimensionless time gives:

$$\left(\frac{x_f}{x_e}\right)^2 \frac{A}{k_f} = \frac{t_{LRi}}{1207.1(\phi c_t)_t \mu\omega} \tag{4.1.26}$$

Assuming a square geometry, i.e., $x_e = y_e$ where:

$$A = x_e^2 \tag{4.1.27}$$

Then,

$$\frac{x_f^2}{k_f} = \frac{t_{LRi}}{1207.1(\phi c_t)_t \mu\omega} \tag{4.1.28}$$

B- The intersection point between the linear flow line and pseudosteady state flow line is:

$$(t_{DA})_{LPSSi} = \frac{1}{16\pi\omega}\left(\frac{x_e}{x_f}\right)^2 \tag{4.1.29}$$

where the subscript LPSSi stands for the intersection point between the linear flow line and pseudosteady state flow line. Substitution for dimensionless time in Equation 4.1.29 yields:

$$\left(\frac{x_e}{x_f}\right)^2 \frac{k_f}{A} = \frac{75.44(\phi c_t)_t \mu}{\omega t_{LPSSi}} \tag{4.1.30}$$

Substituting Equation 4.1.27 into the above equation produces:

$$k_f x_f^2 = \frac{75.44(\phi c_t)_t \mu A^2}{\omega t_{LPSSi}} \tag{4.1.31}$$

C- The intersection point between the radial flow line and pseudosteady state flow line is described by:

$$(t_{DA})_{RPSSi} = \frac{1}{4\pi} \tag{4.1.32}$$

where the subscript RPSSi stands for the intersection point between the radial flow line and pseudosteady state flow line. Substitution for dimensionless time in Equation 4.1.32; gives:

$$A = \frac{k_f t_{RPSSi}}{301.77(\phi c_t)_t \mu} \tag{4.1.33}$$

4.1.5 Characteristic Times: Characteristic times provide unique features for the analysis. The relationship of the characteristic times is described by combining Equations 4.1.25, 4.1.29, and 4.1.32. The new expression can be used for verification.

$$\frac{t_{LRi}}{t_{RPSSi}} = \frac{t_{RPSSi}}{t_{LPSSi}} = \left(\frac{t_{LRi}}{t_{LPSSi}}\right)^{1/2} = 4\omega\left(\frac{x_f}{x_e}\right)^2 \tag{4.1.34}$$

4.1.6 Influence of Wellbore Storage Effects: This section investigates the effect of wellbore storage upon the pressure and pressure derivative behavior of a well with constant surface flow rate on vertically fractured reservoirs. Under practical operating conditions, the initial production from a shut-in well originates from the volume of fluid stored in the wellbore. In tests of fractured wells in low permeability reservoirs, severe storage effects can be encountered. Figures 4.1.7 and 4.1.8 illustrate the effect of wellbore storage on pressure and pressure derivative responses in a vertically fractured reservoir with double porosity of pseudosteady state interporosity flow. These figures show how large and small after-flows affect the shape of the pressure and pressure derivative curves. In the case of a large wellbore storage, the typical behavior of fractured wells is hidden by a unit slope line. However, in the case of a low wellbore storage relative to the size of the fracture, the early time linear fracture of a slope 0.5 can still be observed. Houze[33] mentioned that in the case of high wellbore storage, the linear flow will be completely masked and the usual analysis methods with a low value of skin factor will be applicable. The relationship between x_f and the skin factor is:

$$S = -\ln\left(\frac{x_f}{2r_w}\right) \tag{4.1.35}$$

If the wellbore storage effect is observed, at an early time, then all the pressure and pressure curves merge to a line of slope equal to unity, corresponding to a pure wellbore storage effect. The pressure equation of this straight line given by

$$p_D = \frac{t_D}{C_D} \tag{4.1.36}$$

where C_D is well storage and defined as:

$$C_D = \frac{0.8935\,C}{h(\phi c_t)_t x_f^2} \tag{4.1.37}$$

Substituting the dimensionless variables in the right-hand-side of Equation 4.1.36, gives:

$$\frac{t_D}{C_D} = 2.95\mathrm{x}10^{-4}\,\frac{hk_f}{\mu}\left(\frac{t}{C}\right) \tag{4.1.38}$$

Substituting Equation 4.1.38 and the definition of dimensionless pressure into Equation 4.1.36 provides a solution for the wellbore storage:

$$C = \left(\frac{q_t B}{24}\right)\frac{t}{\Delta p} \tag{4.1.39}$$

where t and Δp are any convenient points on the unit slope line.

The equation of the unit slope line which corresponds to the pressure derivative is:

$$\left(\frac{t_D}{C_D}\right)p_D' = \frac{t_D}{C_D} \tag{4.1.40}$$

where the dimensionless pressure derivative is:

$$p_D' = \left(\frac{26.856h(\phi c_t)_t x_f^2}{q_t B}\right)\Delta p_w' \tag{4.1.41}$$

Then, the equation for the unit slope pressure derivative line can be expressed in real units as follows:

$$C = \left(\frac{q_t B}{24}\right)\frac{t}{(t * \Delta p_w')} \tag{4.1.42}$$

The following expression can be obtained from the intersection point of the unit slope line with the infinite-acting radial flow line:

$$\left(\frac{t_{D_{USRi}}}{C_D}\right) = 0.5 \tag{4.1.43}$$

Then, the wellbore storage in real units becomes:

$$C = \frac{hk_f\, t_{USRi}}{1695\mu} \tag{4.1.44}$$

4.1.7 Transition Period:

Figures 4.1.9 through 4.1.12 illustrate the effect of interporosity flow parameter, λ_f, and dimensionless storage coefficient, ω, on the pressure and the derivative responses in a single-layer, square, vertically fractured reservoir with pseudosteady state interporosity flow. In this case, the interporosity flow parameter, λ_f, is defined as:

$$\lambda_f = 12\, x_f^2 \frac{k_m}{k_f h_m} = \lambda \frac{x_f^2}{r_w^2} \tag{4.1.45}$$

These figures show that the transition occurs during the infinite-acting radial flow. As mentioned earlier, the dimensionless storage coefficient, ω, and interporosity flow parameter, λ, for pseudosteady state, transient matrix flow in a slab system and transient matrix flow in a sugar-cube system can be estimated by several methods previously developed by Engler[63].

If the transition occurs during the linear flow, there are two parallel lines of slope equal to 0.5. The first line is due to the expansion of the fracture network. This flow period is called "fracture storage dominated period" and is represented by Equation 4.1.12. The second line is at the total system dominated period. For this flow period, ω is equal to unity. Therefore, Equation 4.1.12 reduces to:

$$x_f = \frac{2.032 q_t B}{(t * \Delta p'_w)_{2L1} h} \sqrt{\frac{\mu}{k_f (\phi c_t)_t}} \tag{4.1.46}$$

where the subscript 2L1 stands for the linear flow period at the total system dominated period. A very useful equation can be derived if the two straight lines are present:

$$\omega = \left[\frac{(t * \Delta p'_w)_{2L1}}{(t * \Delta p'_w)_{L1}} \right]^2 \tag{4.1.47}$$

This equation is obtained by dividing Equation 4.1.46 by Equation 4.1.12 and can be used to estimate the parameter ω.

Figures 4.1.13 through 4.1.18 illustrate the above discussion. These figures show the effect of the storage coefficient on the pressure and pressure derivative responses in a vertically fractured reservoir with pseudosteady state interporosity flow where the transition occurs during the linear flow period. Next, Figures 4.1.19 through 4.1.21 illustrate the effect of the interporosity flow parameter on the pressure and pressure derivative responses.

Taking the second derivative of the dimensionless pressure equation 2.17, then the minimum derivative point occurs at $(t_{DA} * \Delta p'_{wD})' = 0$. Therefore, an analytic expression for the minimum dimensionless time can be estimated:

$$(t_{DA})_{min} = \frac{\omega}{\lambda} \ln\left(\frac{1}{\omega}\right) \tag{4.1.48}$$

Figure 4.1.22 shows the effect of the storage coefficient on the pressure derivative versus $\lambda_f t_D$ group in a vertically fractured reservoir with pseudosteady state interporosity flow. From this figure, the minimum coordinate of the group $(\lambda_f t_D)_{min}$ was estimated for various values of ω. As a conclusion, the values agree with Equation 4.1.48. However, Figure 16 in reference 81 has been presented for various values of λ and for ω=0.1. Ben Naceur[81] claimed that the value λ t_D of the minimum derivative hump is constant and approximately equal to 0.2. This is not quite right: it is true only for ω=0.1. This can be verified using Equation 4.1.48 and Figure 4.1.22. This figure shows the transition region (depression) in the pressure derivative for various values of ω. This figure gives the value λ t_D equal to 0.23 for ω=0.1. Thus, the obtained value at ω=0.1 agrees with Equation 4.1.48 and the value obtained by Ben Naceur[81].

Figure 4.1.23 shows the transition period occurs during the linear flow period and illustrates the unit slope derivative line. The analytic equation for this unit slope line during the late transition time is:

$$\ln(t_{DA} * p'_{wD})_{US} = \ln\left(\frac{\lambda (t_{DA})_{US}}{2}\right) \tag{4.1.49}$$

where the subscript US stands for unit slope derivative line. The late transition period unit slope line is a unique method for determining interporosity flow parameter, λ_f. The intersection point between the unit slope line with the infinite-acting line is:

$$\lambda_f = \frac{(\phi c_t)_t \mu x_f^2}{0.0002637 k_f t_{RUSi}} \tag{4.1.50}$$

where the subscript RUSi stands for the intersection point between the unit slope line with the infinite-acting line. The above equation is independent of the dimensionless storage coefficient, ω.

The intersection point between the unit slope line with the fracture storage dominated period linear flow line is:

$$\lambda_f = \left[\frac{\pi}{\omega}\frac{(\phi c_t)_t \mu x_f^2}{0.0002637 k_f t_{LUSi}}\right]^{1/2} \tag{4.1.51}$$

where the subscript LUSi stands for the intersection point between the unit slope line with the fracture storage dominated period linear flow line.

The intersection point between the unit slope line with the total system dominated period linear flow line where ω=1 is:

$$\lambda_f = \left[\frac{\pi \quad (\phi c_t)_t \mu x_f^2}{0.0002637 k_f t_{2LUSi}}\right]^{1/2} \tag{4.1.52}$$

where the subscript 2LUSi stands for the intersection point between the unit slope line with the total system dominated period linear flow line.

A very useful equation can be derived if the two linear straight lines are present. The parameter ω can be estimated by dividing Equation 4.1.52 by Equation 4.1.51:

$$\omega = \left[\frac{t_{2LUSi}}{t_{LUSi}}\right]^2 \tag{4.1.53}$$

4.2 Infinite-Conductivity Fracture in Closed Systems

In the infinite-conductivity case, the pressure within the fracture is assumed to be uniform. The pressure response would be the same as the solution of the uniform-flux case, measured at the $x_D=0.732x_f$. It has been shown by Gringarten and Ramey[82] that pressure drop on the fracture can be obtained at $x_D=0$ for uniform-flux, and at $x_D=0.732x_f$ for infinite-conductivity. This section extends the work in the previous section to an infinite-conductivity vertical fracture inside a square naturally fractured reservoir. Figures 4.2.1 and 4.2.2 show the pressure difference between the uniform-flux solution and the infinite-conductivity solution and their derivatives for the double porosity case. The pressure and pressure derivative curves obtained for the infinite-conductivity fracture are qualitatively the same as the uniform-flux solutions; only the shape is slightly different at intermediate times. Figure 4.2.3 illustrates a pressure derivative curve for an infinite-conductivity solution in a naturally fractured reservoir. The curve reveals a fourth dominated flow regime which can be identified by a straight line of slope 0.36. This flow period is called the bi-radial flow and can be used to estimate the fracture half length and permeability. This figure illustrates the existence of four flow regimes in addition to the transition region: (1) the linear flow line of slope 0.5,

(2) the bi-radial flow line of slope 0.36, (3) the infinite-acting radial flow line of a horizontal straight line, and (4) the pseudo-steady state flow line of slope unity. The characteristics of the other three flow periods (linear, radial and pseudosteady state) are the same as discussed earlier for the uniform-flux fracture. However, the characteristic of the bi-radial flow period will be discussed below.

4.2.1 Bi-Radial Flow Period

For homogeneous reservoirs, Tiab[32] presented the following dimensionless pressure derivative for a well intersected by a vertical fracture of infinite-conductivity in a square system:

$$p'_{wD} = 2\pi\left[1+2\sum_{n=1}^{\infty}\exp\left(-4n^2\pi^2 t_{DA}\right)\right]x\left[1+2\sum_{m=1}^{\infty}\exp\left(-4m^2\pi^2 t_{DA}\right)\left(\frac{\sin\left(m\pi\frac{x_f}{x_e}\right)}{m\pi\frac{x_f}{x_e}}\right)\cos\left(0.732m\pi\frac{x_f}{x_e}\right)\right] \qquad (4.2.1)$$

He obtained the same four flow regimes discussed earlier for the case of the infinite-conductivity fracture. Figure 4.2.4 shows the pressure difference between the uniform-flux solution and the infinite-conductivity solution for a homogeneous reservoir. Using the above equation, Figure 4.2.5 illustrates the pressure derivative difference between the uniform-flux solution and the infinite-conductivity solution for a homogeneous reservoir. Figure 4.2.6 illustrates a pressure derivative curve for an infinite-conductivity solution in a naturally fractured reservoir. This figure shows the existence of the bi-radial flow line.

As illustrated by Figures 4.2.1 through 4.2.6 and as indicated by Tiab[32] the bi-radial flow regime cannot be identified from the pressure function. Therefore, he presented an equation of the bi-radial flow period by using the pressure derivative as:

$$t_{DA} * p'_{wD} = 0.769\left(\frac{x_e}{x_f}\right)^{0.72} t_{DA}{}^{0.36} \tag{4.2.2}$$

Figures 4.2.7 and 4.2.10 show the pressure difference between the homogeneous and double porosity systems and their derivatives for the infinite-conductivity solution. These figures show that the double porosity flow curve is unique, corresponding to the homogeneous solution, and the total flow curves depend on the dimensionless storage coefficient, ω. Also, this can be observed from the study presented in the previous section. All the developed equations for the uniform-flux in a double porosity system can be reduced to the homogeneous system by setting ω equal to unity. As a direct consequence, Equation 4.2.2 can be improved for double porosity systems by replacing the dimensionless time in Equation 4.1.20 by:

$$t_{DA} = \frac{t_{DA}}{\omega} \tag{4.2.3}$$

Therefore, Equation 4.2.2 becomes:

$$t_{DA} * p'_{wD} = 0.769\left(\frac{x_e}{x_f}\right)^{0.72} \left(\frac{t_{DA}}{\omega}\right)^{0.36} \tag{4.2.4}$$

Taking the logarithm of both sides of the above equation and substituting for the dimensionless terms yields:

$$\log(t * \Delta p'_w) = 0.36\log(t) + \log[m_{BR}] \tag{4.2.5}$$

where,

$$m_{BR} = \left[\frac{5.589 q_t B\mu}{\omega^{0.36} k_f h}\left(\frac{x_e}{x_f}\right)^{0.72}\left(\frac{k_f}{(\phi c_t)_t \mu A}\right)^{0.36}\right] \tag{4.2.6}$$

As expected, a log-log plot of $(t * \Delta p'_w)$ versus time will yield a straight line of slope equal to 0.36, which is a unique characteristic of the bi-radial flow period, then Equation 4.2.5 becomes:

$$x_f = 10.914\frac{x_e}{\omega^{0.5}}\left(\frac{q_t B\mu}{(t * \Delta p'_w)_{BR1} k_f h}\right)^{1.389}\left(\frac{k_f}{(\phi c_t)_t \mu A}\right)^{0.5} \tag{4.2.7}$$

where $(t * \Delta p'_w)_{BR1}$ is the value of $(t * \Delta p'_w)$ at time one hour on the bi-radial flow straight line. Then, if the linear flow regime is not observed, the half-fracture length, x_f, can be estimated by using Equation 4.2.7.

4.2.2 The Point of Intersection: The intersection of pressure derivative lines for three flow regimes (linear, radial and pseudosteady state) with the bi-radial flow line can be used to identify reservoir parameters.

A- The intersection point between the bi-radial flow line and linear flow line is described by:

$$(t_{DA})_{LBRi} = 0.363\omega\left(\frac{x_f}{x_e}\right)^2 \tag{4.2.8}$$

where the subscripts L, BR and i stand for linear flow period, bi-radial flow period, and intersection respectively. Substitution for dimensionless time gives:

$$\frac{x_f^{\,2}}{k_f} = \frac{t_{LBRi}\,x_e^2}{1376.56(\phi c_t)_t\,\mu\omega A} \tag{4.2.9}$$

Substituting Equation 4.1.27 and assuming a square geometry, i.e. $x_e = y_e$, then,

$$\frac{x_f^2}{k_f} = \frac{t_{LBRi}}{1376.56(\phi c_t)_t\,\mu\omega} \tag{4.2.10}$$

However, for $\left(\dfrac{x_e}{x_f}\right) < 8$, the infinite-acting radial flow period is too short-lived or essentially non-existent. In this case, the fractured permeability can be estimated by combining Equations 4.1.12 and 4.2.10:

$$k_f = \frac{75.39 q_t B\mu}{\left(t * \Delta p'_w\right)_{L1} h} \frac{1}{\sqrt{t_{LBRi}}} \tag{4.2.11}$$

In summary, if the infinite-acting radial flow line is well defined, the fracture permeability, k_f, can be calculated from Equation 4.1.17. Then, if the linear flow line is dominant, determine the half-fracture length from Equation 4.1.12. However, if the bi-radial flow line is much more dominant than the linear flow line, determine the half-fracture length from Equation 4.2.7.

B- The intersection point between the bi-radial flow line and the infinite acting radial flow line is provided by:

$$(t_{DA})_{RBRi} = 0.3024\omega\left(\frac{x_f}{x_e}\right)^2 \tag{4.2.12}$$

where the subscripts BR, R and i stand for bi-radial flow period, radial flow period, and intersection respectively. Substitution for dimensionless time gives:

$$\frac{x_f^2}{k_f} = \frac{t_{RBRi} x_e^2}{1147(\phi c_t)_t \mu \omega A} \tag{4.2.13}$$

Substituting Equation 4.1.27 and assuming a square geometry, i.e. $x_e = y_e$, then,

$$\frac{x_f^2}{k_f} = \frac{t_{RBRi}}{1147(\phi c_t)_t \mu \omega} \tag{4.2.14}$$

C- The intersection point between the bi-radial flow line and the pseudosteady state flow line is described by:

$$(t_{DA})_{PSSBRi} = \frac{0.03755}{\omega^{0.5625}}\left(\frac{x_e}{x_f}\right)^{1.125} \tag{4.2.15}$$

where the subscripts BR and PSS stand for bi-radial flow period and pseudosteady state respectively. Substitution for dimensionless time gives:

$$k_f = \frac{142.4(\phi c_t)_t \mu A}{\omega^{0.5625} t_{PSSBRi}}\left(\frac{x_e}{x_f}\right)^{1.125} \tag{4.2.16}$$

4.2.3 Characteristic Times: A useful relationship can be obtained by combining Equations 4.2.10 and 4.2.14. The new expression can be used for verification.

$$t_{LBRi} = 1.2\, t_{RBRi} \tag{4.2.17}$$

Another relationship can be derived from Equations 4.2.13 and 4.2.15:

$$t_{RBRi} = 8.05\omega^{1.5625}\left(\frac{x_f}{x_e}\right)^{3.125} t_{PSSBRi} \tag{4.2.18}$$

The above equations can be used for verification purposes.

4.3 Procedures

The following step-by-step procedures will demonstrate the applicability of Tiab's Direct Synthesis Technique.

Case 1: Uniform-Flux Fracture, $\left(\frac{x_e}{x_f}\right)>8$

Step 1: Construct a plot of Δp and $(t^*\Delta p_w')$ versus time on a log-log graph and identify the various characteristic points and lines.

Step 2: Read the value of $(t^*\Delta p_w')_R$ corresponding to the infinite-acting radial flow line.

Step 3: Calculate the fracture permeability from Equation 4.1.17.

Step 4: Determine ω and λ as outlined in Reference 63.

Step 5: Verify ω using either Equation 4.1.47 or Equation 4.1.53.

Step 6: Obtain the value of $(t^*\Delta p_w')$ at time t=1 hr from the linear flow line (extrapolated if necessary), $(t^*\Delta p_w')_{L1}$.

Step 7: Calculate the half-fracture length, x_f, from Equation 4.1.12. If the linear flow line portion of $(t^*\Delta p_w')$ is too short or too distorted by near wellbore effect and noise, then x_f should be determined from the half-slope line of Δp_w using Equation 4.1.14; then use Equation 4.1.13 to draw the half-slope line of the pressure derivative curve.

Step 8: Determine the line of intersection of the linear and radial flow line from the graph, i.e. t_{LRi}, using the $(t^*\Delta p_w')$ curve.

Step 9: Calculate the ratio $\frac{x_f^2}{k_f}$ from Equation 4.1.28. Then calculate this ratio using k_f and x_f values obtained in steps 3 and 7 respectively. If the two ratios are approximately equal, then the values of k_f and x_f are correct. If these ratios are significantly different, shift one or both straight lines and repeat Steps 2 through 9 until the ratios are equal

Step 10: Read the value of $(t^*\Delta p_w')_{PSS1}$ from the pseudosteady state line. Calculate the drainage area, A, using Equation 4.1.23.

Step 11: Obtain the time of intersection of the infinite-acting line and the pseudosteady state line, i.e. t_{RPSSi}, from the graph, and calculate A from Equation 4.1.33. If the two values of A in Steps 10 and 11 are approximately equal, then A is correct. If they are distinctly different, then shift left or right and repeat Steps 10 and 11 until Equation 4.1.23 and 4.1.33 give the same value of A.

Step 12: Calculate the interporosity flow parameter after stimulation, λ_f, using Equation 4.1.45.

Step 13: Verify λ_f using Equations 4.1.50, 4.1.51 and 4.1.52.

Step 14: Select any convenient time t_R during the infinite-acting period and read the corresponding value of $(\Delta p_w)_R$; then calculate the skin factor from Equation 4.1.18.

Step 15: Read the value of Δp_w and $(t^*\Delta p_w')$ corresponding to any convenient time t_{PSS} during the pseudosteady state flow portion of the curves and calculate the shape factor C_A from Equation 4.1.24.

Case 2: Uniform-Flux Fracture, $\left(\frac{x_e}{x_f}\right)<8$

In this case, the infinite-acting radial flow regime is not dominant.

Step 1: Construct a plot of Δp and $(t^*\Delta p_w')$ versus time on a log-log graph and identify the various characteristic points and lines.

Step 2: Determine ω as outlined in Reference 63 or use either Equation 4.1.47 or Equation 4.1.53.

Step 3: Obtain the value of $(t^*\Delta p_w')$ at time t=1 hr from the linear flow line (extrapolated if necessary), $(t^*\Delta p_w')_{L1}$.

Step 4: Calculate the half-fracture length, x_f, from Equation 4.1.12. If the linear flow line portion of $(t^*\Delta p_w')$ is too short or too distorted by near wellbore effect and noise, then x_f should be determined from the half-slope line of Δp_w using Equation 4.1.14; then use Equation 4.1.13 to draw the half-slope line of the pressure derivative curve.

Step 5: Read the value of $(t^*\Delta p_w')_{PSS1}$ from the pseudosteady state line. Calculate the drainage area, A, using Equation 4.1.23.

Step 6: Obtain the time of intersection of the infinite-acting line and the pseudosteady state line, i.e. t_{RPSSi}, from the graph, and calculate the fracture permeability, k_f, from Equation 4.1.33.

Step 7: Calculate the fracture permeability from the time of intersection of the two straight lines and Equation 4.1.31. If the two values of k_f in Steps 6 and 7 are approximately equal, then k_f is correct. If they are distinctly different, then shift left or right and repeat Steps 6 and 7 until Equation 4.1.31 and 4.1.33 give the same value of k_f.

Step 8: Determine λ as outlined in Reference 63.

Step 9: Calculate the interporosity flow parameter after stimulation, λ_f, using Equation 4.1.45.

Step 10: Verify λ_f using Equations 4.1.50, 4.1.51 and 4.1.52.

Step 11: Calculate the value of $(t^*\Delta p_w')_R$ from Equation 4.1.17, then calculate the skin factor from Equation 4.1.18.

Case 3: Infinite-Conductivity Fracture, $\left(\frac{x_e}{x_f}\right)$>8

If all three straight lines used in Case 1 (i.e. linear flow line, infinite-acting radial flow line and pseudosteady state flow line) are available, then the fifteenth-step procedure used to analyze the pressure transient test in a uniform-flux fracture is exactly the same for an infinite-conductivity fracture. However, in many tests, the linear flow line portion of the infinite-conductivity fracture is either too short or non-existent. Thus, only the bi-radial, infinite-acting, and pseudosteady state lines can be observed. In this case, the following procedure is recommended.

Step 1: Construct a plot of Δp and $(t^*\Delta p_w')$ versus time on a log-log graph and identify the various characteristic points and lines.

Step 2: Read the value of $(t^*\Delta p_w')_R$ corresponding to the infinite-acting radial flow line.

Step 3: Calculate the fracture permeability from Equation 4.1.17.

Step 4: Determine ω and λ as outlined in Reference 63.

Step 5: Verify ω using either Equation 4.1.47 or Equation 4.1.53.

Step 6: Read the value of $(t^*\Delta p_w')_{PSS1}$ from the pseudosteady state line. Calculate the drainage area, A, using Equation 4.1.23.

Step 7: Obtain the time of intersection of the infinite-acting line and the pseudosteady state line, i.e. t_{RPSSi}, from the graph, and calculate A from Equation 4.1.33. If the two values of A in Steps 6 and 7 are approximately equal, then A is correct. If they are distinctly different then shift left or right and repeat Steps 6 and 7 until Equation 4.1.23 and 4.1.33 give the same value of A.

Step 8: Obtain the value of $(t^*\Delta p_w')$ at time t=1 hr from the bi-radial flow line (extrapolated if necessary), $(t^*\Delta p_w')_{BR1}$.

Step 9: Calculate the half-fracture length, x_f, from Equation 4.2.7.

Step 10: Calculate the ratio $\frac{x_f^2}{k_f}$ using the values k_f and x_f values obtained in steps 3 and 9, respectively.

Step 11: From the graph, determine the time of intersection of the radial flow line and the bi-radial flow line, t_{RBRi}, then calculate the ratio $\frac{x_f^2}{k_f}$ from Equation 4.2.14. If steps 10 and 11 give the same value of $\frac{x_f^2}{k_f}$, then the values of k_f and x_f are correct. If they are different, then shift one or both straight lines (bi-radial and infinite-acting lines), and repeat Steps 2,3,4,6,8,9,10 and 11 until Steps 10 and 11 give the same value of $\frac{x_f^2}{k_f}$.

Step 12: Calculate the interporosity flow parameter after stimulation, λ_f, using Equation 4.1.45.

Step 13: Verify λ_f using Equations 4.1.50, 4.1.51 and 4.1.52.

Step 14: Select any convenient time t_R during the infinite-acting period and read the corresponding value of $(\Delta p_w)_R$; then calculate the skin factor from Equation 4.1.18.

Step 15: Read the value of Δp_w and $(t^*\Delta p_w')$ corresponding to any convenient time t_{PSS} during the pseudosteady state flow portion of the curves and calculate the shape factor C_A from Equation 4.1.24.

Case 4: Infinite-Conductivity Fracture, $\left(\frac{x_e}{x_f}\right)<8$

Step 1: Construct a plot of Δp and $(t^*\Delta p_w')$ versus time on a log-log graph and identify the various characteristic points and lines.

Step 2: Determine ω as outlined in Reference 63 or use either Equation 4.1.47 or Equation 4.1.53.

Step 3: Obtain the value of $(t^*\Delta p_w')$ at time t=1 hr from the linear flow line (extrapolated if necessary), $(t^*\Delta p_w')_{L1}$.

Step 4: Calculate the half-fracture length, x_f, from Equation 4.1.12. If the linear flow line portion of $(t^*\Delta p_w')$ is too short or too distorted by near wellbore effect and noise, then x_f should be determined from the half-slope line of Δp_w using Equation 4.1.14; then use Equation 4.1.13 to draw the half-slope line of the pressure derivative curve.

Step 5: Calculate the fracture permeability, k_f, from Equation 4.2.11.

Step 6: Verify the fracture permeability, k_f, using Equation 4.2.10.

Step 7: Determine λ as outlined in Reference 63.

Step 8: Calculate the interporosity flow parameter after stimulation, λ_f, using Equation 4.1.45.

Step 9: Verify λ_f using Equations 4.1.50, 4.1.51 and 4.1.52.

Step 10: Calculate the value of $(t^*\Delta p_w')_R$ from Equation 4.1.17, then calculate the skin factor from Equation 4.1.18.

y_e/x_e	1.0
ω	0.01
λ	100.0
x_e/x_f	1.0

	Stehfest	Approximation	
T_D	P_D	P_D	Error %
1.00E-08	0.001772	0.001772454	0.026
1.50E-08	0.002171	0.002170804	0.009
2.00E-08	0.002506	0.002506628	0.025
2.50E-08	0.002802	0.002802496	0.018
3.00E-08	0.00307	0.00306998	0.001
3.50E-08	0.003315	0.003315958	0.029
4.00E-08	0.003544	0.003544908	0.026
4.50E-08	0.003759	0.003759942	0.025
5.00E-08	0.003962	0.003963327	0.034
5.50E-08	0.004156	0.004156773	0.019
6.00E-08	0.004341	0.004341608	0.014
6.50E-08	0.004518	0.004518888	0.020
7.00E-08	0.004688	0.004689472	0.031
7.50E-08	0.004852	0.004854065	0.043
8.00E-08	0.005012	0.005013257	0.025
8.50E-08	0.005166	0.005167547	0.030
9.00E-08	0.005316	0.005317362	0.026
9.50E-08	0.005461	0.00546307	0.038
1.00E-07	0.005603	0.005604991	0.036
1.50E-07	0.006861	0.006864684	0.054
2.00E-07	0.007921	0.007926655	0.071
2.50E-07	0.008855	0.008862269	0.082
3.00E-07	0.009697	0.00970813	0.115
3.50E-07	0.010473	0.010485978	0.124
4.00E-07	0.011195	0.011209982	0.134
4.50E-07	0.011872	0.011889982	0.151
5.00E-07	0.012512	0.012533141	0.169
5.50E-07	0.01312	0.01314487	0.190
6.00E-07	0.013701	0.013729368	0.207
6.50E-07	0.014258	0.01428998	0.224
7.00E-07	0.014794	0.014829413	0.239
7.50E-07	0.015311	0.015349901	0.254
8.00E-07	0.01581	0.015853309	0.274
8.50E-07	0.016295	0.016341217	0.284
9.00E-07	0.016764	0.016814974	0.304
9.50E-07	0.017221	0.017275743	0.318
1.00E-06	0.017665	0.017724539	0.337

Table 4.1.1 Comparison between the proposed approximation with the Laplace solution.

y_e/x_e	1.0
ω	0.01
λ	100.0
x_e/x_f	50.0

	Stehfest	Approximation	
T_D	P_D	P_D	Error %
1.00E-12	0.000882	0.000886227	0.48
1.50E-12	0.00108	0.001085402	0.50
2.00E-12	0.001247	0.001253314	0.51
2.50E-12	0.001394	0.001401248	0.52
3.00E-12	0.001527	0.00153499	0.52
3.50E-12	0.001649	0.001657979	0.54
4.00E-12	0.001763	0.001772454	0.54
4.50E-12	0.00187	0.001879971	0.53
5.00E-12	0.001971	0.001981664	0.54
5.50E-12	0.002068	0.002078386	0.50
6.00E-12	0.00216	0.002170804	0.50
6.50E-12	0.002248	0.002259444	0.51
7.00E-12	0.002333	0.002344736	0.50
7.50E-12	0.002415	0.002427032	0.50
8.00E-12	0.002494	0.002506628	0.51
8.50E-12	0.00257	0.002583773	0.54
9.00E-12	0.002645	0.002658681	0.52
9.50E-12	0.002717	0.002731535	0.53
1.00E-11	0.002788	0.002802496	0.52
1.50E-11	0.003415	0.003432342	0.51
2.00E-11	0.003943	0.003963327	0.52
2.50E-11	0.004406	0.004431135	0.52
3.00E-11	0.004829	0.004854065	0.52
3.50E-11	0.005215	0.005242989	0.54
4.00E-11	0.005576	0.005604991	0.52
4.50E-11	0.005914	0.005944991	0.52
5.00E-11	0.006234	0.006266571	0.52
5.50E-11	0.006538	0.006572435	0.53
6.00E-11	0.006829	0.006864684	0.52
6.50E-11	0.007107	0.00714499	0.53
7.00E-11	0.007376	0.007414706	0.52
7.50E-11	0.007634	0.00767495	0.54
8.00E-11	0.007885	0.007926655	0.53
8.50E-11	0.008128	0.008170609	0.52
9.00E-11	0.008363	0.008407487	0.53
9.50E-11	0.008593	0.008637872	0.52
1.00E-10	0.008816	0.008862269	0.52

Table 4.1.1 Comparison between the proposed approximation with the Laplace solution. (To be continued)

y_e/x_e	1.0
ω	0.01
λ	100.0
x_e/x_f	100.0

	Stehfest	Approximation	
T_D	P_D	P_D	Error %
1.00E-12	0.001754	0.001772454	1.05
1.50E-12	0.002149	0.002170804	1.01
2.00E-12	0.002481	0.002506628	1.03
2.50E-12	0.002774	0.002802496	1.03
3.00E-12	0.003039	0.00306998	1.02
3.50E-12	0.003282	0.003315958	1.03
4.00E-12	0.003509	0.003544908	1.02
4.50E-12	0.003722	0.003759942	1.02
5.00E-12	0.003923	0.003963327	1.03
5.50E-12	0.004114	0.004156773	1.04
6.00E-12	0.004297	0.004341608	1.04
6.50E-12	0.004473	0.004518888	1.03
7.00E-12	0.004642	0.004689472	1.02
7.50E-12	0.004805	0.004854065	1.02
8.00E-12	0.004962	0.005013257	1.03
8.50E-12	0.005115	0.005167547	1.03
9.00E-12	0.005263	0.005317362	1.03
9.50E-12	0.005407	0.00546307	1.04
1.00E-11	0.005548	0.005604991	1.03
1.50E-11	0.006795	0.006864684	1.03
2.00E-11	0.007846	0.007926655	1.03
2.50E-11	0.008772	0.008862269	1.03
3.00E-11	0.009608	0.00970813	1.04
3.50E-11	0.010378	0.010485978	1.04
4.00E-11	0.011094	0.011209982	1.05
4.50E-11	0.011767	0.011889982	1.05
5.00E-11	0.012403	0.012533141	1.05
5.50E-11	0.013009	0.01314487	1.04
6.00E-11	0.013587	0.013729368	1.05
6.50E-11	0.014141	0.01428998	1.05
7.00E-11	0.014675	0.014829413	1.05
7.50E-11	0.01519	0.015349901	1.05
8.00E-11	0.015688	0.015853309	1.05
8.50E-11	0.01617	0.016341217	1.06
9.00E-11	0.016638	0.016814974	1.06
9.50E-11	0.017094	0.017275743	1.06
1.00E-10	0.017539	0.017724539	1.06

Table 4.1.1 Comparison between the proposed approximation with the Laplace solution. (To be continued)

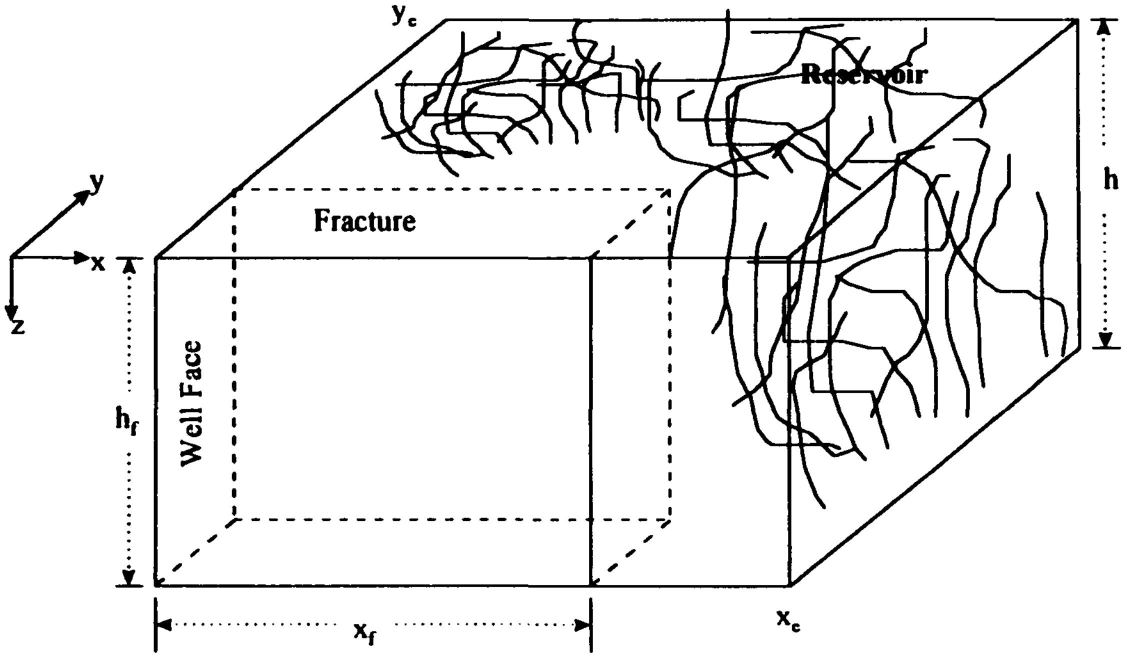

Figure 4.1.1 Vertical fracture in a double porosity reservoir.

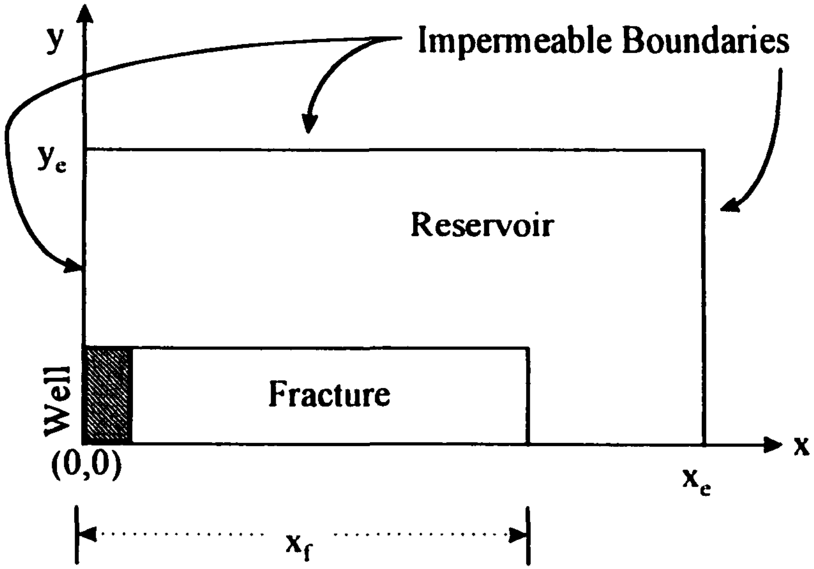

Figure 4.1.2 Plane view.

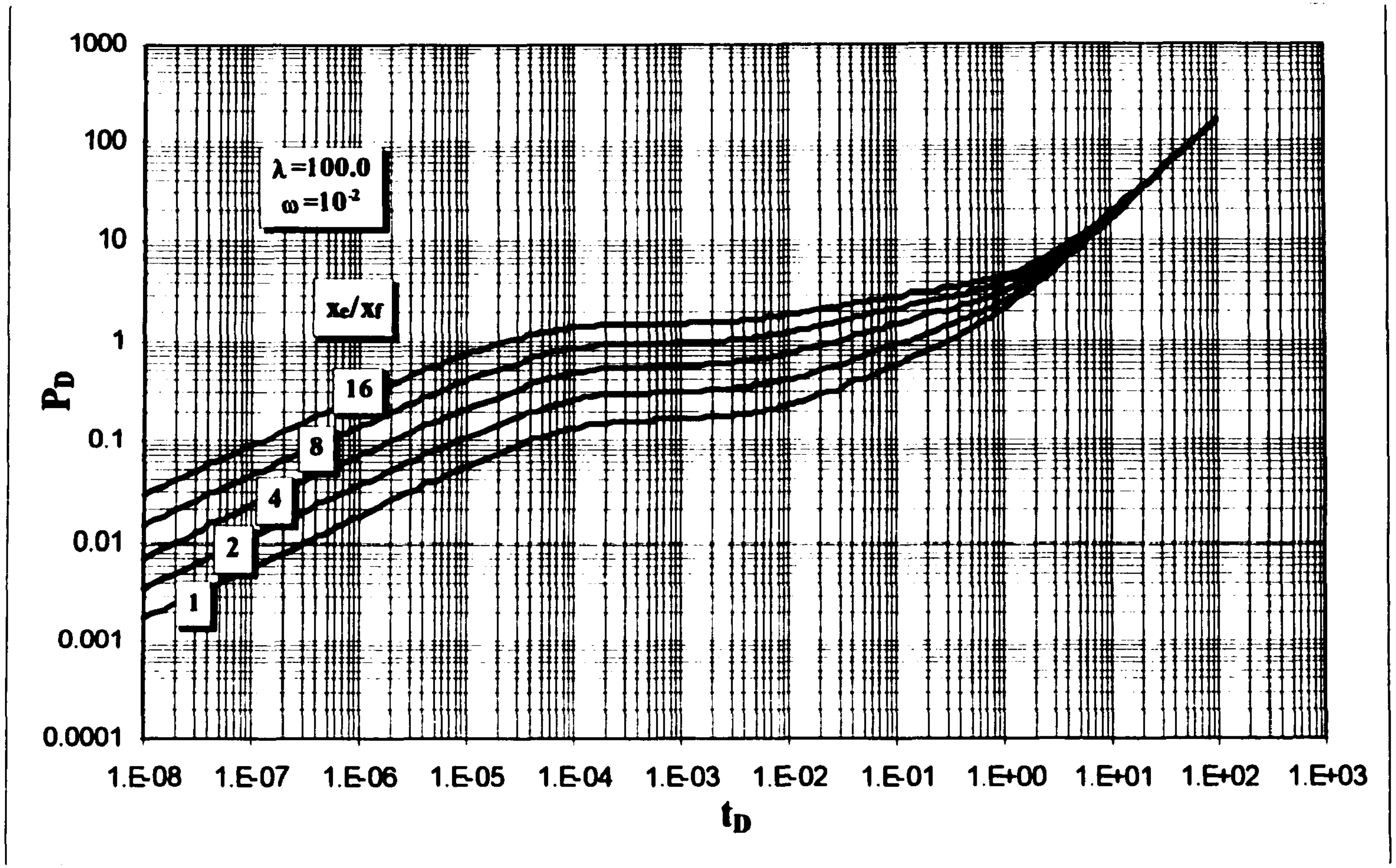

Figure 4.1.3 Characteristics of pressure response in a single-layer square, naturally fractured reservoir with pseudosteady state interporosity flow, ω=0.01 and λ_f=100. Both wellbore storage and skin are ignored.

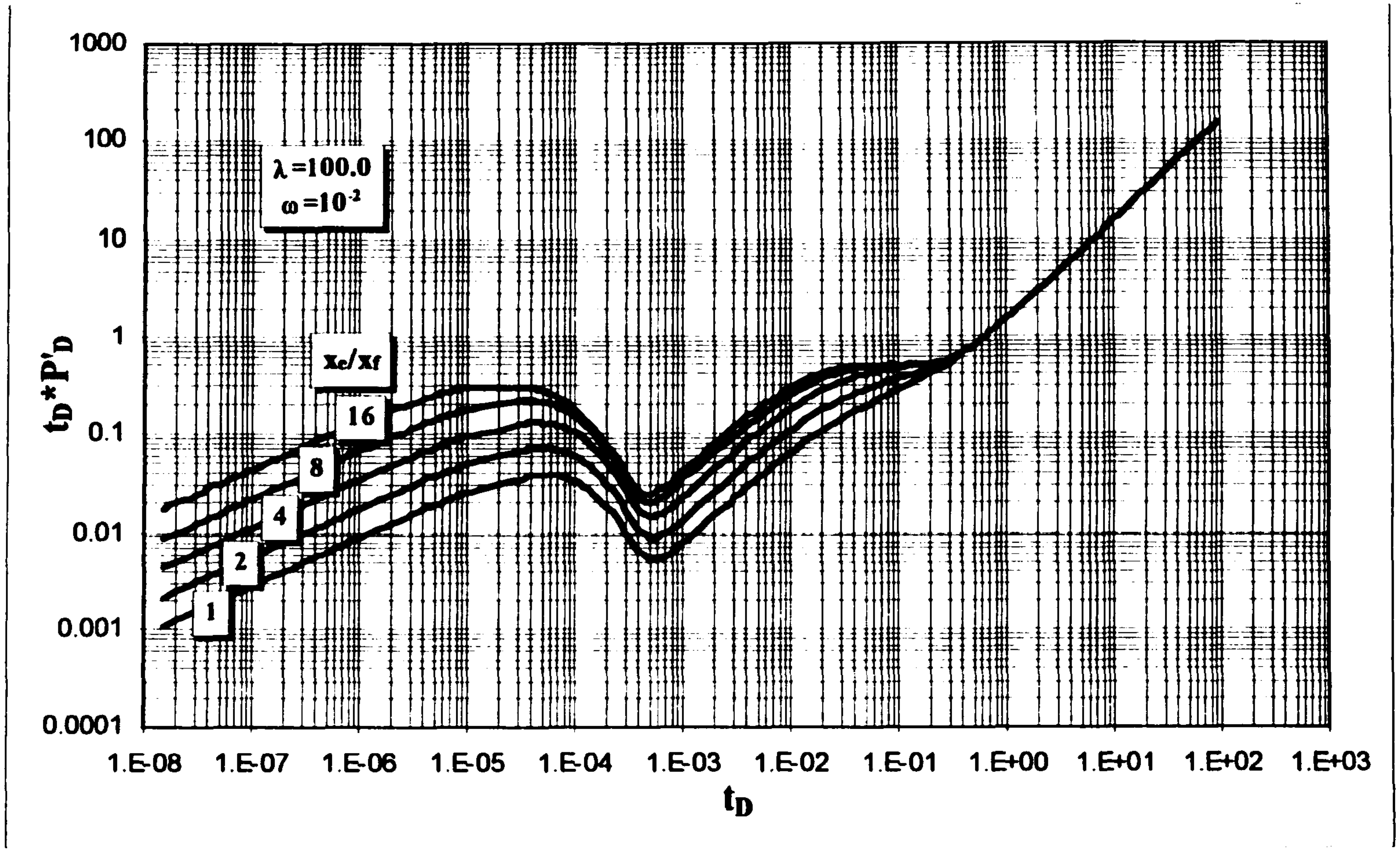

Figure 4.1.4 Characteristics of pressure derivative response in a single-layer square, naturally fractured reservoir with pseudosteady state interporosity flow, ω=0.01 and λ_f=100. Both wellbore storage and skin are ignored.

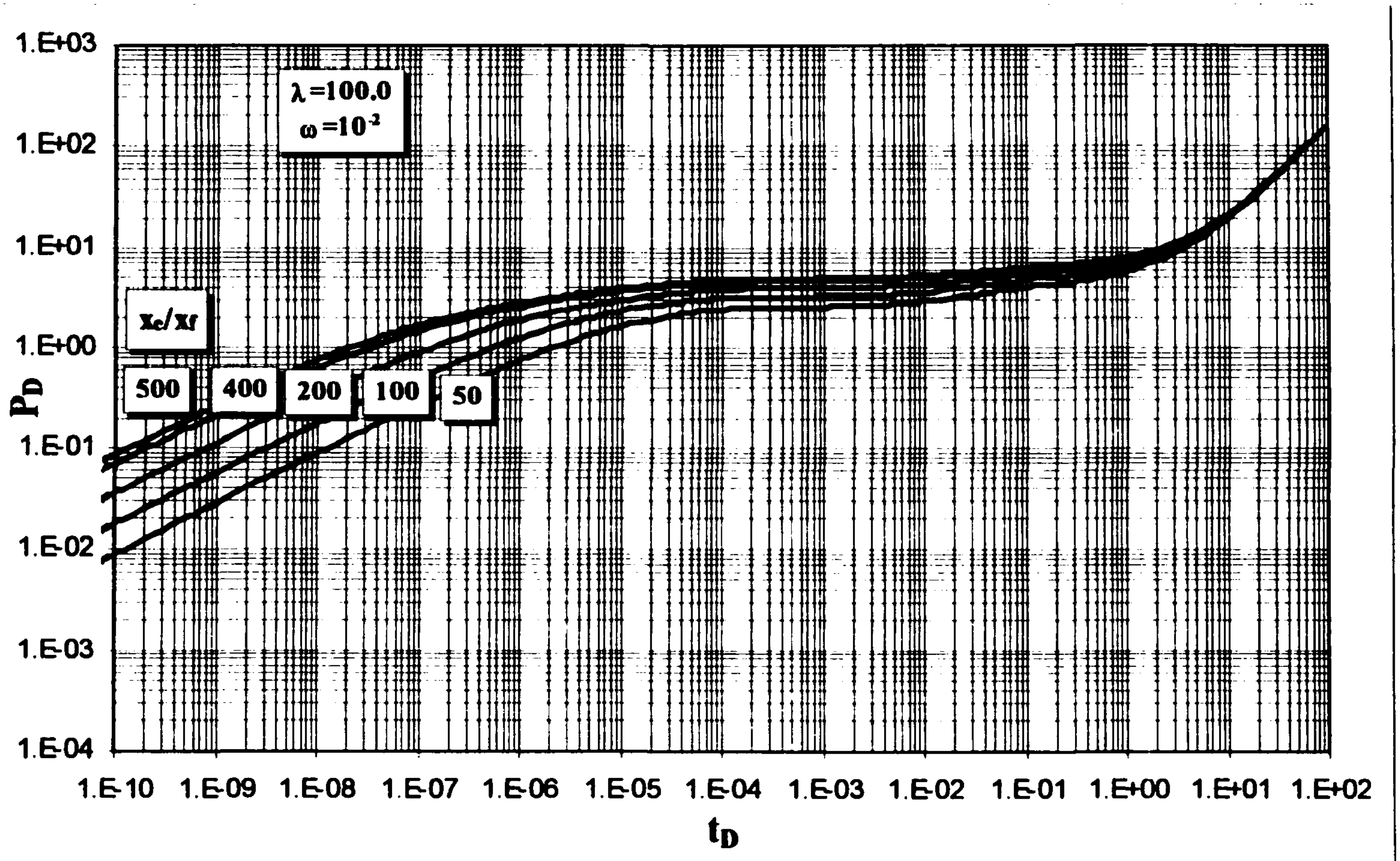

Figure 4.1.5 Characteristics of pressure response in a single-layer square, naturally fractured reservoir with pseudosteady state interporosity flow, ω=0.01 and λ_f=100. Both wellbore storage and skin are ignored.

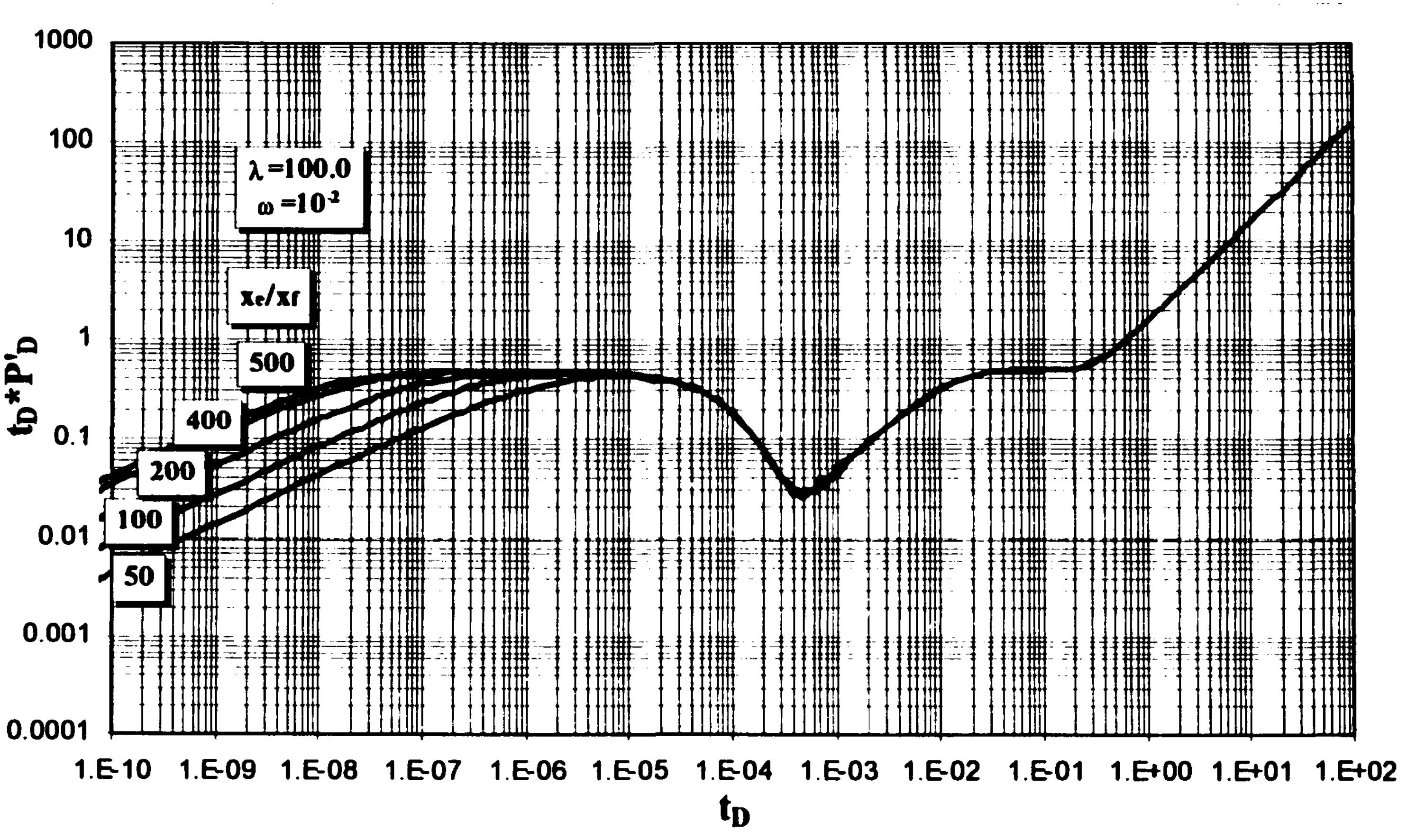

Figure 4.1.6 Characteristics of pressure derivative response in a single-layer square, naturally fractured reservoir with pseudosteady state interporosity flow, ω=0.01 and λ_f=100. Both wellbore storage and skin are ignored.

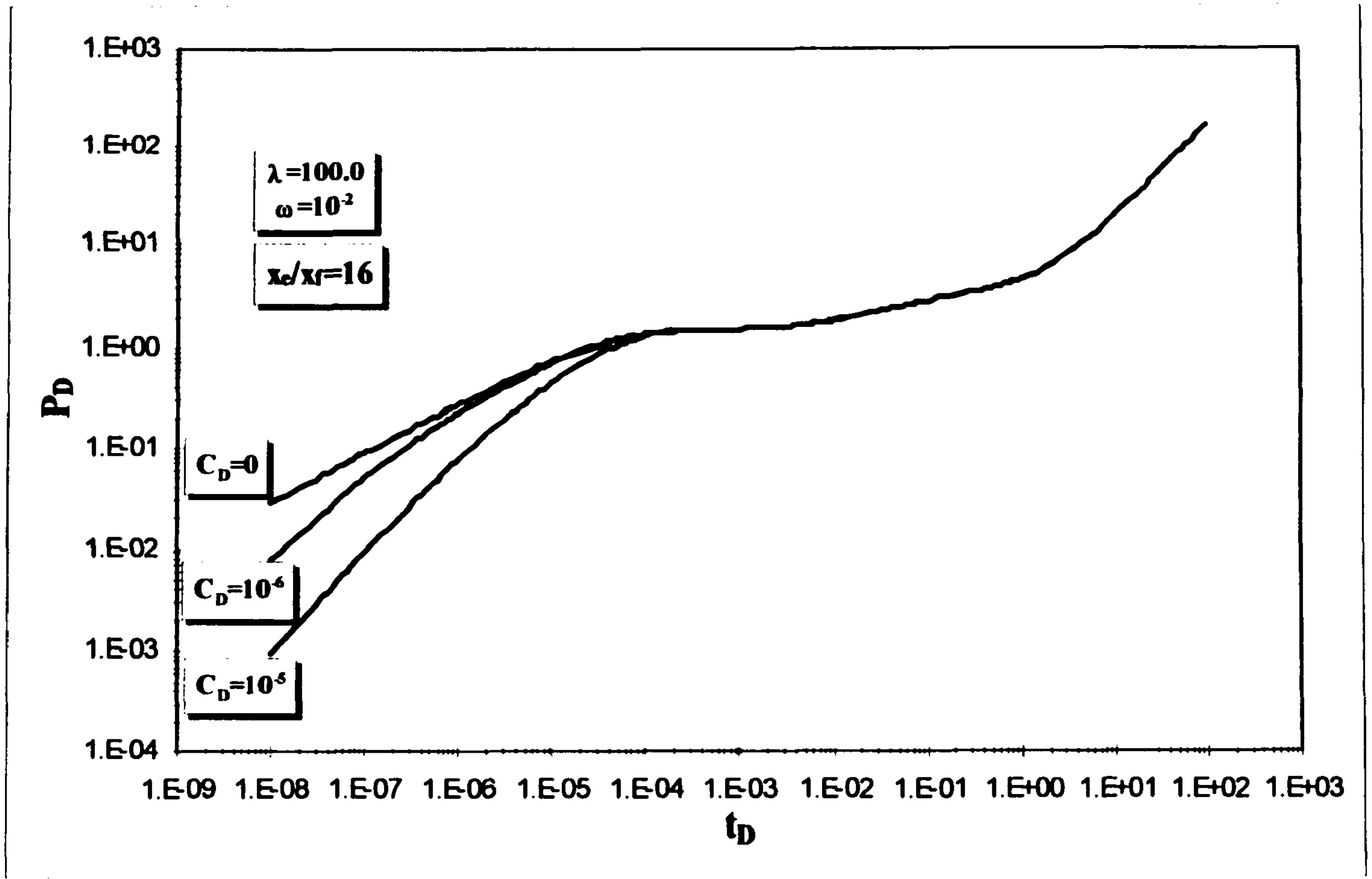

Figure 4.1.7 The effect of wellbore storage on pressure behavior in a vertical fractured reservoir with double porosity of pseudosteady state interporosity flow, ω=0.01 and λ_f=100

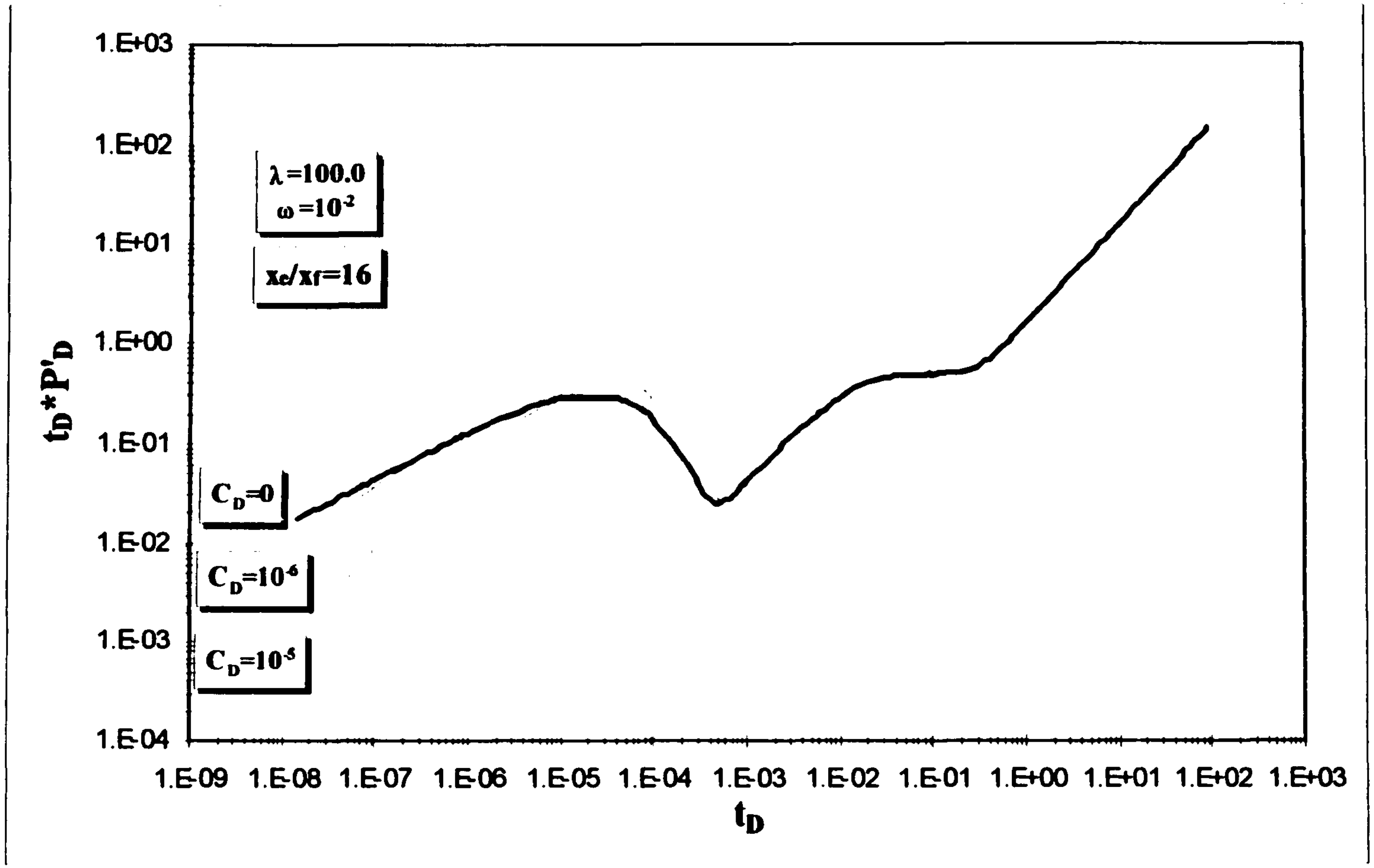

Figure 4.1.8 The effect of wellbore storage on pressure derivative behavior in a vertical fractured reservoir with double porosity of pseudosteady state interporosity flow, ω=0.01 and λ_f=100.

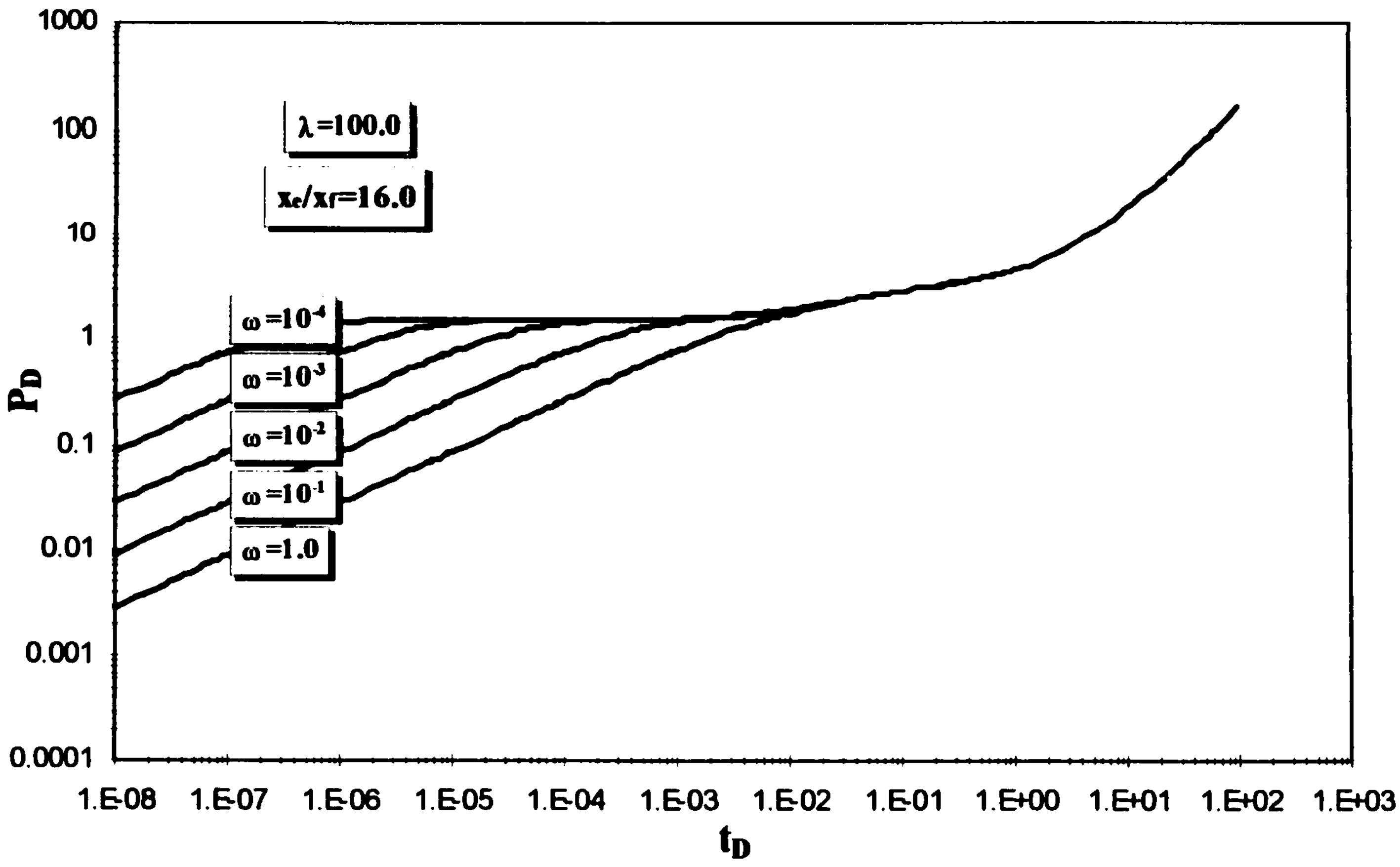

Figure 4.1.9 Effect of storage coefficient on the pressure response in a single-layer square, vertical fractured reservoir with pseudosteady state interporosity flow.

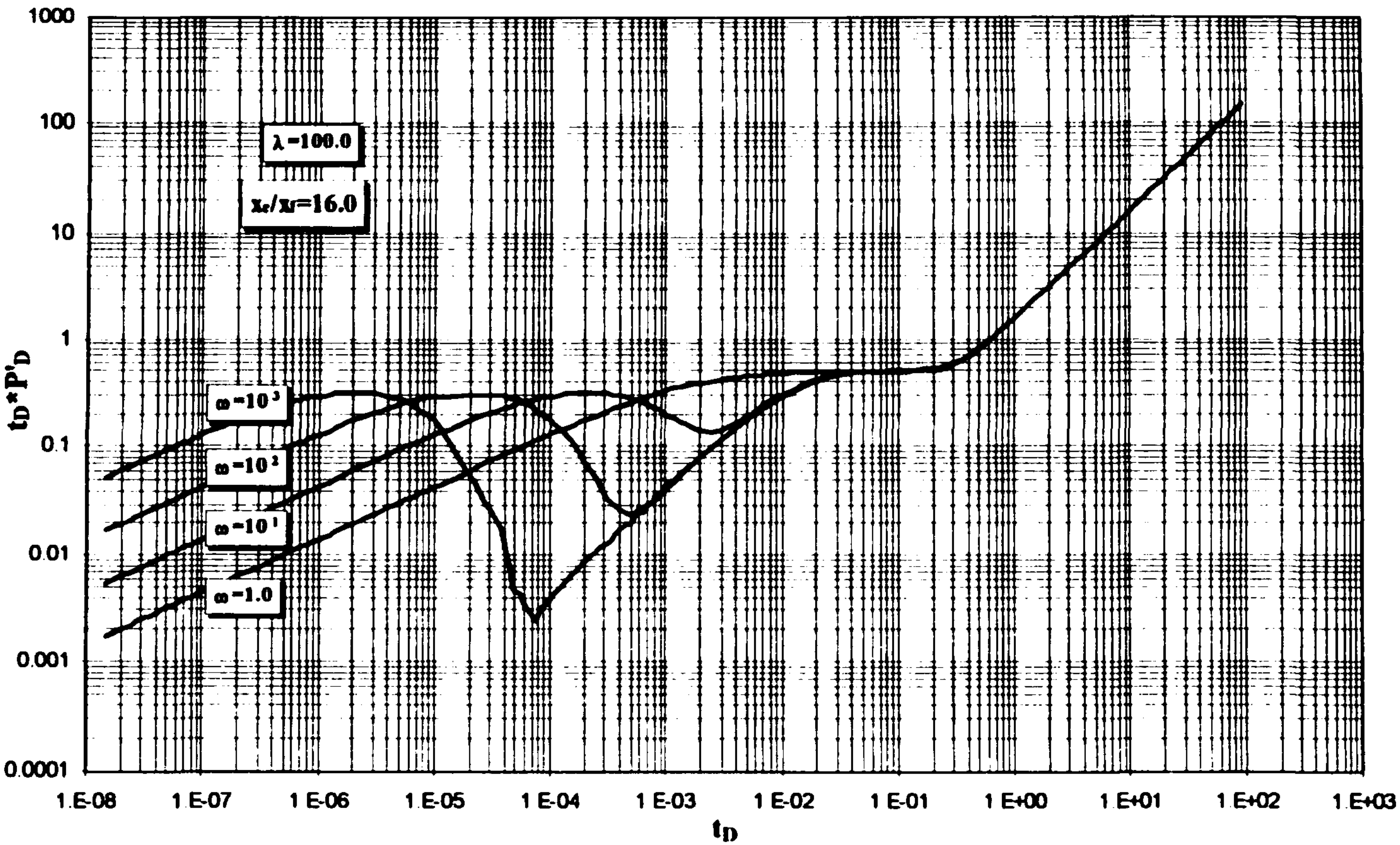

Figure 4.1.10 Effect of storage coefficient on the pressure derivative response in a single-layer square, vertical fractured reservoir with pseudosteady state interporosity flow

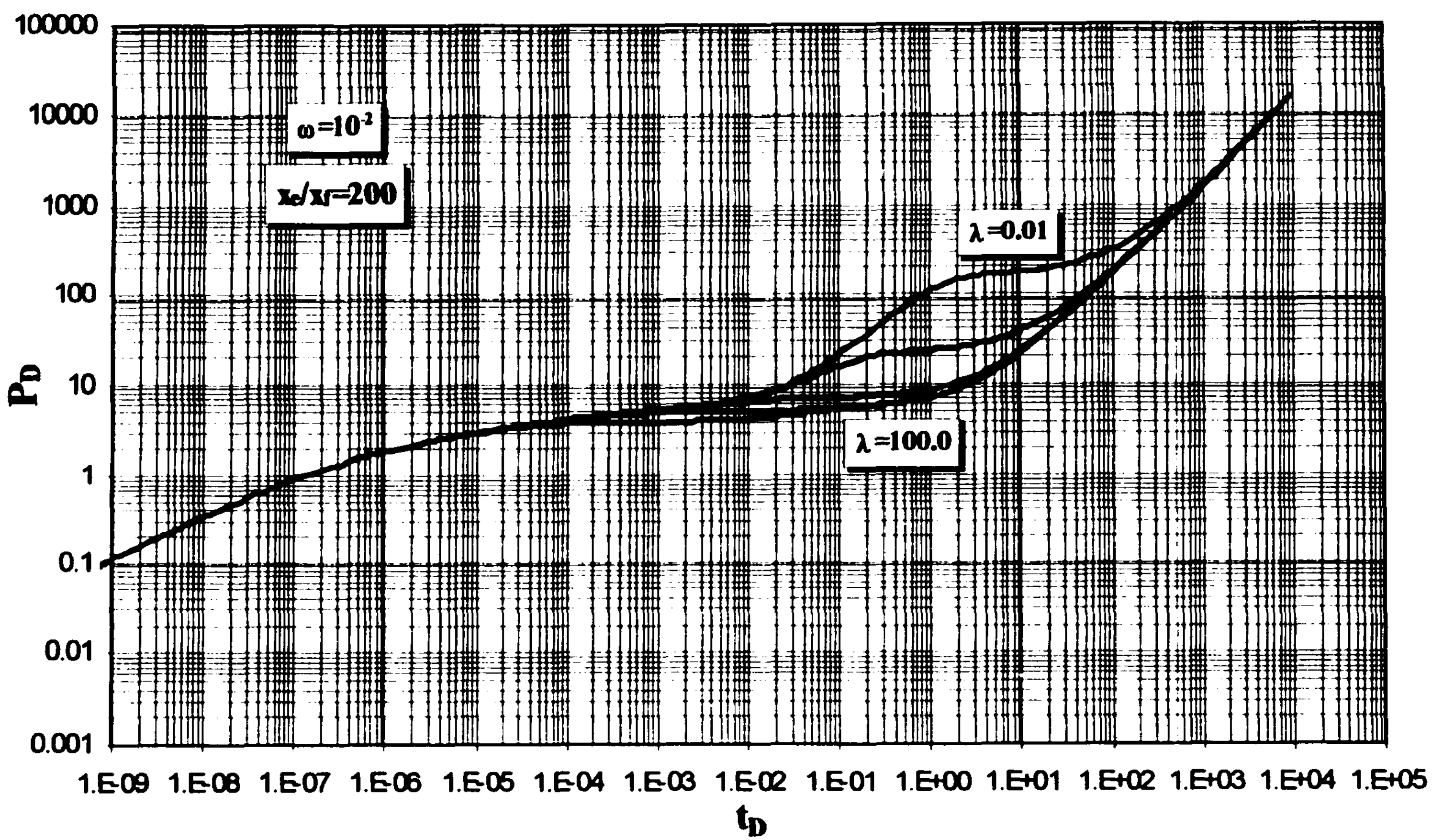

Figure 4.1.11 Effect of interporosity flow parameter on the pressure response in a single-layer square, vertical fractured reservoir with pseudosteady state interporosity flow.

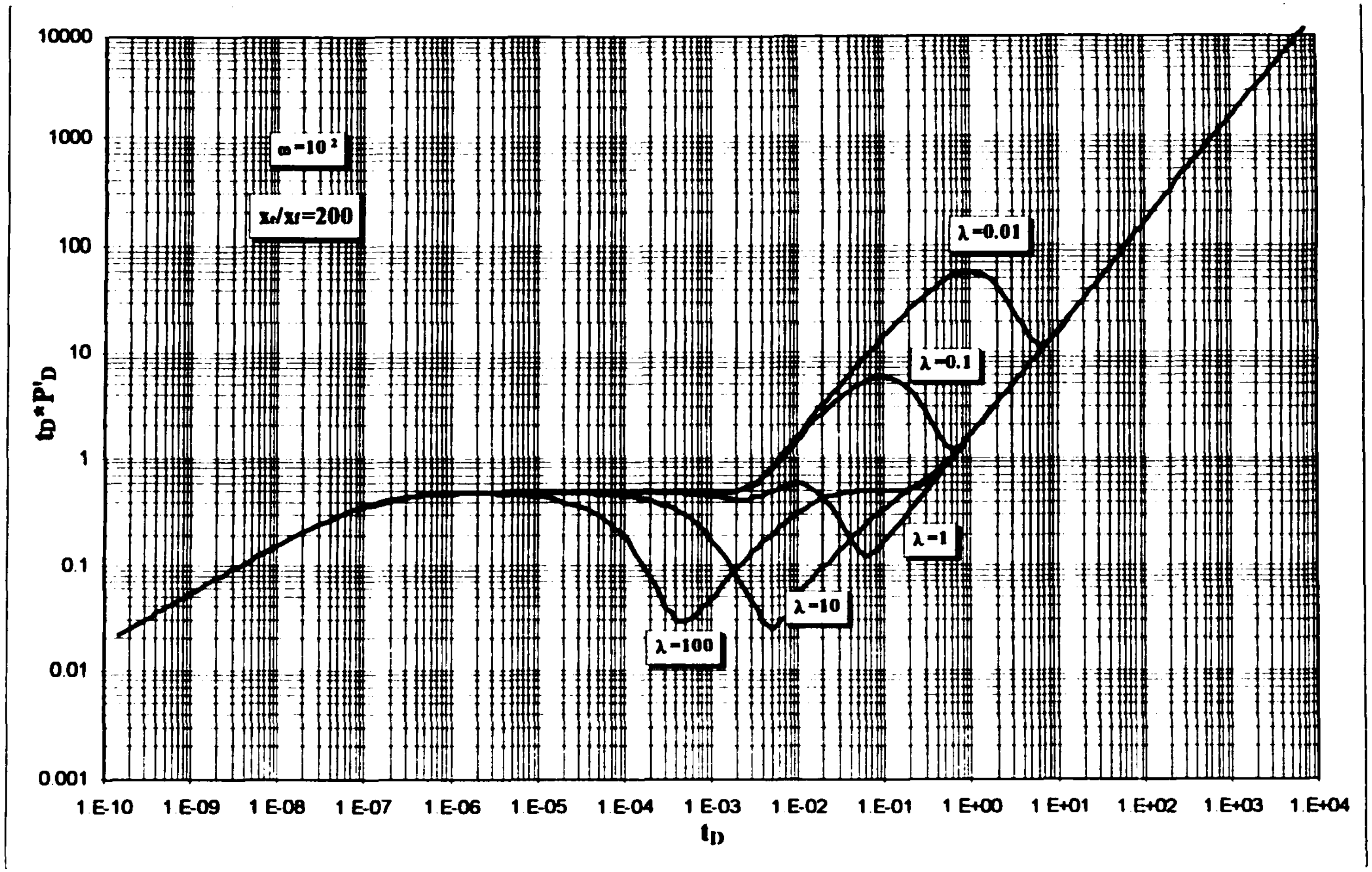

Figure 4.1.12 Effect of interporosity flow parameter on the pressure response in a single-layer square, vertical fractured reservoir with pseudosteady state interporosity flow.

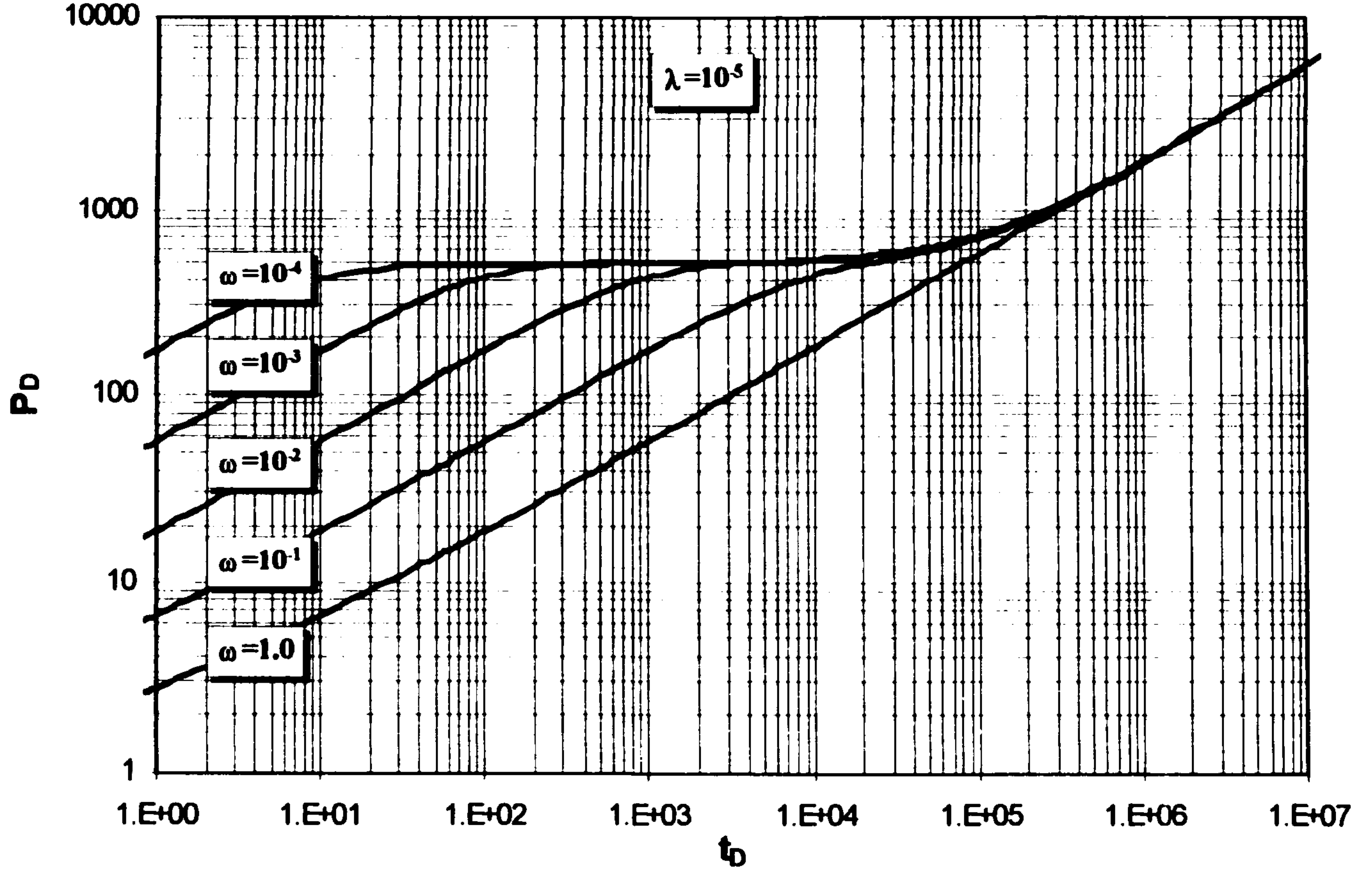

Figure 4.1.13 Effect of storage coefficient on the pressure response in a vertical fractured reservoir with pseudosteady state interporosity flow, $\lambda=10^{-5}$, the transition occurs during the linear flow period.

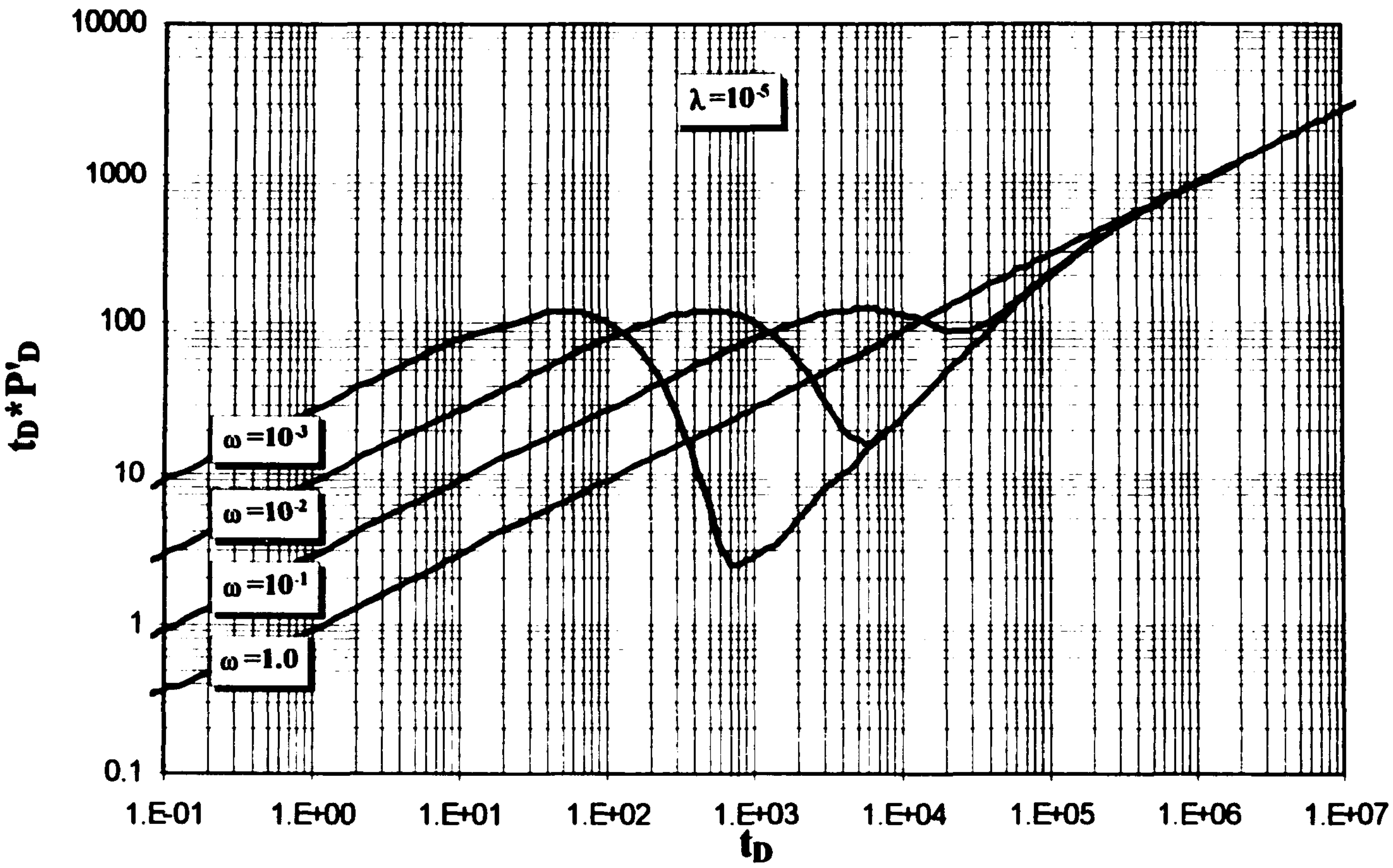

Figure 4.1.14 Effect of storage coefficient on the pressure derivative response in a vertical fractured reservoir with pseudosteady state interporosity flow, $\lambda=10^{-5}$. The transition occurs during the linear flow period.

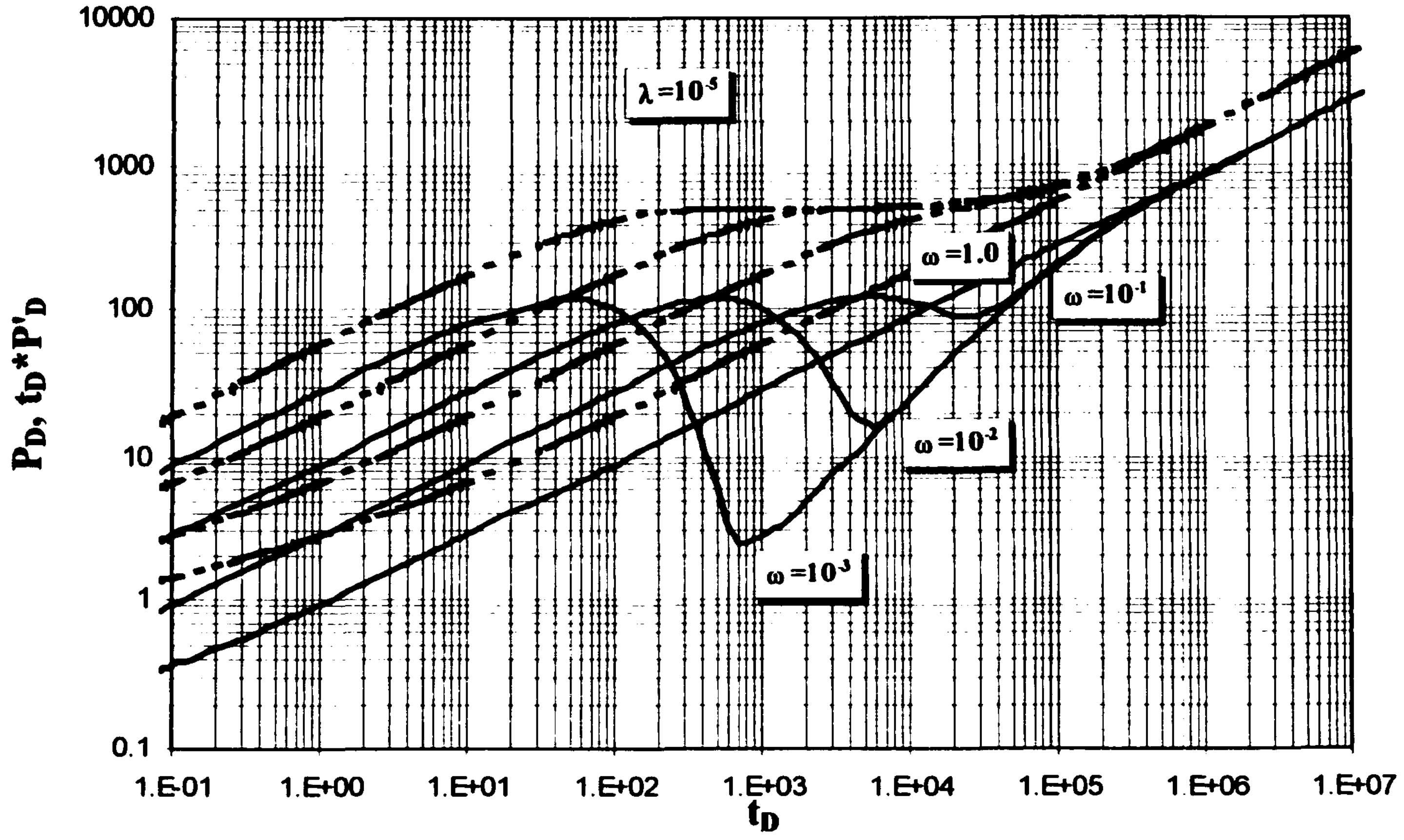

Figure 4.1.15 Effect of storage coefficient on the pressure and pressure derivative responses in a vertical fractured reservoir with pseudosteady state interporosity flow, $\lambda=10^{-5}$. The transition occurs during the linear flow period.

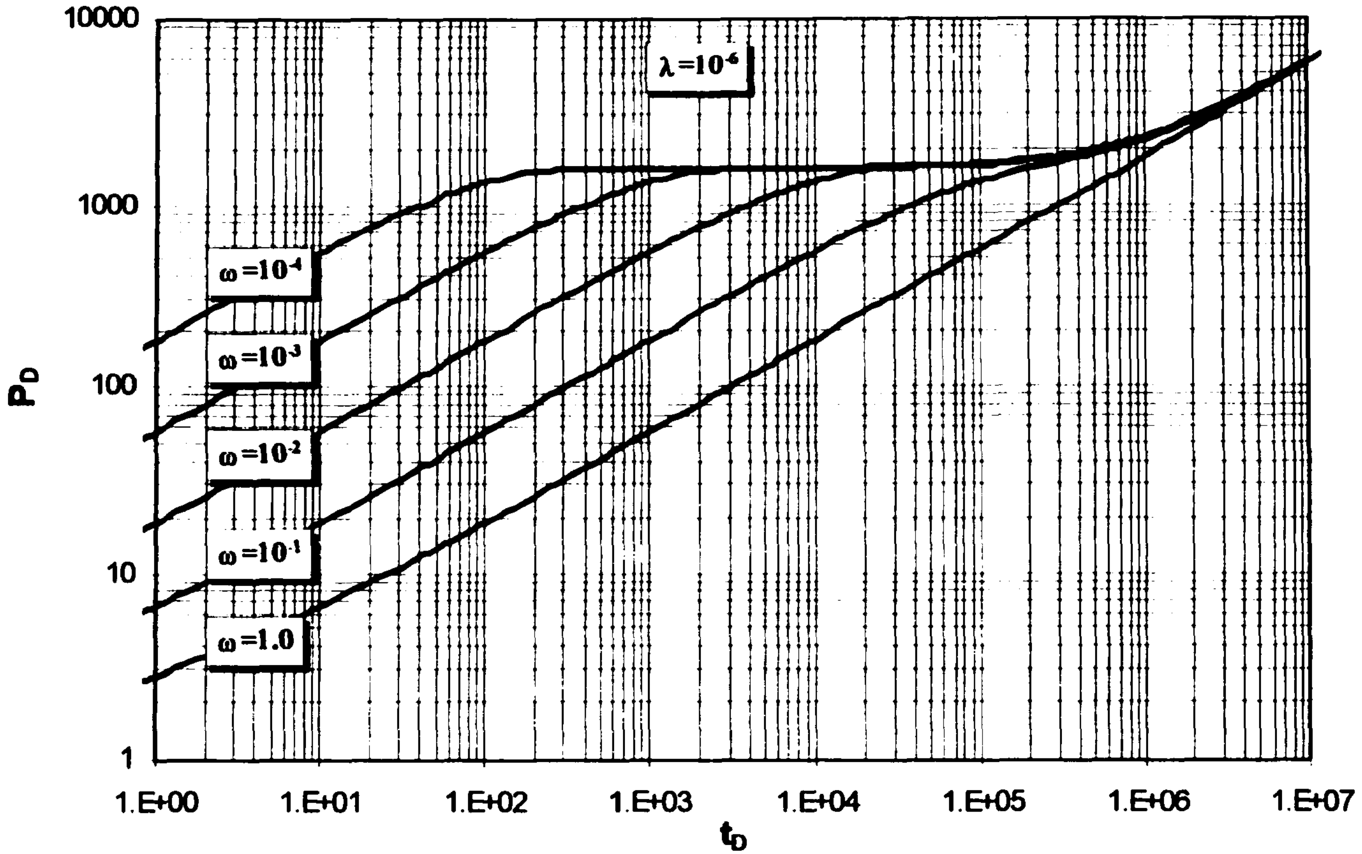

Figure 4.1.16 Effect of storage coefficient on the pressure response in a vertical fractured reservoir with pseudosteady state interporosity flow, $\lambda=10^{-6}$. The transition occurs during the linear flow period.

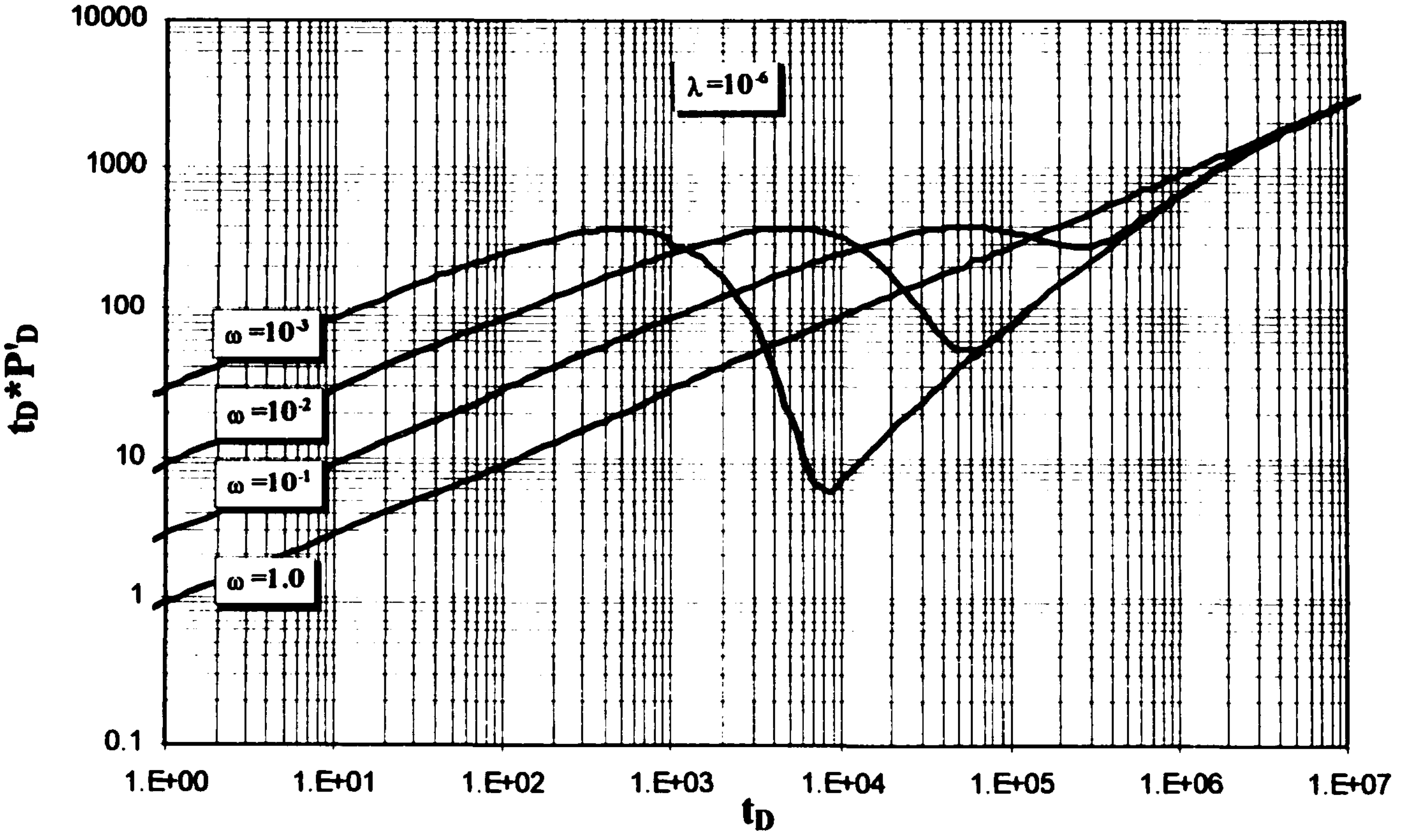

Figure 4.1.17 Effect of storage coefficient on the pressure derivative response in a vertical fractured reservoir with pseudosteady state interporosity flow, $\lambda=10^{-6}$. The transition occurs during the linear flow period.

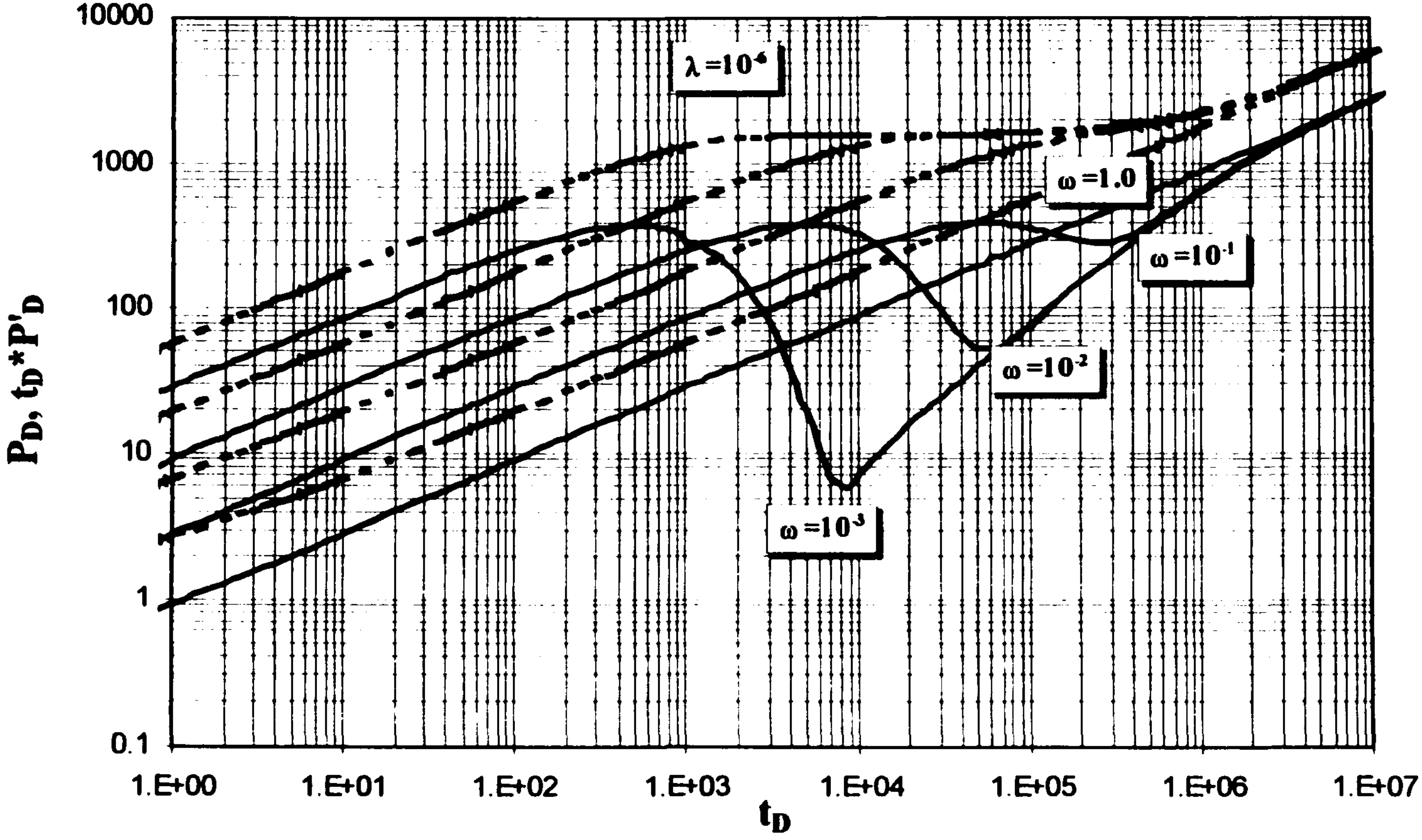

Figure 4.1.18 Effect of storage coefficient on the pressure and pressure derivative responses in a vertical fractured reservoir with pseudosteady state interporosity flow, $\lambda=10^{-6}$. The transition occurs during the linear flow period.

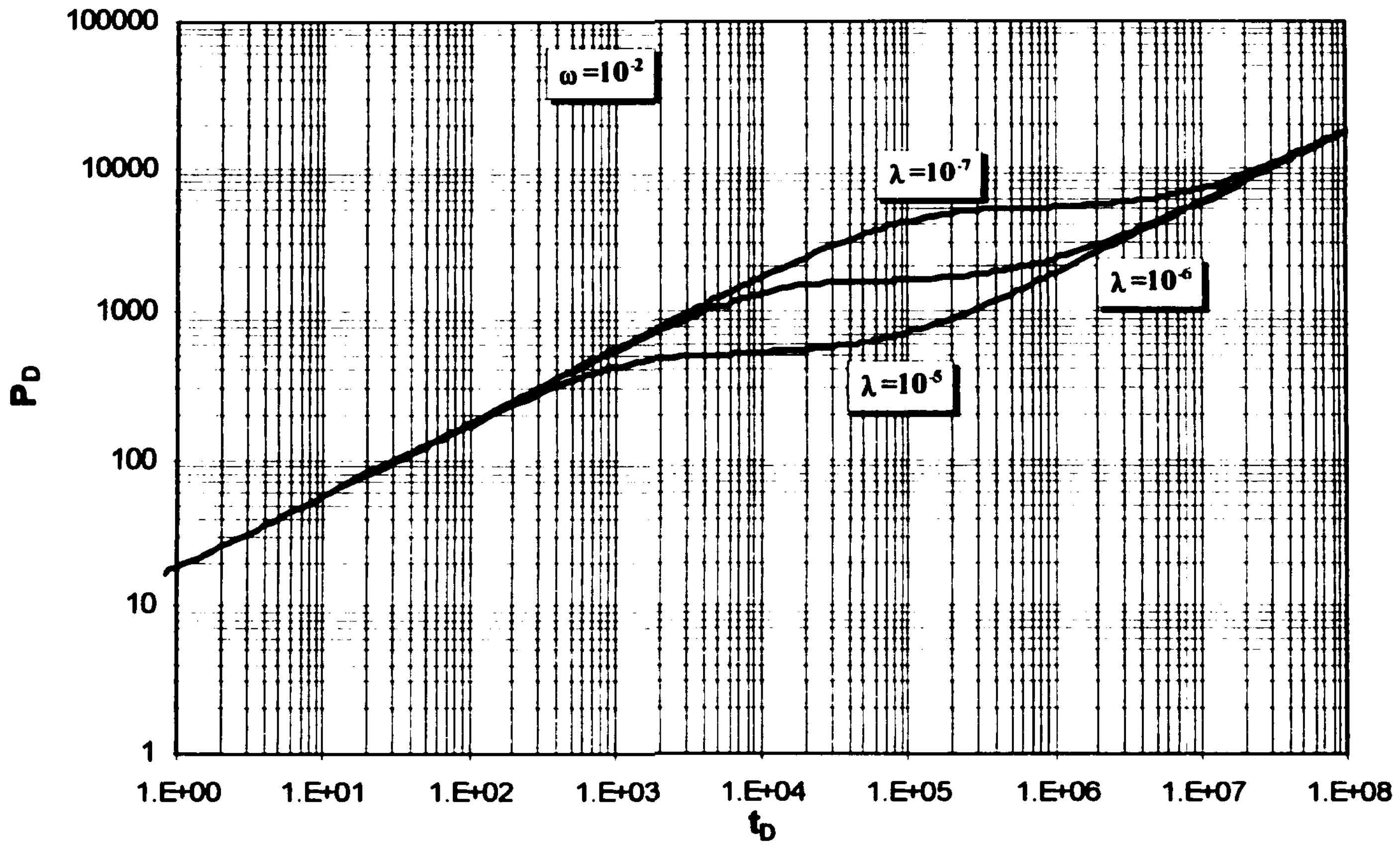

Figure 4.1.19 Effect of interporosity flow parameter on the pressure response in a vertical fractured reservoir with pseudosteady state interporosity flow. The transition occurs during the linear flow period.

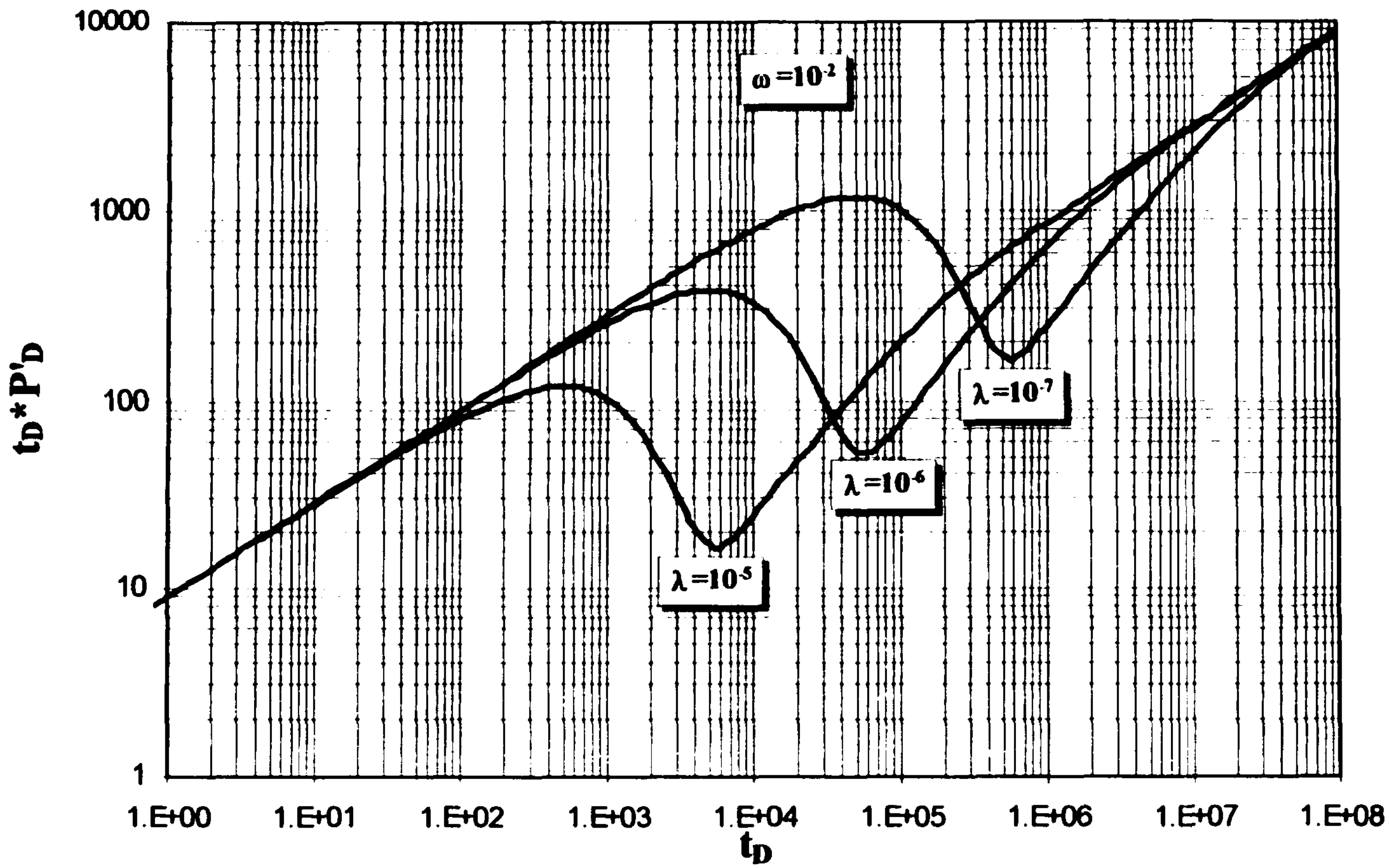

Figure 4.1.20 Effect of interporosity flow parameter on the pressure derivative response in a vertical fractured reservoir with pseudosteady state interporosity flow. The transition occurs during the linear flow period.

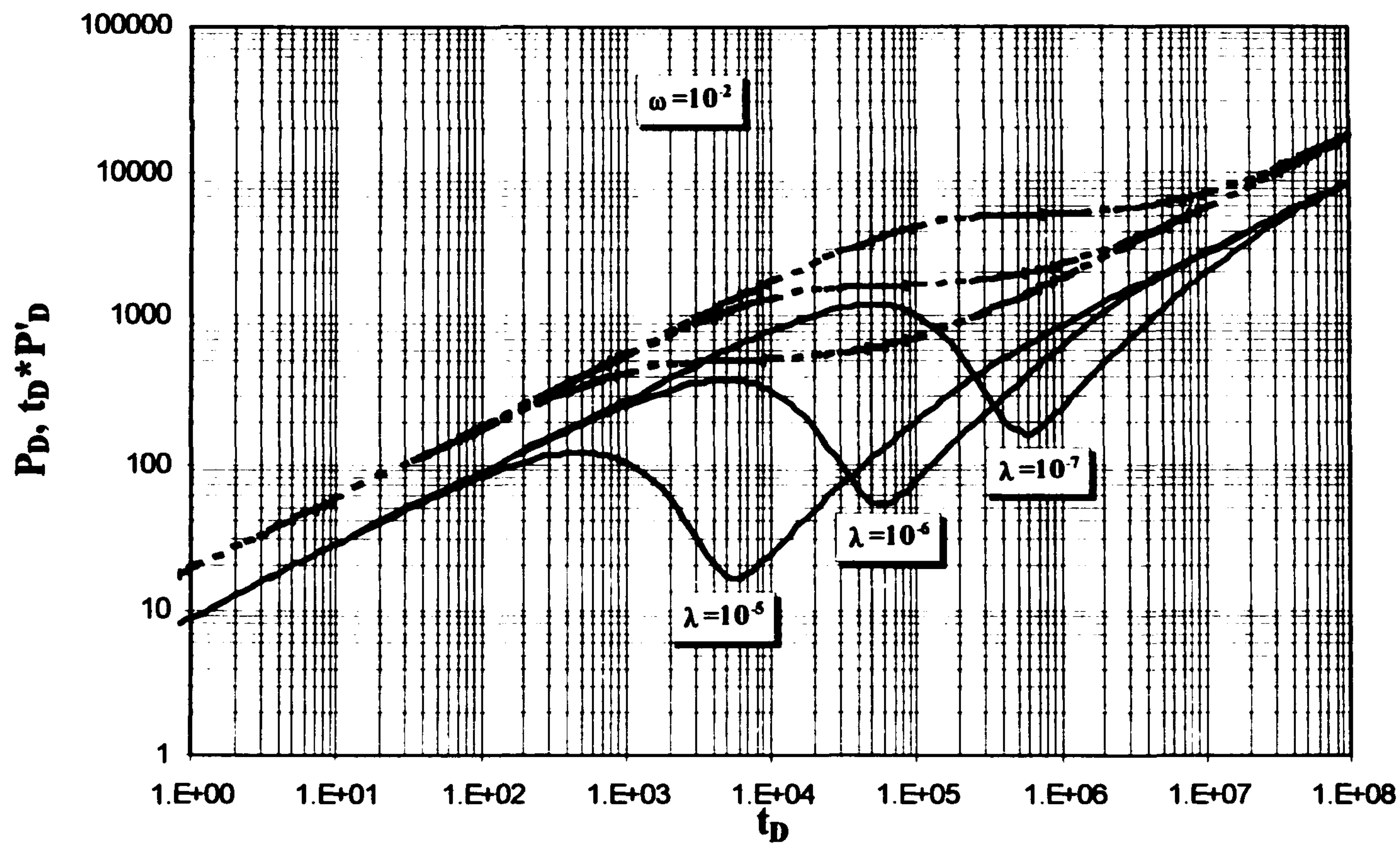

Figure 4.1.21 Effect of interporosity flow parameter on the pressure and pressure derivative responses in a vertical fractured reservoir with pseudosteady state interporosity flow. The transition occurs during the linear flow period.

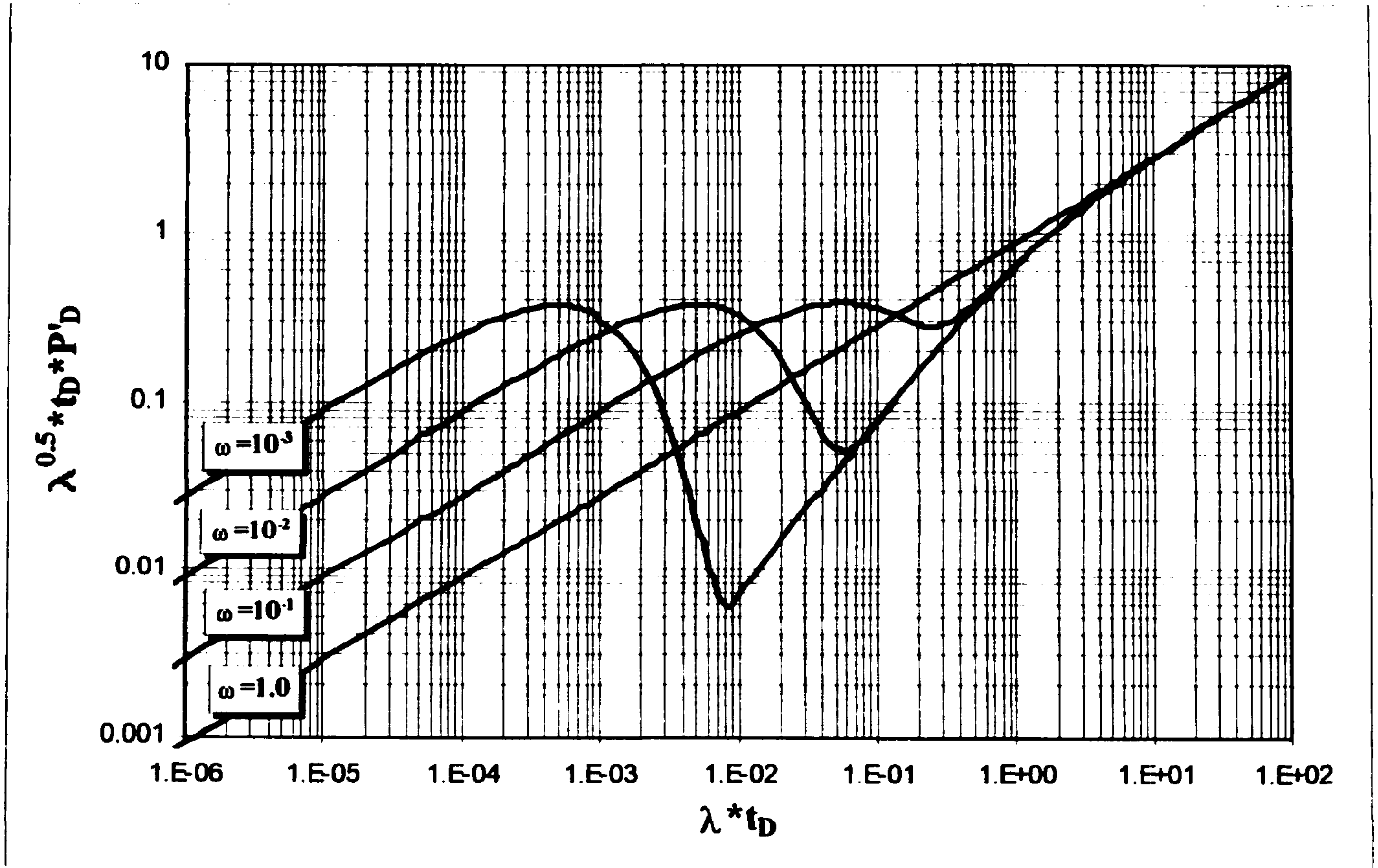

Figure 4.1.22 Effect of storage coefficient on the pressure response in a vertical fractured reservoir with pseudosteady state interporosity flow, λt_D group. The transition occurs during the linear flow period.

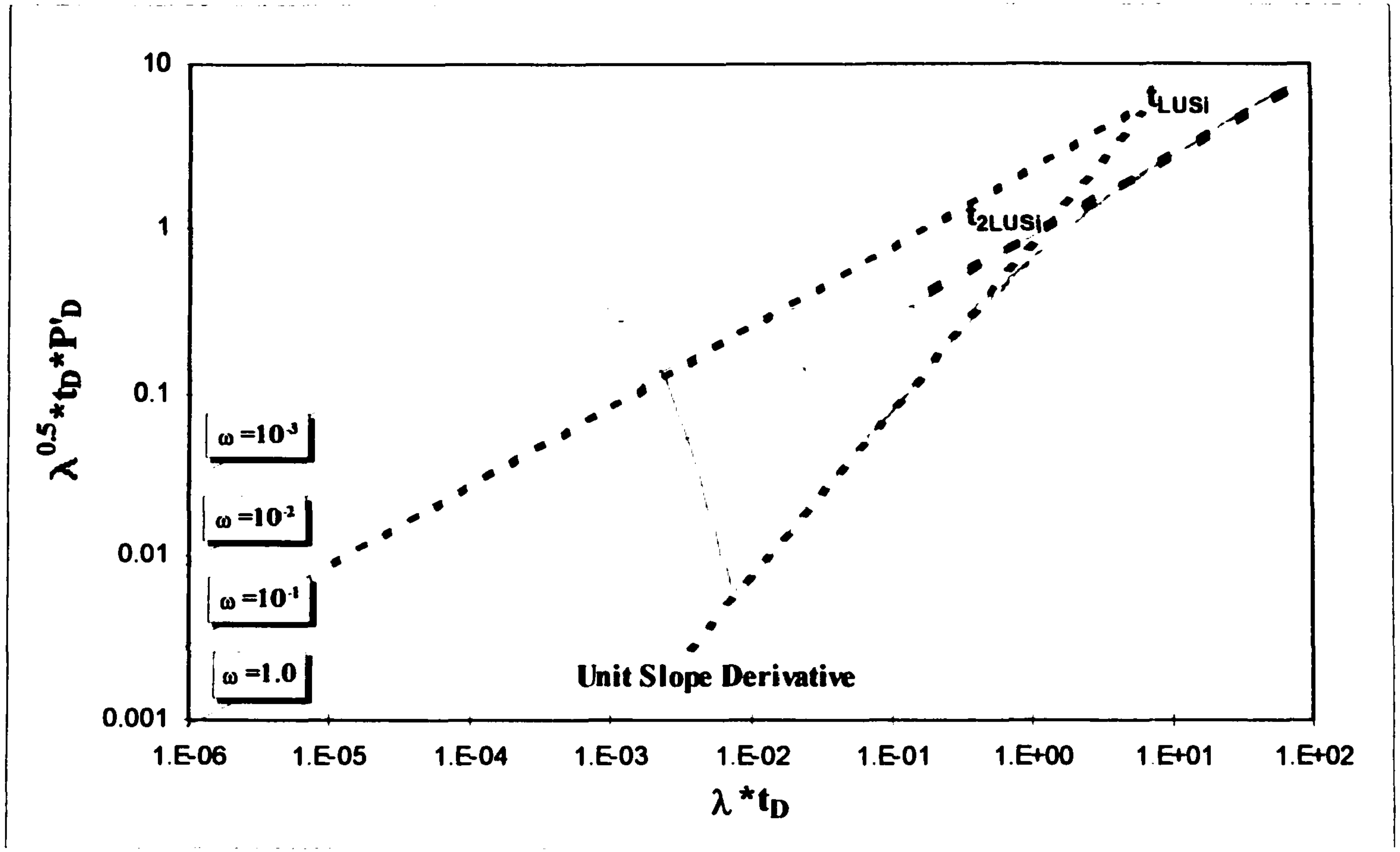

Figure 4.1.23 Transition period during the linear flow period illustrating the unit slope derivative line.

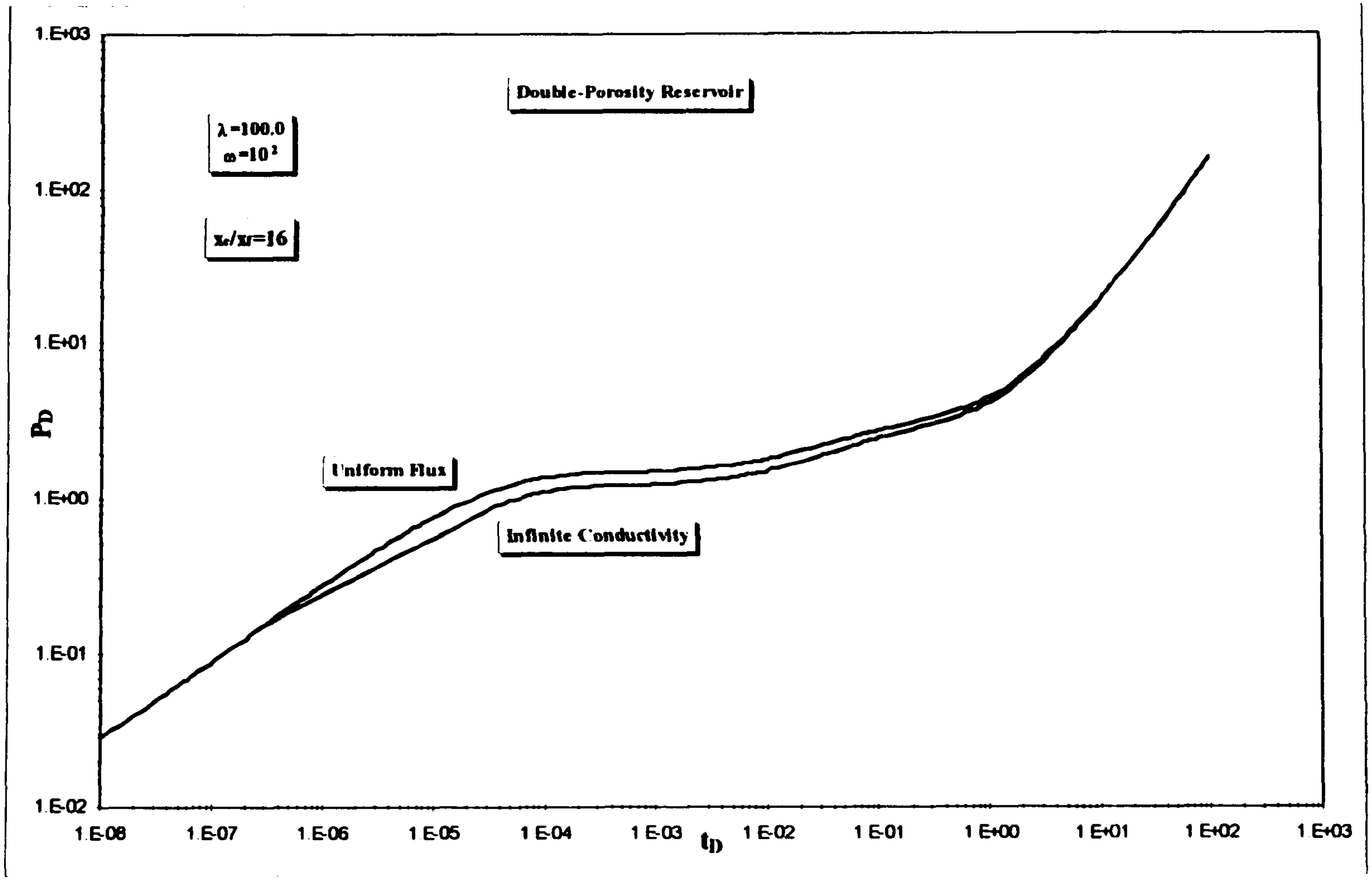

Figure 4.2.1 Pressure curves for uniform-flux solution versus infinite-conductivity in a double porosity reservoir

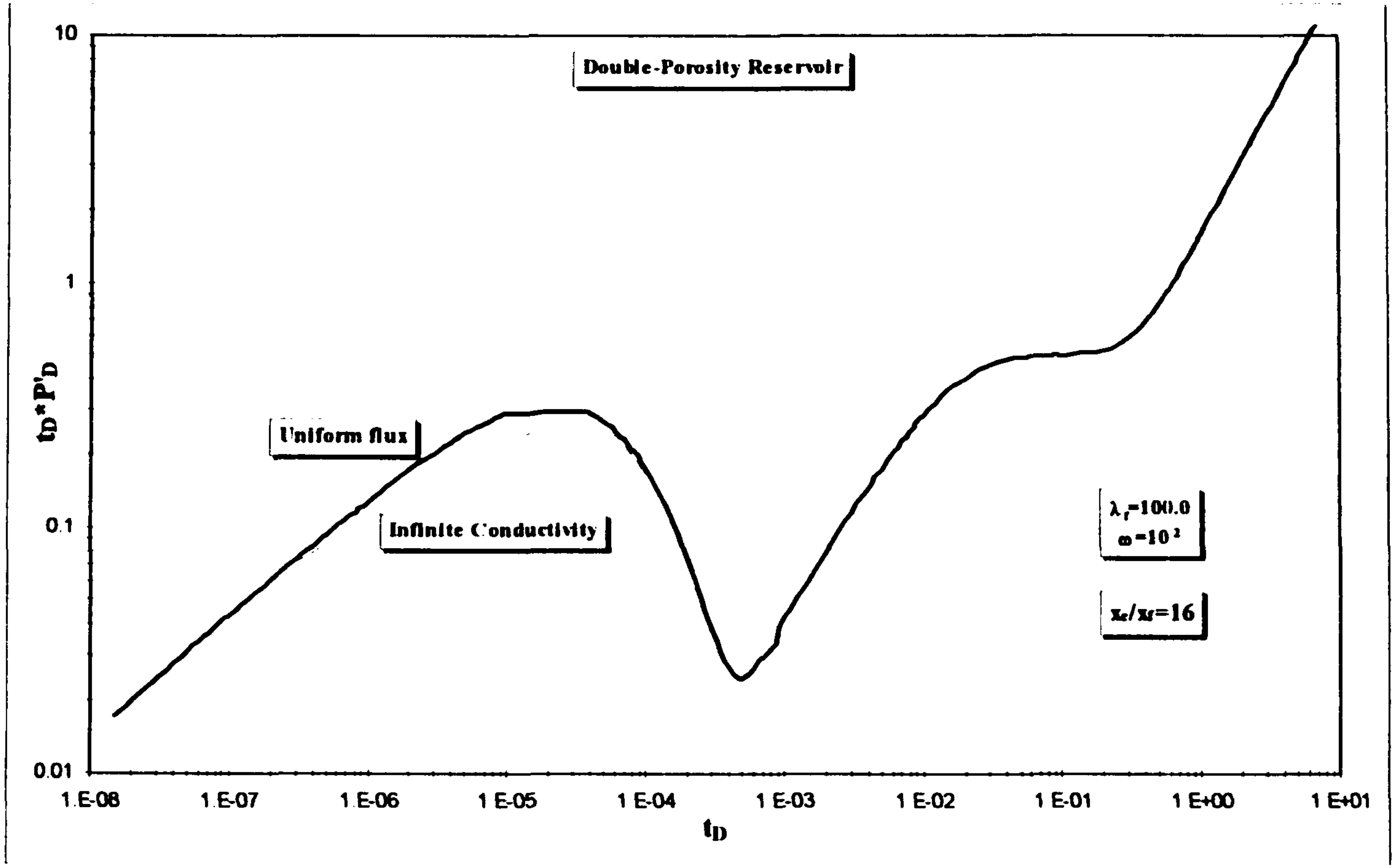

Figure 4.2.2 Pressure derivative curves for uniform-flux solution versus infinite-conductivity in a double porosity reservoir.

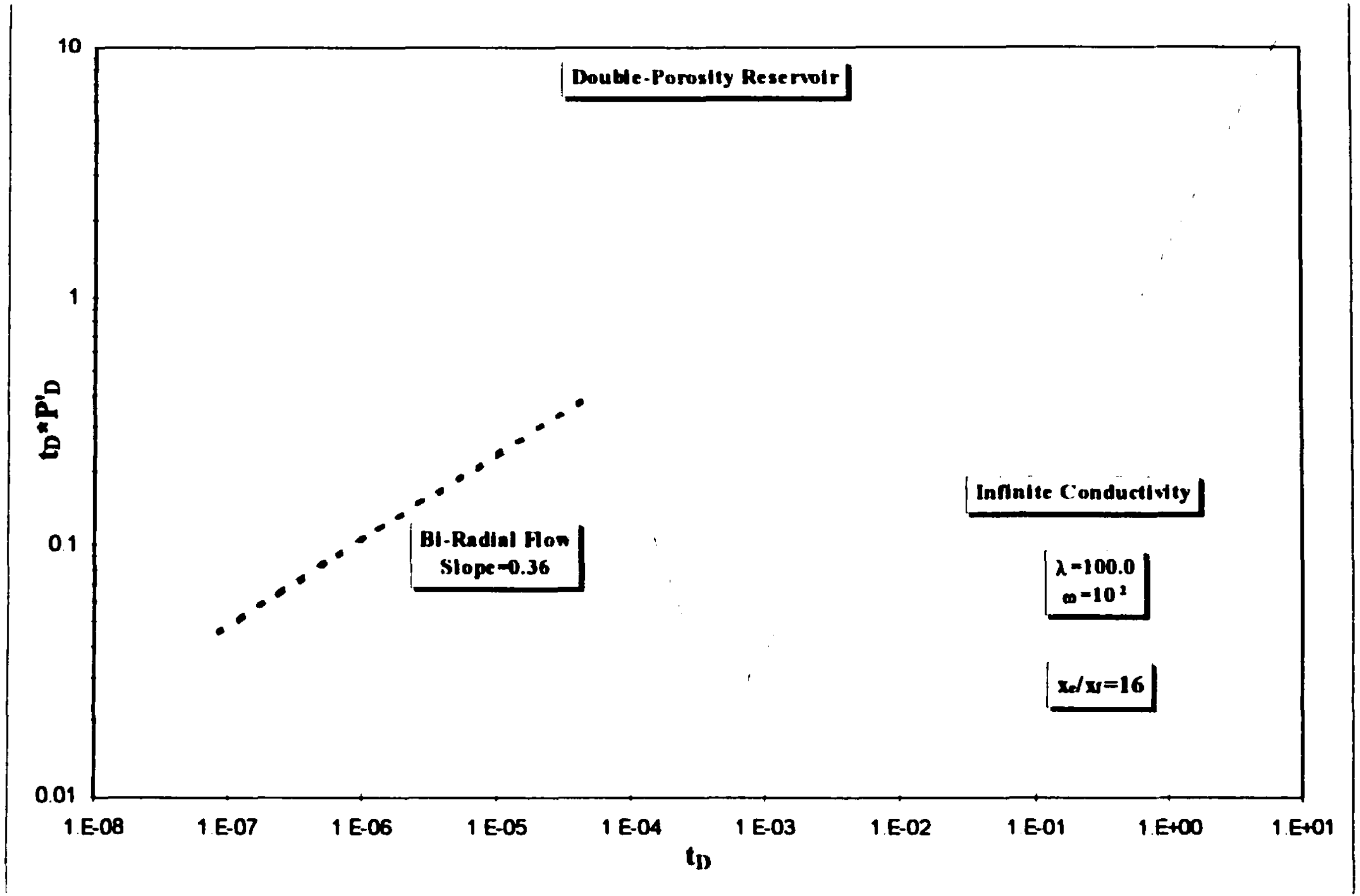

Figure 4.2.3 Pressure derivative curve for infinite-conductivity in a double porosity reservoir.

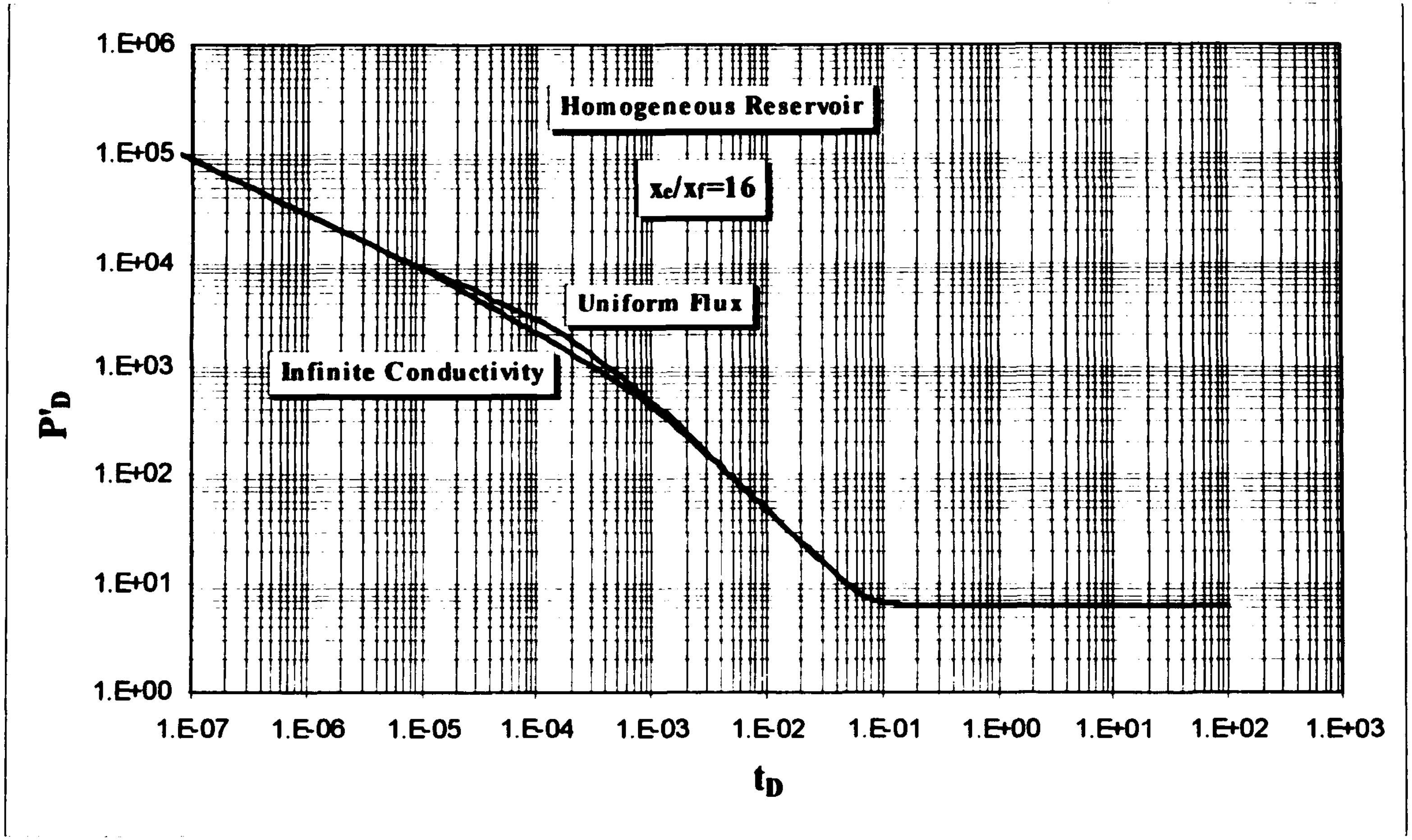

Figure 4.2.4 Pressure derivative curves for uniform-flux solution versus infinite-conductivity in a homogeneous reservoir.

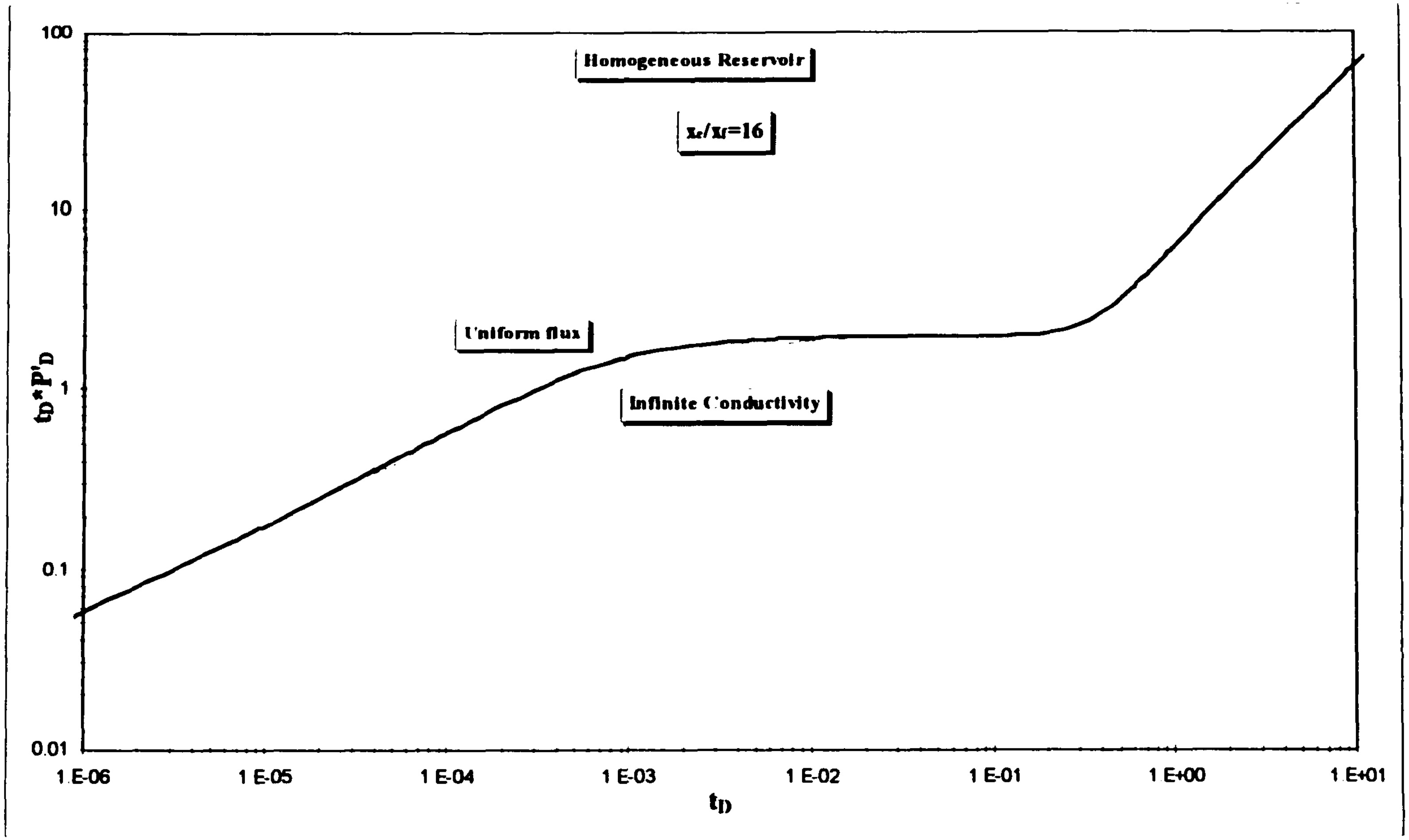

Figure 4.2.5 Pressure derivative curves for uniform-flux solution versus infinite-conductivity in a homogeneous reservoir.

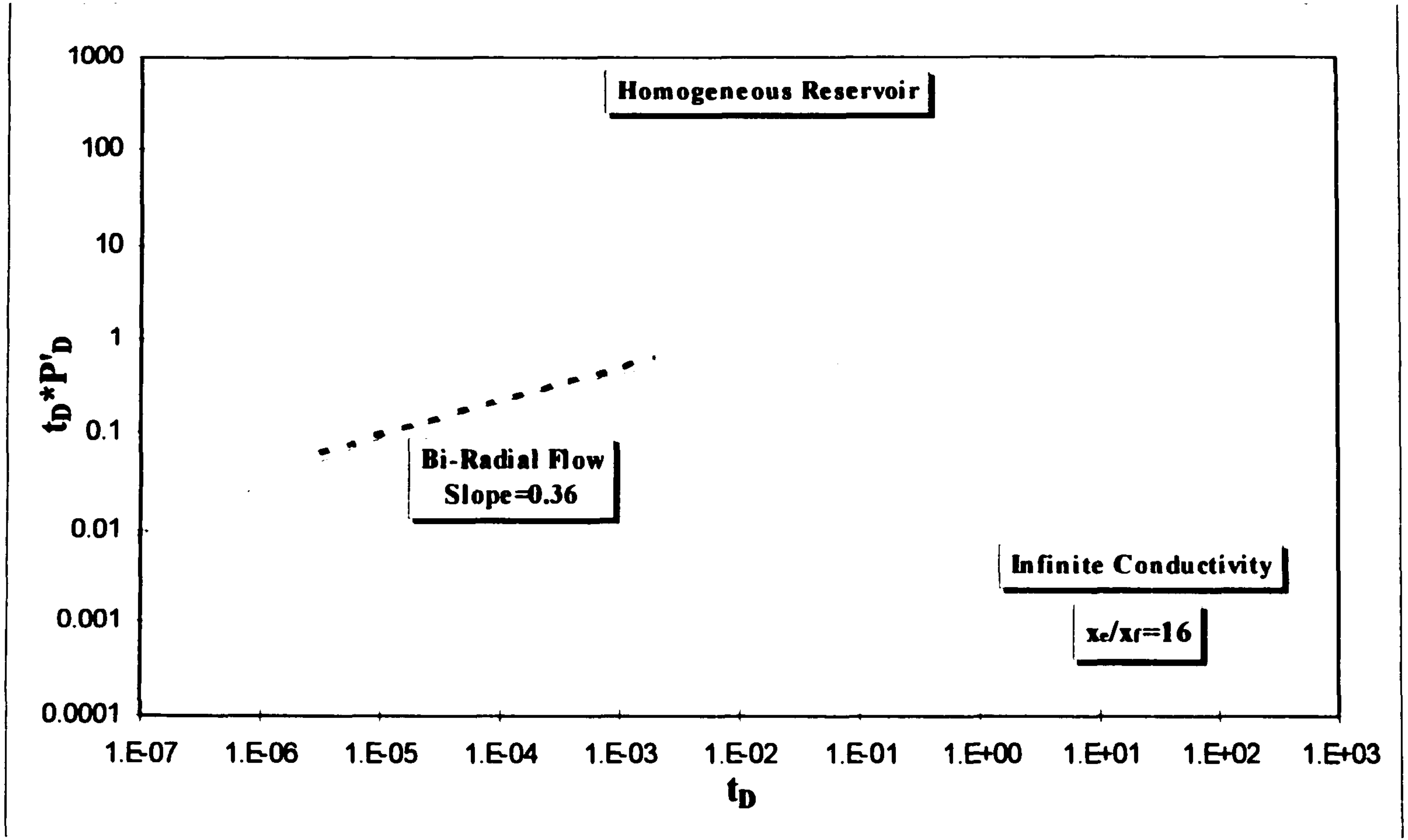

Figure 4.2.6 Pressure derivative curve for infinite-conductivity in a homogeneous reservoir.

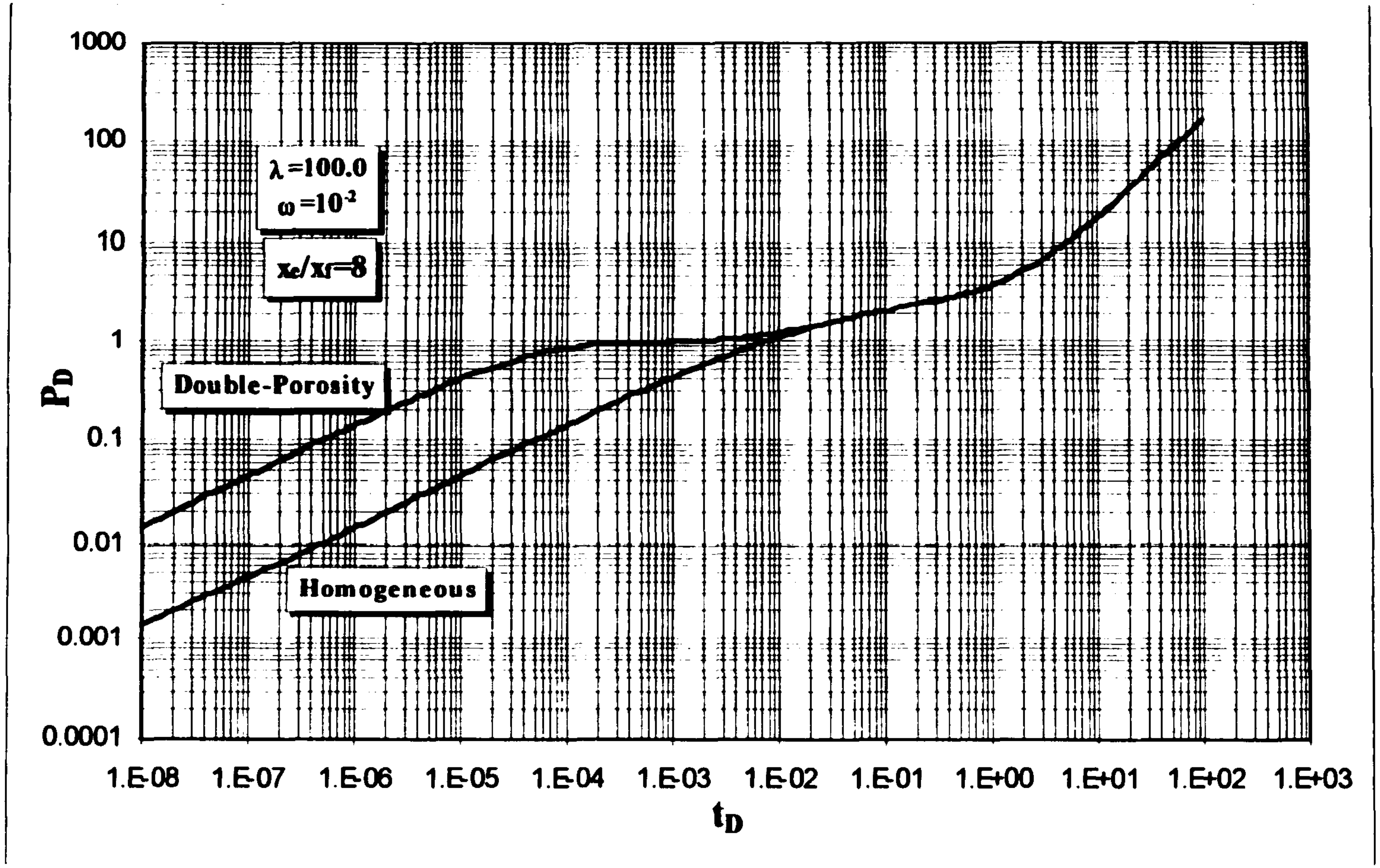

Figure 4.2.7 Pressure curves for infinite-conductivity in homogeneous and double porosity systems, $\left(\frac{x_e}{x_f}\right) = 8$.

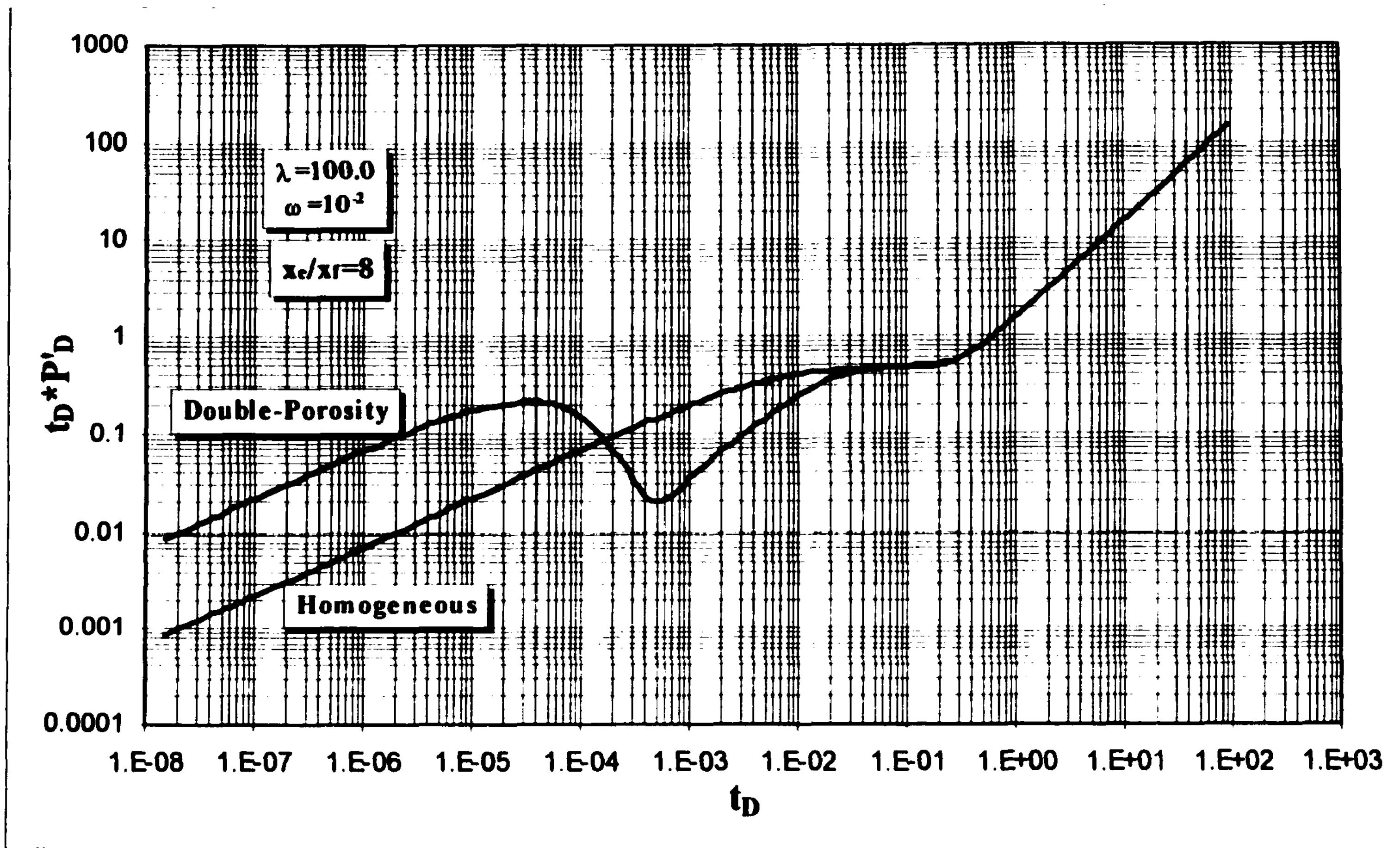

Figure 4.2.8 Pressure derivative curves for infinite-conductivity in homogeneous and double porosity systems, $\left(\frac{x_e}{x_f}\right) = 8$.

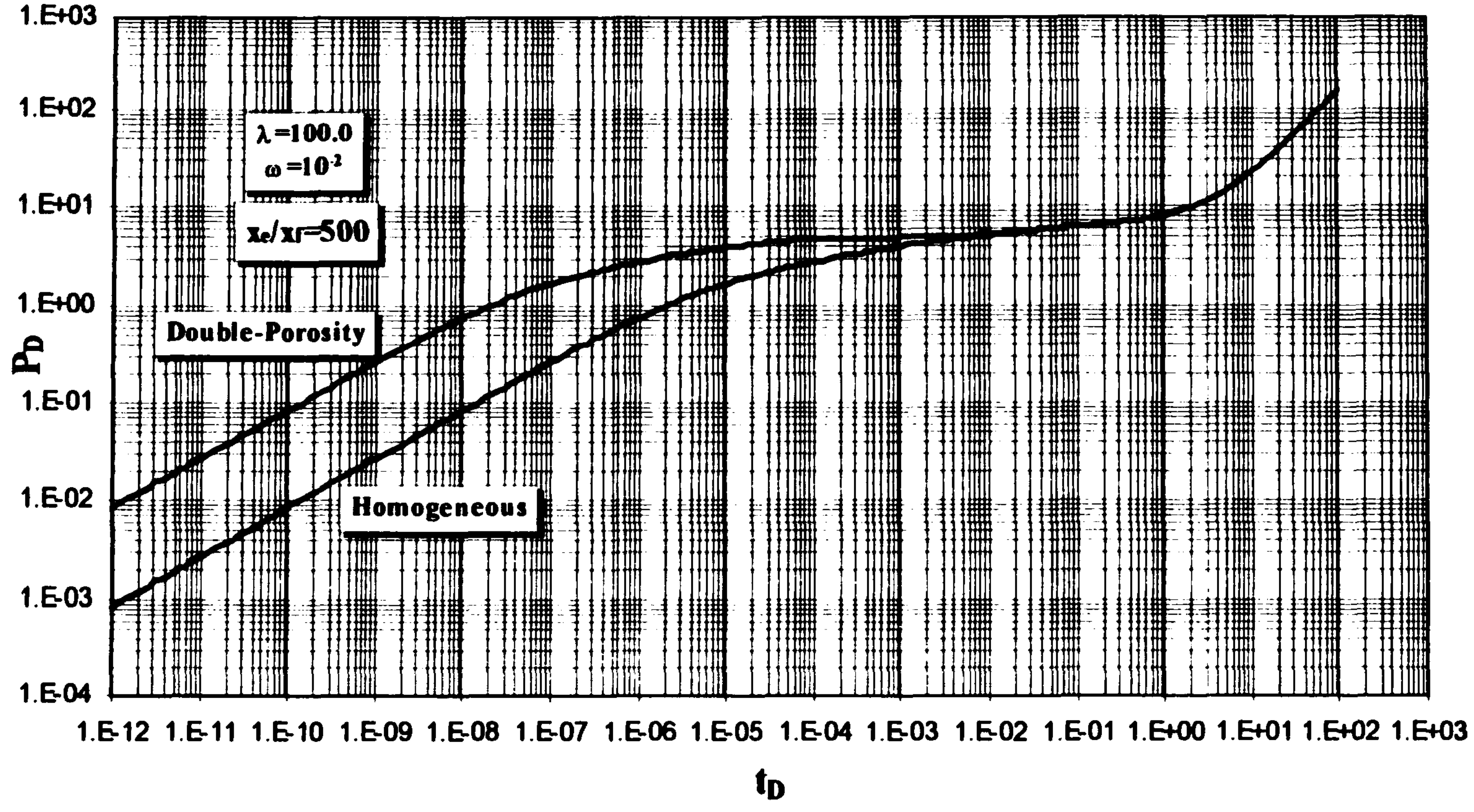

Figure 4.2.9 Pressure curves for infinite-conductivity in homogeneous and double porosity systems, $\left(\frac{x_e}{x_f}\right) = 500$.

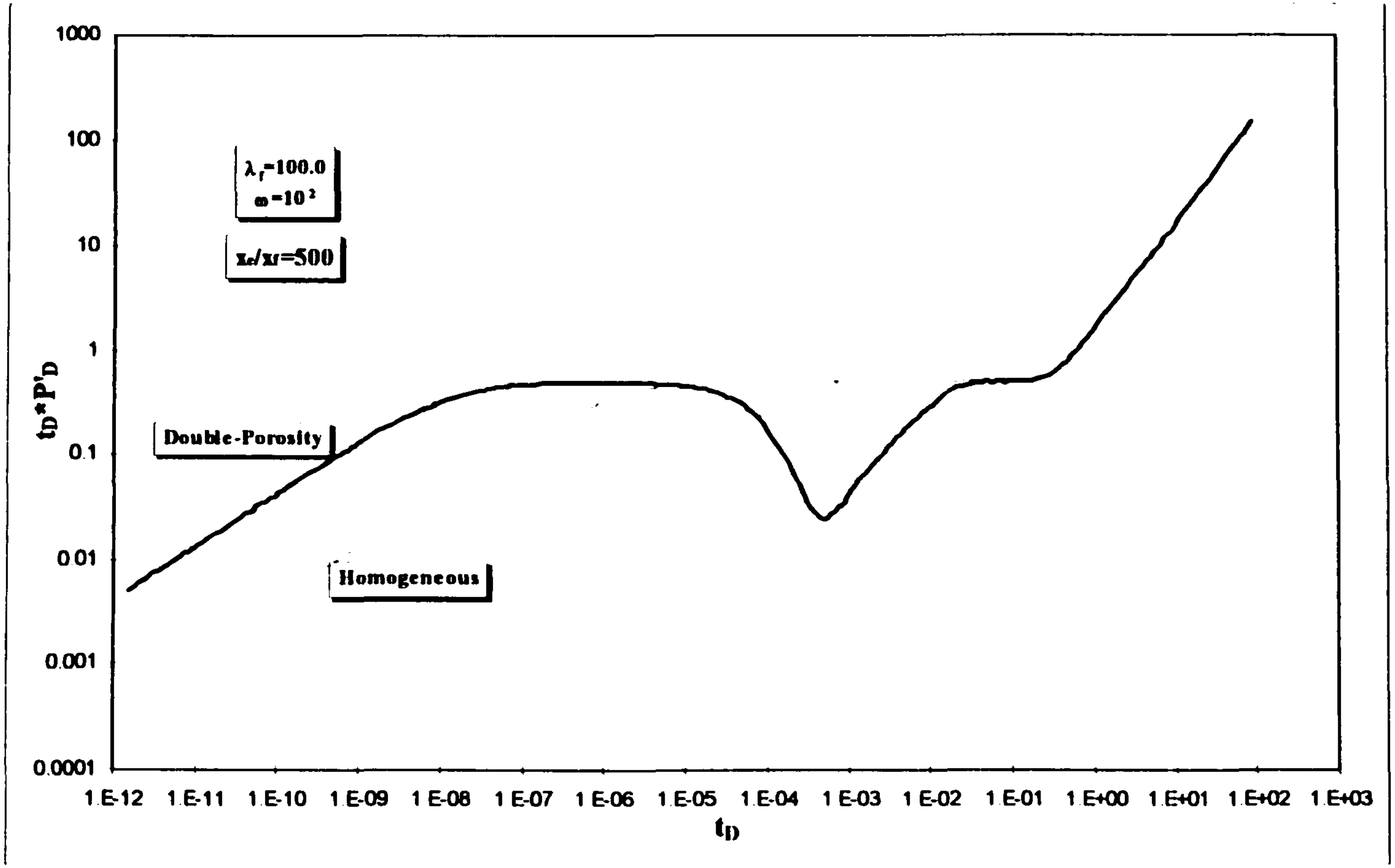

Figure 4.2.10 Pressure derivative curves for infinite-conductivity in homogeneous and double porosity systems, $\left(\frac{x_e}{x_f}\right) = 500$.

CHAPTER 5

APPLICATION OF TIAB'S DIRECT SYNTHESIS TO MULTI-LAYER DOUBLE POROSITY RESERVOIR WITH VERTICAL FRACTURE

Even though there has been a large number of publications on the behavior of pressure analysis, the combined effects of layered and vertically fractured system with double porosity on the pressure behavior needs to be examined. Osman[93-97] presented the pressure behavior of fractured well located in stratified homogeneous reservoirs for the two cases bounded square[94-95] and infinite-acting[93] reservoirs. He studied the behavior of uniform flux[93-95], infinite-conductivity[93-95], and finite-conductivity[96] fractures respectively. He found that the extension of fracture plays the major role in controlling the pressure behavior during early times while the system transmissibility is the major factor during late times. The case of a vertical fractured well inside multi-layered double porosity systems is not treated in literature. This work is intended to fill lacuna in knowledge. The main purpose of this chapter is to study and extend Tiab's Direct Synthesis technique to a vertical fractured multiple layer reservoir with double porosity. Specifically, this study was made on the closed, square, non-communicating, fractured two-layer reservoir producing at a constant flow rate. A new set of dimensionless pressure and pressure derivative versus dimensionless time type curves was generated. These type curves were developed for various values of flow capacity ratio as well as the variations on the fracture penetration ratio of each layer. Then, Tiab's Direct Synthesis Technique was applied to the generated type curves to provide a way of estimating the flow capacity and the fracture length of each layer. It was found that the effect of flow capacity ratio (transmissibility) on pressure derivative curves is significant. The effect of flow capacity ratio is the major factor on the pressure derivative during the late time pseudo-steady state.

The assumptions made in Chapter 4 are applied here. In addition, the reservoir to be studied consists of multiple, horizontal, naturally fractured layers of differing physical properties which are separated from each other by impermeable barriers. The fracture fully penetrates the vertical extent of each layer and is the same length in both sides of the well. In addition, it is convenient to assume gravity effects are negligible, and flow entering the wellbore comes only through the fracture. Each layer has a distinct value of flow capacity. The initial reservoir pressure, p_{int}, in each layer is the same. As the instantaneous wellbore pressure is identical and since the initial pressure is the same in all layers, then the pressure drop must be identical; thus:

$$\Delta p_i = p_{int} - p_i = \Delta p_{i+1} = p_{int} - p_{i+1} = \Delta p \tag{5.1}$$

Further, the sum flow rate from each layer must be equal to the total flow rate; thus:

$$q_t = \sum_{i=1}^{n} q_i \tag{5.2}$$

for i=1, 2, 3, ..., n.

For two-layer reservoirs, the total production rate is equal to the sum of the production rate of each layer:

$$q_t = q_1 + q_2 \tag{5.3}$$

The dimensionless flow rate of each layer is the ratio of the flow rate from the layer of interest to the surface flow rate:

$$q_{fDi} = \frac{q_i}{q_t} \tag{5.4}$$

The unit system is shown schematically in Figure 5.1. Under the assumption of pseudosteady state for interporosity flow between the matrix and fracture system, the dimensionless variables and general solution for wells in multi-layer double porosity reservoirs are discussed in Appendix B. The Laplace transform solution for fractured well in closed rectangular double porosity reservoir is discussed in Appendix G. Mavor and Walkup Jr.[43] presented a general description of the layered commingled model by applying the parallel resistance concept as:

$$\bar{p}_{wD} = \frac{1}{s}\left[C_D s + \sum_{i=1}^{n} \frac{1}{R_i}\right]^{-1} \tag{5.5}$$

where, R_i is the total layer resistance function and C_D is the dimensionless wellbore storage. The resistance terms depend upon the reservoir model selected for each layer.

An analytical expression for the pressure distribution created by the vertical fracture in a double porosity multi-layer reservoir can be obtained by combining the parallel resistance concept presented by Mavor and Walkup Jr.[43] with the Laplace transform solution presented by Liu and Yang[80], where:

$$R_i = \frac{\pi}{2}\left\{\frac{\coth(F_{oi} y_{eDi})}{F_{oi}} + 2\sum_{n=1}^{\infty}\frac{1}{(n\pi x_{fDi})^2}\sin^2(n\pi x_{fDi})\cos(n\pi x_{Di})\frac{\coth(F_{ni} y_{eDi})}{F_{ni}}\right\} + S_i \tag{5.6}$$

and

$$F_{ni} = \left[sf_i(s) + (n\pi)^2 \right]^{1/2} \tag{5.7}$$

All in all, the multi-layer reservoir solution can be modeled with the equivalent single-layer solution. The reservoir permeability and half fracture length of each layer can be then calculated with reasonable confidence.

This work is restricted to the behavior of a single fractured well in the center of a closed square reservoir; therefore:

$$x_e = y_e \tag{5.8}$$

A new set of type curves were developed for the case of a well intercepting a multi-layer vertically fractured reservoir with double porosity. These curves of pressure and pressure derivative can be used to interpret pressure transient tests in fractured wells without using type curve matching method. This can be done by applying Tiab's Direct Synthesis to allow the estimation of the fracture half length, x_{fi}, and fracture permeability, k_{fi}, of each layer. For example, Figures 5.2 through 5.4 illustrate the characteristic pressure and its derivative response in a two layer vertically fractured reservoir with pseudosteady state interporosity flow. Both wellbore storage and skin are ignored. The interpretation presented here utilizes a new version of pressure and pressure derivative type curves including flow capacity ratio and penetration ratio. Based on observations of the sensitivity of the response of these parameters, new correlations have been developed.

5.1 Uniform-Flux Fracture in Closed Systems

On Figure 5.3, the characteristic points and lines available for evaluating the pressure test can be identified. This figure shows the existence of the three flow regimes: (1) the linear flow line of slope 0.5, (2) the infinite-acting radial flow line of a horizontal straight line, and (3) the pseudo-steady state flow line of slope unity, in addition to the transition region. The figure shows the effect of flow capacity ratio on the pressure response where the storage coefficient is held constant ($\omega_1=\omega_2=0.1$), while the permeability-thickness product ratio (flow capacity ratio) is variable. In this figure, the characteristic points and lines available for evaluating the pressure test can be identified.

The infinite-acting radial flow portion of the pressure derivative is a horizontal straight line. Figure 5.3 illustrates that during this flow period, the equation for the pressure derivative is:

$$t_{DA} * p'_{wD} = 0.5 \tag{5.1.1}$$

Substituting the dimensionless pressure and dimensionless time in the above equation yields:

$$\bar{k}h = \frac{70.6 q_t B\mu}{(t * \Delta p'_w)_R} \tag{5.1.2}$$

where the subscript R stands for radial flow line and $\bar{k}$ represents the thickness-averaged value of layer permeabilities. $\bar{k}$ is defined as:

$$\bar{k}h = \sum_{i=1}^{n} k_{fi} h_i \tag{5.1.3}$$

where k_{fi} and h_i refer to the permeability and thickness of layer i, and n is the total number of layers.

The infinite-acting radial flow period observed in the pressure derivative curves is corresponding to all layers, therefore $\bar{k}h$ represents the total thickness-averaged value of layer permeabilities. Therefore, Equation 5.1.2 can be used to calculate the total flow capacity of the well.

The flow capacity of each layer is a very important parameter for characterization of multi-layer vertically fractured reservoirs and therefore must be quantified by direct synthesis. Figure 5.3 illustrates the characteristics of pressure derivative response in a two-layer vertically fractured reservoir with pseudosteady state interporosity flow, $\omega_1=\omega_2=0.1$, where wellbore storage is not considered. An important observation that will be used to develop a correlation for calculating the flow capacity of each layer is that the time of the beginning pseudosteady state line, $(t_{DA})_{bPSS}$, increases with the increase of the flow capacity ratio. It can be concluded from this figure that the length of this stage is influenced by the permeability contrast. The same conclusion has been made by Tariq and Ramey[39] for the case of multi-layer bounded homogeneous reservoirs. Figures 5.1.1 through 5.1.4 show the effect of storage coefficient, ω, and interporosity flow parameter, λ, on the pressure and pressure derivative responses in a two-layer vertically fractured reservoir with pseudosteady state interporosity flow. From these figures, it is clear that the beginning of pseudosteady state flow line is independent from ω and is only a function of λ. The characteristic time, $(t_{DA})_{bPSS}$, can be normalized by the time of the intersection point between the radial flow line and pseudo-steady state flow line, $(t_{DA})_{RPSSi}$, which is defined by Equation 4.1.32. In order to obtain the relationship, the late time pseudosteady state flow lines for different values of flow capacity ratio were presented in Figure 5.4. It is clear from the figure that the results for the case of $\frac{(k_f h)_1}{(k_f h)_2}<8$, are close to the results for an ideal single-layer case. For all other cases, the results are widely different. This means that for $\frac{(k_f h)_1}{(k_f h)_2}<8$, the pressure derivative behavior is equivalent to single-layer system with $\frac{(k_f h)_1}{(k_f h)_2}=1$. Figure 5.1.5 shows the correlation obtained to determine the flow capacity ratio. The empirical equation which fits the correlation, with less than 1% error, is given by:

$$\frac{(k_f h)_1}{(k_f h)_2} = 2.4055\left[\frac{(t)_{bPSS}}{\lambda(t)_{RPSSi}}\right]^2 + 7.9974\left[\frac{(t)_{bPSS}}{\lambda(t)_{RPSSi}}\right] \tag{5.1.4}$$

Figure 5.1.6 shows the correlation between the ratio of flow capacity of layer 1 to total flow capacity, $\frac{(k_f h)_1}{(\bar{k}h)}$, and the ratio of the characteristic times, $\left[\frac{(t)_{bPSS}}{\lambda(t)_{RPSSi}}\right]$.

The developed correlations in Equations 5.1.4 and Figures 5.1.5-6 depend on values obtained from the infinite-acting radial flow line as well as the pseudosteady state flow line. Unfortunately, based on the observation discussed in Chapter 4 that the infinite-acting flow period is dominant only if $\left(\frac{x_e}{x_f}\right)>8$, these correlations are useless for the case $\left(\frac{x_e}{x_f}\right)$ <8. Therefore, alternative correlations were developed to analyze any case in which the infinite-acting flow period is not observed. Figure 5.1.7 shows the flow capacity ratio, $\frac{(k_f h)_1}{(k_f h)_2}$, versus the characteristic time $\left[\frac{(t)_{bPSS}}{\lambda(t)_{min}}\right]$. With less than 1% error, the empirical correlation is given by:

$$\frac{(k_f h)_1}{(k_f h)_2} = 0.0022\left[\frac{(t)_{bPSS}}{\lambda(t)_{min}}\right]^2 + 0.2275\left[\frac{(t)_{bPSS}}{\lambda(t)_{min}}\right] \tag{5.1.5}$$

The present study was conducted to provide a knowledge of flow capacity in each layer using the analytical solution as discussed above. All equations developed in Chapter 4 can be improved to the case of multi-layer double porosity reservoirs using the dimensionless variables presented in Appendix B. Therefore, the multi-layer reservoir solution can be modeled with the equivalent single-layer solution. The reservoir permeability and half fracture length of each layer can be then calculated with reasonable confidence.

From the fracture linear flow period, the fracture length of each layer, x_{fi}, can be estimated by:

$$x_{fi} = \frac{2.032 q_t B}{(t*\Delta p'_w)_{L1}\sqrt{\omega_i}\, h_i}\sqrt{\frac{\mu_i}{k_{fi}\,(\phi c_t)_{ti}}} \tag{5.1.6}$$

where $(t*\Delta p'_w)_{L1}$ is the value of $(t*\Delta p'_w)$ at time one hour on the linear flow straight line.

The fracture length of each layer, x_{fi}, can be determined from the pressure line as:

$$x_{fi} = \frac{4.064 q_t B}{(\Delta p_w)_{L1} \sqrt{\omega_i}\, h_i} \sqrt{\frac{\mu_i}{k_{fi}\, (\phi c_t)_{ti}}} \tag{5.1.7}$$

where $(\Delta p_w)_{L1}$ is the value of (Δp_w) at time one hour on the fracture linear flow straight line.

From the pseudosteady state flow regime, the drainage area of each layer can be calculated as:

$$A_i = \frac{q_t B}{4.27 (t * \Delta p'_w)_{PSS1}\, h_i (\phi c_t)_{ti}} \tag{5.1.8}$$

where the subscript PSS1 stands for the pseudo-steady state flow regime at t=1 hr.

The shape factor of each layer, C_{Ai}, can be solved using the following equation:

$$C_{Ai} = 2.2458 \left(\frac{x_e}{x_f} \right)_i^2 \operatorname{Exp}\left[\left(\frac{0.000527 k_{fi} t_{PSS}}{(\phi c_t)_{ti} \mu_i A_i} \right) \left(1 - \frac{(\Delta p_w)_{PSS}}{(t * \Delta p'_w)_{PSS}} \right) \right] \tag{5.1.9}$$

where t_{PSS} is any convenient time during the pseudosteady state flow line. $(\Delta p_w)_{PSS}$ and $(t * \Delta p'_w)_{PSS}$ are values of (Δp_w) and $(t * \Delta p'_w)$ corresponding to t_{PSS}, respectively.

From the intersection point between the linear flow line and the infinite acting radial flow line, the fracture half-length of each layer can be estimated as:

$$\frac{x_{fi}^2}{k_{fi}} = \frac{t_{LRi}}{1207.1 (\phi c_t)_{ti} \mu_i \omega_i} \tag{5.1.10}$$

The intersection point between the linear flow line and pseudo-steady state flow line yields:

$$k_{fi} x_{fi}^2 = \frac{75.44 (\phi c_t)_{ti} \mu_i A_i^2}{\omega_i t_{LPSSi}} \tag{5.1.11}$$

The intersection point between the radial flow line and pseudo-steady state flow line, gives:

$$A_i = \frac{k_{fi} t_{RPSSi}}{301.77(\phi c_t)_{ti} \mu_i} \tag{5.1.12}$$

The wellbore storage coefficient defined in Equation 4.1.44 becomes:

$$C = \frac{h\bar{k}\, t_{USRi}}{1695\mu} \tag{5.1.13}$$

The transition period was discussed in previous chapters. With minor exception, the basic procedure is the same as for the single-layer system in Chapter 4. For the case of two-layer system, all correlations obtained and applied for the transition period take the layer parameters instead of the average reservoir parameters. For example, Equation 4.1.51 which calculates the interporosity flow parameter, λ_f, becomes:

$$\lambda_{fi} = \left[\frac{\pi}{\omega_i} \frac{(\phi c_t)_{ti} \mu_i x_{fi}^2}{0.0002637 k_{fi} t_{LUSi}} \right]^{1.2} \tag{5.1.14}$$

where the subscript LUSi stands for the intersection point between the unit slope line with the fracture storage dominated period linear flow line.

5.2 Infinite-Conductivity Fracture in Closed Systems

In the infinite-conductivity case, the curve reveals a fourth dominated flow regime which can be identified by a straight line of slope 0.36. This flow period is called the bi-radial flow which can be used to estimate the fracture half length of each layer:

$$x_{fi} = 10.914 \frac{x_{ei}}{\omega_i^{0.5}} \left(\frac{q_t B \mu_i}{\left(t * \Delta p_w'\right)_{BR1} k_{fi} h_i} \right)^{1.389} \left(\frac{k_{fi}}{(\phi c_t)_{ti} \mu_i A_i} \right)^{0.5} \tag{5.2.1}$$

where $(t * \Delta p_w')_{BR1}$ is the value of $(t * \Delta p_w')$ at time one hour on the bi-radial flow straight line. The intersection point between the bi-radial flow line and linear flow line gives:

$$\frac{x_{fi}^2}{k_{fi}} = \frac{t_{LBRi}}{1376.56(\phi c_t)_{ti} \mu_i \omega_i} \tag{5.2.2}$$

However for $\left(\frac{x_e}{x_f} \right) < 8$, the infinite-acting radial flow period is too short-lived or essentially non-existent. In this case, the average permeability can be estimated by:

$$\bar{k}h = \frac{75.39 q_t B \mu}{\left(t * \Delta p_w'\right)_{L1}} \frac{1}{\sqrt{t_{LBRi}}} \tag{5.2.3}$$

The intersection point between the bi-radial flow line and the infinite acting radial flow line yields:

$$\frac{x_{fi}^2}{k_{fi}} = \frac{t_{RBRi}}{1147(\phi c_t)_{ti} \mu_i \omega_i} \tag{5.2.4}$$

From the intersection point between the bi-radial flow line and the pseudosteady state flow line, the following relationship can be obtained:

$$k_{fi} = \frac{142.4(\phi c_t)_{ti}\mu_i A_i}{\omega_i^{0.5625} t_{PSSBRi}} \left(\frac{x_e}{x_f}\right)_i^{1.125} \tag{5.2.5}$$

5.3 Vertical Fracture in Closed Systems with Skin Effects

This section extends the work to include skin effects. Fracture acid stimulation test results in negative skin. Therefore, both positive and negative skin values are considered in this study. Figures 5.3.1 and 5.3.2 illustrate the characteristics of pressure derivative behavior in a two-layer vertically fractured reservoir with pseudosteady state interporosity flow, for various positive and negative skin values respectively. It is clear that the effect layering is a major factor on the pressure derivative curves during the late time pseudo-steady state. Figure 5.3.3 shows the effect of skin on the late time pseudosteady state flow pressure derivative behavior in a two-layer vertically fractured reservoir. In this work, skin is assumed to be equal for both layers. Therefore, the skin can be calculated by using average reservoir parameters and then:

$$S = S_1 = S_2 \tag{5.3.1}$$

where, S, S_1, and S_2 are average skin, skin of layer 1, and skin for layer 2 respectively.

Figures 5.3.4 through 5.3.6 show the characteristics of pressure derivative response in two-layer vertically fractured reservoirs for skin values of -1, 1, and 2 respectively. Figures 5.3.7 through 5.3.13 show the effect of skin on the late time pseudo-steady state flow pressure derivative response in two-layer vertically fractured reservoirs, for various values of skin. The following empirical correlation of $\frac{(k_f h)_1}{(k_f h)_2}$ versus the characteristic time $\left[\frac{(t)_{bPSS}}{\lambda(t)_{min}}\right]$ was developed and shown in Figures 5.3.14 through 5.3.21:

$$\frac{(k_f h)_1}{(k_f h)_2} = F\left[\frac{(t)_{bPSS}}{\lambda(t)_{min}}\right]^2 + G\left[\frac{(t)_{bPSS}}{\lambda(t)_{min}}\right] \tag{5.3.2}$$

where

$$F = 0.0022 \tag{5.3.3}$$

and

$$G = 0.0057\,(S)^2 - 0.0772\,(S) + 0.2275 \tag{5.3.4}$$

Dividing the dimensionless pressure equation by the dimensionless pressure derivative equation results in an expression for skin:

$$S = 0.5\left[\frac{(\Delta p_w)_R}{(t * \Delta p'_w)_R} - \ln\left(\frac{\bar{k} t_R}{(\phi c_t)_t \mu r_w^2}\right) + 7.43\right] \tag{5.3.5}$$

where t_R is any convenient time during the infinite-acting radial flow line and $(\Delta p_w)_R$ is the value of (Δp_w) corresponding to t_R. Note that the calculated skin from equation 5.3.5 is an average value, because the average reservoir parameters are used.

Individual skin factor can be estimated from:

$$S_i = 0.5\left[\frac{(\Delta p_w)_R}{(t * \Delta p'_w)_R} - \ln\left(\frac{k_{fi} t_R}{(\phi c_t)_{ti} \mu_i r_w^2}\right) + 7.43\right] \tag{5.3.6}$$

where t_R is any convenient time during the infinite-acting radial flow line and $(\Delta p_w)_R$ is the value of (Δp_w) corresponding to t_R and i is layer number and could be 1 or 2.

5.4 Pressure Derivative and Flow Rate Behavior in Vertically Fractured Reservoir with Double Porosity

To improve the prediction of the multi-layer reservoir behavior, it is necessary to determine the properties of the various layers. Due to the large number of parameters needed to be estimated in multi-layer vertically fractured double porosity models, the analysis of well test data from fractured reservoirs by using the pressure response alone does not contain sufficient information to determine individual properties. This section presents an analysis procedure for commingled layered systems that is completely analogous to that used for single-layered systems. It is developed from an understanding of the various flow periods described in Chapter 4. Pressure, pressure derivative, and flow rate data can be analyzed to determine individual layer properties, such as flow capacity; half-fracture length; dimensionless storage coefficient, ω; interporosity flow parameter, λ_f; and skin values.

As discussed in Chapter 3, there is an alternative procedure which has been suggested by different authors[43,46,47,64] to calculate an equivalent single layer system from the response of a layered system. They show that the rate normalized pressure of $(\Delta P)/q_{ri}$ from the exact Laplace space solutions gives an equivalent single-layer pressure behavior, where the relative flow rate of each layer is the ratio of the flow rate from the layer of interest to the surface flow rate. The relative flow rate is defined in Equation 3.6.1.

Economides[66] presented a methodology to interpret fractured well tests based on observations of the behavior of fractured wells. He suggested the influence functions in order to allow the interpretation of drawdown data. He stated that the influence function gives an equivalent single layer pressure behavior. Economides said that "the simplest form of the influence function is dividing the pressure difference by the corresponding flow rate,"[66] i.e., $\Delta p/q$ for oil.

As mentioned earlier, Osman[93-97] presented the pressure behavior of fractured well located in stratified homogeneous reservoirs for the bounded square[94-95] and infinite-acting[93] reservoirs. He studied the behavior of uniform flux[93-95], infinite-conductivity[93-95] and finite-conductivity[96] fractures respectively. He found[96-97] (1997) that fractional production rate from different layers is a good measure of reservoir and fracture characteristics. The superposition technique was applied to develop simple equations that can be used to analyze the simultaneously measured sand-face after-flow rate and down-hole pressure data for the linear flow period. These equations were used combined with those for the pseudoradial flow period to devise a new method of analysis.

The case of a vertically fractured well inside multi-layered double porosity systems are not treated in the literature. This work presents a mathematical model which describes pressure tests in vertically fractured wells. A new simple method of analysis based on this model is presented for pressure tests. This method is useful for the analysis of simultaneously measured down-hole sand-face rate and pressure.

This work addresses the problem of interpretation of layered vertically fractured double porosity reservoir in commingled wells. The Laplace space for pressure of vertically fractured well in a single-layer double porosity reservoir is defined in Equation G.39. The Equation can be modified for the case of multi-layer reservoir as:

$$\bar{\bar{p}}_{fD} = \frac{\pi}{2}\bar{q}_{fD}\left\{\frac{\coth(F_{oi}y_{eDi})}{F_{oi}} + 2\sum_{n=1}^{\infty}\frac{1}{(n\pi x_{fDi})^2}\sin^2(n\pi x_{fDi})\frac{\coth(F_{ni}y_{eDi})}{F_{ni}}\right\} \quad (5.4.1)$$

The sum of the dimensionless flow rate from each layer must be equal to the total flow rate; thus Equation G.25 becomes:

$$\bar{q}_{fD} = \frac{1}{s}\sum_{i=1}^{n} q_{fDi} = \frac{1}{s}\sum_{i=1}^{n}\left(\frac{q_i}{q_t}\right) \quad (5.4.2)$$

where n is the sum of layers. Equation 5.4.1 can be solved by combining the above condition with the following condition:

$$\bar{p}_{wD} = \bar{\bar{p}}_{fD} \quad (5.4.3)$$

The Laplace transform for pressure of vertically fractured well in a multi-layer double porosity reservoir results in:

$$\bar{p}_{wD} = \frac{\pi}{2}\sum_{i=1}^{n} q_{fDi}\left\{\frac{\coth(F_{oi}y_{eDi})}{F_{oi}} + 2\sum_{n=1}^{\infty}\frac{1}{(n\pi x_{fDi})^2}\sin^2(n\pi x_{fDi})\frac{\coth(F_{ni}y_{eDi})}{F_{ni}}\right\} \quad (5.4.4)$$

The single-layer Laplace transform in a multi-layered system can be developed from the above equation as:

$$\bar{p}_{wDi} = \frac{\pi}{2} q_{fDi}\left\{\frac{\coth(F_{oi}y_{eDi})}{F_{oi}} + 2\sum_{n=1}^{\infty}\frac{1}{(n\pi x_{fDi})^2}\sin^2(n\pi x_{fDi})\frac{\coth(F_{ni}y_{eDi})}{F_{ni}}\right\} \quad (5.4.5)$$

The major conclusion from the above discussion is that the log-log plot of pressure change and derivative group divided by the layer dimensionless flow, q_{fDi}, versus time is sufficient to define the various flow periods. As a consequence, the approach presented here will allow to determine the individual properties of a single layer in a multi-layer fractured reservoir. This observation agrees with the influence function approach suggested by Economides[66].

Although the total flow rate from the well is constant, the fractional production rate from a particular layer q_i varies with time[97]. Superposition technique in time is applied to Equation 5.4.5 takes into account such variation. Thus, the dimensionless pressure at the time of each measured point can be given by:

$$\bar{p}_{wDi} = \sum_{j=1}^{N} \left(q_{fDi,j} - q_{fDi,j-1} \right) R_i (t_N - t_{j-1}) \tag{5.4.6}$$

where R_i is defined in Equation 5.4. i=1,2,.....,n layers. The same observation was found by Osman[97] (1997) for pressure behavior of fractured well located in stratified homogeneous reservoirs for the two cases bounded square[94-95] and infinite-acting[93] reservoirs. Therefore, he recommended to measure fractional flow during testing. For the infinite-acting case, pressure derivative plots reveal three dominated flow regimes: linear flow period, transition period, and infinite-acting radial period. The case of closed system reveals an additional flow period, called the pseudo-steady state flow regime. All flow regimes will be discussed below.

The dimensionless variables for multi-layer fractured double porosity reservoir case has been defined and presented in Appendix B. Chapter 4 further presents the direct synthesis method for interpreting pressure transient tests in single-layer fractured reservoirs. As a direct consequence, a log-log plot of $(\Delta P_w)/(q_{fDi})$ and $(t^*\Delta P'_w)/(q_{fDi})$ versus time can be used in developing the analysis procedure that combines the defined dimensionless variables in Appendix B and the work presented in Chapter 4. Subsequently, it is possible to estimate the individual properties of a single layer in a multi-layer fractured reservoir.

From fracture linear flow period, the fracture length of each layer, x_{fi}, can be estimated by:

$$x_{fi} = \frac{2.032 q_t B}{\left[\frac{(t * \Delta p'_w)}{q_{fDi}}\right]_{L1} \sqrt{\omega_i}\, h_i} \sqrt{\frac{\mu_i}{k_{fi}\,(\phi c_t)_{fi}}} \tag{5.4.7}$$

where $\left[\frac{(t * \Delta p'_w)}{q_{fDi}}\right]_{L1}$ is the value of $\left[\frac{(t * \Delta p'_w)}{q_{fDi}}\right]$ at time one hour on the linear flow straight line.

The fracture length of each layer, x_{fi}, can be determined from the pressure line as:

$$x_{fi} = \frac{4.064 q_t B}{\left(\frac{\Delta p_w}{q_{fDi}}\right)_{L1} \sqrt{\omega_i}\, h_i} \sqrt{\frac{\mu_i}{k_{fi}\,(\phi c_t)_{fi}}} \tag{5.4.8}$$

where $\left(\frac{\Delta p_w}{q_{fDi}}\right)_{L1}$ is the value of $\left(\frac{\Delta p_w}{q_{fDi}}\right)$ at time one hour on the fracture linear flow straight line.

From the infinite-acting radial flow line, layer permeability can by calculated as:

$$k_{fi} = \frac{70.6 q_t B \mu_i}{\left[\frac{(t * \Delta p'_w)}{q_{fDi}}\right]_{R} h_i} \tag{5.4.9}$$

where the subscript R stands for radial flow line.

From the pseudosteady state flow regime, the drainage area of each layer can be calculated as:

$$A_i = \frac{q_t B}{4.27\left[\dfrac{(t * \Delta p'_w)}{q_{fDi}}\right]_{PSS1} h_i (\phi c_t)_{ti}} \tag{5.4.10}$$

where the subscript PSS1 stands for the pseudosteady state flow regime at t=1 hr.

The shape factor of each layer, C_{Ai}, can be solved using the following equation:

$$C_{Ai} = 2.2458\left(\frac{x_e}{x_f}\right)_i^2 \mathrm{Exp}\left[\left(\frac{0.000527 k_{fi} t_{PSS}}{(\phi c_t)_{ti}\mu_i A_i}\right)\left(1 - \frac{\left(\Delta p_w / q_{fDi}\right)_{PSS}}{\left(t * \Delta p'_w / q_{fDi}\right)_{PSS}}\right)\right] \tag{5.4.11}$$

where t_{PSS} is any convenient time during the pseudosteady state flow line. $\left(\Delta p_w / q_{fDi}\right)_{PSS}$ and $\left(t * \Delta p'_w / q_{fDi}\right)_{PSS}$ are values of $\left(\Delta p_w / q_{fDi}\right)$ and $\left(t * \Delta p'_w / q_{fDi}\right)$ corresponding to t_{PSS}, respectively.

For the infinite-conductivity case, the fracture half-length of each layer can be estimated from the bi-radial flow line as:

$$x_{fi} = 10.914 \frac{x_{ei}}{\omega_i^{0.5}}\left(\frac{q_t B \mu_i}{\left(t * \Delta p'_w / q_{fDi}\right)_{BR1} k_{fi} h_i}\right)^{1.389}\left(\frac{k_{fi}}{(\phi c_t)_{ti}\mu_i A_i}\right)^{0.5} \tag{5.4.12}$$

where $\left(t * \Delta p'_w / q_{fDi}\right)_{BR1}$ is the value of $\left(t * \Delta p'_w / q_{fDi}\right)$ at time one hour on the bi-radial flow straight line.

The infinite-acting radial flow period is too short-lived or essentially non-existent for $\left(\frac{x_e}{x_f}\right) < 8$. Then the layer permeability can be estimated by:

$$k_{fi} = \frac{75.39 q_t B \mu_i}{\left(t * \Delta p'_w / q_{fDi}\right)_{Li} h_i} \frac{1}{\sqrt{t_{LBRi}}} \tag{5.4.13}$$

Individual skin factor can be calculated as:

$$S_i = 0.5\left[\frac{\left(\Delta p_w / q_{fDi}\right)_R}{\left(t * \Delta p'_w / q_{fDi}\right)_R} - \ln\left(\frac{k_{fi} t_R}{(\phi c_t)_{ti} \mu_i r_w^2}\right) + 7.43\right] \tag{5.4.14}$$

where t_R is any convenient time during the infinite acting radial flow line and $\left(\Delta p_w / q_{fDi}\right)_R$ is the value of $\left(\Delta p_w / q_{fDi}\right)$ corresponding to t_R.

5.5 Procedures

The following step-by-step procedures will demonstrate the applicability of Tiab's Direct Synthesis Technique.

Case 1: Uniform-Flux Fracture in Multi-Layer Closed Systems with no Skin

Step 1: Construct a plot of Δp and $(t^*\Delta p_w')$ versus time on a log-log graph and identify the various characteristic points and lines.

Step 2: Read the value of $(t^*\Delta p_w')_R$ corresponding to the infinite-acting radial flow line.

Step 3: Calculate the total flow capacity of the reservoir, $\bar{k}h$, using Equation 5.1.2.

Step 4: Determine ω and λ as outlined in Reference 63.

Step 5: Verify ω using either Equation 4.1.47 or Equation 4.1.53.

Step 6: Calculate $\left[\dfrac{(t)_{bPSS}}{\lambda(t)_{RPSS}}\right]$ and $\left[\dfrac{(t)_{bPSS}}{\lambda(t)_{min}}\right]$ ratios.

Step 7: Determine the ratio $\dfrac{(k_f h)_1}{(k_f h)_2}$ using either Equation 5.1.4 or Equation 5.1.5.

Step 8: Calculate the ratio $\dfrac{(k_f h)_1}{(\bar{k}h)}$ using Equation 3.2.9.

Step 9: Calculate the flow capacity ratio of Layer 1 using Equation 3.2.7.

Step 10: Calculate the flow capacity ratio of Layer 2 using Equation 3.2.11.

Step 11: Obtain the value of $(t^*\Delta p_w')$ at time t=1 hr from the linear flow line (extrapolated if necessary), $(t^*\Delta p_w')_{L1}$.

Step 12: Calculate the half-fracture length, x_f, from Equation 5.1.6. If the linear flow line portion of $(t^*\Delta p_w')$ is too short or too distorted by near wellbore effect and noise, then x_f should be determined from the half-slope line of Δp_w using Equation 5.1.7; then use Equation 4.1.13 to draw the half-slope line of the pressure derivative curve.

Step 13: Determine the line of intersection of the linear and radial flow line from the graph, i.e. t_{LRi}, using the $(t^*\Delta p_w')$ curve.

Step 14: Calculate the ratio $\frac{x_{fi}^2}{k_{fi}}$ from Equation 5.1.10. Then calculate this ratio using k_{fi} and x_{fi} values obtained in steps 9,10 and 12 respectively. If the two ratios are approximately equal, then the values of k_{fi} and x_{fi} are correct. If these ratios are significantly different, shift one or both straight lines, and repeat Steps 2 through 14 until the ratios are equal.

Step 15: Read the value of $(t^*\Delta p_w')_{PSS1}$ from the pseudosteady state line. Calculate the drainage area, A_i, using Equation 5.1.8.

Step 16: Obtain the time of intersection of the infinite-acting line and the pseudosteady state line, i.e. t_{RPSSi}, from the graph, and calculate A_i from Equation 5.1.12. If the two values of A_i in Steps 15 and 16 are approximately equal, then A_i is correct. If they are distinctly different then shift left or right and repeat Steps 15 and 16 until Equation 5.1.8 and 5.1.12 give the same value of A_i.

Step 17: Calculate the interporosity flow parameter after stimulation, λ_{fi}, using Equation 4.1.45.

Step 18: Verify λ_{fi} using Equations 4.1.50, 4.1.51 and 4.1.52.

Step 19: Select any convenient time t_R during the infinite-acting period and read the corresponding value of $(\Delta p_w)_R$; then calculate the skin factor of each layer from Equation 5.3.6.

Step 20: Read the value of Δp_w and $(t^*\Delta p_w')$ corresponding to any convenient time t_{PSS} during the pseudosteady state flow portion of the curves and calculate the shape factor C_{Ai} from Equation 5.1.9.

Case 2:Infinite-Conductivity Fracture in Multi-Layer Closed Systems with no Skin

Step 1: Construct a plot of Δp and $(t^*\Delta p_w')$ versus time on a log-log graph and identify the various characteristic points and lines.

Step 2: Read the value of $(t^*\Delta p_w')_R$ corresponding to the infinite-acting radial flow line.

Step 3: Calculate the total flow capacity of the reservoir, $\bar{k}h$, using Equation 5.1.2.

Step 4: Determine ω and λ as outlined in Reference 63.

Step 5: Verify ω using either Equation 4.1.47 or Equation 4.1.53.

Step 6: Calculate $\left[\dfrac{(t)_{bPSS}}{\lambda(t)_{RPSS}}\right]$ and $\left[\dfrac{(t)_{bPSS}}{\lambda(t)_{\min}}\right]$ ratios.

Step 7: Determine the ratio $\dfrac{(k_f h)_1}{(k_f h)_2}$ using either Equation 5.1.4 or Equation 5.1.5.

Step 8: Calculate the ratio $\dfrac{(k_f h)_1}{(\bar{k}h)}$ using Equation 3.2.9.

Step 9: Calculate the flow capacity ratio of Layer 1 using Equation 3.2.7.

Step 10: Calculate the flow capacity ratio of Layer 2 using Equation 3.2.11.

Step 11: Read the value of $(t^*\Delta p_w')_{PSS1}$ from the pseudosteady state line. Calculate the drainage area, A_i, using Equation 5.1.8.

Step 12: Obtain the time of intersection of the infinite-acting line and the pseudosteady state line, i.e. t_{RPSSi}, from the graph, and calculate A_i from Equation 5.1.12. If the two values of A_i in Steps 15 and 16 are approximately equal, then A_i is correct. If they are distinctly different then shift left or right and repeat Steps 15 and 16 until Equation 5.1.8 and 5.1.12 give the same value of A_i.

Step 13: Obtain the value of $(t^*\Delta p_w')$ at time t=1 hr from the bi-radial flow line (extrapolated if necessary), $(t^*\Delta p_w')_{BR1}$.

Step 14: Calculate the half-fracture length of each layer, x_{fi}, from Equation 5.2.1.

Step 15: Calculate the ratio $\frac{x_{fi}^2}{k_{fi}}$ of each layer using the values k_{fi} and x_{fi} values obtained in steps 9,10 and 14 respectively.

Step 16: From the graph, determine the time of intersection of the radial flow line and the bi-radial flow line, t_{RBRi}, then calculate the ratio $\frac{x_{fi}^2}{k_{fi}}$ from Equation 5.2.4. If steps 15 and 16 give the same value of $\frac{x_{fi}^2}{k_{fi}}$, then the values of k_{fi} and x_{fi} are correct. If they are different, then shift one or both straight lines (bi-radial and infinite-acting lines) and repeat Steps 9,10,13,14,15 and 16 until Steps 15 and 16 give the same value of $\frac{x_{fi}^2}{k_{fi}}$.

Step 17: Calculate the interporosity flow parameter after stimulation, λ_{fi}, using Equation 4.1.45.

Step 18: Verify λ_{fi} using Equations 4.1.50, 4.1.51 and 4.1.52.

Step 19: Select any convenient time t_R during the infinite-acting period and read the corresponding value of $(\Delta p_w)_R$; then calculate the skin factor of each layer from Equation 5.3.6.

Step 20: Read the value of Δp_w and $(t^*\Delta p_w')$ corresponding to any convenient time t_{PSS} during the pseudosteady state flow portion of the curves and calculate the shape factor C_{Ai} from Equation 5.1.9.

Case 3: Uniform-Flux Fracture in Multi-Layer Closed Systems with Skin

Step 1: Construct a plot of Δp and $(t^*\Delta p_w')$ versus time on a log-log graph and identify the various characteristic points and lines.

Step 2: Read the value of $(t^*\Delta p_w')_R$ corresponding to the infinite-acting radial flow line.

Step 3: Calculate the total flow capacity of the reservoir, $\bar{k}h$, using Equation 5.1.2.

Step 4: Determine ω and λ as outlined in Reference 63.

Step 5: Verify ω using either Equation 4.1.47 or Equation 4.1.53.

Step 6: Calculate $\left[\dfrac{(t)_{bPSS}}{\lambda(t)_{\min}}\right]$ ratio.

Step 7: Calculate the skin factor using Equation 5.3.5.

Step 8: Determine the ratio $\frac{(k_f h)_1}{(k_f h)_2}$ using Equation 5.3.2.

Step 9: Calculate the ratio $\frac{(k_f h)_1}{(\bar{k}h)}$ using Equation 3.2.9.

Step 10: Calculate the flow capacity ratio of Layer 1 using Equation 3.2.7.

Step 11: Calculate the flow capacity ratio of Layer 2 using Equation 3.2.11.

Step 12: Obtain the value of $(t^*\Delta p_w')$ at time t=1 hr from the linear flow line (extrapolated if necessary), $(t^*\Delta p_w')_{L1}$.

Step 13: Calculate the half-fracture length, x_f, from Equation 5.1.6. If the linear flow line portion of $(t^*\Delta p_w')$ is too short or too distorted by near wellbore effect and noise, then x_f should be determined from the half-slope line of Δp_w using Equation 5.1.7; then use Equation 4.1.13 to draw the half-slope line of the pressure derivative curve.

Step 14: Determine the line of intersection of the linear and radial flow line from the graph, i.e. t_{LRi}, using the $(t^*\Delta p_w')$ curve.

Step 15: Calculate the ratio $\frac{x_{fi}^2}{k_{fi}}$ from Equation 5.1.10. Then calculate this ratio using k_{fi} and x_{fi} values obtained in steps 9,10 and 12 respectively. If the two ratios are approximately equal, then the values of k_{fi} and x_{fi} are correct. If these ratios are significantly different, shift one or both straight lines and repeat Steps 2 through 14 until the ratios are equal.

Step 16: Read the value of $(t^*\Delta p_w')_{PSS1}$ from the pseudosteady state line. Calculate the drainage area, A_i, using Equation 5.1.8.

Step 17: Obtain the time of intersection of the infinite-acting line and the pseudosteady state line, i.e. t_{RPSSi}, from the graph, and calculate A_i from Equation 5.1.12. If the two values of A_i in Steps 15 and 16 are approximately equal, then A_i is correct. If they are distinctly different then shift left or right and repeat Steps 15 and 16 until Equation 5.1.8 and 5.1.12 give the same value of A_i.

Step 18: Calculate the interporosity flow parameter after stimulation, λ_{fi}, using Equation 4.1.45.

Step 19: Verify λ_{fi} using Equations 4.1.50, 4.1.51 and 4.1.52.

Step 20: Select any convenient time t_R during the infinite-acting period and read the corresponding value of $(\Delta p_w)_R$; then calculate the skin factor of each layer from Equation 5.3.6.

Step 21: Read the value of Δp_w and $(t^*\Delta p_w')$ corresponding to any convenient time t_{PSS} during the pseudosteady state flow portion of the curves and calculate the shape factor C_{Ai} from Equation 5.1.9.

Case 4: Infinite-Conductivity Fracture in Multi-Layer Closed Systems with Skin

Step 1: Construct a plot of Δp and $(t^*\Delta p_w')$ versus time on a log-log graph and identify the various characteristic points and lines.

Step 2: Read the value of $(t^*\Delta p_w')_R$ corresponding to the infinite-acting radial flow line.

Step 3: Calculate the total flow capacity of the reservoir, $\bar{k}h$, using Equation 5.1.2.

Step 4: Determine ω and λ as outlined in Reference 63.

Step 5: Verify ω using either Equation 4.1.47 or Equation 4.1.53.

Step 6: Calculate $\left[\frac{(t)_{bPSS}}{\lambda(t)_{min}}\right]$ ratio.

Step 7: Calculate the skin factor using Equation 5.3.5.

Step 8: Determine the ratio $\frac{(k_f h)_1}{(k_f h)_2}$ using Equation 5.3.2.

Step 9: Calculate the ratio $\frac{(k_f h)_1}{(\bar{k}h)}$ using Equation 3.2.9.

Step 10: Calculate the flow capacity ratio of Layer 1 using Equation 3.2.7.

Step 11: Calculate the flow capacity ratio of Layer 2 using Equation 3.2.11.

Step 12: Read the value of $(t^*\Delta p_w')_{PSS1}$ from the pseudosteady state line. Calculate the drainage area, A_i, using Equation 5.1.8.

Step 13: Obtain the time of intersection of the infinite-acting line and the pseudosteady state line, i.e. t_{RPSSi}, from the graph, and calculate A_i from Equation 5.1.12. If the two values of A_i in Steps 15 and 16 are approximately equal, then A_i is correct. If they are distinctly different then shift left or right and repeat Steps 15 and 16 until Equation 5.1.8 and 5.1.12 give the same value of A_i.

Step 14: Obtain the value of $(t^*\Delta p_w')$ at time t=1 hr from the bi-radial flow line (extrapolated if necessary), $(t^*\Delta p_w')_{BR1}$.

Step 15: Calculate the half-fracture length of each layer, x_{fi}, from Equation 5.2.1.

Step 16: Calculate the ratio $\frac{x_{fi}^2}{k_{fi}}$ of each layer using the values k_{fi} and x_{fi} values obtained in steps 9,10 and 14 respectively.

Step 17: From the graph, determine the time of intersection of the radial flow line and the bi-radial flow line, t_{RBRi}, then calculate the ratio $\frac{x_{fi}^2}{k_{fi}}$ from Equation 5.2.4. If steps 15 and 16 give the same value of $\frac{x_{fi}^2}{k_{fi}}$, then the values of k_{fi} and x_{fi} are correct. If they are different, then shift one or both straight lines (bi-radial and infinite-acting lines) and repeat Steps 9,10,13,14,15 and 16 until Steps 15 and 16 give the same value of $\frac{x_{fi}^2}{k_{fi}}$.

Step 18: Calculate the interporosity flow parameter after stimulation, λ_{fi}, using Equation 4.1.45.

Step 19: Verify λ_{fi} using Equations 4.1.50, 4.1.51 and 4.1.52.

Step 20: Select any convenient time t_R during the infinite-acting period and read the corresponding value of $(\Delta p_w)_R$; then calculate the skin factor of each layer from Equation 5.3.6.

Step 21: Read the value of Δp_w and $(t^*\Delta p_w')$ corresponding to any convenient time t_{PSS} during the pseudosteady state flow portion of the curves and calculate the shape factor C_{Ai} from Equation 5.1.9.

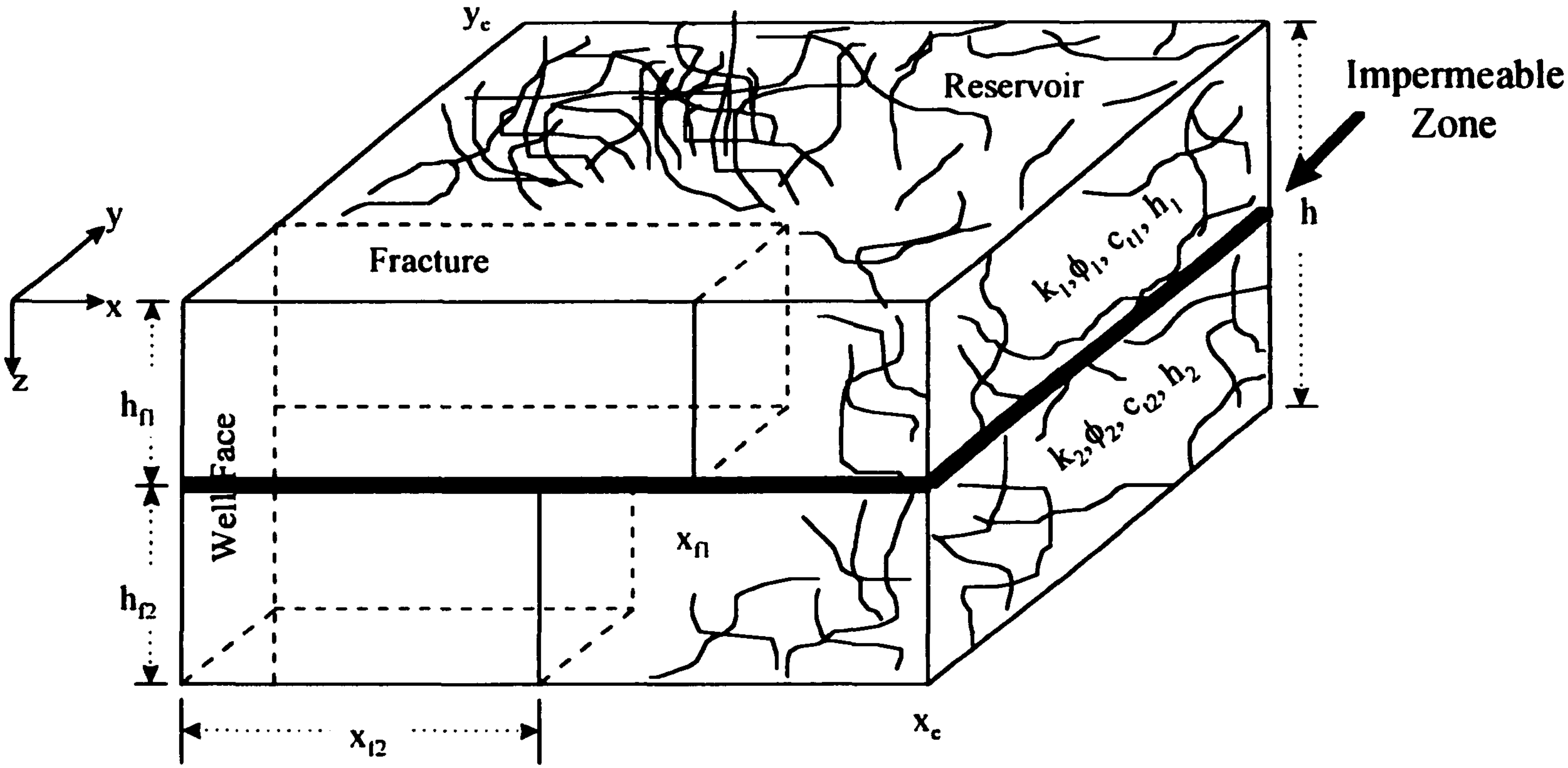

Figure 5.1 Vertical fracture in a multi-layer double porosity reservoir.

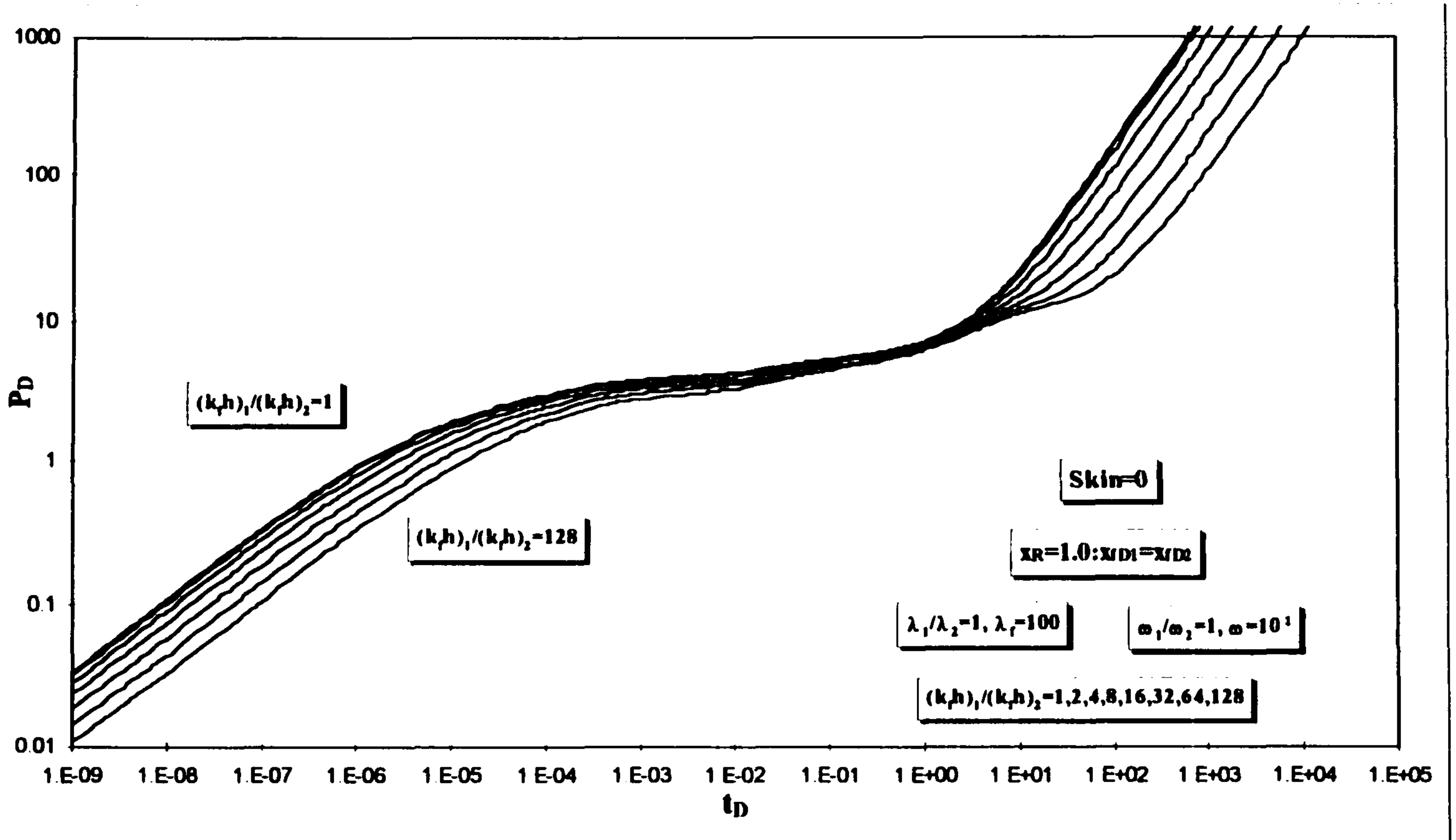

Figure 5.2 Characteristics of pressure behavior in a two-layer vertical fractured reservoir with pseudosteady state interporosity flow, $\omega_1=\omega_2=0.1$ and $\lambda_{f1}=\lambda_{f2}=100$. Both wellbore storage and skin are ignored.

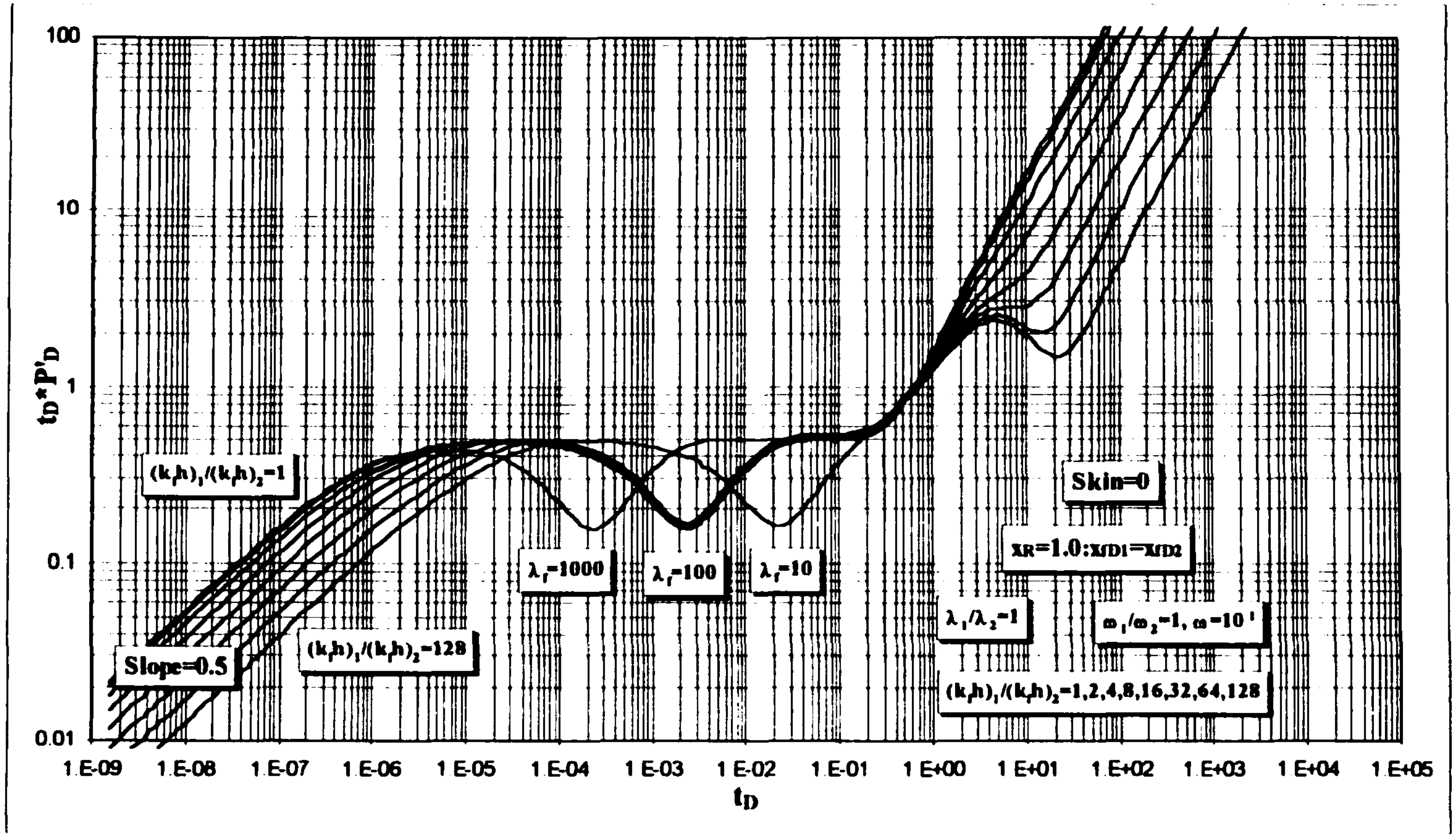

Figure 5.3 Characteristics of pressure derivative behavior in a two-layer vertical fractured reservoir with pseudosteady state interporosity flow, $\omega_1=\omega_2=0.1$.
Both wellbore storage and skin are ignored.

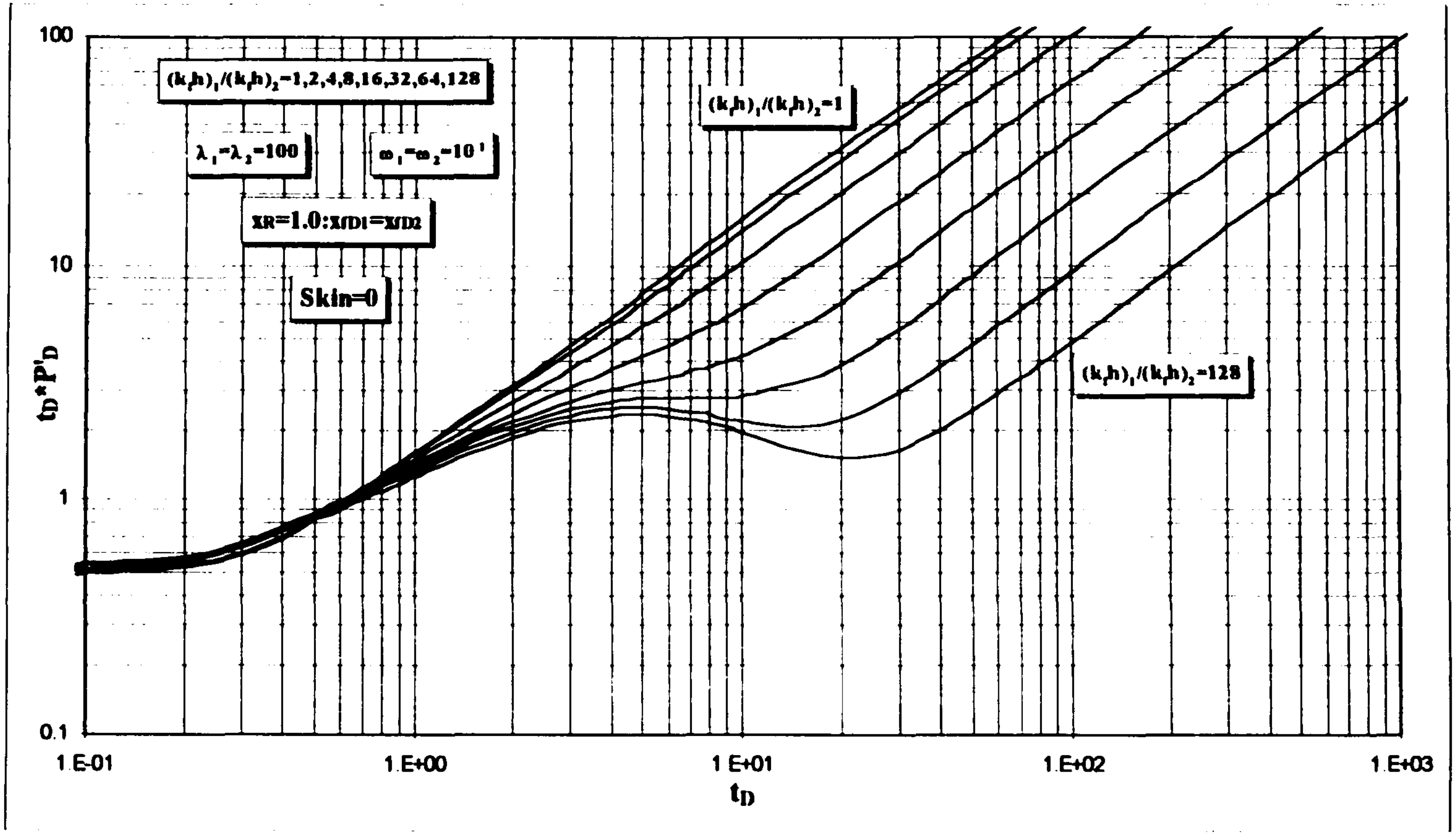

Figure 5.4 The effect of the flow capacity ratio on the late time pseudo-steady state flow pressure derivative behavior in a two-layer vertical fractured reservoir with pseudosteady state interporosity flow, $\omega_1=\omega_2=0.1$ and $\lambda_{f1}=\lambda_{f2}=100$. Both wellbore storage and skin are ignored.

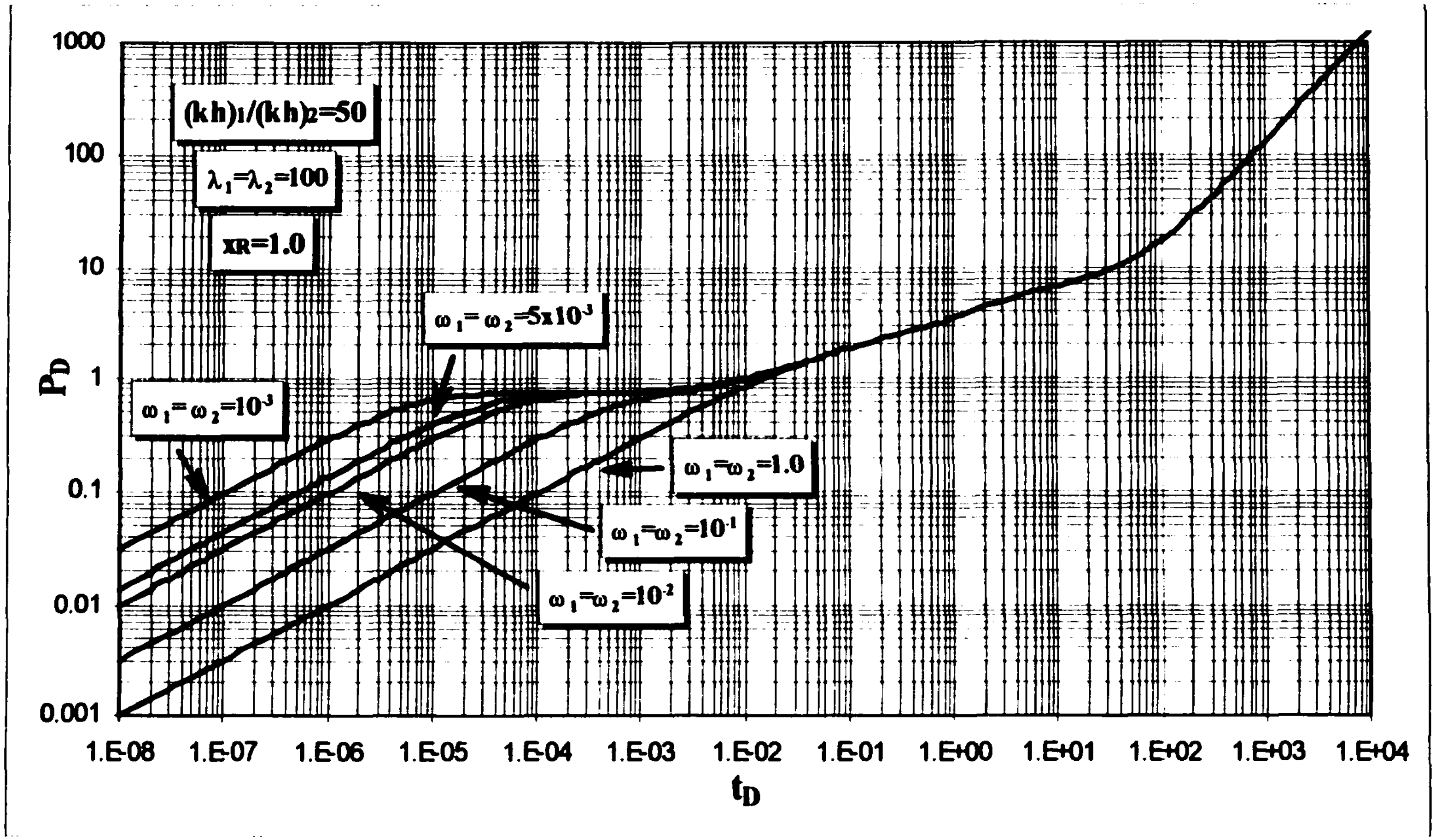

Figure 5.1.1 Effect of storage coefficient on the pressure response in a two-layer vertical fractured reservoir with pseudosteady state interporosity flow, $\frac{(kh)_1}{(kh)_2} = 50$.

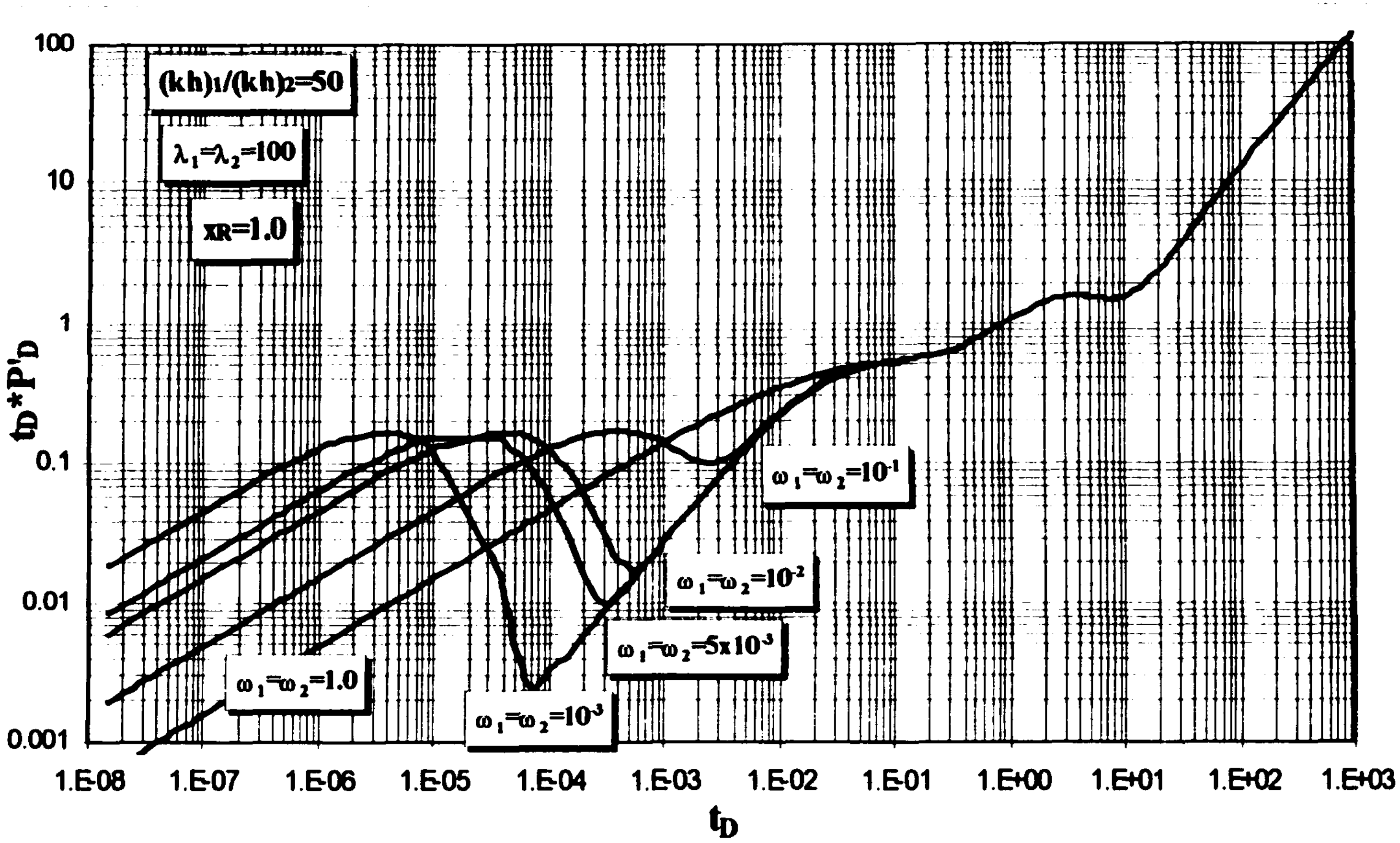

Figure 5.1.2 Effect of storage coefficient on the pressure derivative response in a two-layer vertical fractured reservoir with pseudosteady state interporosity flow, $\frac{(kh)_1}{(kh)_2} = 50$.

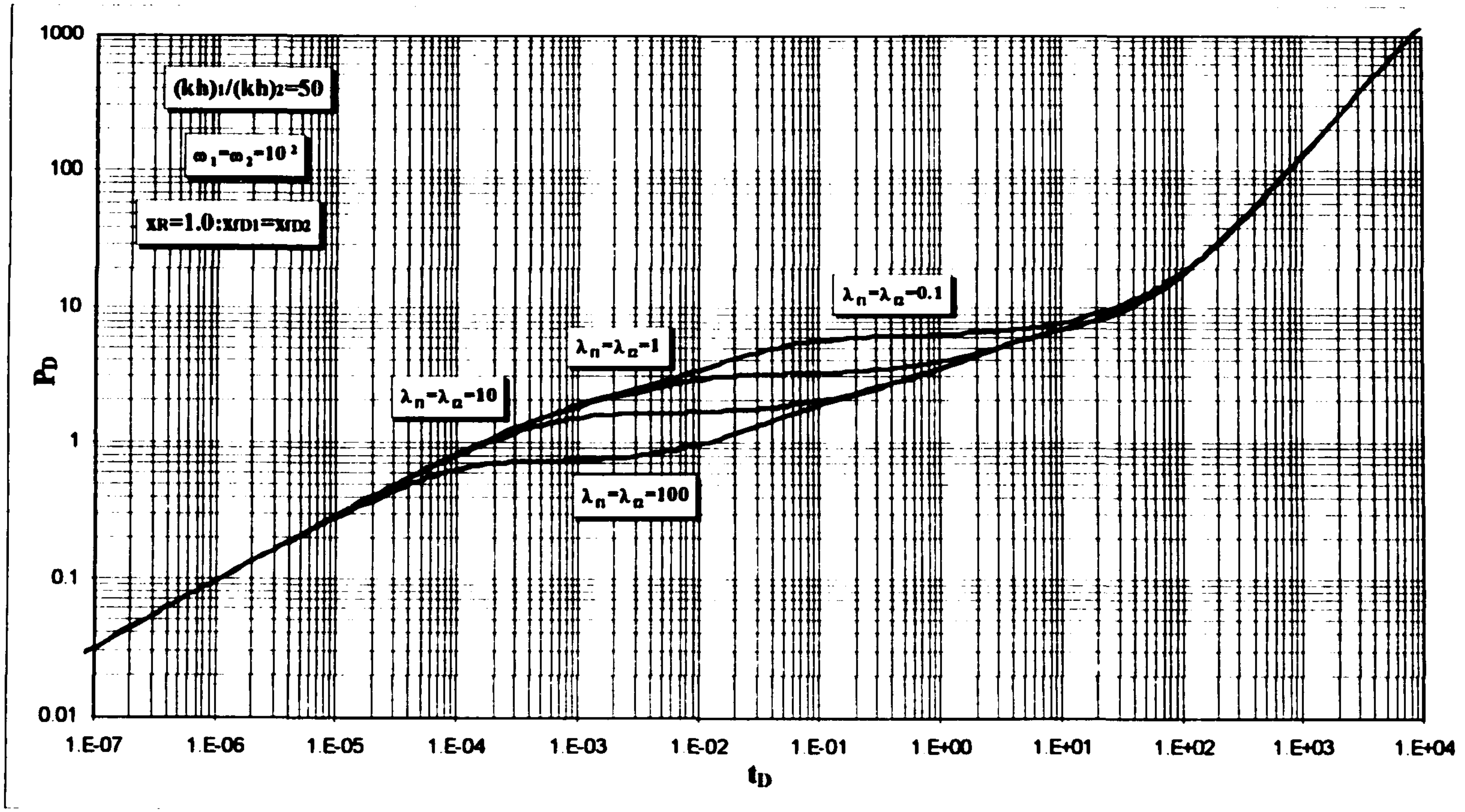

Figure 5.1.3 Effect of interporosity flow parameter on the pressure response in a two-layer vertical fractured reservoir with pseudosteady state interporosity flow, $\frac{(kh)_1}{(kh)_2} = 50$.

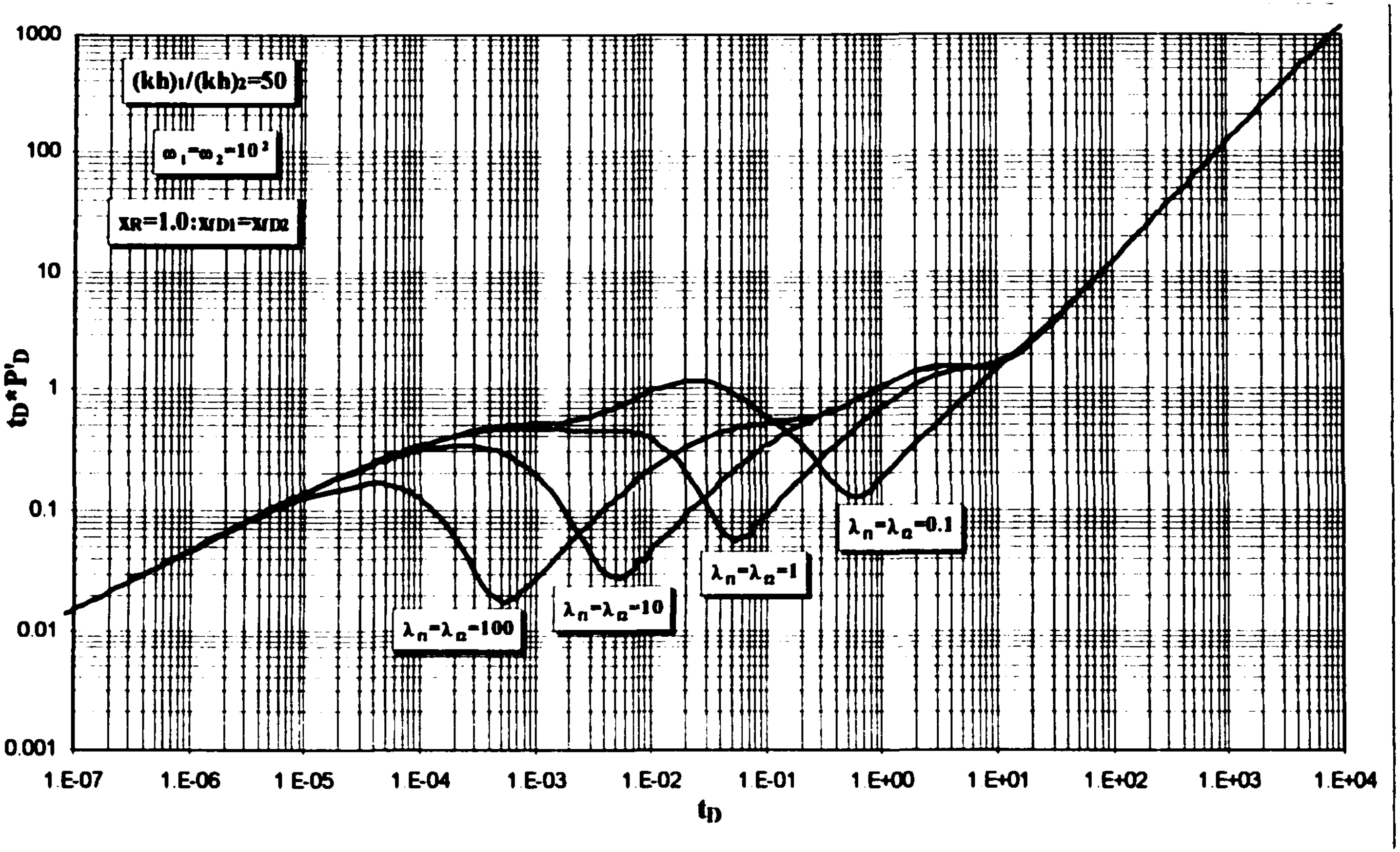

Figure 5.1.4 Effect of interporosity flow parameter on the pressure derivative response in a two-layer vertical fractured reservoir with pseudosteady state interporosity flow, $\frac{(kh)_1}{(kh)_2} = 50$.

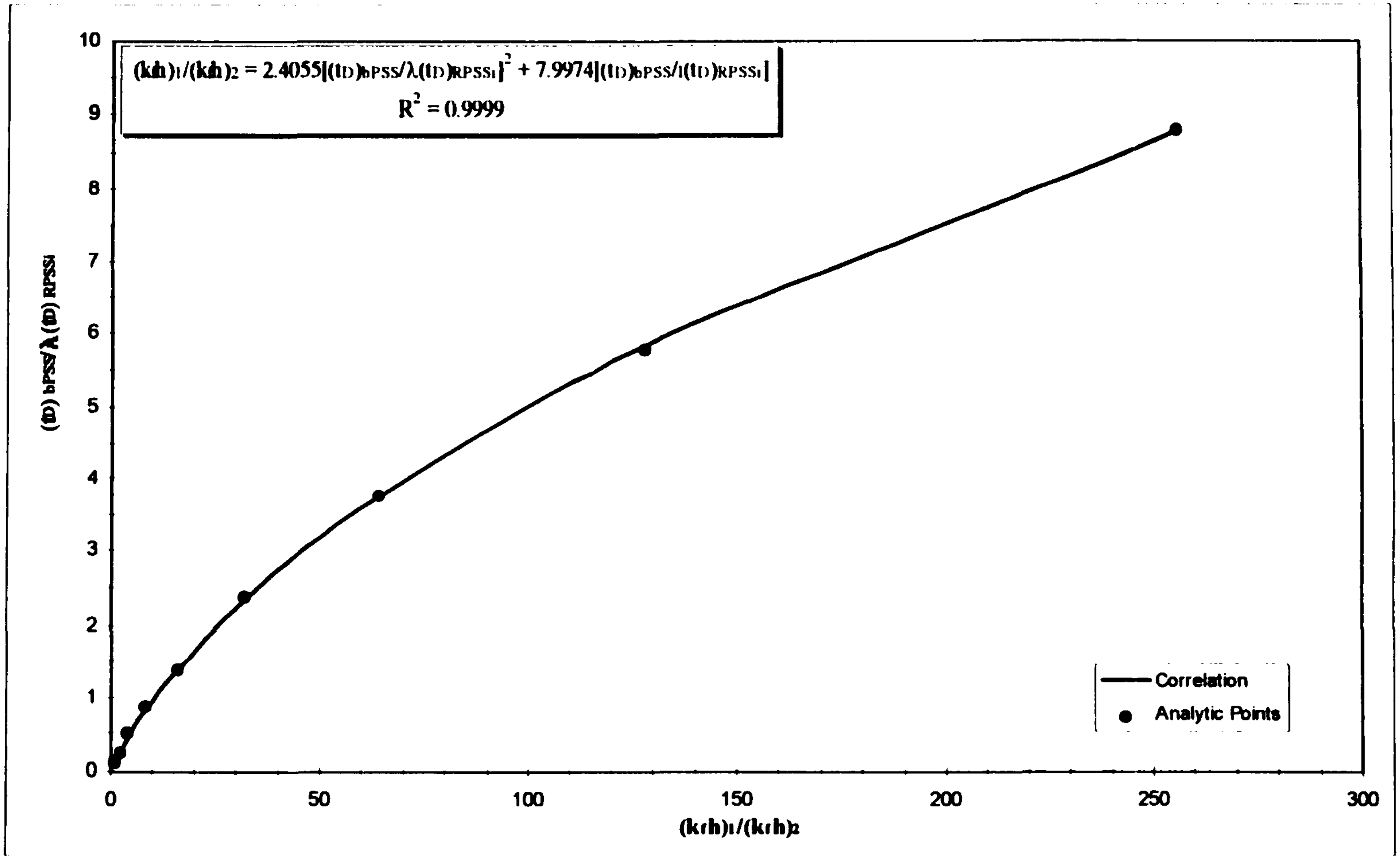

Figure 5.1.5 Correlation between flow capacity ratio and ratio of characteristic times, skin=0.

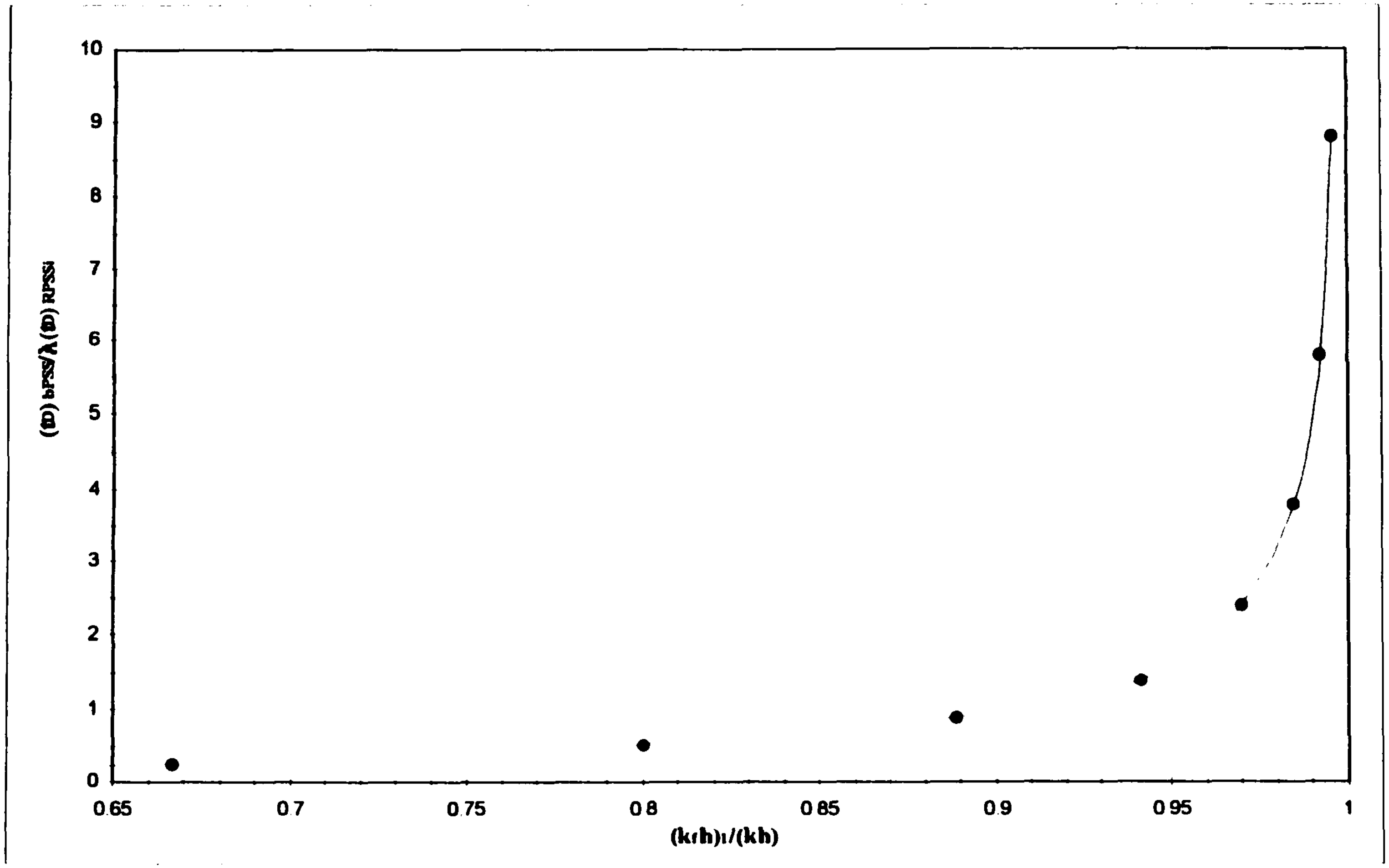

Figure 5.1.6 Correlation between the total flow capacity and ratio of characteristic times, Skin=0.

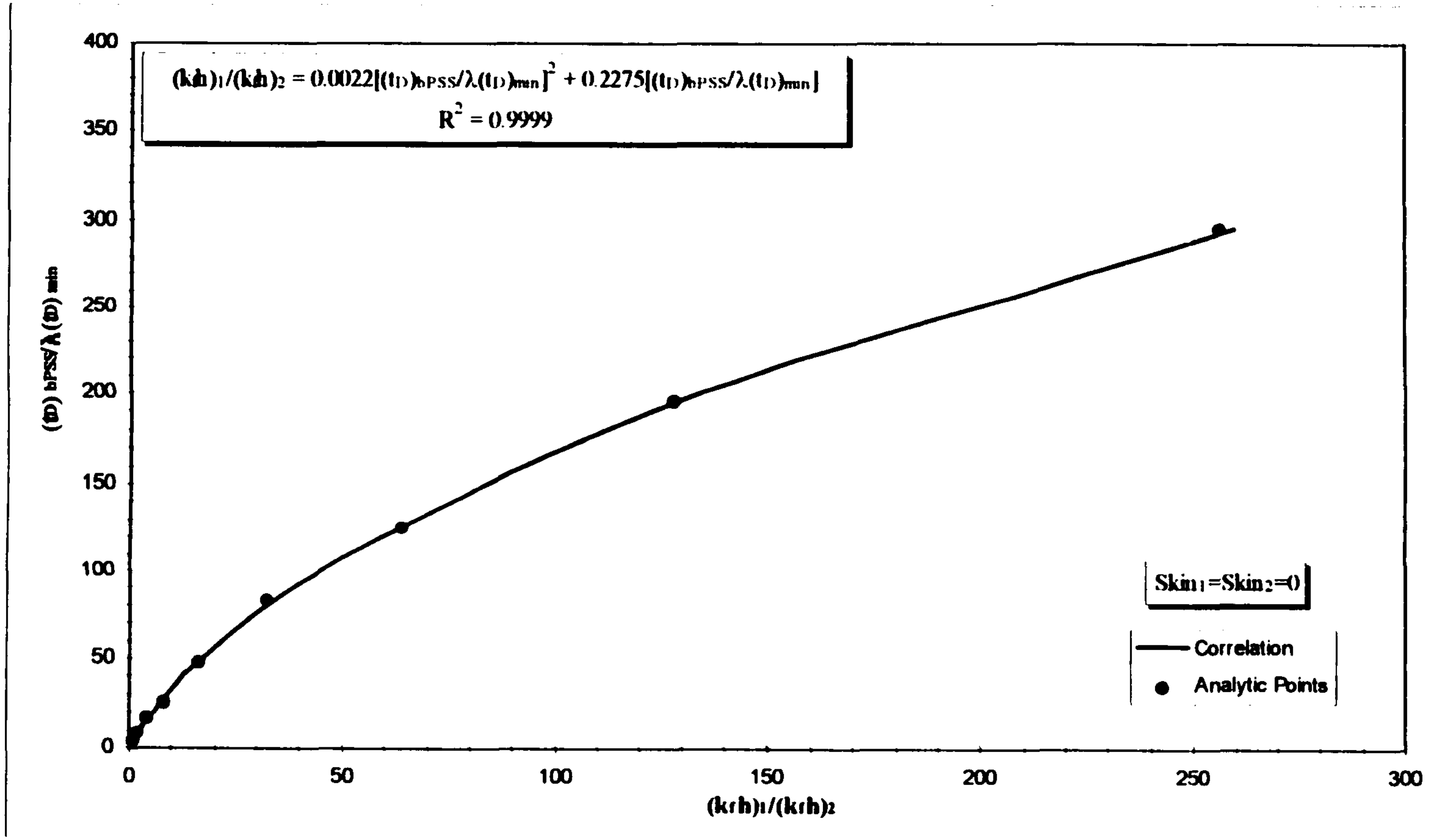

Figure 5.1.7 Correlation between the flow capacity ratio and ratio of characteristic times, Skin=0.

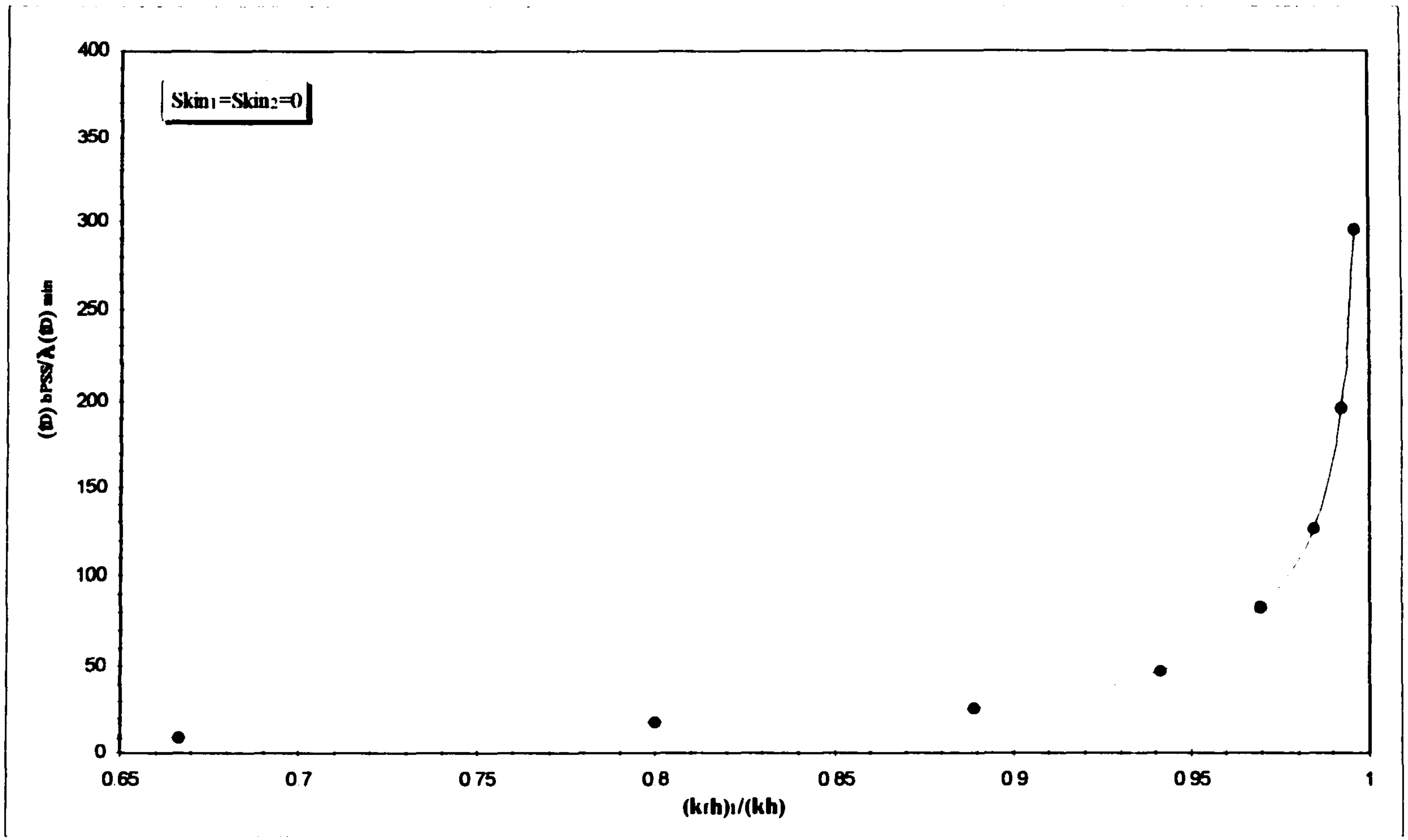

Figure 5.1.8 Correlation between the total flow capacity ratio and ratio of characteristic times, skin=0.

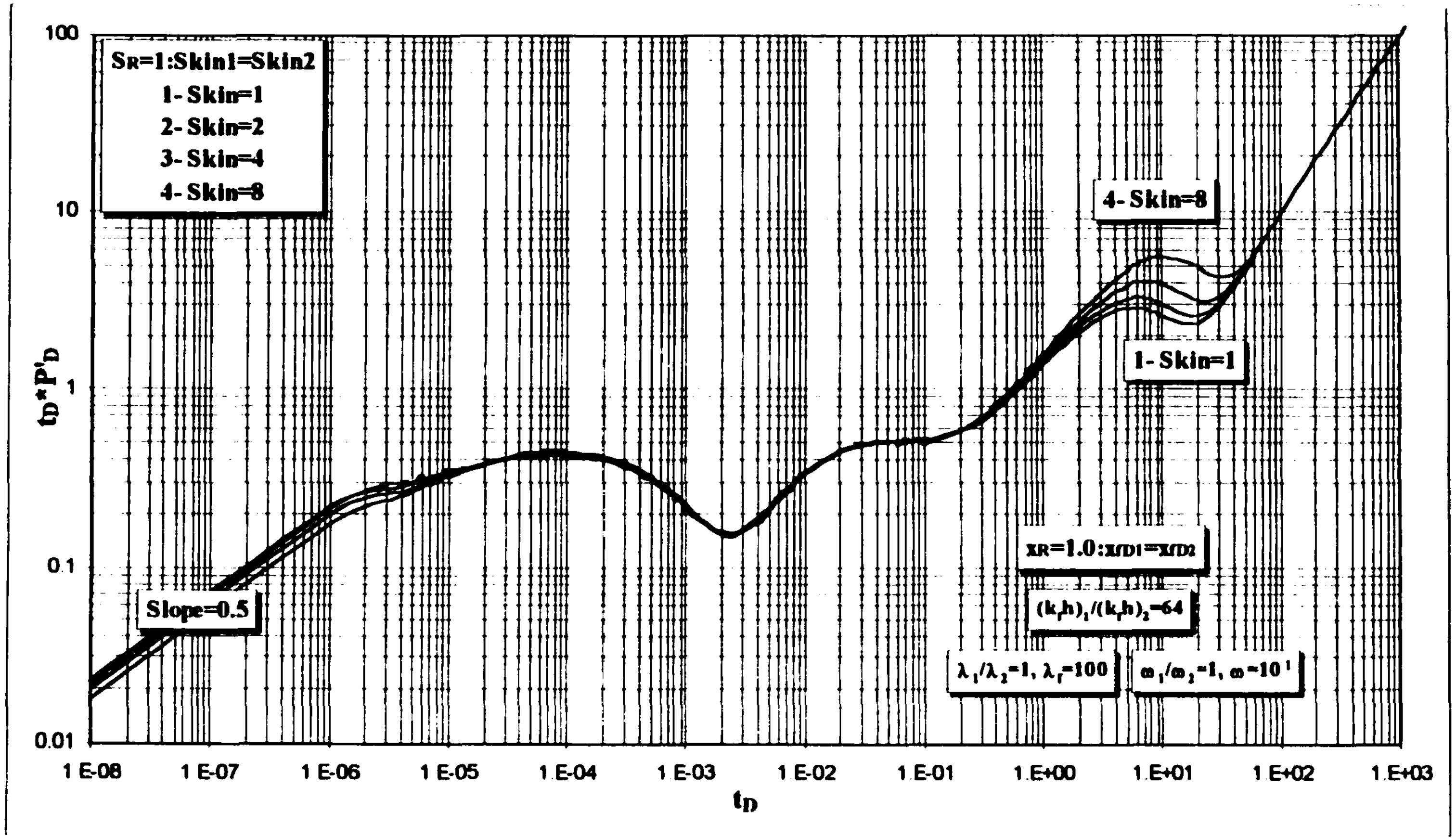

Figure 5.3.1 Characteristics of pressure derivative behavior in a two-layer vertical fractured reservoir with pseudosteady state interporosity flow, $\omega_1=\omega_2=0.1$ and $\lambda_{f1}=\lambda_{f2}=100$, for various values of positive skin.

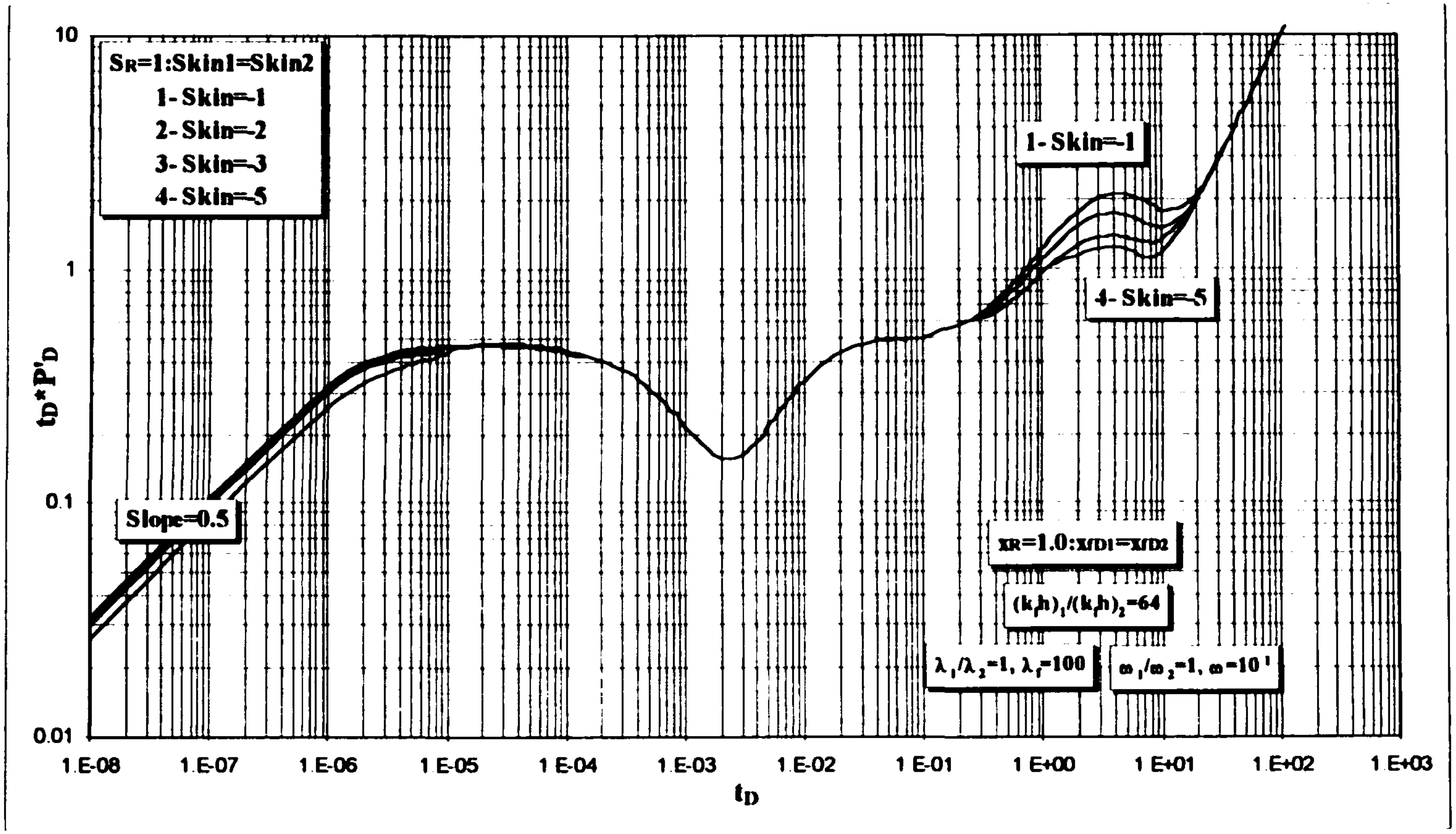

Figure 5.3.2 Characteristics of pressure derivative behavior in a two-layer vertical fractured reservoir with pseudosteady state interporosity flow, $\omega_1=\omega_2=0.1$ and $\lambda_{f1}=\lambda_{f2}=100$, for various values of negative skin.

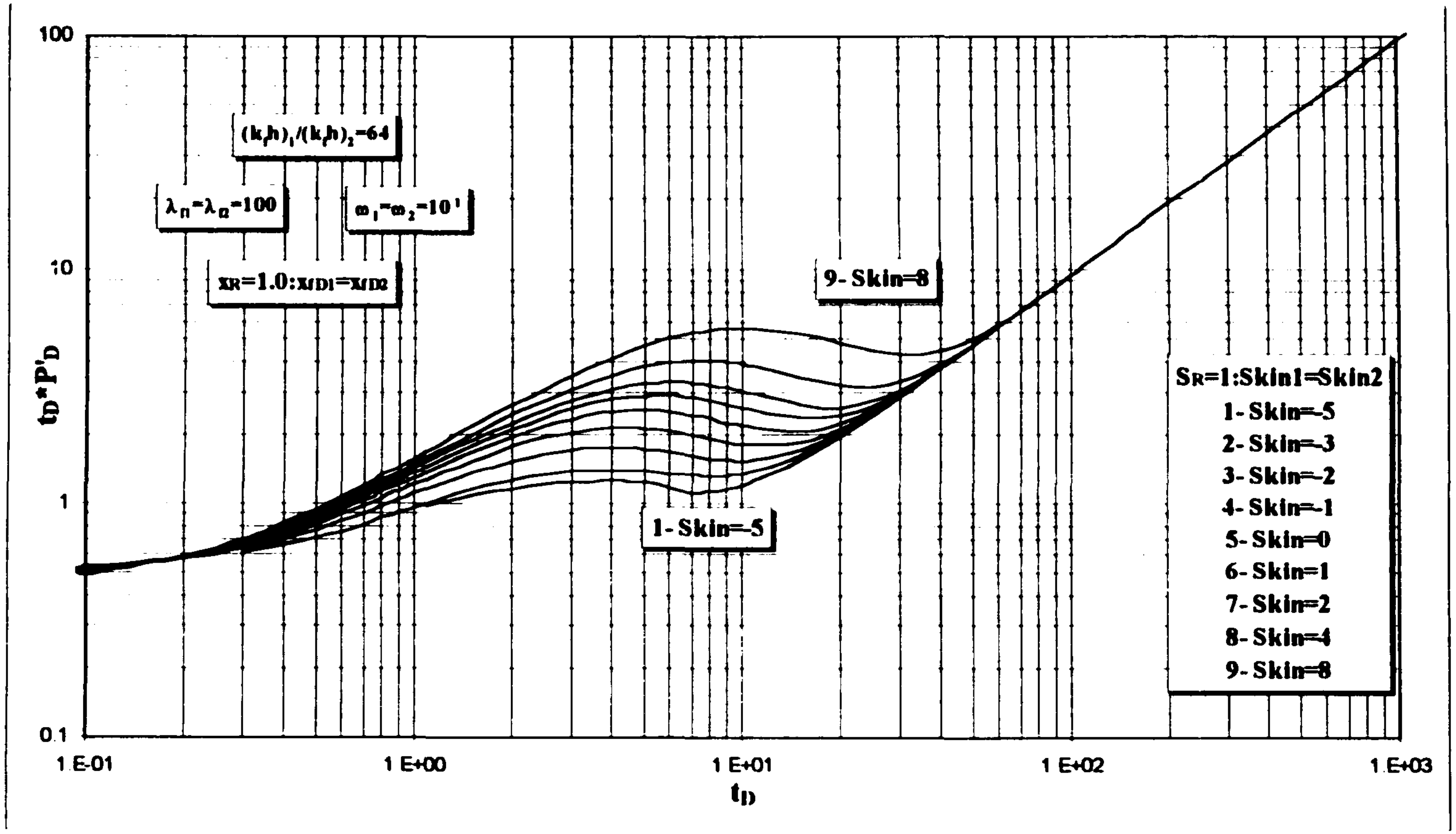

Figure 5.3.3 The effect of skin on the late time pseudo-steady state flow pressure derivative behavior in a two-layer vertical fractured reservoir with pseudosteady state interporosity flow, $\omega_1=\omega_2=0.1$ and $\lambda_{f1}=\lambda_{f2}=100$.

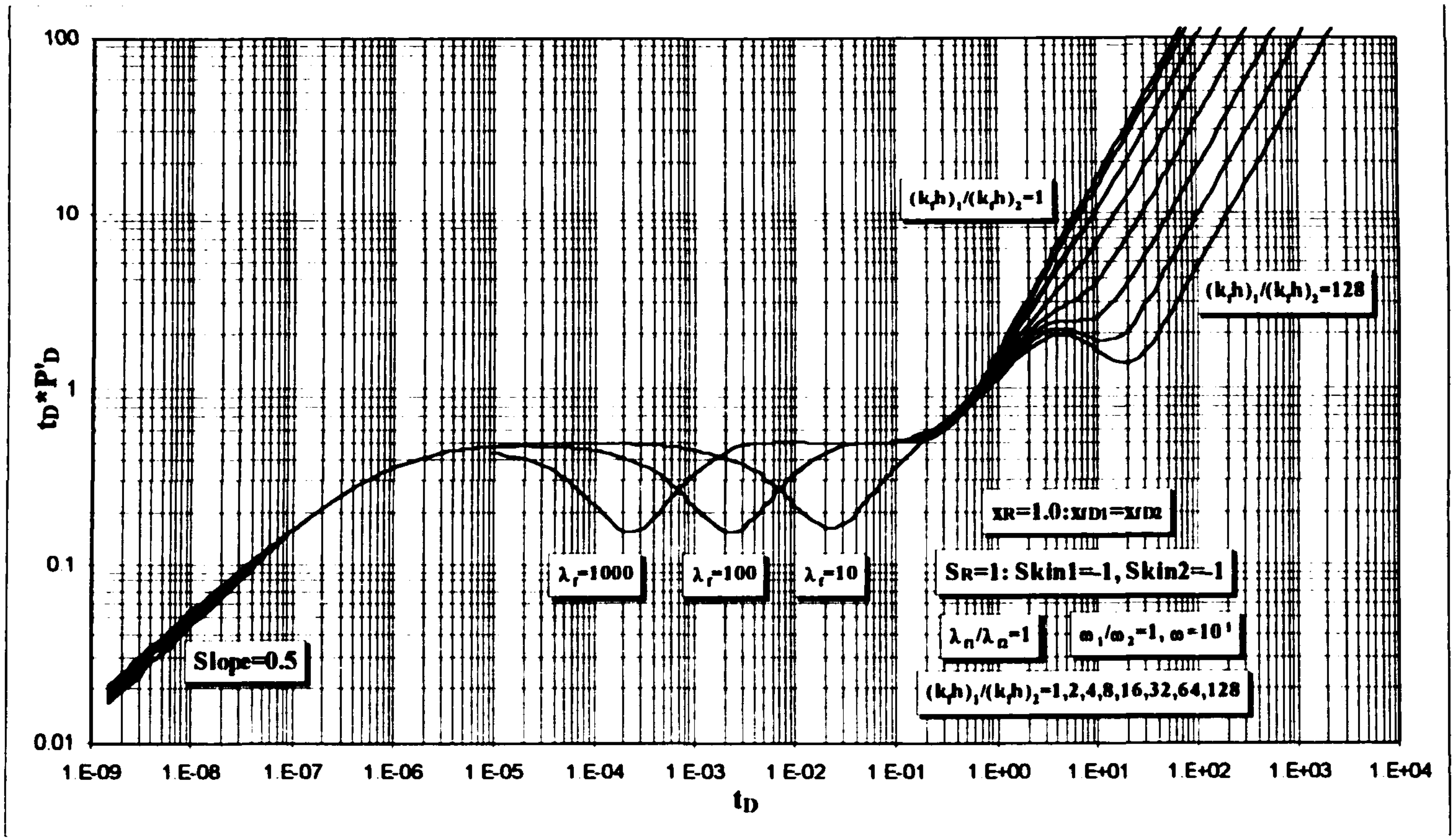

Figure 5.3.4 Characteristics of pressure derivative behavior in a two-layer vertical fractured reservoir with pseudosteady state interporosity flow, $\omega_1=\omega_2=0.1$ and $\lambda_{f1}=\lambda_{f2}=100$. Skin=-1.

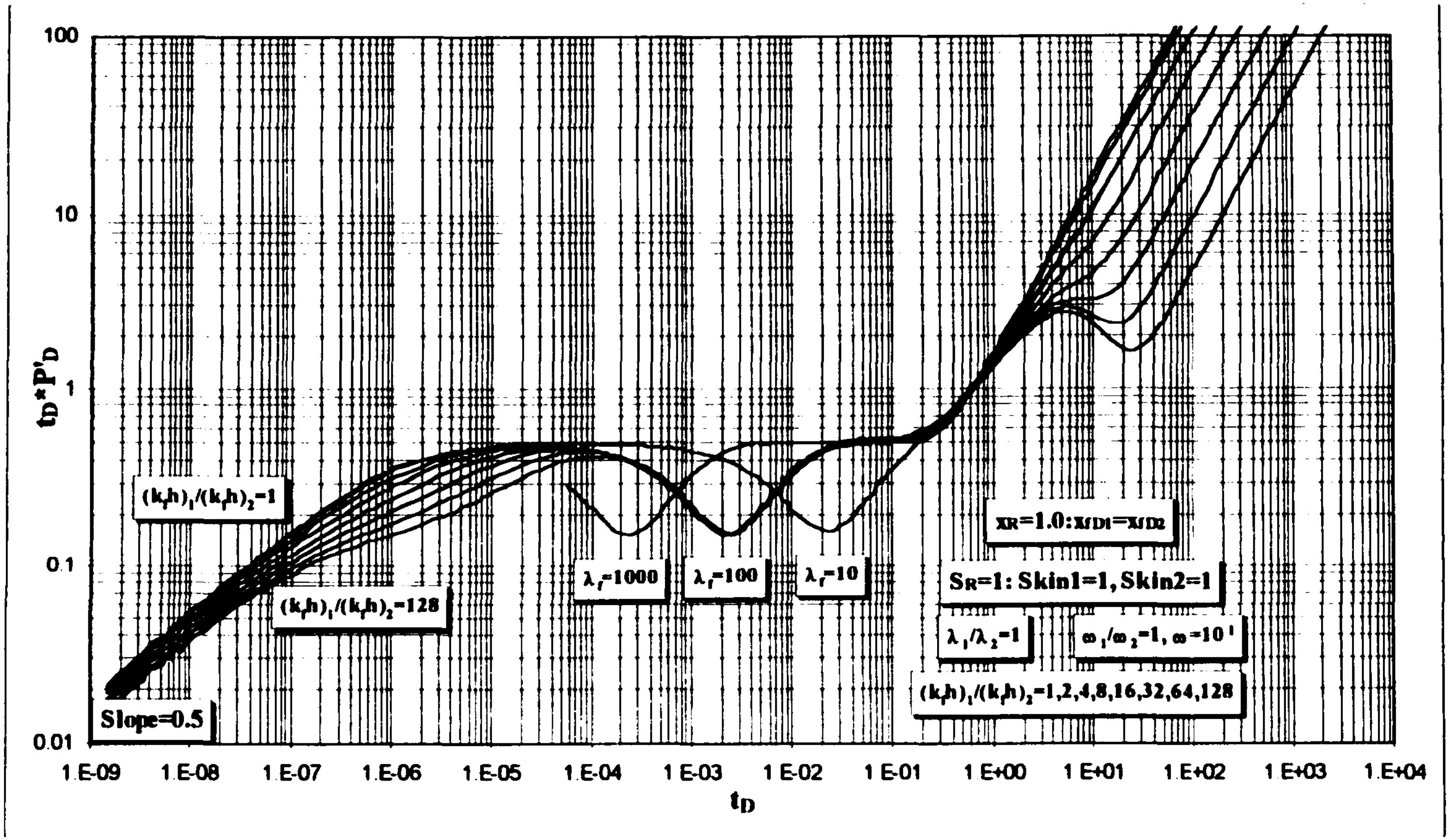

Figure 5.3.5 Characteristics of pressure derivative behavior in a two-layer vertical fractured reservoir with pseudosteady state interporosity flow, $\omega_1=\omega_2=0.1$ and $\lambda_{f1}=\lambda_{f2}=100$. Skin=1.

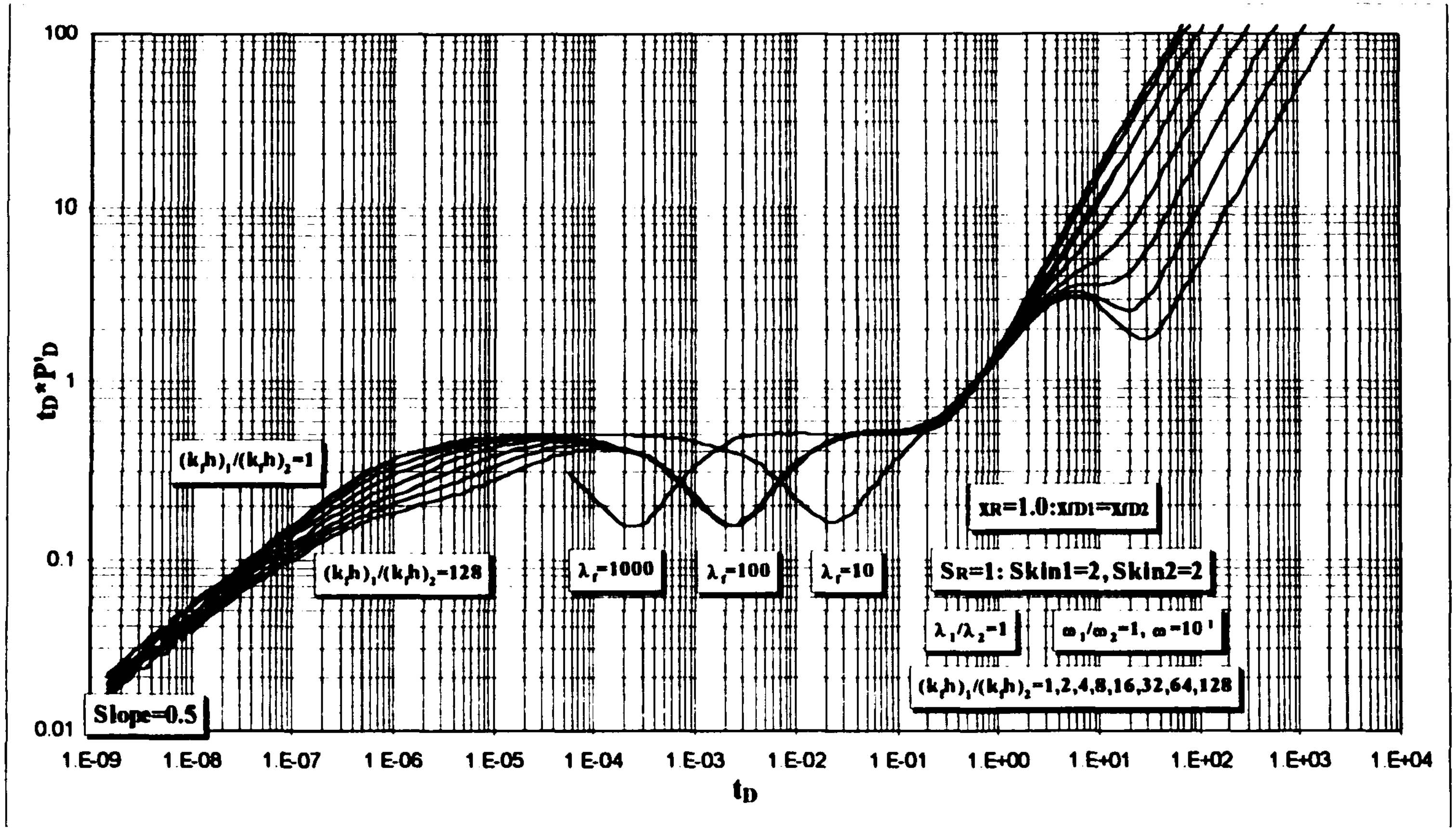

Figure 5.3.6 Characteristics of pressure derivative behavior in a two-layer vertical fractured reservoir with pseudosteady state interporosity flow, $\omega_1=\omega_2=0.1$ and $\lambda_{f1}=\lambda_{f2}=100$. Skin=2.

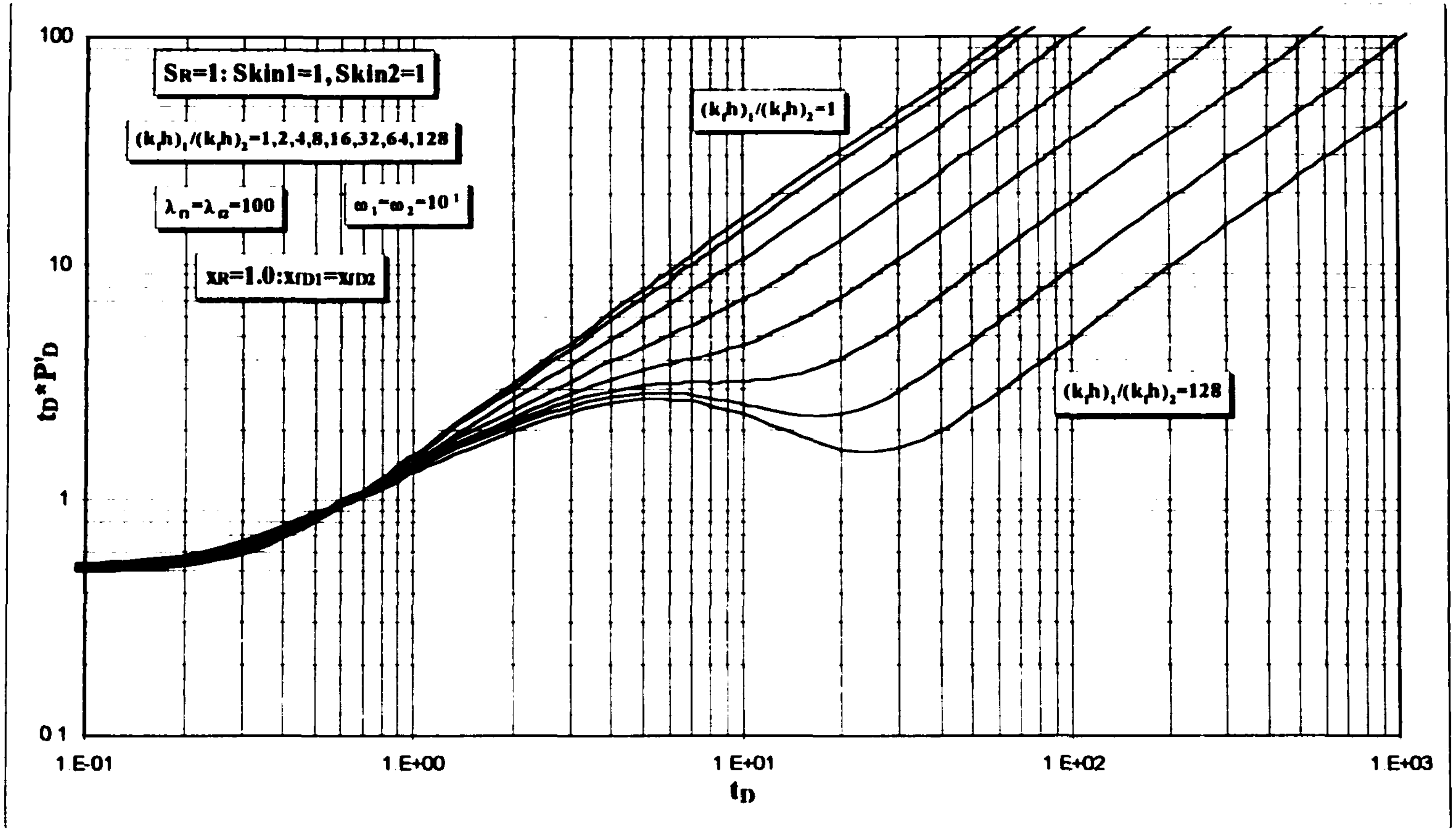

Figure 5.3.7 The effect of skin on the late time pseudo-steady state flow pressure derivative behavior in a two-layer vertical fractured reservoir with pseudosteady state interporosity flow, $\omega_1=\omega_2=0.1$ and $\lambda_{f1}=\lambda_{f2}=100$. Skin=1.

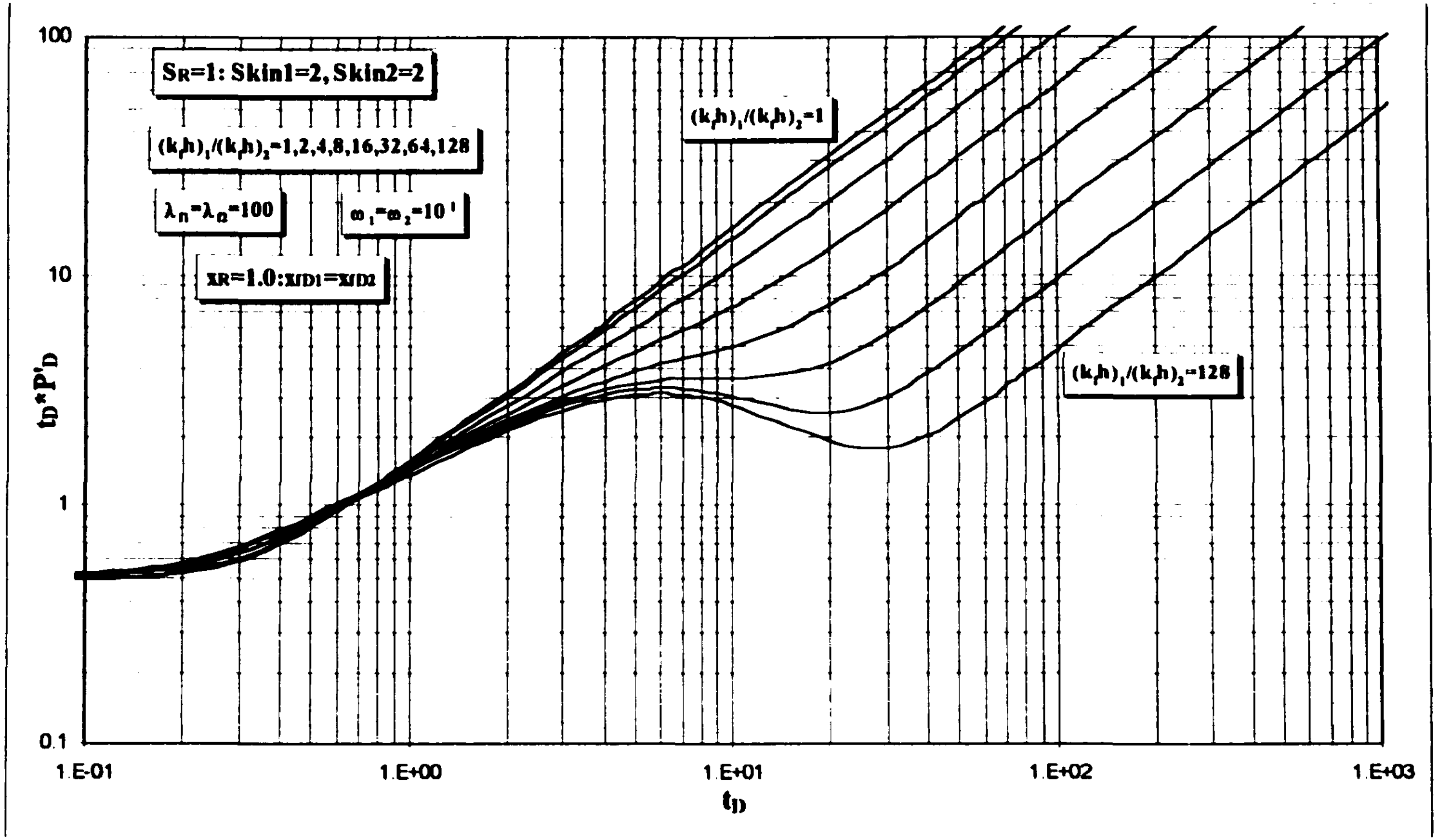

Figure 5.3.8 The effect of skin on the late time pseudo-steady state flow pressure derivative behavior in a two-layer vertical fractured reservoir with pseudosteady state interporosity flow, $\omega_1=\omega_2=0.1$ and $\lambda_{f1}=\lambda_{f2}=100$. Skin=2.

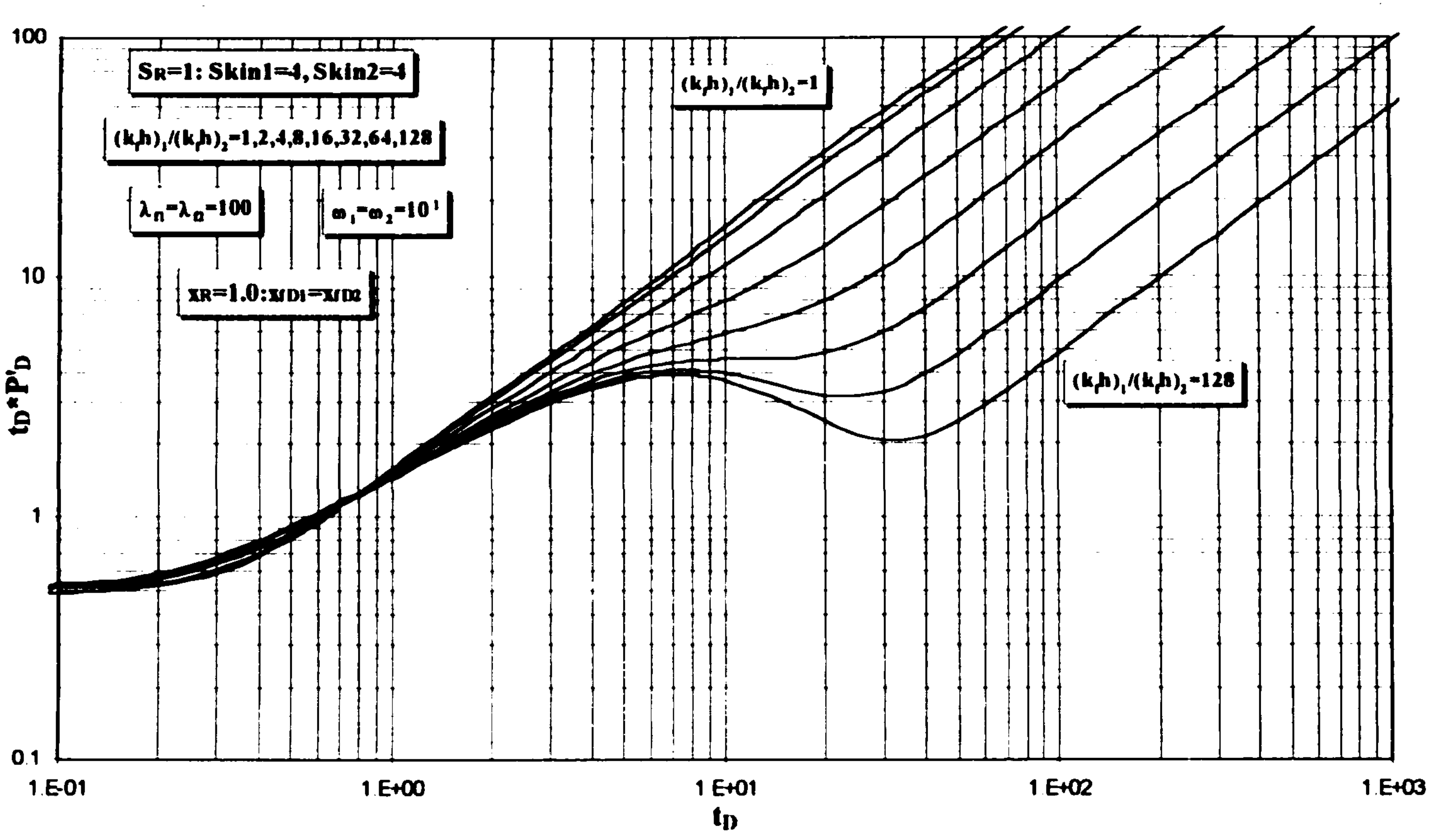

Figure 5.3.9 The effect of skin on the late time pseudo-steady state flow pressure derivative behavior in a two-layer vertical fractured reservoir with pseudosteady state interporosity flow, $\omega_1=\omega_2=0.1$ and $\lambda_{f1}=\lambda_{f2}=100$. Skin=4

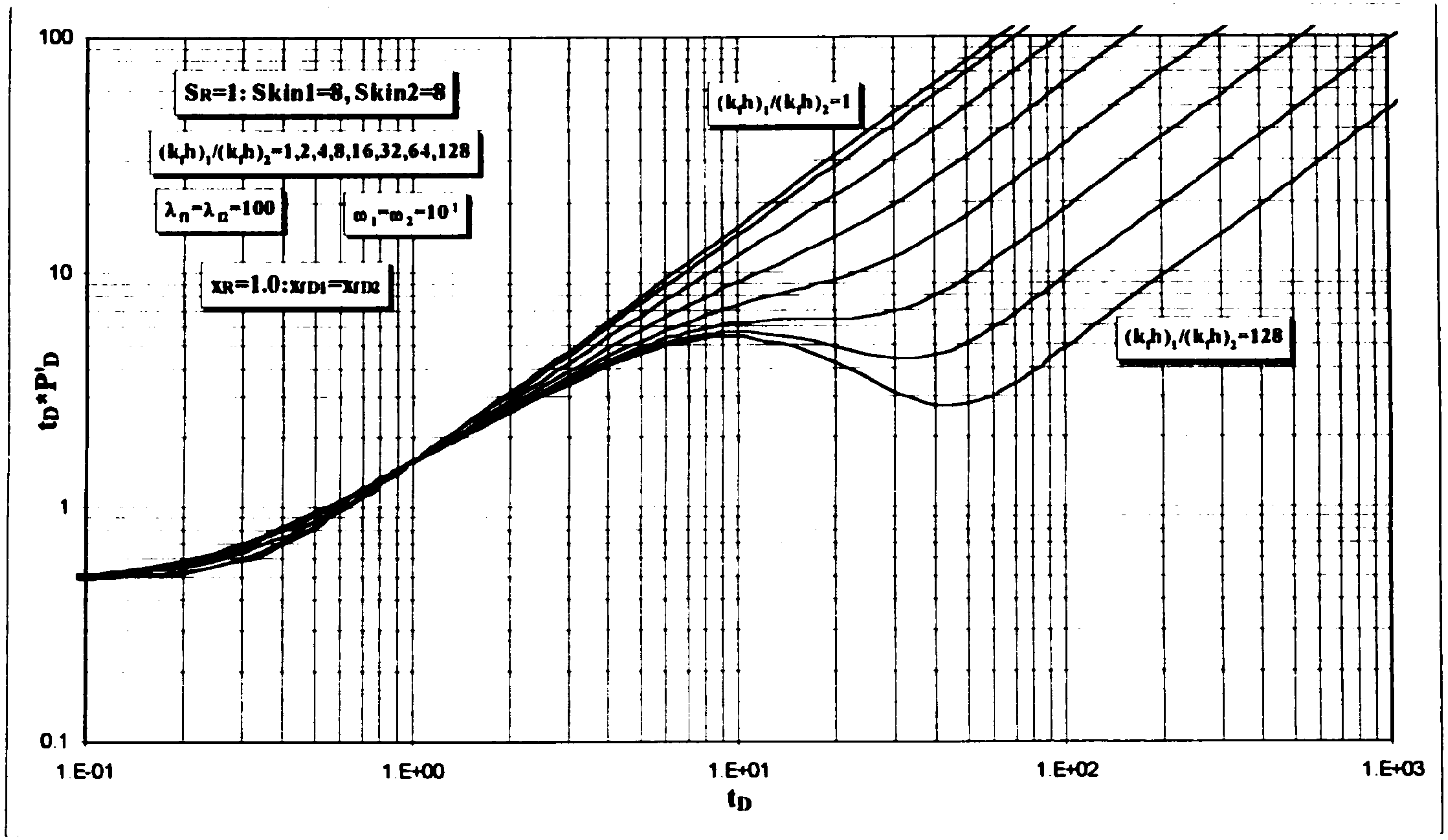

Figure 5.3.10 The effect of skin on the late time pseudo-steady state flow pressure derivative behavior in a two-layer vertical fractured reservoir with pseudosteady state interporosity flow, $\omega_1=\omega_2=0.1$ and $\lambda_{f1}=\lambda_{f2}=100$. Skin=8.

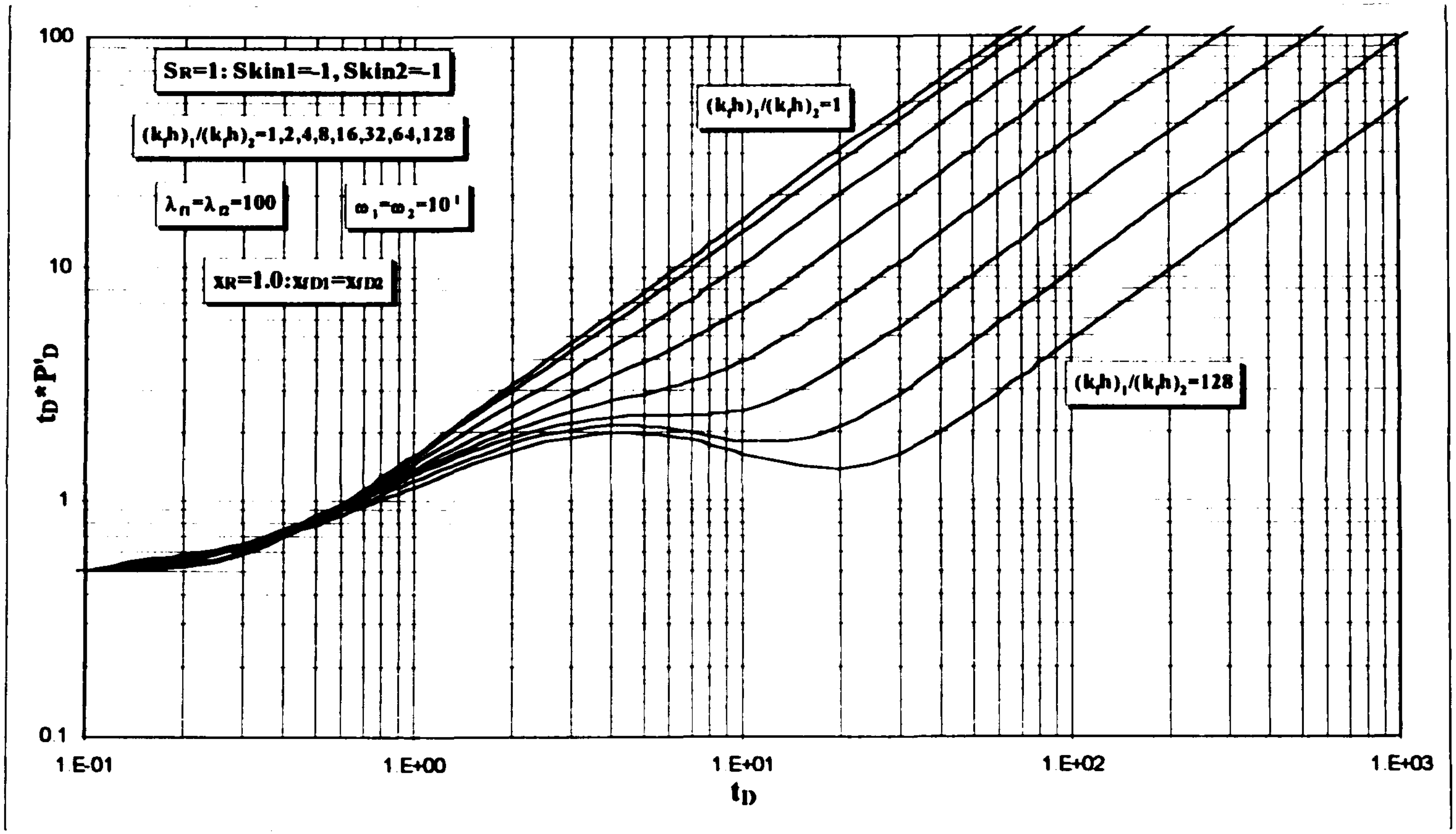

Figure 5.3.11 The effect of skin on the late time pseudo-steady state flow pressure derivative behavior in a two-layer vertical fractured reservoir with pseudosteady state interporosity flow, $\omega_1=\omega_2=0.1$ and $\lambda_{f1}=\lambda_{f2}=100$. Skin=-1.

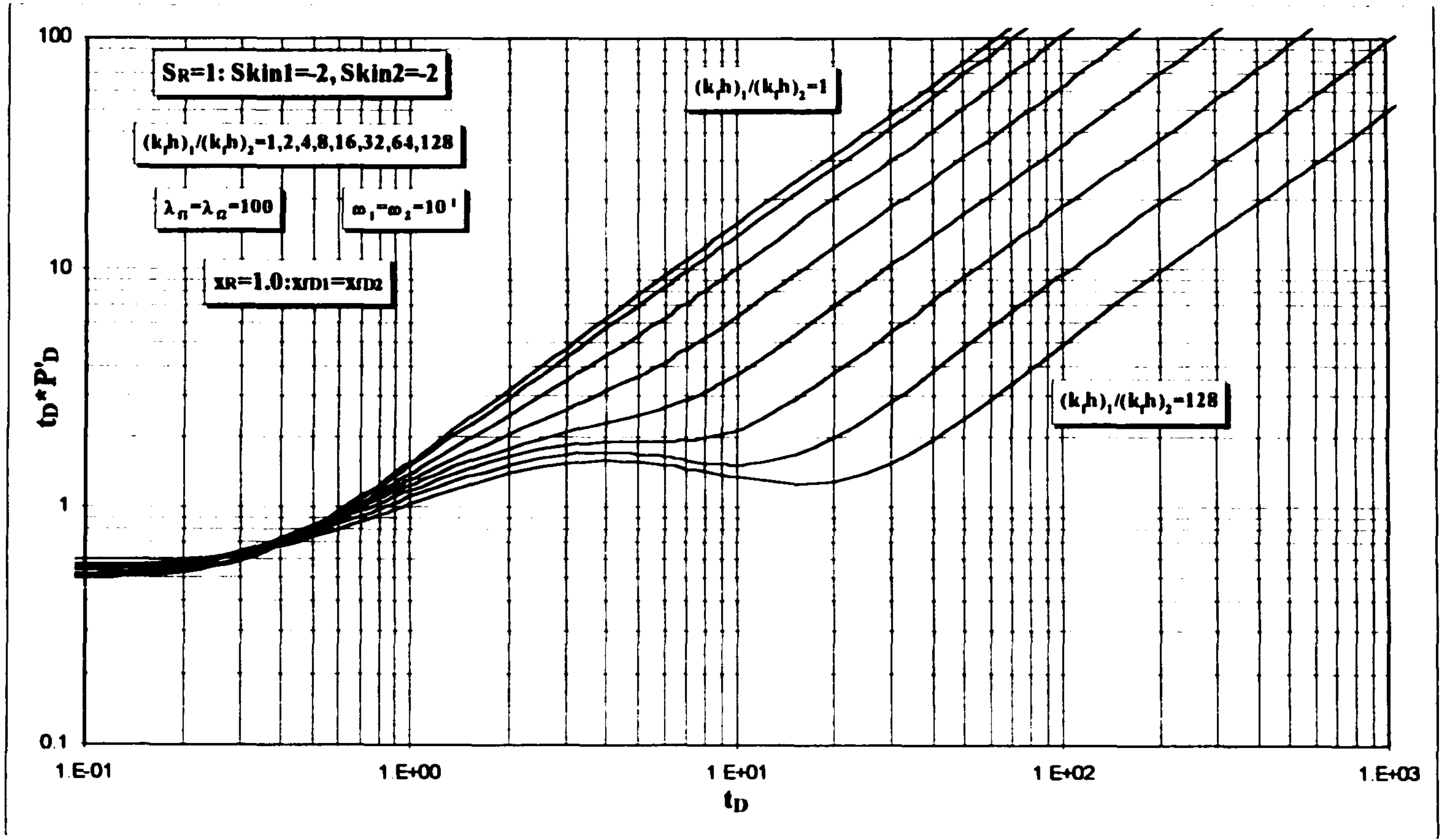

Figure 5.3.12 The effect of skin on the late time pseudo-steady state flow pressure derivative behavior in a two-layer vertical fractured reservoir with pseudosteady state interporosity flow, $\omega_1=\omega_2=0.1$ and $\lambda_{f1}=\lambda_{f2}=100$. Skin=-2.

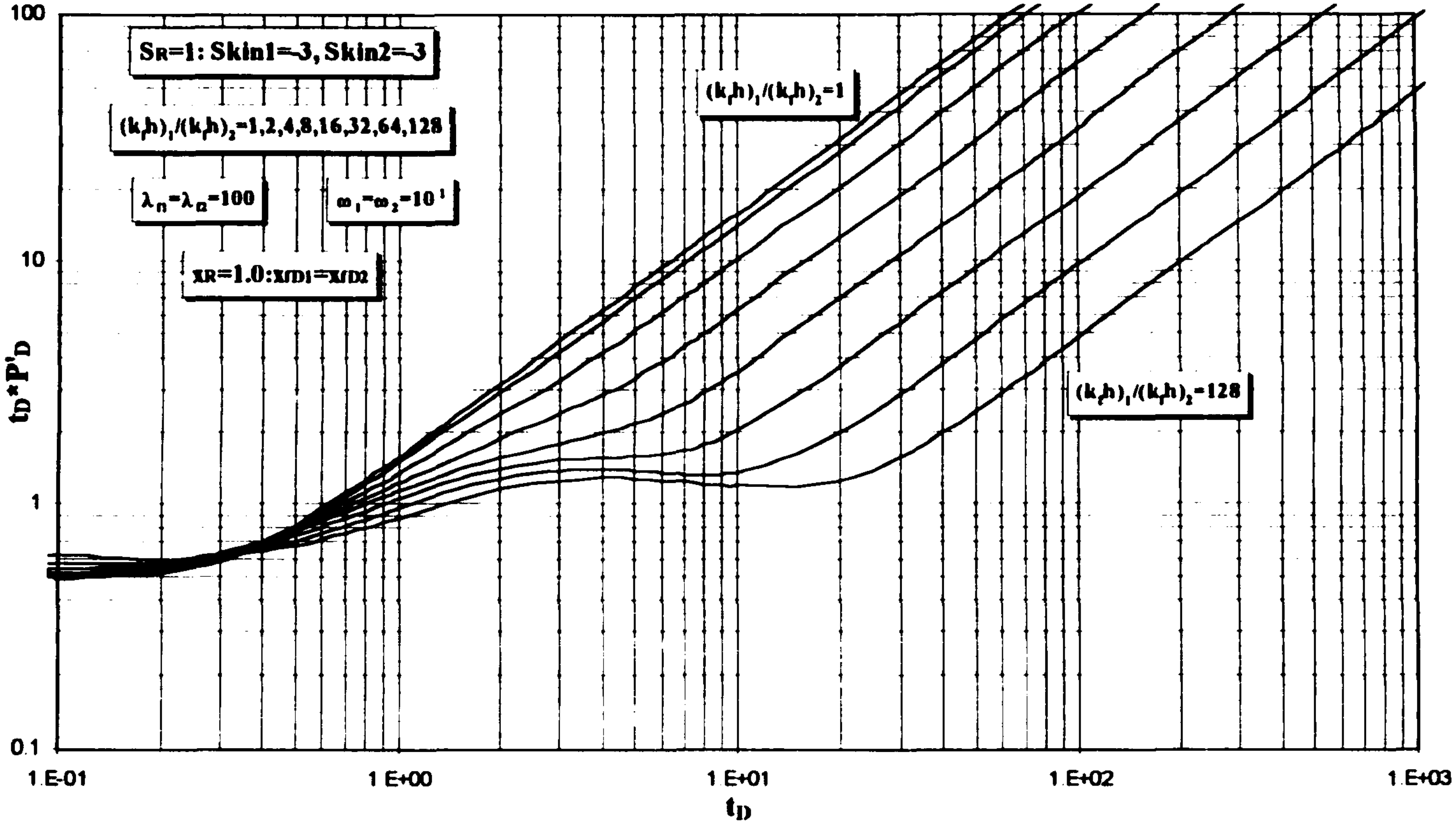

Figure 5.3.13 The effect of skin on the late time pseudo-steady state flow pressure derivative behavior in a two-layer vertical fractured reservoir with pseudosteady state interporosity flow, $\omega_1=\omega_2=0.1$ and $\lambda_{f1}=\lambda_{f2}=100$. Skin=-3.

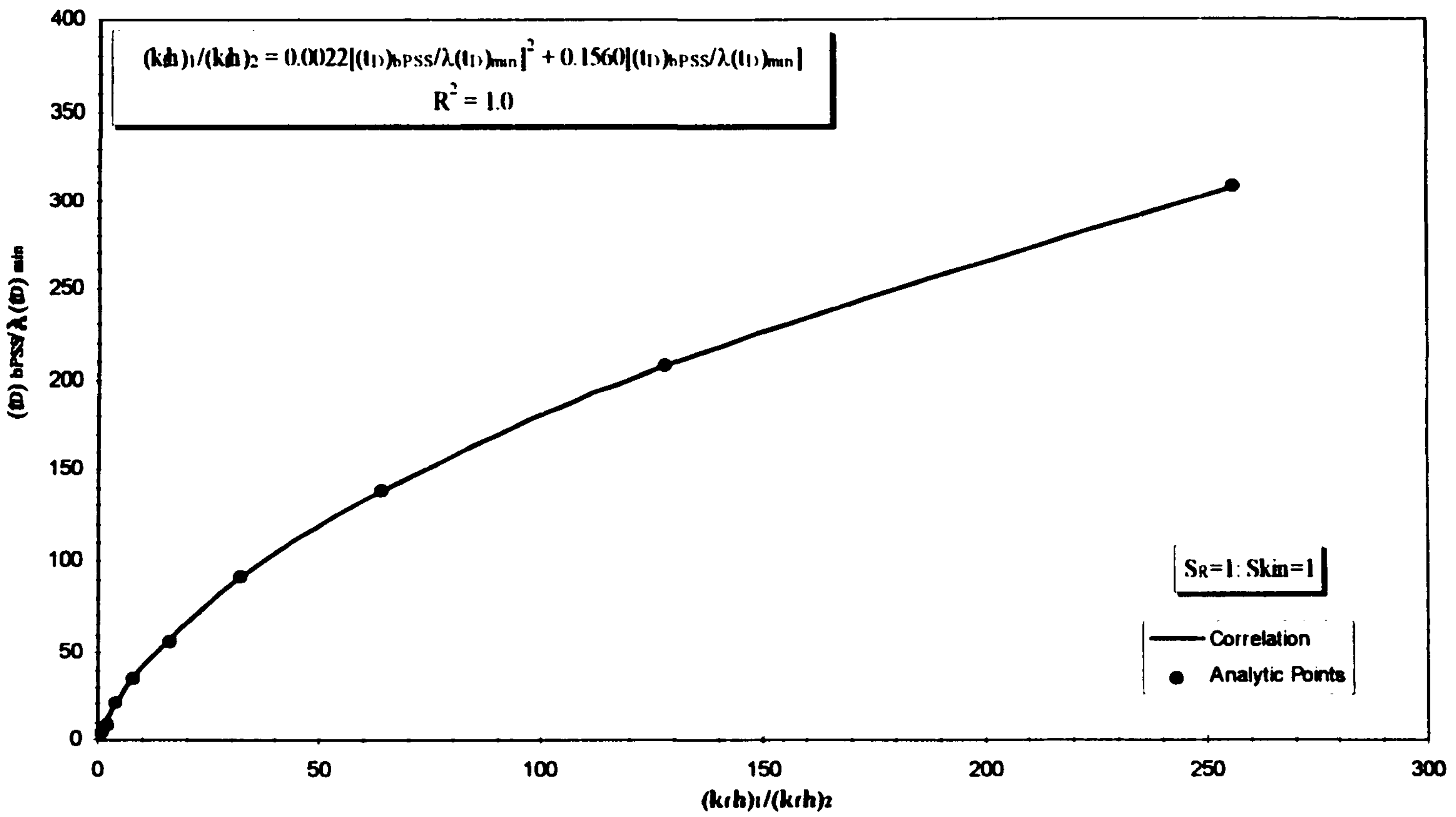

Figure 5.3.14 Correlation between the flow capacity ratio and ratio of characteristic times, Skin=1.

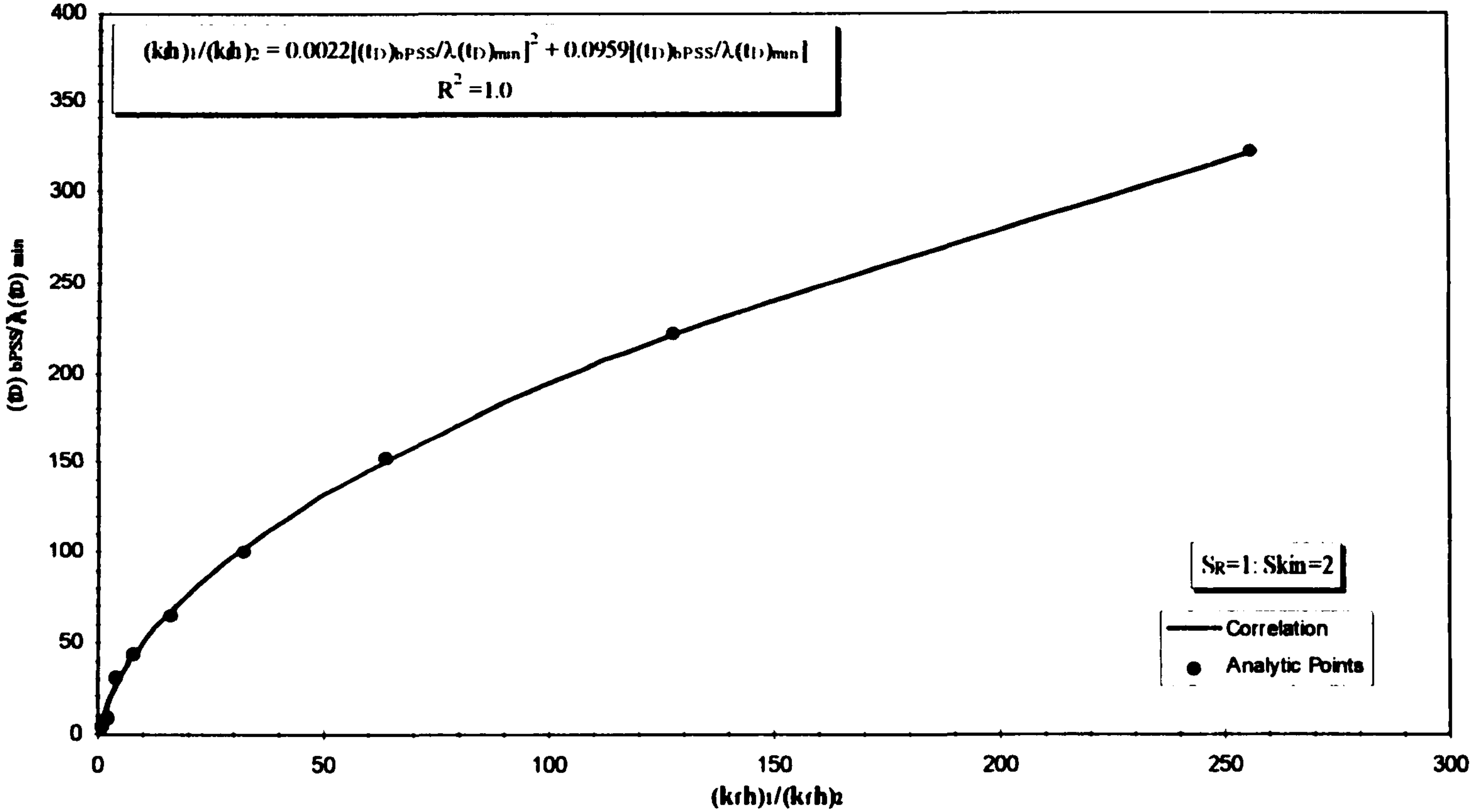

Figure 5.3.15 Correlation between the flow capacity ratio and ratio of characteristic times, Skin=2.

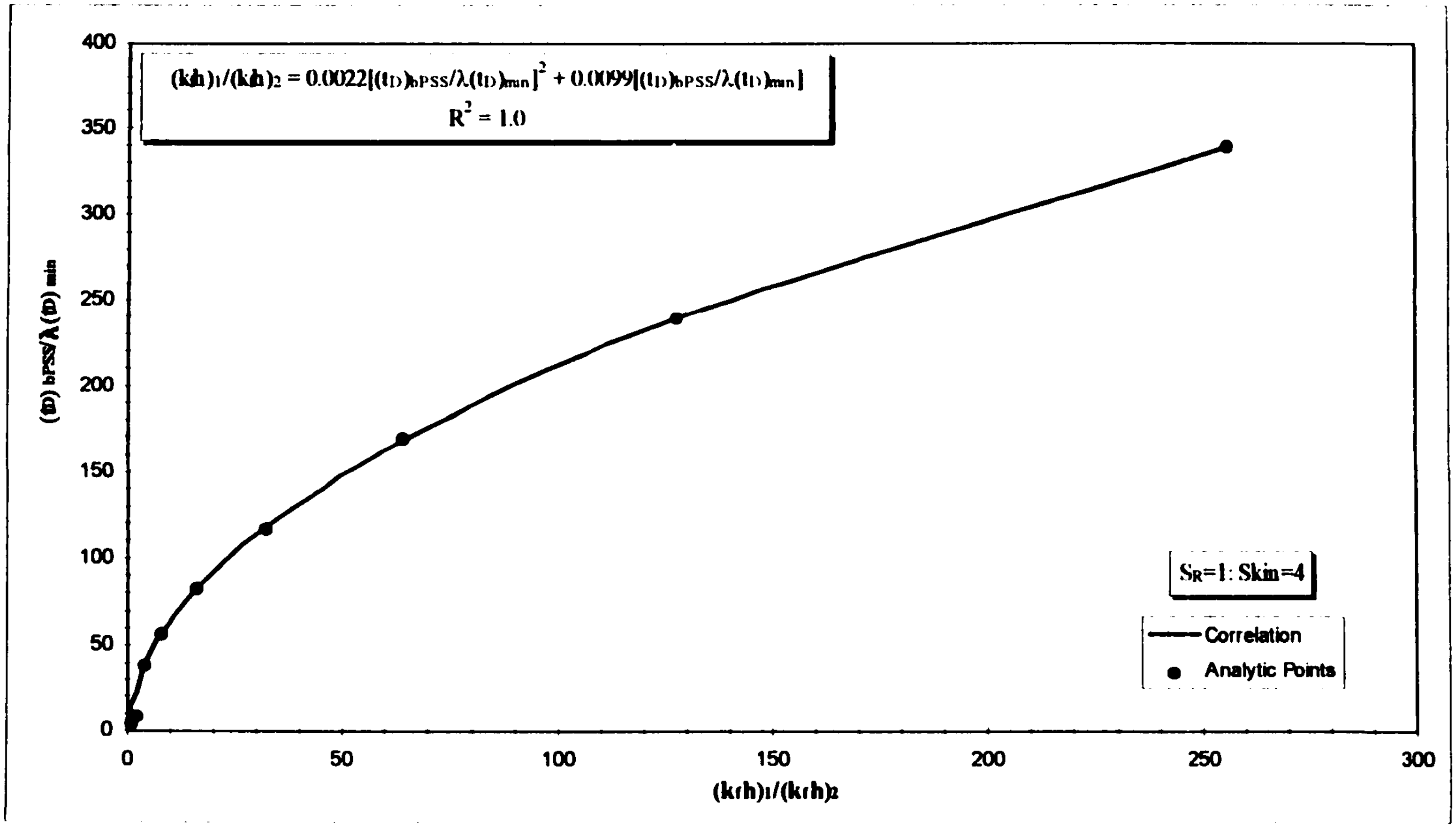

Figure 5.3.16 Correlation between the flow capacity ratio and ratio of characteristic times, Skin=4.

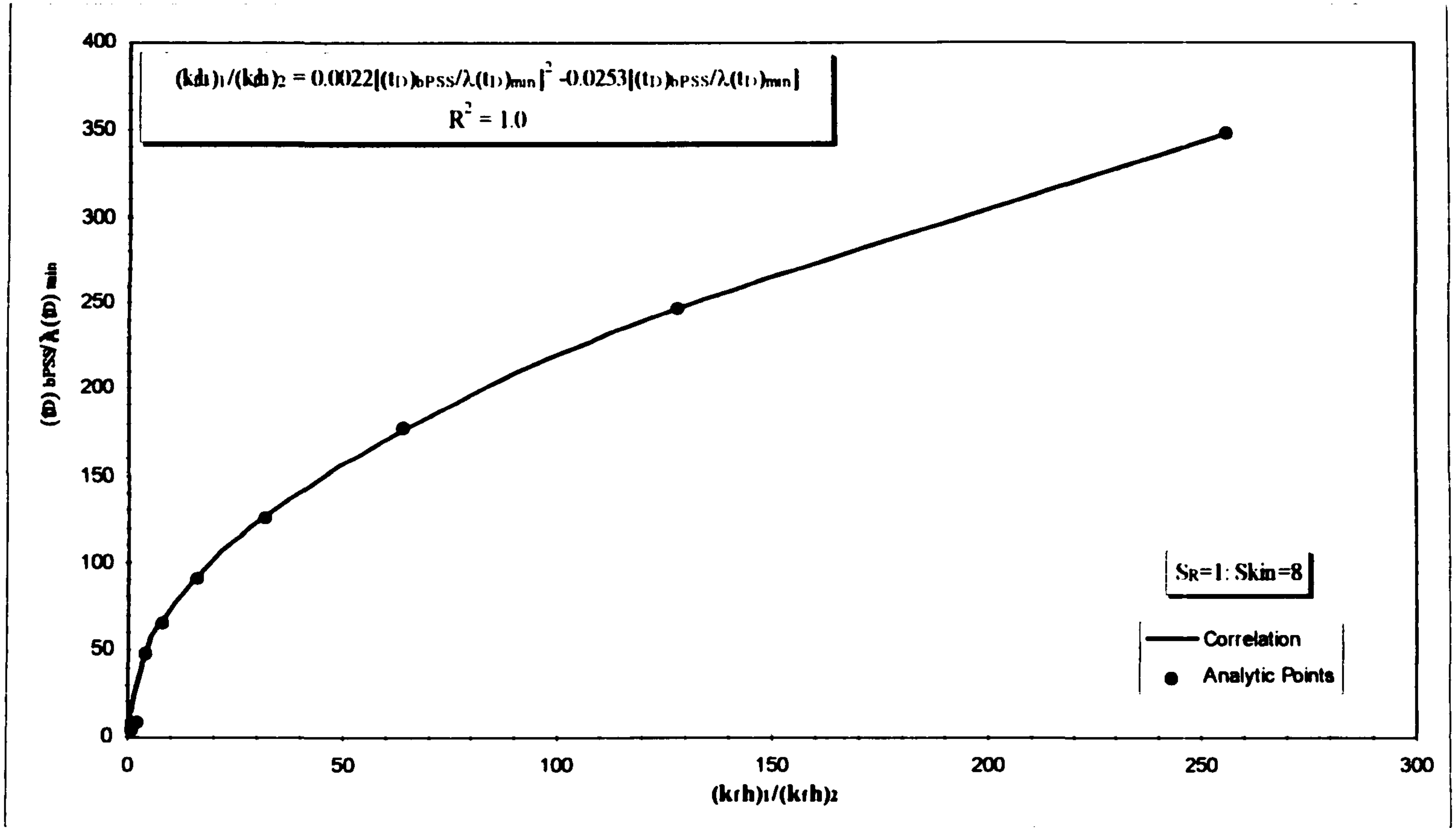

Figure 5.3.17 Correlation between the flow capacity ratio and ratio of characteristic times, Skin=8.

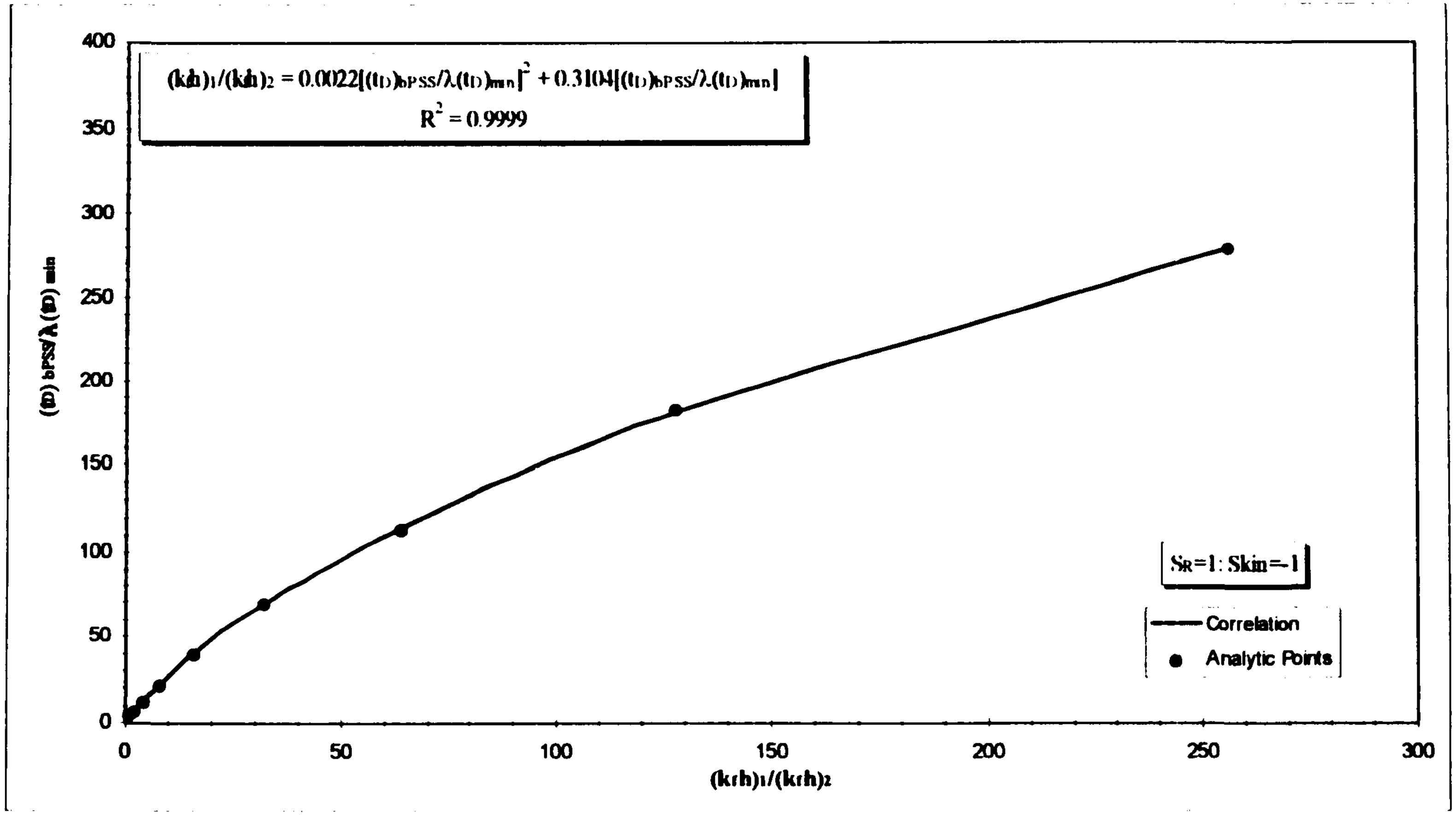

Figure 5.3.18 Correlation between the flow capacity ratio and ratio of characteristic times, Skin=-1.

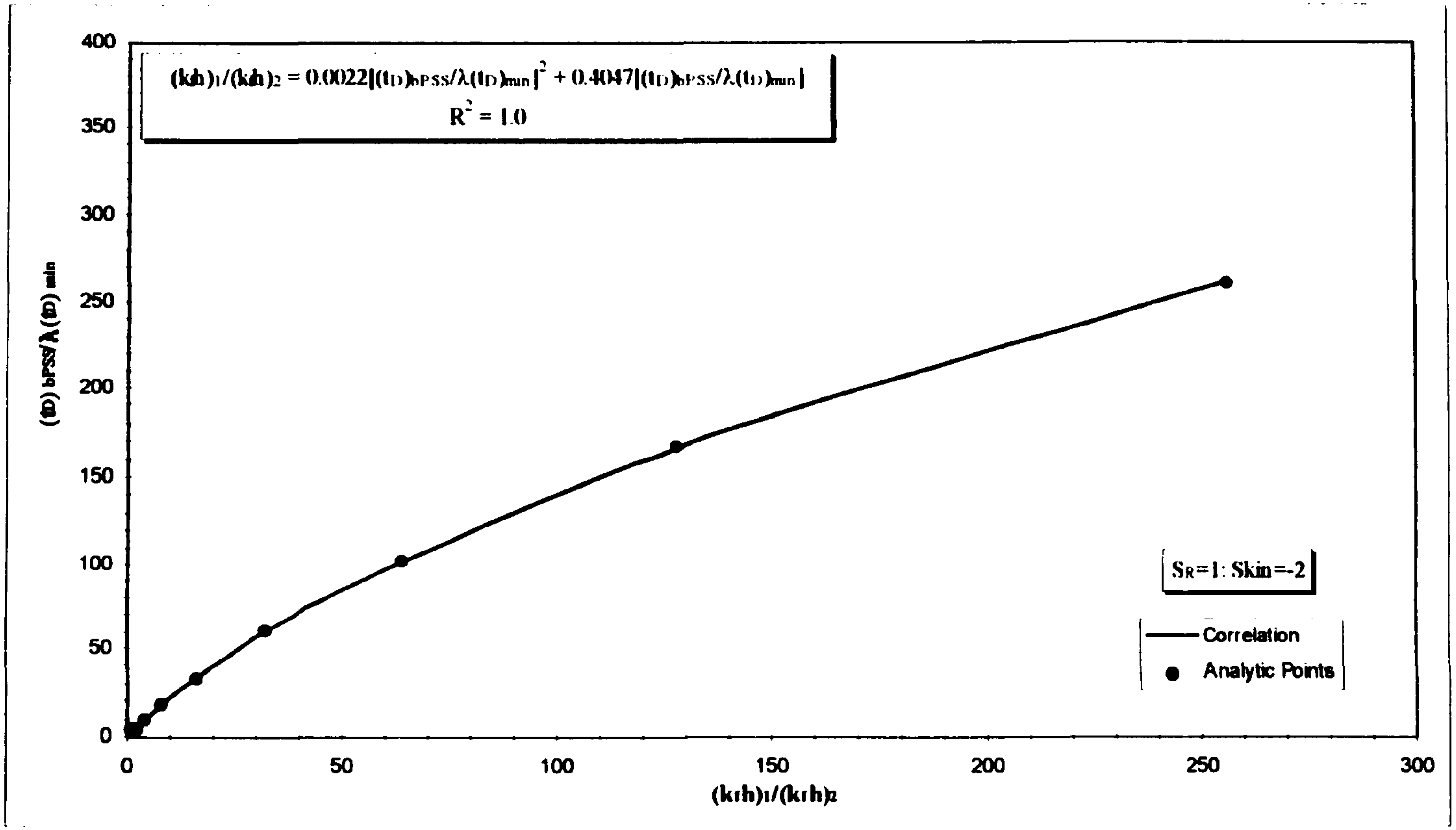

Figure 5.3.19 Correlation between the flow capacity ratio and ratio of characteristic times, Skin=-2.

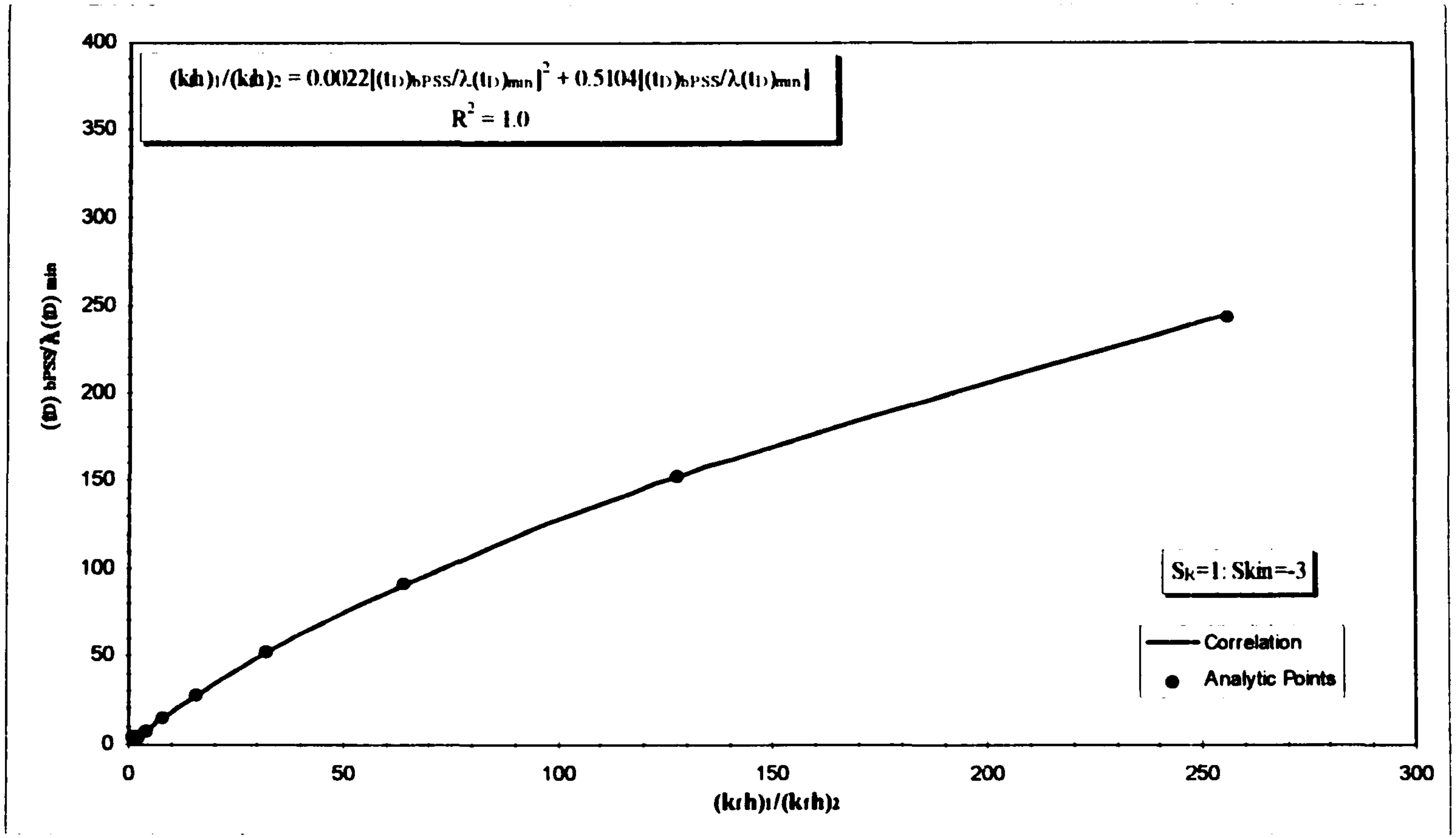

Figure 5.3.20 Correlation between the flow capacity ratio and ratio of characteristic times, Skin=-3.

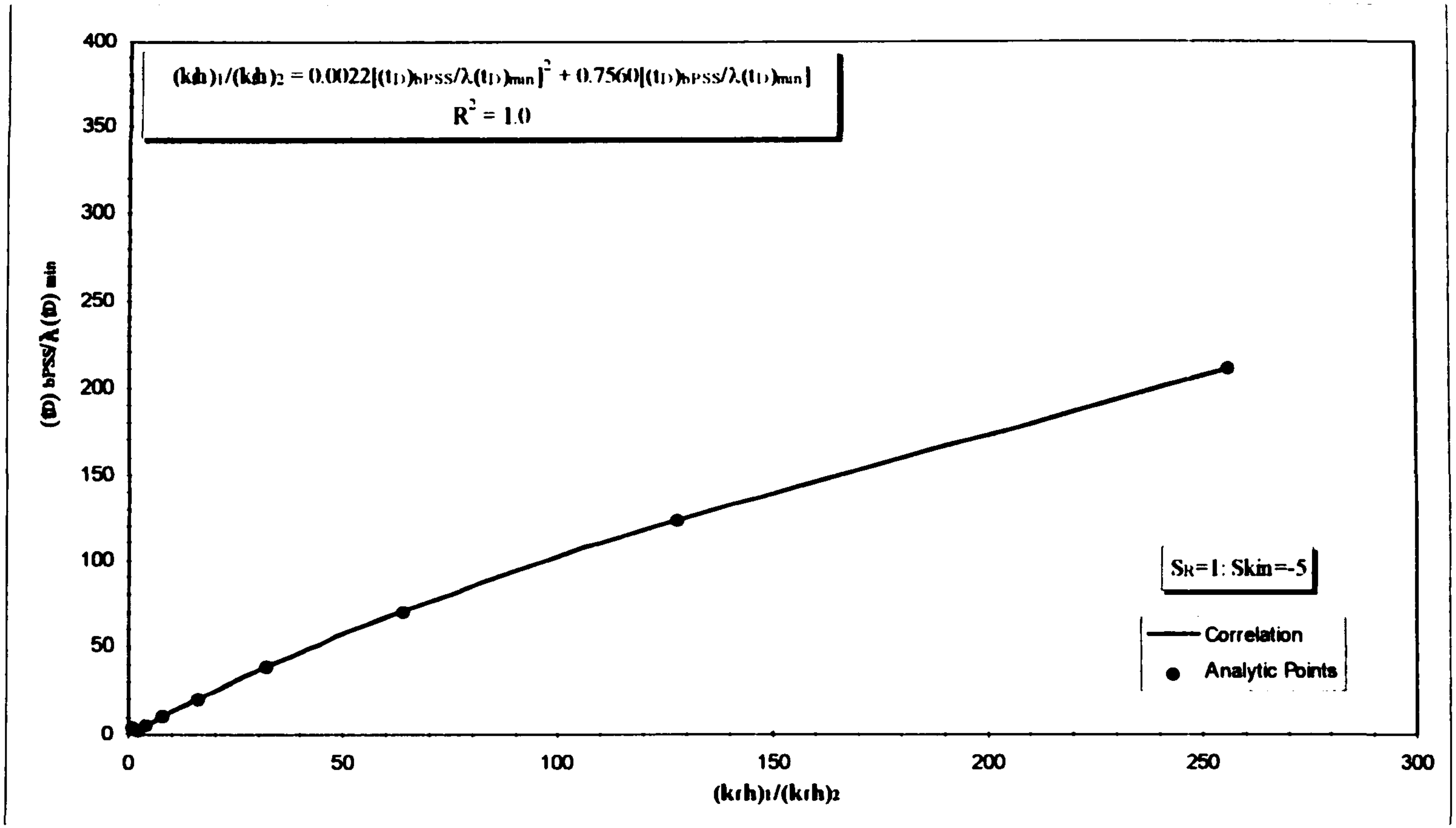

Figure 5.3.21 Correlation between the flow capacity ratio and ratio of characteristic times, Skin=-5.

CHAPTER 6

APPLICATIONS

To show the potential of the analysis and accuracy of the direct synthesis technique, the following examples of actual pressure data were analyzed by the application of Tiab's direct synthesis technique.

Example 6.1:

Ehlig-Economides et. al.[44] presented a reservoir which has three zones in commingled production, as shown in Figure 6.1. Zones 1 and 3 are fissured; Zone 2 is not. The pressure derivative curve of the total system is shown in Figure 6.2 with the characteristic points and lines labeled. The following reservoir and fluid data are given:

Zone Thicknesses:	Porosities:
Zone 1: h_{Z1}= 40 ft	$\phi_{Z1} = 0.27$
Zone 2: h_{Z2}= 40 ft	$\phi_{Z2} = 0.21$
Zone 3: h_{Z3}= 240 ft	$\phi_{Z3} = 0.27$

Formation Volume Factor: B=1.2 bbl/STB

Oil Viscosity: μ= 1 cp

Total Compressibility: c_t= $2.1\text{x}10^{-5}$ psi^{-1}

Wellbore Radius: r_w= 0.25 ft

Flow Rate of Zone 1: q_{Z1}= 9.02 bbl/day

Flow Rate of Zone 2: q_{Z2}= 89.98 bbl/day (Simulated)

Flow Rate of Zone 3: q_{Z3}= 538 bbl/day (Simulated)

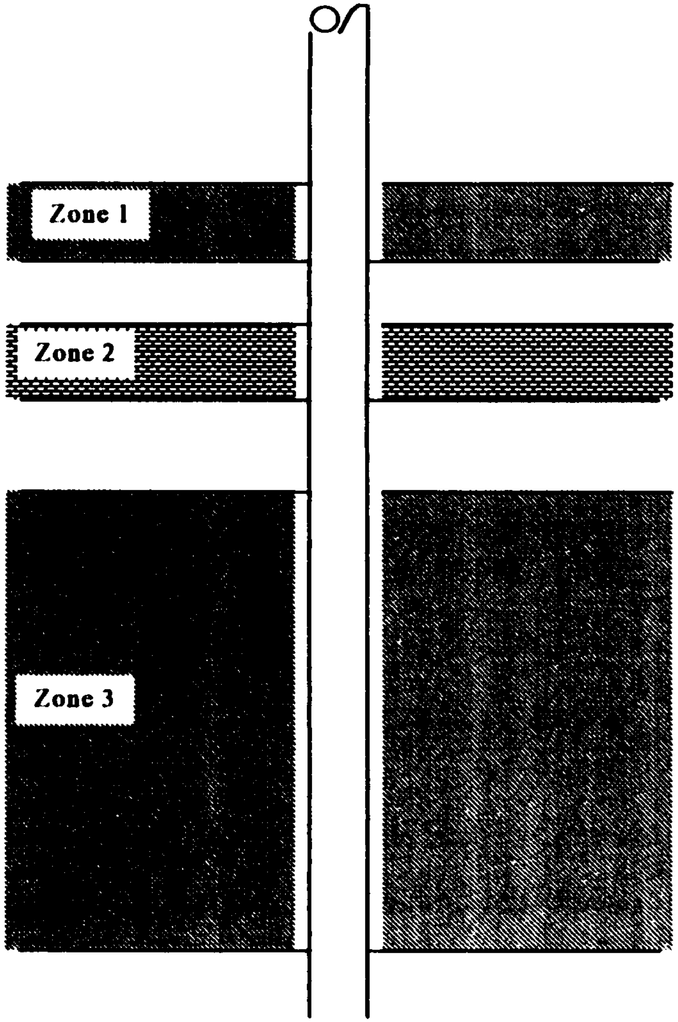

Figure 6.1 The commingled reservoir tested in Example 6.1.

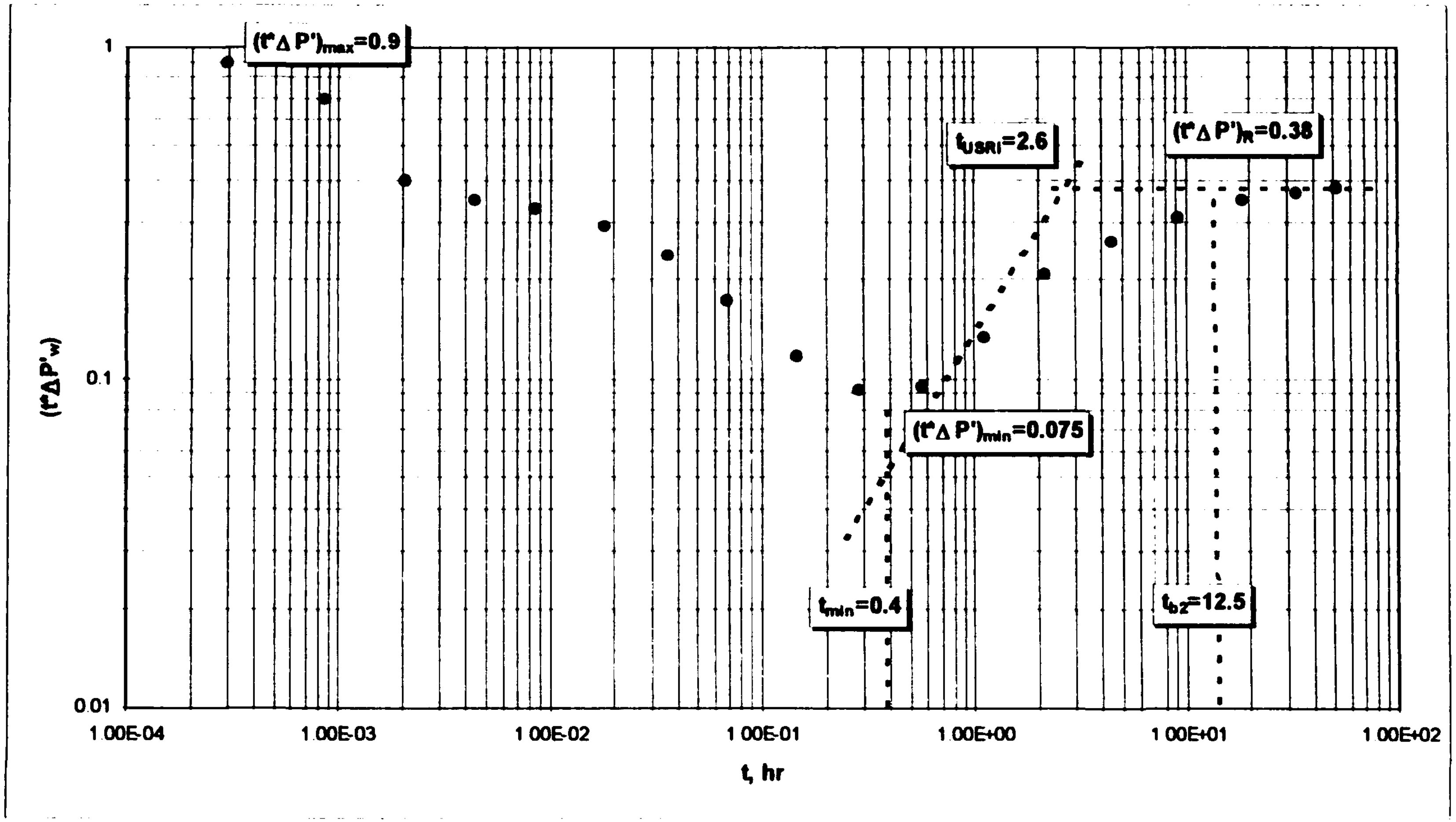

Figure 6.2 Pressure derivative data for Example 6.1. (Ehlig-Economides et. al.[44])

The total reservoir storage, $\overline{\phi c_t h}$ can immediately be determined from Equation 3.1.6, as:

$$\overline{\phi c_t h} = 0.001764 \ \text{psi}^{-1}.\text{ft}$$

then, $\overline{\phi c_t} = 0.55\text{x}10^{-5} \ \text{psi}^{-1}$

and $\bar{\phi} = 0.26$

Using Equation 3.2.5, and from the late time infinite acting radial flow period, the total fracture permeability is:

$$\bar{k} = \frac{70.6 q_t B\mu}{(t * \Delta p'_w)_{R1} \ \text{h}} = \frac{70.6(637)(1)(1.2)}{(0.38)(320)} = 443.75 \text{ md}$$

Ehlig-Economides et. al.[44] obtained the combination group C_De^{2s} of each zone using type curve matching: Zone 1 is C_De^{2s}= 15, and Zone 3 is C_De^{2s}=10. Therefore, the average C_De^{2s} is equal to 12.5. The constant E can be estimated by substituting the average value of C_De^{2s} into Equation 3.4.3:

$$E = 0.3945 \ \text{Ln}(12.5) + 1.6386 = 2.635$$

The constant D is given by Equation 3.4.2, and is equal to 0.15.

Now to determine the flow capacity ratio, $\frac{(k_f h)_1}{(k_f h)_2}$, the pressure derivative ratio, $\frac{(t * \Delta p'_w)_{max}}{(t * \Delta p'_w)_R}$, must be identified and calculated from the pressure derivative curve:

$$\frac{(t * \Delta p'_w)_{max}}{(t * \Delta p'_w)_R} = \frac{0.9}{0.38} = 2.368$$

then using Equation 3.4.1:

$$\frac{(k_f h)_1}{(k_f h)_2} = Exp\left\{-\frac{1}{0.15}\left[\frac{0.9}{0.38} - 2.635\right]\right\} = 5.45$$

The ratio $\frac{(k_f h)_1}{(\bar{k}h)}$ can be estimated from Equation 3.2.9:

$$\frac{(k_f h)_1}{(\bar{k}h)} = \frac{\dfrac{(k_f h)_1}{(k_f h)_2}}{\dfrac{(k_f h)_1}{(k_f h)_2} + 1} = \frac{5.45}{5.45 + 1} = 0.845$$

The flow capacity of the first layer is given by Equation 3.2.7 as:

$$(k_f h)_1 = (\bar{k}h)\frac{(k_f h)_1}{(\bar{k}h)} = (443.75)(320)(0.845) = 119990 \text{ md.ft}$$

This reservoir has three zones, therefore:

$$(\bar{k}h) = (k_f h)_{Z1} + (k_f h)_{Z2} + (k_f h)_{Z3}$$

where,

$$(k_f h)_1 = (k_f h)_{Z3} = 119990 \text{ md.ft}$$

and $\quad (k_f h)_2 = (k_f h)_{Z1} + (k_f h)_{Z2}$

Then, Equation 3.2.11 gives the flow capacity $(k_f h)_2$:

$$(k_f h)_2 = (\bar{k}h) - (k_f h)_1 = (443.75)(320) - 119990 = 22000 \text{ md.ft}$$

Zone 2 is homogeneous and its permeability, k, has been obtained by Ehlig-Economides et. al.[44]. The permeability of Zone 2 is equal to 500 md. Therefore, the flow capacity of Zone 1, $(k_f h)_{Z1}$, is:

$$(kh)_{Z1} = (k_f h)_2 - (k_f h)_{Z2} = 22000 - (500)(40) = 2000 \text{ md.ft}$$

The permeability of each zone can be estimated as follows:

$$(k_f)_{Z1} = \frac{2000}{40} = 50 \text{ md}$$

$$(k_f)_{Z2} = 500 \text{ md}$$

$$(k_f)_{Z3} = \frac{119990}{240} = 500 \text{ md}$$

Figure 6.3 exhibits the dual porosity response, characterized by initial and final plateaus in the derivative corresponding to fissure and total system radial flow, respectively. The valley between the two flat ports represents a transition from the early time flow period to the late time regime. The next step determines whether the minimum point is influenced by the wellbore storage. The value of the time ratio of minimum-to-peak is greater than 10; therefore it meets the condition of Equation 2.32, i.e. the minimum coordinate is not influenced by wellbore storage effects. Then, the dimensionless storage coefficient, ω, is calculated from Equation 2.27 as:

$$\omega = 0.15866\left(\frac{(t * \Delta p'_w)_{min}}{(t * \Delta p'_w)_R}\right) + 0.54653\left(\frac{(t * \Delta p'_w)_{min}}{(t * \Delta p'_w)_R}\right)^2$$

$$\omega = 0.15866\left(\frac{0.075}{0.38}\right) + 0.54653\left(\frac{0.075}{0.38}\right)^2 = 0.052$$

Independent verification is possible:

$$\omega = 0.19211\left(\frac{5t_{min}}{t_{b2}}\right) + 0.80678\left(\frac{5t_{min}}{t_{b2}}\right)^2 \tag{6.1}$$

$$\omega = 0.19211\left(\frac{5(0.4)}{12.5}\right) + 0.80678\left(\frac{5(0.4)}{12.5}\right)^2 = 0.051$$

The interporosity flow parameter, λ, can be confirmed by two separate equations, i.e., based on the minimum coordinates, and the intersection of the late transition unit slope line with the late time radial flow period. From Equation 2.29:

$$\lambda = \frac{42.5h(\phi c_t)_t r_w^2}{qB}\left(\frac{(t*\Delta p'_w)_{min}}{t_{min}}\right)$$

$$\lambda = \frac{42.5(320)(0.55x10^{-5})(0.25)^2}{(637)(1.2)}\left(\frac{0.075}{0.4}\right) = 1.14x10^{-6}$$

and from Equation 2.30:

$$\lambda = \frac{(\phi c_t)_t \mu r_w^2}{0.0002637k_{fb}}\left(\frac{1}{t_{USRi}}\right) = \frac{1}{\alpha t_{USRi}}$$

$$\lambda = \frac{(0.55x10^{-5})(1)(0.25)^2}{0.0002637(443.75)}\left(\frac{1}{2.6}\right) = 1.13x10^{-6}$$

The above example shows the potential of the analysis and accuracy of the direct synthesis technique because the direct synthesis method offers independent verification.

Example 6.2:

This example is analyzed using the rate-normalized pressure approach described in Section 3.6. The reservoir and fluid data are given in Example 6.1. Ehlig-Economides et al.[44] analyzed the two dual porosity zones, presented in the previous example, using the standard dual porosity type curves which include the pressure derivate[18]. They obtained an equivalent transient pressure derivative behavior using the rate-normalized pressure derivative. The obtained curves are identical to that of the single layer pressure transients which would result if the layers were isolated in the wellbore by packers. The rate-normalized pressure derivative is used in this example to isolate the single-layer pressure derivative transients from the pressure derivative transient of the total system which is presented in Example 6.1. The pressure derivative curves of Zone 1 and Zone 3 are shown in Figures 6.3 and 6.4 respectively. The characteristic points and lines are labeled in these figures. The fracture permeabilities of Zone 1 and Zone 3 can be calculated from the late time radial flow derivative line. Using Equation 3.2.5, the fracture permeability of Zone 1 is:

$$(k_f)_{Z1} = \frac{70.6 q_t B\mu}{\dfrac{(t*\Delta p'_w)_{R1}}{\Delta q_r} h} = \frac{70.6(9.02)(1)(1.2)}{(0.38)(40)} = 50.2 \text{ md}$$

and the fracture permeability of Zone 3 is:

$$(k_f)_{Z3} = \frac{70.6 q_t B\mu}{\dfrac{(t*\Delta p'_w)_{R1}}{\Delta q_r} h} = \frac{70.6(538)(1)(1.2)}{(0.38)(240)} = 500.4 \text{ md}$$

The dimensionless storage coefficient, ω, of Zone 1 is calculated from Equation 2.27 as:

$$\omega_{Z1} = 0.15866\left(\frac{0.012}{0.38}\right) + 0.54653\left(\frac{0.012}{0.38}\right)^2 = 0.0055$$

and the dimensionless storage coefficient, ω, of Zone 3 is:

$$\omega_{Z3} = 0.15866\left(\frac{0.07}{0.38}\right) + 0.54653\left(\frac{0.07}{0.38}\right)^2 = 0.048$$

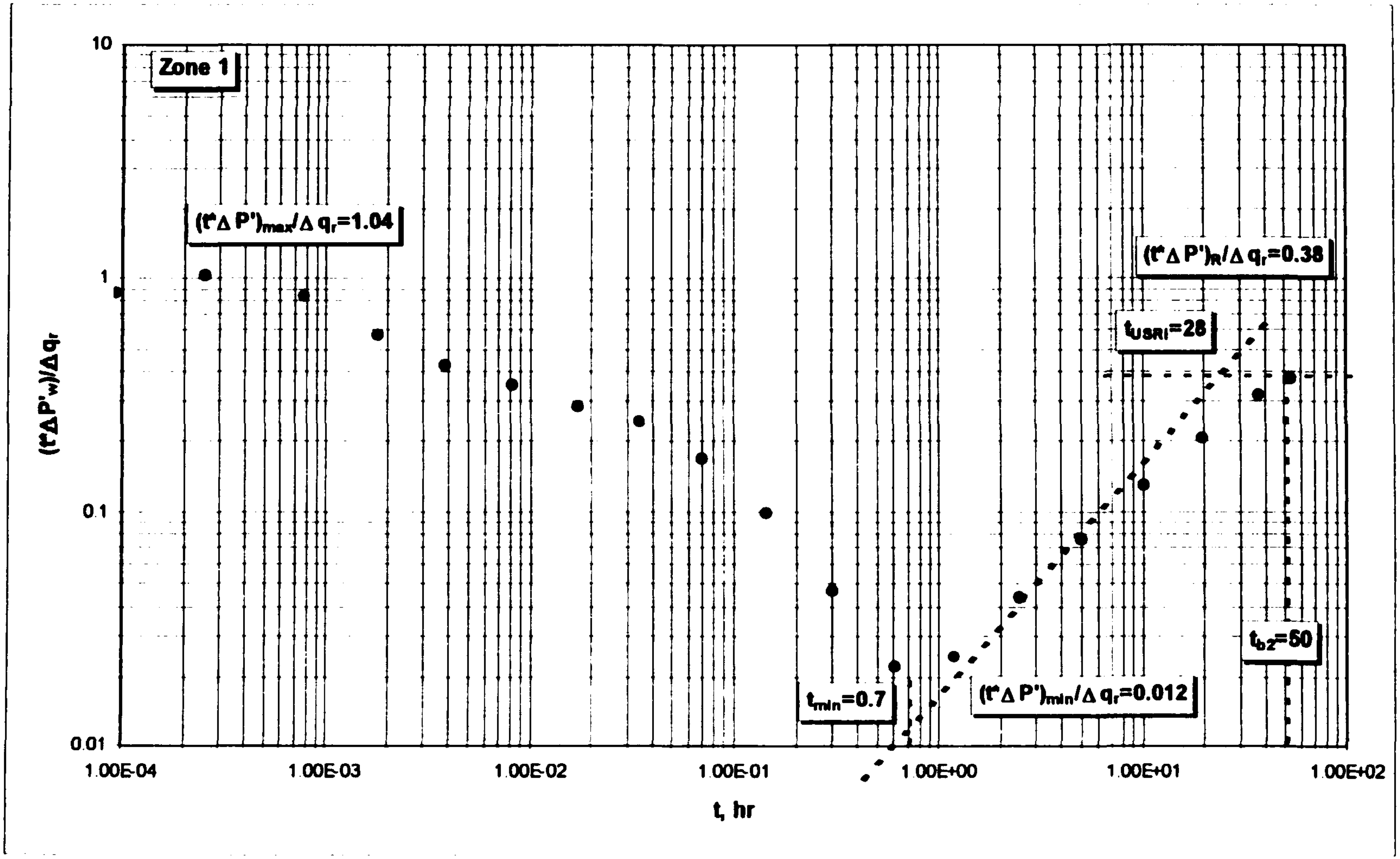

Figure 6.3 Pressure derivative data of zone 1 for Example 6.2. (Ehlig-Economides et. al.[44])

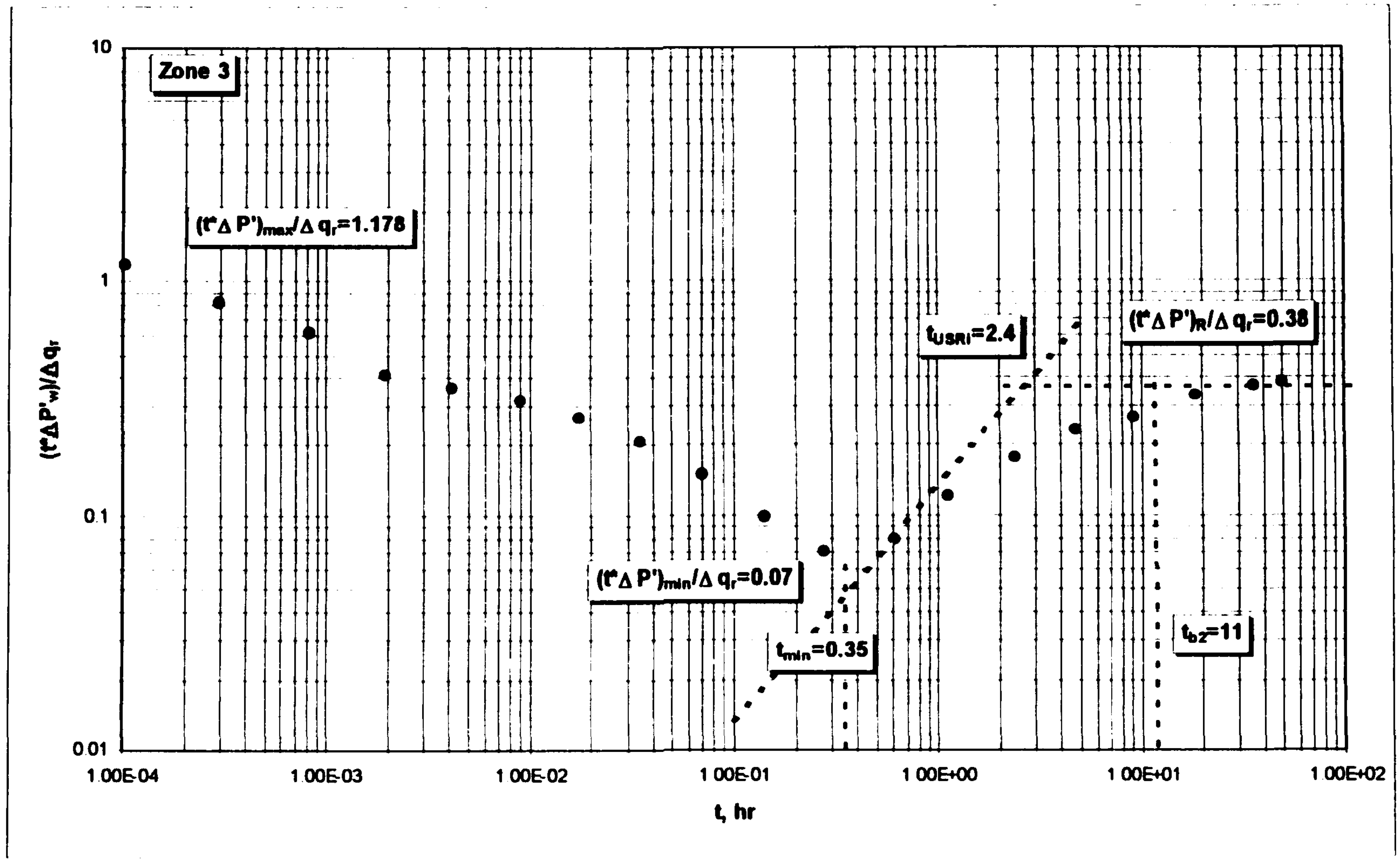

Figure 6.4 Pressure derivative data of zone 3 for Example 6.2. (Ehlig-Economides et. al.[44])

Independent verification is possible; Equation 6.1 yields:

$$\omega_{Z3} = 0.19211\left(\frac{5(0.35)}{11}\right) + 0.80678\left(\frac{5(0.35)}{11}\right)^2 = 0.05$$

For Zone 1, the interporosity flow parameter can calculated from Equation 2.29:

$$\lambda_{Z1} = \frac{42.5(40)(0.27)(2.1x10^{-5})(0.25)^2}{(9.02)(1.2)}\left(\frac{0.012}{0.7}\right) = 9.5x10^{-7}$$

and can be confirmed from Equation 2.30:

$$\lambda_{Z1} = \frac{(0.27)(2.1x10^{-5})(1)(0.25)^2}{0.0002637(50)}\left(\frac{1}{28}\right) = 9.5x10^{-7}$$

For Zone 3, the interporosity flow parameter can calculated from Equation 2.29:

$$\lambda_{Z3} = \frac{42.5(240)(0.27)(2.1x10^{-5})(0.25)^2}{(538)(1.2)}\left(\frac{0.07}{0.35}\right) = 1.12x10^{-6}$$

and can be confirmed from Equation 2.30:

$$\lambda_{Z3} = \frac{(0.27)(2.1x10^{-5})(1)(0.25)^2}{0.0002637(500)}\left(\frac{1}{2.4}\right) = 1.12x10^{-6}$$

Parameter	Type Curve	Direct Type Curve Synthesis
k_{fZ1}, md	50.4	50.2
k_{fZ3}, md	501	500.4
ω_{Z1}	0.005	0.0055
ω_{Z3}	0.05	0.05
λ_{Z1}	$1.25x10^{-8}$	$9.5x10^{-7}$
λ_{Z3}	$1.25x10^{-8}$	$1.12x10^{-6}$

Table 6.1 Comparison of Results

It can be concluded from the previous examples that the total system behavior is similar to that of Zone 3, because Zone 3 represents most of the total permeability thickness. Comparing Ehlig-Economides et. al.[44] type curve matching with direct synthesis results in several observations. The naturally fractured parameters obtained from the direct synthesis are believed more accurate than those from type curve matching because the direct synthesis method offers independent verification. The difference in the interporosity flow parameter between the type curve matching and the direct synthesis is a direct result of the simulated flow rates for Zones 2 and 3 and the choice of the transition flow period. The difference in ω_{Z1} can be directly attributed to the minimum pressure derivative coordinate determined by each technique. Unfortunately, this test was not run long enough to capture the radial flow derivative line; therefore, this essential flow period must be inferred from the scarce late time radial flow period data.

Example 6.3:

Britt et. al.[56] used type curve matching to interpret the pressure falloff test discussed below. The well has been acidized several times prior to the last fracture stimulation in 1983. A post frac pressure falloff test was performed using both a downhole shut-in device and a quartz pressure gauge. Figure 6.5 is a log-log plot of pressure and pressure derivative change versus time behavior. The plot shows the early time data is dominated by the fracture and late time data is dominated by the total system. Also, the figure shows a transition period between the early and late times. The data exhibits a unique behavior

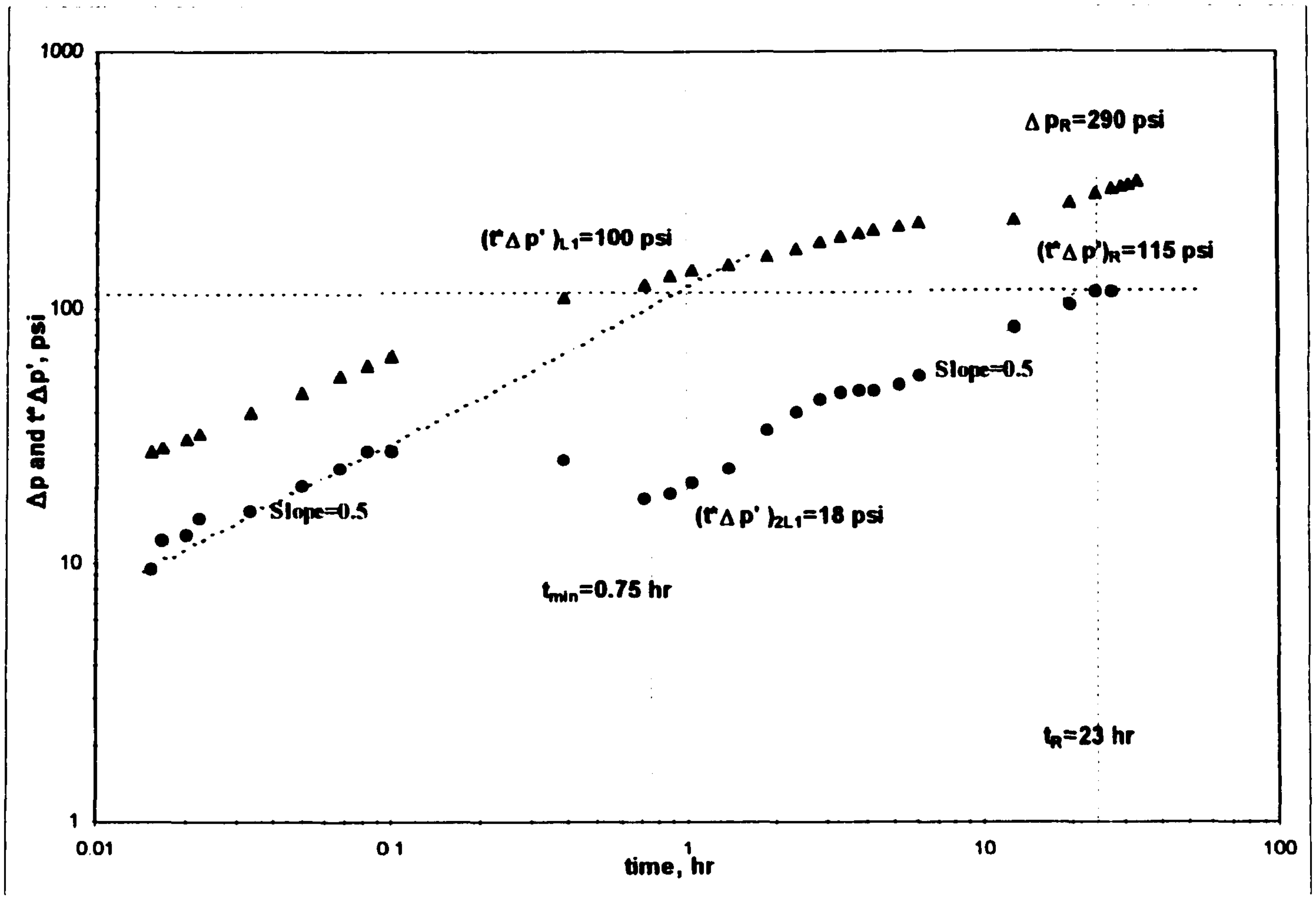

Figure 6.5 Pressure and pressure derivative data for Example 6.3 (Britt et al.[56])

which is indicative of a naturally fractured reservoir with vertical fracture. The following reservoir and fluid data are given:

q= 1050 bbl/day	B= 1 bbl/STB
μ= 0.7 cp	c_t= 9.5x10-6 psi^{-1}
ϕ= 0.085	k= 3.33 md
h= 135 ft	

The plot shows that the transition occurs during the linear flow; therefore, there are two parallel lines of slope equal to 0.5. The first line is due to the expansion of the fracture net work. This flow period is called "fracture storage dominated period" and is represented by Equation 4.1.12. The second line is the total system dominated period. For this flow period ω is equal to unity. A very useful equation was derived and presented in Equation 4.1.17:

$$\omega = \left[\frac{(t * \Delta p'_w)_{2L1}}{(t * \Delta p'_w)_{L1}}\right]^2 = \left[\frac{18}{100}\right]^2 = 0.032$$

Independent verification is possible from Equation 2.27:

$$(t * \Delta p'_w)_{\min} = 17$$

$$(t * \Delta p'_w)_R = 115$$

$$\omega = 0.15866\left(\frac{17}{115}\right) + 0.54653\left(\frac{17}{115}\right)^2 = 0.035$$

The fracture permeability can be estimated from the infinite acting radial flow line of the pressure derivative using Equation 4.1.17:

$$k_f = \frac{70.6 q_t B\mu}{(t * \Delta p'_w)_R h} = \frac{70.6(1050)(1)(0.7)}{(135)(115)} = 3.34 \text{ md}$$

Fracture linear flow period behavior occurs at early time, then the fracture length, x_f, can be calculated using Equation 4.1.12:

$$x_f = \frac{2.032 q_t B}{(t * \Delta p'_w)_{L1} \sqrt{\omega} h} \sqrt{\frac{\mu}{k_f (\phi c_t)_t}}$$

$$x_f = \frac{2.032(1050)(1)}{(100)\sqrt{0.032}(135)} \sqrt{\frac{0.7}{(9.5x10^{-6})(0.085)(3.34)}} = 450 \text{ ft}$$

and the fracture length, x_f, can be confirmed from the second line which is at the total system dominated period. Therefore, Equation 4.1.46 must be used:

$$x_f = \frac{2.032(1050)(1)}{(18)(135)} \sqrt{\frac{0.7}{(9.5x10^{-6})(0.085)(3.34)}} = 447.3 \text{ ft}$$

For a well intercepting a square, vertically fractured reservoir with double porosity, the interporosity flow parameter, λ_f, is defined in Equation 4.1.45:

$$\lambda_f = 12\, x_f^2 \frac{k_{ma}}{k_f h_m} = \lambda \frac{x_f^2}{r_w^2}$$

The interporosity flow parameter, λ_f, can be calculated using Equation 2.31:

$$\lambda_f = \frac{(\phi c_t)_t \mu x_f^2}{0.0002637 k_{fb}} \left(\frac{\omega \ln(1/\omega)}{t_{min}} \right)$$

$$\lambda_f = \frac{(0.085)(9.5x10^{-6})(0.7)(450)^2}{0.0002637(3.34)} \left(\frac{(0.032)\ln(1/0.032)}{0.75} \right) = 19.1$$

For verification, Equation 2.29 is used to determine λ_f based on the minimum coordinates:

$$\lambda_f = \frac{42.5(135)(0.085)(9.5x10^{-6})(450)^2}{(1050)(1)}\left(\frac{17}{0.75}\right) = 20$$

and $$\lambda = 20\left(\frac{r_w}{450}\right)^2 = 9.87x10^{-5} r_w^2$$

Assume r_w= 0.25 ft, then:

$$\lambda = 6.17x10^{-6}$$

The radial flow period is influenced by the skin which can be calculated Equation 4.1.18:

$$S = 0.5\left[\frac{(\Delta p_w)_R}{(t*\Delta p'_w)_R} - \ln\left(\frac{k_f t_R}{(\phi c_t)_f \mu r_w^2}\right) + 7.43\right]$$

$$S = 0.5\left[\frac{290}{115} - \ln\left(\frac{(3.34)(23)}{(0.085)(9.5x10^{-5})(0.7)(0.25)^2}\right) + 7.43\right] = -4.6$$

Parameter	Type Curve	Direct Type Curve Synthesis
k_f, md	3.33	3.34
x_f, ft	442	447-450
ω	---	0.032
λ	---	$6.17x10^{-6}$
λ_f	---	20
Skin	-4.2	-4.6

Table 6.2 Comparison of Results

Britt et. al.[56] used the pressure type curves of homogenous reservoirs with hydraulic fracture to analyze this falloff test. Therefore, they were not able to estimate the interporosity flow parameter and the dimensionless storage coefficient. Unfortunately, this test was not run long enough to capture the radial flow derivative line and therefore this essential flow period must be inferred from the scarce late time radial flow period data. Notice the difference in skin value. This difference is a result of the choice of the late time infinite acting radial flow derivative line or the assumed wellbore radius value. Comparing Britt et. al.[56] type curve matching with direct synthesis results in an excellent agreement in estimating k_f, and x_f.

As a conclusion, the applications show that Tiab's Direct Synthesis Technique is very useful when the late time infinite-acting radial flow line is not well developed due to the lack of data.

CHAPTER 7

DISCUSSION
CONCLUSIONS AND RECOMMENDATIONS

7.1 Discussion

The literature review shows that although hundreds of papers on well test analysis treated different situations of wells located in oil reservoirs, to the best of my knowledge none of them studied the case of multi-layer double porosity reservoirs with vertical fractures. Therefore, this work examines the pressure behavior of multi-layer naturally fractured reservoirs with and without hydraulic (vertical) fracturing. This study utilizes the layered reservoir without cross-flow. A technique known as "Tiab's Direct Synthesis" is applied to pressure tests, increasing the accuracy and reliability of the information. This technique gives direct estimates of reservoir parameters and fracture characteristics without using type curve matching. New analytical and empirical expressions were developed as a result of this study. However, to make these correlations universal, normalized forms are derived. Most of the results are presented in the general form of dimensionless variables. The results presented in this work are applicable to both drawdown and buildup well testing. This research shows that the pressure derivative is a powerful diagnostic tool for analyzing pressure transient data.

The development of the direct synthesis procedure for a commingled multi-layer infinite-acting, naturally fractured reservoir is examined. Mathematical formulation is presented and type curves for wellbore pressure and its derivative are generated. A new set of type curves is developed and presented for both transient and pseudo-steady state flow including wellbore storage. For simplification, only a two-layer system without cross-flow is considered. However, the results provided here can be generalized to muli-layer systems. Derivations of $f(s)_i$ function to simulate three types of double porosity response are presented in this study. The types are: (1) pseudo-steady state matrix flow; (2) transient matrix flow of a slab geometry; and (3) transient matrix flow of a sugar-cube geometry. The derived function $f(s)$ converts the single porosity solution into the corresponding multi-layer dual porosity reservoir solution. One of the most important results obtained is that the significant transient event in interpreting a production data from an infinite, multi-layer reservoir is the initial flow period. It is important to note that the shapes of either pressure or pressure derivative curves for the layered reservoir are similar to those of a single-layer reservoir. Thus the shape of the well response will not be useful in identifying the layered nature of the formation. As a result, new empirical correlations were developed to solve the flow capacity in each layer. Both cases are considered, with and without wellbore storage. The effect of the dimensionless storage coefficient, ω, and the interporosity flow parameter, λ, is investigated by observing the pressure and pressure derivative responses. A very important observation was found that for $\frac{\lambda_1}{\lambda_2} > 100$, the derivative curve has two depressions. As a direct consequence, individual values of λ and ω can be estimated. The first depression gives values of λ and ω for one layer, and the second depression gives values of λ and ω for the other layer.

Further, the study presents an analysis procedure for commingled layered, double porosity systems that is completely analogous to that used for single layered systems.

The analysis is based on a plot of pressure change (ΔP) divided by relative rate change (Δq_{ri}) versus time. Then, the direct synthesis technique was applied to develop simple equations that can be used to determine individual layer properties, such as permeability, dimensionless storage coefficient, ω, interporosity flow parameter, λ, and skin values. The analysis can be applied for both infinite-acting and bounded naturally fractured reservoirs.

This study addressed the problem of the pressure behavior of a well crossed by a uniform-flux and infinite-conductivity vertical fracture and located in a multi-layered bounded square reservoir with a double porosity system. A mathematical model is applied to the case of a single-layer system and type curves for wellbore pressure and its derivative are generated. The advantage of these analytically produced type curves over the previously published work is the addition of the pressure derivative. The main applications of the proposed technique are to determine the reservoir properties and fracture-half length. Useful correlations were developed to determine the dimensionless storage coefficient, ω, and interporosity flow parameter, λ. The nature of the fracture (uniform-flux and infinite-conductivity vertical fracture) has minor effects on the pressure derivative. The nature of the fracture affects only the time to the end of the fracture linear flow period. The type curves obtained for the infinite-conductivity fracture are qualitatively the same as the uniform-flux solutions. Only the shape is slightly different at intermediate times. In the case of the uniform-flux vertical fracture, type curves show the existence of three flow regimes: (1) the linear flow line of slope 0.5, (2) the infinite-acting radial flow line of a horizontal straight line, and (3) the pseudo-steady state flow line of slope unity, in addition to the transition region. Infinite-conductivity vertical fracture case reveals a fourth dominated flow regime which can be identified by a straight line of slope 0.36. This flow period is called the bi-radial flow. It was found that the pressure and the pressure derivative are mainly controlled by the fracture extension into the formation. Unfortunately, the infinite-acting flow period is dominant only if $\left(\frac{x_e}{x_f}\right) > 8$.

Relationships were developed for multi-layer systems. New points and lines are identified by applying the direct synthesis analysis which improves the interpretation. The study shows that the direct synthesis technique is simple and accurate because the analysis couples the pressure data with the analytical equations. A new set of dimensionless pressure and pressure derivative versus dimensionless time type curves were generated. Tiab's Direct Synthesis Technique was applied to the generated type curves to provide a way of estimating the flow capacity and the fracture length of each layer. It was found that the effect of flow capacity ratio on pressure derivative curves is significant. The effect of flow capacity ratio is the major factor on the pressure derivative curves during the late time pseudo-steady state. Thus, different correlations were obtained to determine individual layer flow capacity ratio. It was shown that for $\frac{(k_f h)_1}{(k_f h)_2} < 8$, the pressure derivative behavior is equivalent to single-layer system with $\frac{(k_f h)_1}{(k_f h)_2} = 1$.

This work presents a mathematical model which describes pressure tests in commingled vertically fractured double porosity reservoirs. A new simple method of analysis based on this model is presented for pressure tests. This method is useful for the analysis of simultaneously measured down-hole sand-face rate and pressure. Tiab's Direct Synthesis Technique was applied to develop simple equations that can be used to analyze the simultaneously measured downhole pressure and sand-face flow rate. Based on this study, the fractional flow rate comes from each layer is a good source of data which can be coupled with pressure response to estimate individual layer properties. Thus, it is recommended to measure the layer sand-face flow rate during pressure testing in a multi-layered reservoir.

This study shows that the drilling operation is a good source of data from which the changing in skin factor and damage radius along the well depth can be quantified. Knowledge of the extension of a formation damaged region is considered essential for the preparation of an appropriate fracture stimulation design. A simplified model is developed and presented in Appendix F illustrating the variability of the damage zone along the depth of a vertical well.

Finally, there is no doubt that the importance of the results derived from this study have a major impact on improving the interpretation of pressure behaviors of multi-layer systems. To show the potential of the analysis and accuracy of Tiab's Direct Synthesis Technique, examples of pressure test data were analyzed by the application of direct synthesis technique. Thus, it is believed that while the proposed models and correlations are a result of theoretical development, they still can be used for practical purposes.

7.2 Conclusions

The following conclusions are drawn in this study:

(1) It is important to note that the shapes of either pressure or pressure derivative curves for the double porosity layered reservoir are similar to those of a single-layer reservoir.

(2) The pressure transient of a single phase and slightly compressible fluid flow in a multi-layer infinite, isotropic, double porosity system is extended to the application of Tiab's Direct Synthesis Technique.

(3) A very important observation was found that for $\frac{\lambda_1}{\lambda_2} > 100$, the pressure derivative curve has two depressions. As a direct consequence, individual values of λ and ω can be estimated.

(4) The peak points on pressure derivative curves are more affected by wellbore storage than by skin.

(5) This study addressed the problem of the pressure behavior of a well crossed by a vertical fracture and located in a double porosity reservoir. It was found that the infinite-acting flow radial period is dominant only if $\left(\frac{x_e}{x_f}\right) > 8$.

(6) The nature of the fracture (uniform-flux or infinite-conductivity vertical fracture) has minor effects on pressure derivative. The nature of the fracture affects only the time to the end of the fracture linear flow period.

(7) The effect of flow capacity ratio is the major factor on the pressure derivative curves during the late time pseudo-steady state. As a result, new empirical expressions were developed to estimate the flow capacity ratio by observing the beginning of the pseudo-steady state flow period.

(8) The results for the case of $\frac{(k_f h)_1}{(k_f h)_2} < 8$, are close to the results for an ideal single-layer case. For all other cases, the results are widely different.

(9) The proposed technique provides accurate determination results of the individual layer properties; e.g., fractured permeability, skin factor, dimensionless storage coefficient, interporosity flow parameter, and half-fracture length (if applicable).

(10) Based on the proposed study, it is recommended that the layer sand-face flow rate be measured during pressure testing in a multi-layered reservoir.

7.3 Recommendations

The following brief recommendations are suggested for further study in the area that examines of multi-layered reservoirs:

(1) This work can be extended to include horizontal reservoirs.

(2) Further extension of this work can include non-Newtonian fluid flow in both homogeneous and heterogeneous reservoirs.

(3) The pressure derivative can be extended to consider vertically fractured wells in a bounded rectangular reservoir with various values of the long side to the short side ratio.

NOMENCLATURE

A	area, ft^2
B	formation volume factor, rb/stb
c_t	total compressibility, psi^{-1} (Pa^{-1})
c_{ti}	compressibility of layer i, psi^{-1} (Pa^{-1})
C	wellbore storage coefficient, bbl/psi (m^3/Pa)
C_A	shape factor of the primary system, ft (m)
C_D	dimensionless wellbore storage
$f(s)$	function converts the single porosity solution into the corresponding dual porosity reservoir solution
h	total formation thickness, ft (m)
h_i	formation thickness of layer i, ft (m)
$\bar{k}$	permeability (thickness-averaged value) defined in Equation 3.3, md (m^2)
k_{fi}	permeability of layer i, md (m^2)
K_0	modified Bessel functions of the second kind, zeroth order
K_1	modified Bessel functions of the second kind, first order
n	number of layers
p	reservoir pressure, psi (Pa)
p_D	dimensionless pressure
p_{wD}	dimensionless bottom-hole pressure

p_{int} initial pressure, psi (Pa)

p_w bottom-hole pressure, psi (Pa)

p'_D dimensionless pressure derivative

p'_{wD} dimensionless bottom-hole pressure derivative

Δp pressure difference (p_w- p_{int}), psi (Pa)

$\Delta p'$ pressure difference derivative, psi (Pa)

q_t flow rate, stbd (m^3/s)

q_i flow rate of layer i, stbd (m^3/s)

q_{ti} relative flow rate of layer i defined in Equation 3.43

r_e reservoir outer radius, ft (m)

r_w wellbore radius, ft (m)

s Laplace operator

S skin factor

t test time, hour (second)

t_D dimensionless time

x_e half side of rectangle in x-axis, ft (m)

x_f fracture-half length, ft (m)

x_{fi} fracture-half length of layer i, ft (m)

y_e half side of rectangle in y-axis, ft (m)

Greek Symbols

α_i' interporosity flow shape factor, ft^{-1} (m^{-1})

α_i layer storage ratio defined in Equation B-19

β_i layer mobility ratio defined in Equation B-17

λ interporosity flow parameter

μ viscosity, cp ($Pa.s^n.m^{1-n}$)

ϕ porosity

ϕ_i porosity of layer i

$\overline{\phi c_t}$ defined in Equation 3.4

ω dimensionless storage coefficient

Subscripts

1 layer number 1

2 layer number 2

b1 beginning of first radial flow period

b2 beginning of second radial flow period

D dimensionless

e value at outer boundary

f fracture value

i value of layer i

L	linrear
int	initial value
m	matrix value
max	maximum
min	minimum
PSS	pseudo-steady state
R	radial
t	total
w	value at wellbore

<u>SI Metric Conversion Factors</u>

cp x 1.0	E-03 = Pa.s
ft x 3.048	E-01 = m
ft^2 x 9.290304	E-02 = m^2
bbl x 1.589873	E-01 = m^3
md x 9869233	E-04 = m^2
psi x 6.894757	E+03 = Pa
psi^{-1} x 1.450377	E-04 = Pa^{-1}

REFERENCES

1. Cinco-ley, H.: "Well-Test Analysis for Naturally Fractured Reservoirs," JPT, January 1996.
2. Warren, J.E. and Root, P.J.: "The Behavior of Naturally Fractured Reservoirs," SPEJ (Sept. 1963) 245-255; Trans., AIME, 228.
3. Kazemi, H.: "Pressure Transient Analysis of Naturally Fractures Reservoirs with Uniform Fracture Distribution," SPEJ, (Dec. 1969), 451-462.
4. Tiab, D.: "Modern Core Analysis Manuscript", Internal Core Lab Publication, May 1993.
5. Prison , S.J.: "How to Map Fracture Development from Wells Logs," World Oil, 164, no. 4, March 1967, p. 106-114.
6. Stehfest, H.: "Numerical Inversion Of Laplace Transform," Communications of the ACM (Jan 1970) Volume 13, No. 1, pp 47-49.
7. Pollard, P.: " Evaluation of Acid Treatments from Pressure Buildup Analysis," Trans., AIME (1959) 216, 38-43.
8. Barenblatt, G.I. and Zheltov, Y.P.: "Fundamentl Equations of Filtration of Homogeneous Liquids in Fissures Rocks," Sovet Physics, Doklady (1960) 5, 522.
9. Barenblatt, G.I., Zheltov, Y.P. and Kochina, I.N.: "Basic Concepts in the Theory of Seepage of Homogeneous Liquids in Fissured Rocks," PMM, Vol. 24 (1960) 5, 852-864.
10. Odeh, A.A.: "Unsteady-State Behavior of Naturally Fractured Reservoirs," SPEJ (March 1965), 60-66.

11. De Swaan, O.A.: "Analytic Solutions for Determining Naturally Fractured Reservoir Properties by Well Testing," SPEJ (June 1976), 117-122.

12. Earlougher, R. C.: Advances In Well Testing Analysis: Monograph series, SPE, Dallas, 1977, Vol. 5, 126-127.

13. Mavor, M. J. and Cinco Ley, H.: "Transient Pressure Behavior of Naturally Fractured Reservoirs," SPE 7977, presented at the 1979 California Regional Meeting of the SPE, held in Venture, California, April 18-20, 1979.

14. Bourdet, D. and Gringarten, A.C.: "Determination of fissure volume and Block Size in Fractured Reservoir By Type-Curve Analysis," SPE 9293, presented at 55th Annual Fall Tech. Conf. And Exh. Of the SPE, held in Dallas, TX, Sept. 21-24, 1980.

15. Lai, C.H., Bodvarson, G.S., Tsang, C.F. and Witherspoon, P.A.: "A New Model for Well Test Data Analysis for Naturally Fractured Reservoirs," SPE 11688 presented at the March 1983 California Regional Meeting in Ventura, CA.

16. Streltsova, T.D.: "Well Pressure Behavior of a Naturally Fractures Reservoir," SPEJ, (Oct. 1983), 769-780.

17. Bourdet, D. Ayoub, J. A., Whittle, T. M. Pirard, Y. M., and Knlazeff, V.: "Interpreting Well Tests In Fractured Reservoirs," World Oil, Oct. 1983, 77-87.

18. Bourdet, D., Alagoa, A., Ayoub, J. A., and Pirard, Y. M.: "New Type Curves Aid Analysis of Fissured Zone Well Tests," World Oil, April 1984, 111-125.

19. Blasingame, T. A. and Lee, W. J.: "Properties of Homogeneous Reservoirs, Naturally Fractured Reservoirs, and Hydraulic fractured Reservoirs from Decline

Curve Analysis," SPE 15018, presented at the Permian Basin Oil & Gas recovery Conference of the SPE held in Midland, TX, March 13-14, 1985.

20. Onur, M. and Satman, A.: "New Type Curves to Determine Naturally Fractured Reservoir Parameters," SPE Technical Publications, SPE 23830, Sept. 16, 1991.

21. Hyes, M. R. L. and Vaughan,, A. E.: "A New Type Curve for Well Testing In Anisotropic Formations," SPE 23099, presented at the Offshore Europe Conference held in Aberdeen, Sept. 1991.

22. Engler, T. and Tiab, D.: "Analysis of Pressure and Pressure Derivative Without Type Curve Matching: 4.Naturally Fractured Reservoirs," Journal of Petroleum Science and Engineering 15 (1996) 127-138.

23. Russel, D. G., and Truitt, N. E.: "Transient Pressure Behavior In Vertically Fractured Reservoirs," J. Pet. Tech., Oct. 1964, 159-170.

24. Cinco-Ley, H., Samaniego-V, F., and Domingueza, N.: "Transient Pressure Behavior For A Well With A Finite Conductivity Vertical Fracture," SPE 6014 presented at the 51st Annual Fall Technical Conference And Exhibition of the SPE, New Orleans, La. (Oct. 3-6, 1976).

25. Cinco-Ley, H., Samaniego-V, F.: "Effect Of Wellbore Storage And Damage On The Transient Behavior Of Vertically Fractured Wells," SPE 6752, presented at the 52nd Annual Fall Technical Conference And Exhibition of the SPE, Denver, Colorado, Oct. 9-12, 1977.

26. Baker, B. J., and Ramey, H. J., Jr.: "Transient Flow To Finite Conductivity Vertical Fractures," SPE 7489, presented at the 53rd Annual Fall Technical Conference And Exhibition of the SPE, Houston, Texas, Oct. 1-3, 1978.

27. Cinco-Ley, H., Samaniego-V, F.: "Transient Pressure Analysis For Fractured Wells," SPE 7490, presented at the 53rd Annual Fall Technical Conference And Exhibition of the SPE, Houston, Texas, Oct. 1-3, 1978.

28. Hanley, E. J., and Bandyopadhyay, P.: "Pressure Transient Behavior Of The Uniform Infulx Finite Conductivity Fracture," SPE 8278, presented at the 54th Annual Fall Technical Conference And Exhibition of the SPE, Las Vegas, Nevada, Sept. 23-26, 1979.

29. Ahmed, U.: "Transient Pressure Analysis Of Hydraulically Fractured Wells In The Western Tight Sands," SPE 10878, presented at the Rocky Mountain Regional Meeting of the SPE, Billing, MT., May 19-21, 1982.

30. Puthigai, S. K., and Tiab, D.: "Application of P'D Function to vertically Fractured wells-Field Cases," SPE 11028, presented at the 57th Annual Fall Technical Conference And Exhibition of the SPE, New Orleans, Sept. 26-29, 1982.

31. Tiab, D.: "Direct Type-Curve Synthesis Of Pressure Transient Tests," SPE 18992, prepared for presentation at the SPE Joint Rocky Mountain Regional/Low Permeability Reservoirs Symposium and Exhibition held in Denver, Colorado, March 6-8, 1989.

32. Tiab, D.: "Analysis of Pressure and Pressure Derivative Without Type Curve Matching: Vertically Fractured Wells In Closed Systems," Journal of Petroleum Science and Engineering 11 (1994) 323-333.

33. Houze, O.P., Horne, R., and Ramey, H.J. Jr.: "Infinite Conductivity Vertical Fracture In A Reservoir With Double Porosity Behavior," SPE 12778 presented at the 1984 SPE California Regional Meeting, Long Beach, April 11-13.

34. Lancaster, D.E., and Gatens, J.M.: "Practical Well Test Analysis Methods For Hydraulically Fractured Wells In A Dual-Porosity Resrviors," SPE 15924 presented at the SPE Estern Regional Meeting held in Columbus, Ohio, November 12-14, 1986.

35. Cinco-Ley, H., and Meng, H.: "Pressure Transient Analysis Of Wells With Finite Conductivity Vertical Fractures In Double Porosity Reservoirs," SPE 18172 presented at the 63rd Annual Technical Conference and Exhibition of the SPE held in Houston, TX, October 2-6, 1988.

36. Liu Ci-Qun and Yang-Jim: "The Approximate Analytical Solutions Of Transient Pressure For A Finite-Conductivity Vertical Fracture In A Reservoir With Double Porosity," SPE 19439 was provided to the SPE for distribution and possible publication in an SPE journal, 1989.

37. Russel, D.G., and Prats, M.: "The Practical Aspects Of Interlayer Crossflow," J. Pet. Tech. (June 1962) 589-594.

38. Lefkovits, H.C. et al.: "A Study of the Behaviour of Bounded Reservoirs Composed of Stratified Layers," SPEJ (March 1961) 43-58; Trans AIME, 222.

39. Tariq, S.M., Ramey, H.J Jr.: "Drawdown Behaviour of a Well with Storage and Skin Effect Communicating with Layer of Different Radii with Other Characteristics," SPE 7453 presented at the 1978 SPE Annual Technical Conference and Exhibitions, Houston (Oct 1-3).

40. Raghavan. R, Prijambodo. R., and Reynolds, A.C.: "Well Test Analysis for Wells producing Layered Reservoir with cross flow," SPEJ' (June 1985) 380-395.

41. Satman, A.: "An Analytical Study of Transient Flow in Stratified Systems with Fluid Banks," SPE 10264 presented at the 1981 Annual Meeting. San Antonio, TX, Oct. 5-7.

42. Gao, Chengtai, and Chan-Qing: "The Determination of Total Productivity By a Constant pressure Flow Test and The Crossflow Behavior in Multilayer Reservoirs," SPE 12581, This paper was prepared for presentation at the 1994 Easten Regional Conference & Exhibition held in Charleston, WV, USA, 8-10 November 1984.

43. Ehlig-Economides, C. A. and Joseph, J. A.: "A New Test For Determination Of Individual Layer Properties In A Multilayered Reservoir," SPE 14167, presented at the 60th Annual Tech. Con., SPE of AIME, Las Vegas, Nevada, September 23-25, 1985.

44. Ehlig-Economides, C. and Joseph, J. and Vik, S.A.: "Evaluation Of Single-Layer Transients In A Multilayered System," SPE 15860, This paper was prepared for presentation at the SPE European Petroleum Conference held in London, 20-22 October, 1986.

45. Joseph, J., Nai-Fu, F., and Gui, L.T.: "A Study Of Pressure Transient Behavior In Bounded Two-Layered Reservoirs: Shengli Field, China," This paper was prepared for presentation at the 61st Annual Fall technical Conference and Exhibition of the Society of Petroleum Engineers held in New Orleans, LA October 5-8 1986.

46. Kucuk, F., Karakas, M., and Ayestaran, L.: "Well Testing And Analysis Techniques For Layered Reservoirs," SPE 13081, SPE Formation Evaluation, August 1986, 342-354.

47. Mavor, M.J., and Walkup, G.W. Jr.: "Application of the Parallel Resistance Concept to Well Test Analysis of Multilayered Reservoirs," SPE 15117, This paper was prepared for presentation at the 56th California Regional Meeting of the Society of Petroleum Engineers held in Oakland CA, April 2-4.

48. Hatzignatiou, D.G., Ogbe, D.O., Dehghani, K, and Economides, M.J.: "Interference Behaviour in Multilayered Composite reservoirs," SPE 16766 presented at the 1987 Annual Meeting, Dallas, TX, Sept. 27-30.

49. Shah, P.C., Karakas, M., Kuchuk, F., and Ayestaran, L.C.: "Estimation of the Permeabilities and Skin Factors in Layered Reservoirs with Downhole Rate and Pressure Data," SPE 14131, SPE Formation Evaluation, September 1988, 555-566.

50. Anbarci, K Grader, A.S., and Ertckin, T.: "Determination of Front Locations in Multilayer Composite Reservoir," SPE 19799 presented at the 1989 Annual Meeting, San Antonio, TX, Oct. 8-11.

51. Larsen, L.: "Boundary Effects In Pressure Transient Data From Layered Reservoirs," SPE 19797, 64th Annual Technical Conference and Exhibition, San Antonio, TX, October 8-11, 1989.

52. Bidaux, P., Whittle, T.M., Coveney, P.J., and Gringarten, A.C.: "Analysis of Pressure and Rate Transient Data From Wells in Multilayered Reservoirs: Theory and Aplication," SPE 24679, This paper was prepared for presentation at the 67th Annual Conference and Exhibition of the Society of Petroleum Engineers held in Washington, DC, October 4-7, 1992.

53. Gomes, E., and Ambastha, A.K.: "An Analitycal Pressure-Transient Model for Multilayered, Composite Reservoirs With Pseudostady-State Formation Crossflow," SPE 26049, This paper was prepared at the Western Regional Meeting held in Anchorage, Alaska, U.S.A., 26-28 May 1993.

54. Bennett, C. O., Reynolds, A. C., Raghavan, R., and Elbel, J. L.: "Performance Of Finite-Conductivity, Vertical Fractured Wells In Single-Layer Reservoir," SPE 11029, SPE Formation Evaluation, August 1986, 399-412.

55. Bennett, C. O., Raghavan, R, and Reynolds, A. C.: "Analysis of Finite-Conductivity fractures intercepting multilayer commingled reservoirs," SPE 11030, SPE Formation Evaluation (June 1986) 259-274.

56. Britt, L. K., and Bennett, C. O.: "Determination of Fracture Conductivity in Moderate-Permeability reservoirs using the Bilinear flow concepts," SPE 14165, This paper was presented at the 60th Annual Technical Conference and Exhibition of the SPE, Las Vegas, NV, September 22-25, 1985.

57. Oshinuga, A. D.: "Pressure Transient Behavior of Vertically Fractured Wells in a Closed Square Multilayered Reservoir Using the Principle Of dual-porosity system," Master Thesis, The University of Southwestern Louisiana, May 1988.

58. Okoye, C. U., Oshinuga, A. D., and Ghalambor, A.: "Pressure Transient Behavior In Multilayer Vertically Fractured Gas Reservoir With Finite Conductivity," SPE 18960, This paper was presented at the SPE Joint Rocky Mountain Regional/Low Permeability Reservoirs Symposium and Exhibition, Denver, Colorado, March 6-8, 1989.

59. Okoye, C. U., Oshinuga, A. D., and Ghalambor, A.: "Pressure Transient Behavior of Vertically Fractured Wells in a Closed Square Multilayered Reservoir," SPE 20136, This paper was presented at the 1990 Permain Basin Oil and Gas Recovery Conference, Midland, Texas, March 8-9, 1990.

60. Tiab, D. and Kumar, A.: "Detection and Location of Two Parallel sealing Faults Around a Well," JPT (Oct. 1980) 1701-1708.

61. Tiab, D.: "Analysis Of Pressure And Pressure Derivatives Without Type-Curve Matching-Skin And Wellbore Storage," Journal of Petroleum Science and Engineering 12 (1995) 171-181.

62. Horn, R.N., 1990: Modern Well Test Analysis. Petroway Inc., Palo Alto, CA.

63. Engler, T.: "Interpretation Of Pressure In Tests In Naturally Fractured Reservoirs By The Direct Synthesis Technique," Ph.D. Dissertation, The University of Oklahoma, Norman, Oklahoma 1995.

64. Earlougher, R. C. Jr., et. al.: "Some Characteristics Of Pressure Buildup Behavior In Bounded Multiple-Layered Reservoirs Without Crossflow," J. Pet. Tech. (Oct. 1974) 1178-1186.

65. Kucuk, F. and Ayestaran, L.: "Analysis Of Simultaneously Measured Pressure And Sandfaca Flow Rate In Transient Well Testing," J. Pet. Tech. (February 1985) 323-334, SPE 12177, presented in San Francisco CA, October 5-8 1983.

66. Economides, M.J.: "Observations And Recommendations In The Evaluation Of Tests Of Hydraulically Fractured Wells," SPE 16396 Presents at the SPE/DOE Low Permeability Reservoirs Symposium held in Denver, Colorado, May 18-19, 1987.

67. Serra, K., Reynolds, A., and Raghavan, R.: "New Pressure Transient Analysis Methods For Naturally Fractured Reservoirs," JPT (Dec. 1983) 2271-2283.

68. Stewart, G. and Ascharasobbu, F.: "Well Test Interpretation For Naturally Fractured Reservoirs," SPE 18173 presented at the 1988 Annual Technical Conference, Houston, Tx.

69. Kazemi, H.: "Pressure Buildup In Reservoir Limit Testing Of Stratified System," J. Pet. Tech. (April 1970) 503-511.

70. Cobb, W.M., Ramey, H.J., Jr. And Miller, F.C.: "Well-Test Analysis For Wells Producing From Commingled Zones," J. Pet. Tech. (Jan. 1972) 27-37.

71. Raghavan, R., Topaloglu, H.N., Cobb, W.M. and Ramey, H.J.Jr.: "Well-Testing Analysis From Wells Producing From Two Commingled Zones Of Unequal Thickness," J. Pet. Tech. (Sept. 1974) 1035-1043.

72. Kazemi, H., Seth, M.S., and Thomas, G. W.: "The Interpretation Of Interference Tests In Naturally Fractured Reservoirs With Uniform Fracture Distribution," Soc. Pet. Eng. J. (1969) 463.

73. Odeh, A.S.: "Unsteady State Behavior Of Naturally Fractured Reservoirs," J. Pet. Tech. (1976) 1295.

74. Crawford, G.E., Hagedorn, A.R. and Pierce, A. E.: "Analysis Of Pressure Buildup Tests In A Naturally Fractured Reservoir," J. Pet. Tech. (1976) 1295.

75. Najurieta, H. L.: "A Theory For Pressure Transient Analysis In Naturally Fractured Reservoirs," J. Pet. Tech. (1980) 1241.

76. Stewart, G. Wittmann, M.J. and van Golf-Racht, T.: "The Application Of The Repeat Formation Tester To The Analysis Of Naturally Fractured Reservoirs," SPE 10181, Paper Presented to 56th Annual Fall Conference of SPE, San Antonio (Oct. 1981).

77. Gringarten, A. C.: "Interpretation Of Tests In Fissured Reservoirs And Multi-Layered Reservoirs With Double Porosity Behavior; Theory And Practice," SPE 10044, Paper Presented To Technical Symposium of SPE, Bejing (March 1982).

78. Waldren, D., and Corrigan, A.F.: "An Engineering And Geological Review Of The Problems Encountered In Simulating Naturally Fractured Reservoirs," SPE 13717, Paper Presented At The SPE 1985 Middle East Technical Conference and Exhibition held in Bahrain, March 11-14, 1985.

79. Olarewaju, J. S., Lee, W. J.: "Pressure Behavior Of Layered And Dual Porosity Reservoirs In The Presence Of Wellbore Effects," SPE 17302, SPE Formation Evaluation, September 1989, pp 397-405.

80. Liu Ci-Qun and Yang Jie: "Transient Pressure Behavior With Regard To Wellbore Storage And Skin Effects For A Vertically Fractured Well In Dual-Porosity System," SPE 21466, Jun 4, 1990.

81. Ben Naceur, K., and Economides, M. J.: "Production From Naturally Fissured Reservoirs Intercepted By A Vertical Hydraulic Fracture," SPE 17425, SPE Formation Evaluation, December 1989, 550.

82. Gringartin, A. C., and Ramey, H. J. Jr: "The Use Of Source And Gresn's Function In Solving Unsteady-Flow Problems In Reservoirs," SPEJ (Oct. 1973) 285-295.

83. van Everdingan, A. F. and Hurst, W.: "The Application of the Laplace transformation to Flow Problems in Reservoirs," trans., AIME, (December 1949) 305-324.

84. Morales, R. H., Brown, E., Norman, W. D., DeBonis, V., Mathews, M., Park, E. I., Brown, D.: "Mechanical Skin Damage on Wells," SPE 30459, paper was presented at SPE Annual Technical Conference & Exhibition held in Dallas USA, 22-25 Oct., 1995.

85. Hawkins, M.F.: "A Note On The Skin Effect," Trans., AIME, Vol. 207, 356-357 (1956).

86. Van Everdingen, A.F.: "The Skin Effect And Its Influence On The Productive Capacity Of A Well," Trans., AIME, Vol. 198, 171 (1953).

87. Hurst, W.: "Establishment Of The Skin Effect And Its Impediment To Fluid Flow Into A Wellbore," Pet. Eng., Oct. (1953) 25, B-6.

88. Engler, T.W., Osisanya, S., and Tiab, D.: "Measuring Skin While Drilling," SPE 29526.

89. Ferguson,C.K. and Klotz, J.A.: "Filtration From Mud During Drilling," SPE 289-G, Trans. AIME, 1954, 201, 29-42.

90. Peaceman, D.W.: "Interpretation Of Well Block Pressures In Numerical Reservoir Simulation With Nonsquare Grid Blocks And Anisotropic Permeability," SPE 10528, SPEJ, June 1983.

91. Hurst, W., Clark, J.D., and Brauer, E.B.: "The Skin Effect In Producing Wells," JPT (November 1969) 1483-1489.

92. Donaldson, E.C., and Chernoglazov, V.: "Characterization Of Drilling Mud Fluid Invasion," J. of Pet. Sci. and Eng. (1987) 1, 3-13.

93. Osman, M. E.: "Pressure Analysis Of A Fractured Well In A Multi-Layered Reservoir," Journal of Petroleum Science and Engineering 9 (1993) 49-66.

94. Osman, M. E.: "Well Testing Of A Fractured Well In A Multi-Layered Bounded Square," SPE 24533 presented at 5th Abu Dhabi Petroleum Conference, 18-20 May 1992.

95. Osman, M. E.: "Well Testing Of A Fractured Well In A Multi-Layered Bounded Square," SPE 24533, ADSPE 1604.

96. Osman, M. E.: "Transient Pressure Analysis For Wells In Multi-Layered Reservoir With Finite Conductivity Fractures," SPE 25665, presented at the SPE Middle East Oil Technical Conference & Exhibition held in Bahrain, 3-6 April 1993.

97. Osman, M. E., Almehaideb, A. A., and Abou-Kassem, J. H.: "A New Conventional Method Of Analysis For Well Tests In Hydraulically Fractured Wells Using Down-Hole Pressure And Sand-Face Rates," SPE 37798, presented at the SPE Middle East Oil Technical Conference & Exhibition held in Bahrain, 15-18 March, 1997.

98. Cinco-Ley, H., and Samaniego-V, F.: "Transient Pressure Analysis: Finite Conductivity Vertical Fracture Case Versus Damaged Fracture Case," SPE 10179 presented at the 56th SPE Annual Technical Conference And Exhibition, San Antonio, TX, Oct. 5-7, 1981.

99. Usman, A.: "Transient Pressure Analysis Of Hydraulic Fractured Wells In The Western Tight Sands," SPE 10878, presented at the Rocky Mountain Regional Meeting of the SPE held in Billings, MT, May 19-21, 1982.

100. Aguilera, R.: Naturally Fractured Reservoirs, Petroleum Publishing Company, Tulsa, 1980.

101. Aguilera, R.: "Well Test Analysis of Multi-Layered Naturally Fractured Reservoirs," Journal of Canadian Petroleum Technology, Vol. 39, No. 7, July 2000, 31-37.

102. Mattax, C.C., and Dalton, R.L.: Reservoir Simulation, SPE, Monograph Vol. 13 (1990) 33.

APPENDIX A

COMPUTER MODELS

Computer programs are written on FORTRAN 77 and were compiled using the Microsoft FORTRAN Power Station Software. They can be run in any 486 PC compatible (or higher) that contains Windows 95. The input variables have to be modified when the main program is run. The programs will search for these variables when executed. A typical data for the input variables are well explained in the following examples:

Case 1: Multi-Layer Double Porosity Reservoirs:

Input Data File:

Dimensionless fracture storativity. Layer #1:
0.1
Dimensionless fracture storativity. Layer #2:
0.1
Iterporosity flow coefficient. Layer #1:
1.0E-5
Iterporosity flow coefficient. Layer #2:
1.0E-5
Thichness. Layer #1:
100.0
Thichness. Layer #2:
100.0
Permeability. Layer #1:
32.0
Permeability. Layer #2:
1.0
CDe2S:
1.0E2
Number of data:
21
Dimensionless Time
1.00E-01
2.50E-01
5.00E-01
1.00E+00

2.50E+00
5.00E+00
1.00E+01
2.50E+01
5.00E+01
1.00E+02
2.50E+02
5.00E+02
1.00E+03
2.50E+03
5.00E+03
1.00E+04
2.50E+04
5.00E+04
1.00E+05
2.50E+05
6.00E+05

Simulator output results are organized in an output file, which can be opened using Ward Pad or Note Pad. An example of output file is summarized below.

Output Data File:

C_De^{2S}	$(kh)_1/(kh)$	$(kh)_1/(kh)_2$
100	0.969697	32.00

TD	PD
1.00E-01	0.091998
2.50E-01	0.231801
5.00E-01	0.443171
1.00E+00	0.820323
2.50E+00	1.697782
5.00E+00	2.648844
1.00E+01	3.652244
2.50E+01	4.654367
5.00E+01	5.153654
1.00E+02	5.560746
2.50E+02	6.046042
5.00E+02	6.393143
1.00E+03	6.721416
2.50E+03	7.116317
5.00E+03	7.363523
1.00E+04	7.54861
2.50E+04	7.70737

5.00E+04	7.828177
1.00E+05	8.018178
2.50E+05	8.394227
6.00E+05	8.822577

and the computer code of the numerical inversion is shown below.

```
CCCCCCCCCCCCCCCCCCCCCCCCCCCCCCCCCCCCCCCCCCCCCCCCCCCCCCCCCCCC
C                                                          C
C                     JALAL F. OWAYED                      C
C THIS PROGRAM CAN BE USED TO GENERATE TD VS PD AND TD*PD CURVES C
C   FOR WELLS IN MULTI-LAYER NATURALLY FRACTURED RESERVOIRS.    C
C                                                          C
CCCCCCCCCCCCCCCCCCCCCCCCCCCCCCCCCCCCCCCCCCCCCCCCCCCCCCCCCCCC
   PROGRAM NFR2L

      DOUBLE PRECISION P,Z,FACT,OMEGA1,LAMBDA1,OMEGA2,LAMBDA2
      INTEGER J,K,JA,SN,H
      REAL FA,PD,V(200),XH(200)
      COMMON/MODEL CD,OMEGA1,LAMBDA1,OMEGA2,LAMBDA2,XH1,XH2,XK1,XK2
      COMMON/MOD1/SKIN1,SKIN2,CDE2S
      OPEN(UNIT=6,FILE='IN-2LNFR.DAT',STATUS='UNKNOWN')
      OPEN(UNIT=10,FILE='OUT-2LNFR.DAT',STATUS='UNKNOWN')

            READ(6,*)
            READ(6,*)OMEGA1
            READ(6,*)
            READ(6,*)OMEGA2
            READ(6,*)
            READ(6,*)LAMBDA1
            READ(6,*)
            READ(6,*)LAMBDA2
            READ(6,*)
            READ(6,*)XH1
            READ(6,*)
            READ(6,*)XH2
            READ(6,*)
            READ(6,*)XK1
            READ(6,*)
            READ(6,*)XK2
            READ(6,*)
            READ(6,*)CDE2S
            READ(6,*)
            READ(6,*)K
            READ(6,*)

      XHB=XH1+XH2
      XKB=(XK1*XH1+XK2*XH2)/XHB
      XB1=XKB/XK1
      XB2=XKB/XK2
      XXX1=XK1*XH1/(XHB*XKB)
      XXX2=XK1*XH1/(XK2*XH2)

      WRITE(10,222)
222   FORMAT(4X,'CDe2S',6X,'(kh)1/(kh)',3X,'(kh)1/(kh)2')
      WRITE(10,223)CDE2S,XXX1,XXX2
223   FORMAT(2X,F10.2,2X,F9.6,4X,F9.2)

      WRITE(10,111)
111   FORMAT(6X,'TD',10X,'PD')
```

```
      DO 10 JA=1,K
      READ(6,*)T
      N=8
      H=N/2
      XH(1)=2.0/FACT(H-1)
      DO 20 I=2,H
      XH(I)=(I**H*FACT(2*I))/(FACT(H-I)*FACT(I)*FACT(I-1))
20    CONTINUE
      SN=2*(H-H/2*2)-1
      DO 30 I=1,N
      V(I)=0.0
      IF(I.LT.H) THEN
      I1=I
      ELSE
      I1=H
      ENDIF
      K1=INT((FLOAT(I)+1.0)/2.0)
      DO 40 K=K1,I1
      V(I)=V(I)+XH(K)/(FACT(I-K)*FACT(2*K-I))
40 CONTINUE
      V(I)=SN*V(I)
      SN=-SN
30    CONTINUE
      FA=0.0
      B=DLOG(2.D0)/T
      DO 50 J=1,N
      Z=B*J
      FA=FA+V(J)*P(Z)
50    CONTINUE
      FA=FA*B
      PD=FA
      WRITE(10,100)T,PD
100   FORMAT(3X,E9.2,2X,F16.6)
10    CONTINUE
      STOP
      END

      DOUBLE PRECISION FUNCTION FACT(NX)
      INTEGER NX
      IF(NX.EQ.0) THEN
      FACT=1
      ELSE
      FACT=1
      DO 80 I=1,NX
      FACT=FACT*I
80    CONTINUE
      ENDIF
      RETURN
      END

      DOUBLE PRECISION FUNCTION P(S)
      DOUBLE PRECISION S,PI,OMEGA1,LAMBDA1,OMEGA2,LAMBDA2
      DOUBLE PRECISION FS1,FS2
      COMMON/MODEL/CD,OMEGA1,LAMBDA1,OMEGA2,LAMBDA2,XH1,XH2,XK1,XK2
      COMMON/MOD1/SKIN1,SKIN2,CDE2S

C     BRESSURE TRANSIENT BEHAVIOR OF WELLS IN DOUBLE POROSITY RESERVOOIRS.
      PI=3.14159265
      XHB=XH1+XH2
      ALFA1=1.0
      ALFA2=1.0
      XKB=(XK1*XH1+XK2*XH2)/XHB
      XB1=XKB/XK1
      XB2=XKB/XK2

C     PSEUDOSTEADY STATE MATRIX FLOW
      FS1=OMEGA1*XB1+((ALFA1-OMEGA1)*XB1*LAMBDA1)/((ALFA1-OMEGA1)
```

```
      &                    *S+LAMBDA1)
      E1=(FS1*S)**0.5
      FS2=OMEGA2*XB2+((ALFA2-OMEGA2)*XB2*LAMBDA2)/((ALFA2-OMEGA2)
      &                    *S+LAMBDA2)
      E2=(FS2*S)**0.5

C     TRANSIENT MATRIX FLOW OF A SLAB GEOMETRY
C     FS1=OMEGA1*XB1+XB1*((ALFA1-OMEGA1)*LAMBDA1/(3.0*S))**0.5
C     &                    *DTANH(3.0*(ALFA1-OMEGA1)*S/LAMBDA1)**0.5
C     E1=(FS1*S)**0.5
C     FS2=OMEGA2*XB2+XB2*((ALFA2-OMEGA2)*LAMBDA2/(3.0*S))**0.5
C     &                    *DTANH(3.0*(ALFA2-OMEGA2)*S/LAMBDA2)**0.5
C     E2=(FS2*S)**0.5

C     TRANSIENT MATRIX FLOW OF A SUGAR-CUBE GEOMETRY
C     FS1=OMEGA1*XB1+(LAMBDA1*XB1/(5.0*S))*((15.0*(ALFA1-OMEGA1)
C     & *S/LAMBDA1)**0.5*(1.0/(DTANH(15.0*(ALFA1-OMEGA1)*S/LAMBDA1)
C     & **0.5))-1.0)
C     E1=(FS1*S)**0.5
C     FS2=OMEGA2*XB2+(LAMBDA2*XB2/(5.0*S))*((15.0*(ALFA2-OMEGA2)
C     & *S/LAMBDA2)**0.5*(1.0/(DTANH(15.0*(ALFA2-OMEGA2)*S/LAMBDA2)
C     & **0.5))-1.0)
C     E2=(FS2*S)**0.5

C     WITHOUT WELLBORE STOREGE (MULTI-LAYER RESERVOIR)
C     P1=bessk0(E1)/(S*E1*bessk1(E1))
C     P2=bessk0(E2)/(S*E2*bessk1(E2))
C     P=(P1+P2)/2.0

C     WITH WELLBORE STOREGE AND NO SKIN(MULTI-LAYER RESERVOIR)
C     P1=bessk0(E1)/(S*E1*bessk1(E1))
C     P2=bessk0(E2)/(S*E2*bessk1(E2))
C     P=(P1+P2)/2.0
C     P=1.0/(CD*S*S+(1.0/P))

C     WITH WELLBORE STOREGE AND SKIN [CDe2S] (MULTI-LAYER RESERVOIR)
      DOWN11=1.78107*SQRT((S*FS1)/CDE2S)
      DOWN21=LOG(2.0/DOWN11)
      DOWN31=S+(1.0/DOWN21)
      P1=1.0/(S*DOWN31)

      DOWN12=1.78107*SQRT((S*FS2)/CDE2S)
      DOWN22=LOG(2.0/DOWN12)
      DOWN32=S+(1.0/DOWN22)
      P2=1.0/(S*DOWN32)
      P=(P1+P2)/2.0

      RETURN
      END

      FUNCTION gammln(xx)
  REAL gammln,xx
  INTEGER j
  DOUBLE PRECISION ser,stp,tmp,x,y,cof(6)
  SAVE cof,stp
  DATA cof,stp/76.18009172947146d0,-86.50532032941677d0,
 *24.01409824083091d0,-1.231739572450155d0,.1208650973866179d-2,
 *-.5395239384953d-5,2.5066282746310005d0/
  x=xx
  y=x
  tmp=x+5.5d0
  tmp=(x+0.5d0)*log(tmp)-tmp
  ser=1.000000000190015d0
  do 11 j=1,6
   y=y+1.d0
   ser=ser+cof(j)/y
11  continue
```

```
      gammln=tmp+log(stp*ser/x)
      return
      END
C  (C) Copr. 1986-92 Numerical Recipes Software &j$S9R3#1"`.

            FUNCTION bessk0(x)
      REAL bessk0,x
CU    USES bessi0
      REAL bessi0
      DOUBLE PRECISION p1,p2,p3,p4,p5,p6,p7,q1,q2,q3,q4,q5,q6,q7,y
      SAVE p1,p2,p3,p4,p5,p6,p7,q1,q2,q3,q4,q5,q6,q7
      DATA p1,p2,p3,p4,p5,p6,p7/-0.57721566d0,0.42278420d0,0.23069756d0,
     *0.3488590d-1,0.262698d-2,0.10750d-3,0.74d-5/
      DATA q1,q2,q3,q4,q5,q6,q7/1.25331414d0,-0.7832358d-1,0.2189568d-1,
     *-0.1062446d-1,0.587872d-2,-0.251540d-2,0.53208d-3/
      if (x.le.2.0) then
        y=x*x/4.0
        bessk0=(-log(x/2.0)*bessi0(x))+(p1+y*(p2+y*(p3+y*(p4+y*(p5+y*
     *(p6+y*p7))))))
      else
        y=(2.0/x)
        bessk0=(exp(-x)/sqrt(x))*(q1+y*(q2+y*(q3+y*(q4+y*(q5+y*(q6+y*
     *q7))))))
      endif
      return
      END
C  (C) Copr. 1986-92 Numerical Recipes Software &j$S9R3#1"`.

            FUNCTION bessi0(x)
      REAL bessi0,x
      REAL ax
      DOUBLE PRECISION p1,p2,p3,p4,p5,p6,p7,q1,q2,q3,q4,q5,q6,q7,q8,q9,y
      SAVE p1,p2,p3,p4,p5,p6,p7,q1,q2,q3,q4,q5,q6,q7,q8,q9
      DATA p1,p2,p3,p4,p5,p6,p7/1.0d0,3.5156229d0,3.0899424d0,
     *1.2067492d0,0.2659732d0,0.360768d-1,0.45813d-2/
      DATA q1,q2,q3,q4,q5,q6,q7,q8,q9/0.39894228d0,0.1328592d-1,
     *0.225319d-2,-0.157565d-2,0.916281d-2,-0.2057706d-1,0.2635537d-1,
     *-0.1647633d-1,0.392377d-2/
      if (abs(x).lt.3.75) then
        y=(x/3.75)**2
        bessi0=p1+y*(p2+y*(p3+y*(p4+y*(p5+y*(p6+y*p7)))))
      else
        ax=abs(x)
        y=3.75/ax
        bessi0=(exp(ax)/sqrt(ax))*(q1+y*(q2+y*(q3+y*(q4+y*(q5+y*(q6+y*
     *(q7+y*(q8+y*q9))))))))
      endif
      return
      END
C  (C) Copr. 1986-92 Numerical Recipes Software &j$S9R3#1"`.

            FUNCTION bessk1(x)
            REAL bessk1,x
CU    USES bessi1
      REAL bessi1
      DOUBLE PRECISION p1,p2,p3,p4,p5,p6,p7,q1,q2,q3,q4,q5,q6,q7,y
      SAVE p1,p2,p3,p4,p5,p6,p7,q1,q2,q3,q4,q5,q6,q7
      DATA p1,p2,p3,p4,p5,p6,p7/1.0d0,0.15443144d0,-0.67278579d0,
     *-0.18156897d0,-0.1919402d-1,-0.110404d-2,-0.4686d-4/
      DATA q1,q2,q3,q4,q5,q6,q7/1.25331414d0,0.23498619d0,-0.3655620d-1,
     *0.1504268d-1,-0.780353d-2,0.325614d-2,-0.68245d-3/
      if (x.le.2.0) then
        y=x*x/4.0
        bessk1=(log(x/2.0)*bessi1(x))+(1.0/x)*(p1+y*(p2+y*(p3+y*(p4+y*
     *(p5+y*(p6+y*p7))))))
      else
        y=2.0/x
```

```
    bessk1=(exp(-x)/sqrt(x))*(q1+y*(q2+y*(q3+y*(q4+y*(q5+y*(q6+y*
   *q7))))))
   endif
   return
   END
C  (C) Copr. 1986-92 Numerical Recipes Software &jSS9R3#1"`.

             FUNCTION bessi1(x)
   REAL bessi1,x
   REAL ax
   DOUBLE PRECISION p1,p2,p3,p4,p5,p6,p7,q1,q2,q3,q4,q5,q6,q7,q8,q9,y
   SAVE p1,p2,p3,p4,p5,p6,p7,q1,q2,q3,q4,q5,q6,q7,q8,q9
   DATA p1,p2,p3,p4,p5,p6,p7/0.5d0,0.87890594d0,0.51498869d0,
   *0.15084934d0,0.2658733d-1,0.301532d-2,0.32411d-3
   DATA q1,q2,q3,q4,q5,q6,q7,q8,q9/0.39894228d0,-0.3988024d-1,
   *-0.362018d-2,0.163801d-2,-0.1031555d-1,0.2282967d-1,-0.2895312d-1,
   *0.1787654d-1,-0.420059d-2/
   if (abs(x).lt.3.75) then
    y=(x/3.75)**2
    bessi1=x*(p1+y*(p2+y*(p3+y*(p4+y*(p5+y*(p6+y*p7))))))
   else
    ax=abs(x)
    y=3.75/ax
    bessi1=(exp(ax)/sqrt(ax))*(q1+y*(q2+y*(q3+y*(q4+y*(q5+y*(q6+y*
   *(q7+y*(q8+y*q9))))))))
    if(x.lt.0.)bessi1=-bessi1
   endif
   return
   END
C  (C) Copr. 1986-92 Numerical Recipes Software &jSS9R3#1"`.
```

<u>Case 2:</u> Single-Layer Double Porosity Reservoir with Vertical Fracture

<u>Input Data File:</u>

Xe/Xf:
16.0
Ye/Xe:
1.0
Dimensionless fracture storativity:
0.01
Iterporosity flow coefficient:
100.0
CD:
0.0
Number of data:
21
Dimensionless Time
1.00E-01
2.50E-01
5.00E-01
1.00E+00
2.50E+00

5.00E+00
1.00E+01
2.50E+01
5.00E+01
1.00E+02
2.50E+02
5.00E+02
1.00E+03
2.50E+03
5.00E+03
1.00E+04
2.50E+04
5.00E+04
1.00E+05
2.50E+05
6.00E+05

and the computer code of the numerical inversion is shown below.

```
CCCCCCCCCCCCCCCCCCCCCCCCCCCCCCCCCCCCCCCCCCCCCCCCCCCCCCCCCCCCCCCCCC
C                                                                C
C                    JALAL F. OWAYED                             C
C     THIS PROGRAM CAN BE USED TO GENERATE TD VS PD AND TD*PD CURVES FOR   C
C        VERTICAL FRACTURED WELLS IN NATURALLY FRACTURED RESERVOIRS.       C
C                                                                C
CCCCCCCCCCCCCCCCCCCCCCCCCCCCCCCCCCCCCCCCCCCCCCCCCCCCCCCCCCCCCCCCCC
      PROGRAM VF1LNF

      DOUBLE PRECISION P,Z,FACT,OMEGA,LAMBDA,XEFD,YED
      DOUBLE PRECISION CD
      INTEGER J,K,JA,SN,H
      REAL FA,PD,V(200),XH(200)
      COMMON/MODEL/OMEGA,LAMBDA,XEFD,YED
      COMMON/MODL1/CD

      OPEN(UNIT=6,FILE='IN-VF1LINF.DAT',STATUS='UNKNOWN')
      OPEN(UNIT=10,FILE='OUT-VF1LINF.DAT',STATUS='UNKNOWN')

            READ(6,*)
            READ(6,*)XEFD
            READ(6,*)
            READ(6,*)YED
            READ(6,*)
            READ(6,*)OMEGA
            READ(6,*)
            READ(6,*)LAMBDA
            READ(6,*)
            READ(6,*)CD
            READ(6,*)
            READ(6,*)K
            READ(6,*)

      WRITE(10,111)
111   FORMAT(6X,'TD',10X,'PD')
      DO 10 JA=1,K
      READ(6,*)T
```

```
      N=8
      H=N/2
      XH(1)=2.0/FACT(H-1)
      DO 20 I=2,H
      XH(I)=(I**H*FACT(2*I))/(FACT(H-I)*FACT(I)*FACT(I-1))
 20   CONTINUE
      SN=2*(H-H/2*2)-1
      DO 30 I=1,N
      V(I)=0.0
      IF(I.LT.H) THEN
      I1=I
      ELSE
      I1=H
      ENDIF
      K1=INT((FLOAT(I)+1.0)/2.0)
      DO 40 K=K1,I1
      V(I)=V(I)+XH(K)/(FACT(I-K)*FACT(2*K-I))
40 CONTINUE
      V(I)=SN*V(I)
      SN=-SN
 30   CONTINUE
      FA=0.0
      B=DLOG(2.D0)/T
      DO 50 J=1,N
      Z=B*J
      FA=FA+V(J)*P(Z)
 50   CONTINUE
      FA=FA*B
      PD=FA
      WRITE(10,100)T,PD
100   FORMAT(3X,E9.2,2X,F16.6)
10    CONTINUE
      STOP
      END

      DOUBLE PRECISION FUNCTION FACT(NX)
      INTEGER NX
      IF(NX.EQ.0) THEN
      FACT=1
      ELSE
      FACT=1
      DO 80 I=1,NX
      FACT=FACT*I
 80   CONTINUE
      ENDIF
      RETURN
      END

      DOUBLE PRECISION FUNCTION P(S)
      DOUBLE PRECISION S,PI,OMEGA,LAMBDA,XEFD,YED
      DOUBLE PRECISION XFD,E,E1,E1SUM,Q0,QN
      DOUBLE PRECISION CD
C     DOUBLE PRECISION CD,SKIN
      DOUBLE PRECISION FS
      COMMON/MODEL/OMEGA,LAMBDA,XEFD,YED
      COMMON/MODL1/CD

C       BRESSURE TRANSIENT BEHAVIOR OF WELLS WITH UNIFORM-FLUX
C             VERTICAL FRACTURES IN DOUBLE POROSITY RESERVOOIRS.

      PI=3.14159265
      XFD=1.0/XEFD

C     PSEUDOSTEADY STATE MATRIX FLOW
      FS=((1.0-OMEGA)*OMEGA*S+LAMBDA)/((1.0-OMEGA)*S+LAMBDA)

C     TRANSIENT MATRIX FLOW OF A SLAB GEOMETRY
```

```
C         FS=OMEGA+((1.0-OMEGA)*LAMBDA/(3.0*S))**0.5*DTANH(3.0*(1.0-OMEGA)*S
C         &                    /LAMBDA)**0.5

C         TRANSIENT MATRIX FLOW OF A SUGAR-CUBE GEOMETRY
C         FS=OMEGA+(LAMBDA/(5.0*S))*((15.0*(1.0-OMEGA)*S/LAMBDA)**0.5
C         &                    *(1.0/(DTANH(15.0*(1.0-OMEGA)*S/LAMBDA)**0.5))-1.0)

          E1=0.0
          E1SUM=0.0
          DO 555 N=1,1000
          Q0=(S*FS)**0.5
          QN=(S*FS+N**2.0*PI**2.0)**0.5

C         UNIFORM-FLUX VERTICALLY FRACTURED WELLS IN CLOSED SYSTEMS.
          E1=(1.0/(N**2.0*PI**2.0*XFD**2.0))*(DSIN(N*PI*XFD))**2.0*
          &  (1.0/(DTANH(QN*YED)*QN))

          E1SUM=E1SUM+E1
 555      CONTINUE
          E=(PI/2.0)*(1.0/(DTANH(Q0*YED)*Q0)+2.0*E1SUM)

C         WITH WELLBORE STOREGE
          P=1.0/(CD*S**2.0+1.0/(E/S))

          RETURN
          END
```

Case 3: Multi-Layer Double Porosity Reservoir with Vertical Fracture

Input Data File:

Xe/Xf. Layer #1:
64.0
Xe/Xf. Layer #2:
64.0
Ye/Xe:
1.0
Dimensionless fracture storativity. Layer #1:
0.1
Dimensionless fracture storativity. Layer #2:
0.1
Iterporosity flow coefficient. Layer #1:
100.0
Iterporosity flow coefficient. Layer #2:
100.0
Thichness. Layer #1:
100.0
Thichness. Layer #2:
100.0
Permeability. Layer #1:
16.0
Permeability. Layer #2:
1.0

Skin1, Layer #1:
2.0
Skin2, Layer #2:
2.0
Wellbore Storage:
0.0
Number of data:
21
Dimensionless Time
1.00E-01
2.50E-01
5.00E-01
1.00E+00
2.50E+00
5.00E+00
1.00E+01
2.50E+01
5.00E+01
1.00E+02
2.50E+02
5.00E+02
1.00E+03
2.50E+03
5.00E+03
1.00E+04
2.50E+04
5.00E+04
1.00E+05
2.50E+05
6.00E+05

and the computer code of the numerical inversion is shown below.

```
CCCCCCCCCCCCCCCCCCCCCCCCCCCCCCCCCCCCCCCCCCCCCCCCCCCCCCCCCC
C                                                        C
C                  JALAL F. OWAYED                       C
C   THIS PROGRAM CAN BE USED TO GENERATE TD VS PD AND TD*PD CURVES FOR   C
C   VERTICAL FRACTURED WELLS IN MULTI-LAYERED NATURALLY FRACTURED RESERVOIRS.   C
C                                                        C
CCCCCCCCCCCCCCCCCCCCCCCCCCCCCCCCCCCCCCCCCCCCCCCCCCCCCCCCCC
      PROGRAM VF2LNF

      DOUBLE PRECISION P,Z,FACT,OMEGA1,LAMBDA1,OMEGA2,LAMBDA2
      INTEGER J,K,JA,SN,H
      REAL FA,PD,V(200),XH(200)
      COMMON/MODEL/CD,OMEGA1,LAMBDA1,OMEGA2,LAMBDA2,XH1,XH2,XK1,XK2
      COMMON/MOD/XEFD1,XEFD2,YED,SKIN1,SKIN2

      OPEN(UNIT=6,FILE='IN-VF2LINF.DAT',STATUS='UNKNOWN')
      OPEN(UNIT=10,FILE='OUT-VF2LINF.DAT',STATUS='UNKNOWN')

            READ(6,*)
            READ(6,*)XEFD1
```

```
              READ(6,*)
              READ(6,*)XEFD2
              READ(6,*)
              READ(6,*)YED
              READ(6,*)
              READ(6,*)OMEGA1
              READ(6,*)
              READ(6,*)OMEGA2
              READ(6,*)
              READ(6,*)LAMBDA1
              READ(6,*)
              READ(6,*)LAMBDA2
              READ(6,*)
              READ(6,*)XH1
              READ(6,*)
              READ(6,*)XH2
              READ(6,*)
              READ(6,*)XK1
              READ(6,*)
              READ(6,*)XK2
              READ(6,*)
              READ(6,*)SKIN1
              READ(6,*)
              READ(6,*)SKIN2
              READ(6,*)
              READ(6,*)CD
              READ(6,*)
              READ(6,*)K
              READ(6,*)

      WRITE(10,111)
111   FORMAT(6X,'TD',10X,'PD')
      DO 10 JA=1,K
      READ(6,*)T
      N=8
      H=N/2
      XH(1)=2.0/FACT(H-1)
      DO 20 I=2,H
      XH(I)=(I**H*FACT(2*I))/(FACT(H-I)*FACT(I)*FACT(I-1))
20    CONTINUE
      SN=2*(H-H/2*2)-1
      DO 30 I=1,N
      V(I)=0.0
      IF(I.LT.H) THEN
      I1=I
      ELSE
      I1=H
      ENDIF
      K1=INT((FLOAT(I)+1.0)/2.0)
      DO 40 K=K1,I1
      V(I)=V(I)+XH(K)/(FACT(I-K)*FACT(2*K-I))
40 CONTINUE
      V(I)=SN*V(I)
      SN=-SN
30    CONTINUE
      FA=0.0
      B=DLOG(2.D0)/T
      DO 50 J=1,N
      Z=B*J
      FA=FA+V(J)*P(Z)
50    CONTINUE
      FA=FA*B
      PD=FA
      WRITE(10,100)T,PD
100   FORMAT(3X,E9.2,2X,F16.6)
10    CONTINUE
      STOP
```

```
      END

      DOUBLE PRECISION FUNCTION FACT(NX)
      INTEGER NX
      IF(NX.EQ.0) THEN
      FACT=1
      ELSE
      FACT=1
      DO 80 I=1,NX
      FACT=FACT*I
 80   CONTINUE
      ENDIF
      RETURN
      END

      DOUBLE PRECISION FUNCTION P(S)
      DOUBLE PRECISION S,PI,OMEGA1,LAMBDA1,OMEGA2,LAMBDA2
      DOUBLE PRECISION FS1,FS2
      DOUBLE PRECISION XFD1,XFD2,EA,EB,EEA,EEB,EASUM,EBSUM,Q0,QN,E1,E2
      COMMON/MODEL/CD,OMEGA1,LAMBDA1,OMEGA2,LAMBDA2,XH1,XH2,XK1,XK2
      COMMON/MOD/XEFD1,XEFD2,YED,SKIN1,SKIN2

C     BRESSURE TRANSIENT BEHAVIOR OF WELLS WITH UNIFORM-FLUX VERTICAL
C             FRACTURES IN MULTI-LAYERED DOUBLE POROSITY RESERVOOIRS.

      PI=3.14159265
      XFD1=1.0/XEFD1
      XFD2=1.0/XEFD2
      XHB=XH1+XH2
      ALFA1=1.0
      ALFA2=1.0
      XKB=(XK1*XH1+XK2*XH2)/XHB
      XB1=XKB/XK1
      XB2=XKB/XK2

C     PSEUDOSTEADY STATE MATRIX FLOW
      FS1=OMEGA1*XB1+((ALFA1-OMEGA1)*XB1*LAMBDA1)/((ALFA1-OMEGA1)
      &               *S+LAMBDA1)
      E1=(FS1*S)
      FS2=OMEGA2*XB2+((ALFA2-OMEGA2)*XB2*LAMBDA2)/((ALFA2-OMEGA2)
      &               *S+LAMBDA2)
      E2=(FS2*S)

C     TRANSIENT MATRIX FLOW OF A SLAB GEOMETRY
C     FS1=OMEGA1*XB1+XB1*((ALFA1-OMEGA1)*LAMBDA1/(3.0*S))**0.5
C     &               *DTANH(3.0*(ALFA1-OMEGA1)*S/LAMBDA1)**0.5
C     E1=(FS1*S)
C     FS2=OMEGA2*XB2+XB2*((ALFA2-OMEGA2)*LAMBDA2/(3.0*S))**0.5
C     &               *DTANH(3.0*(ALFA2-OMEGA2)*S/LAMBDA2)**0.5
C     E2=(FS2*S)

C     TRANSIENT MATRIX FLOW OF A SUGAR-CUBE GEOMETRY
C     FS1=OMEGA1*XB1+(LAMBDA1*XB1/(5.0*S))*((15.0*(ALFA1-OMEGA1)
C     & *S/LAMBDA1)**0.5*(1.0/(DTANH(15.0*(ALFA1-OMEGA1)*S/LAMBDA1)
C     & **0.5))-1.0)
C     E1=(FS1*S)
C     FS2=OMEGA2*XB2+(LAMBDA2*XB2/(5.0*S))*((15.0*(ALFA2-OMEGA2)
C     & *S/LAMBDA2)**0.5*(1.0/(DTANH(15.0*(ALFA2-OMEGA2)*S/LAMBDA2)
C     & **0.5))-1.0)
C     E2=(FS2*S)

C     LAYER #1:
      EA=0.0
      EASUM=0.0
      DO 555 N=1,1000
      Q0=(E1)**0.5
      QN=(E1+N**2.0*PI**2.0)**0.5
```

```
C     UNIFORM-FLUX VERTICALLY FRACTURED WELLS IN CLOSED SYSTEMS.
      EA=(1.0/(N**2.0*PI**2.0*XFD1**2.0))*(DSIN(N*PI*XFD1))**2.0*
     & (1.0/(DTANH(QN*YED)*QN))

      EASUM=EASUM+EA
 555  CONTINUE
      EEA=(PI/2.0)*(1.0/(DTANH(Q0*YED)*Q0)+2.0*EASUM)

C     LAYER #2:
      EB=0.0
      EBSUM=0.0
      DO 565 N=1,1000
      Q0=(E2)**0.5
      QN=(E2+N**2.0*PI**2.0)**0.5

C     UNIFORM-FLUX VERTICALLY FRACTURED WELLS IN CLOSED SYSTEMS.
      EB=(1.0/(N**2.0*PI**2.0*XFD2**2.0))*(DSIN(N*PI*XFD2))**2.0*
     & (1.0/(DTANH(QN*YED)*QN))

      EBSUM=EBSUM+EB
 565  CONTINUE
      EEB=(PI/2.0)*(1.0/(DTANH(Q0*YED)*Q0)+2.0*EBSUM)

C     WITH SKIN (MULTI-LAYER RESERVOIR)- THIS EQUATION IS
      P=1.0/(S*(1.0/(EEA+SKIN1)+1.0/(EEB+SKIN2))/2.0)
      RETURN
      END
```

APPENDIX B

GENERAL SOLUTION

For an n-layer double porosity system, each layer is considered to have isotropic property. Small and constant compressibility, single phase, radial flow, and small pressure gradients are assumed in each layer. The partial differential equation with the above assumptions is defined as:

$$\frac{\partial^2 p_{fi}}{\partial r^2} + \frac{1}{r}\frac{\partial p_{fi}}{\partial r} = \left(\frac{\phi_f c_f \mu}{k_f}\right)_i \frac{\partial p_{fi}}{\partial t} - \left(\frac{\mu}{k_f}\right)_i q_{mi} \tag{B-1}$$

The initial and boundary conditions are:

$$p_{fi}(r,0) = p_{int} \tag{B-2}$$

$$p_{fi}(\infty,t) = p_{int} \tag{B-3}$$

$$r_w \left.\frac{\partial p_{fi}}{\partial r}\right|_{r=r_w} = -\frac{q_t \mu_i B}{2\pi h_i k_{fi}} \tag{B-4}$$

Rewriting the above equations in dimensionless forms yields:

$$\frac{\partial^2 p_{fDi}}{\partial r_D^2} + \frac{1}{r_D}\frac{\partial p_{fDi}}{\partial r_D} = \omega_i \beta_i \frac{\partial p_{fDi}}{\partial t_D} + q_{mDi} \tag{B-5}$$

$$p_{fDi}(r_D,0) = 0 \tag{B-6}$$

$$p_{fDi}(\infty,t_D) = 0 \tag{B-7}$$

$$\left.\frac{\partial p_{fDi}}{\partial r_D}\right|_{r_D=1} = -1 \tag{B-8}$$

where the dimensionless variables are defined by the following equations:

$$p_{fDi} = \frac{2\pi k_{fi} h_i (p_{init} - p_{fi})}{q_t B \mu_i} \tag{B-9}$$

$$p_{mDi} = \frac{2\pi k_{mi} h_i (p_{init} - p_{mi})}{q_t B \mu_i} \tag{B-10}$$

$$p_{wD} = \frac{2\pi \bar{k} h (p_{init} - p_w)}{q_t B \mu} \tag{B-11}$$

$$t_D = \frac{\bar{k} t}{\overline{\phi c_t} \mu r_w^2} \tag{B-12}$$

$$r_D = \frac{r}{r_w} \tag{B-13}$$

$$\lambda_i = \alpha_i' r_w^2 \left(\frac{k_m}{\mu} \right)_i \left(\frac{\mu}{\bar{k}} \right) \tag{B-14}$$

For slab:

$$\alpha_i' = \frac{12}{h_{mi}^2} \tag{B-15}$$

and for spherical matrix blocks:

$$\alpha_i' = \frac{15}{r_{mi}^2} \tag{B-16}$$

$$\beta_i = \left(\frac{\bar{k}}{\mu} \right) \left(\frac{\mu}{k_f} \right)_i \tag{B-17}$$

$$\omega_i = \left[\frac{\phi_f c_{tf}}{\phi_f c_{tf} + \phi_m c_{tm}} \right]_i \tag{B-18}$$

$$\alpha_i = \frac{\left[\phi_f c_{tf} + \phi_m c_{tm}\right]_i}{\overline{\phi c_t}} \tag{B-19}$$

$$\frac{\partial^2 \overline{p}_{fDi}}{\partial r_D^2} + \frac{1}{r_D}\frac{\partial \overline{p}_{fDi}}{\partial r_D} = \omega_i \beta_i s \overline{p}_{fDi} + \overline{q}_{mDi} \tag{B-20}$$

$$\overline{p}_{fDi}(\infty, s) = 0 \tag{B-21}$$

$$\frac{\partial \overline{p}_{fDi}}{\partial r_D} = -\frac{1}{s} \tag{B-22}$$

$$\frac{\partial^2 \overline{p}_{fDi}}{\partial r_D^2} + \frac{1}{r_D}\frac{\partial \overline{p}_{fDi}}{\partial r_D} = s f(s)_i \overline{p}_{fDi} \tag{B-23}$$

The function $f(s)_i$ converts the single porosity solution into the corresponding dual porosity layered reservoir solution. Derivations for $f(s)_i$ functions to simulate three types of double porosity response are presented in the following Appendices. The types are: (1) pseudo-steady state matrix flow; (2) transient matrix flow of a slab geometry; and (3) transient matrix flow of a sugar-cube geometry.

APPENDIX C

PSEUDO-STEADY STATE MATRIX FLOW

Waren and Root[2] defined the matrix volumetric flux for a single layer reservoir. The definition can be modified and presented for a multi-layer system as:

$$q_{mi} = -\left(\phi_m c_m\right)_i \frac{\partial p_{mi}}{\partial t} \tag{C-1}$$

Presenting the above equation in dimensionless form gives:

$$q_{mDi} = \beta_i\left(\alpha_i - \omega_i\right)\frac{\partial p_{mDi}}{\partial t_D} \tag{C-2}$$

The pressure in the matrix is described by a pseudosteady state condition:

$$\left(\phi_m c_m\right)_i \frac{\partial p_{mi}}{\partial t} = \frac{\alpha_i' k_{mi}}{\mu_i}(p_{fi} - p_{mi}) \tag{C-3}$$

or, in dimensionless form:

$$\beta_i\left(\alpha_i - \omega_i\right)\frac{\partial p_{mDi}}{\partial t_D} = \lambda_i(p_{fDi} - p_{mDi}) \tag{C-4}$$

An expression for the dimensionless source in terms of dimensionless fracture pressure can be obtained by applying the Laplace transform and coupling Equations C-2 and C-4:

$$\overline{q}_{mDi} = \frac{\beta_i\left(\alpha_i - \omega_i\right)s\lambda_i}{\left(\alpha_i - \omega_i\right)s + \lambda_i}\overline{p}_{fDi} \tag{C-5}$$

Then, the f_i function is required to simulate the double porosity behavior under pseudosteady state flow assumption between matrix and fracture and can be obtained by substituting the dimensionless source equation into Equation (B-23):

$$f(s)_i = \omega_i\beta_i + \frac{(\alpha_i - \omega_i)\beta_i\lambda_i}{(\alpha_i - \omega_i)s + \lambda_i} \tag{C-6}$$

The above derived equation agreed with the one presented by Mavor and Walkup Jr.[47]

APPENDIX D

TRANSIENT MATRIX FLOW OF A SLAB GEOMETRY

De Swaan[11] developed the analytical equations for the asymptotes (two parallel straight lines) considering transient matrix flow and both slab (layer) and sugar-cube geometries. The matrix source term is given by:

$$q_{mi} = \left(\frac{V_m \phi_m c_m}{V_f}\right)_i \int_0^t \frac{\partial \Delta p_{fi}}{\partial \tau} f_{bh}(t-\tau)d\tau \tag{D-1}$$

where f_{bh} is the normalized flux corresponding to a unit pressure change on the block surface. Converting Equation (D-1) into dimensionless form gives:

$$q_{mDi} = (\alpha_i - \omega_i)\int_0^{t_D} \frac{\partial p_{fDi}}{\partial \tau_D} f_{bh}(t_D - \tau_D)d\tau_D \tag{D-2}$$

Applying the Laplace transform to the above equation yields:

$$\bar{q}_{mDi} = \beta_i(\alpha_i - \omega_i)s\bar{p}_{fDi}\bar{f}_{bh} \tag{D-3}$$

The following equation describes the flow in the matrix:

$$\frac{\partial^2 \Delta p_{mi}}{\partial z^2} = \frac{1}{\eta_{mi}}\frac{\partial \Delta p_{mi}}{\partial t} \tag{D-4}$$

and the initial and boundary conditions are:

$$\Delta p_{mi}(z,0) = 0 \qquad \text{(D-5))}$$

$$\Delta p_{mi}(\frac{h_{mi}}{2},0) = \Delta p_{fi} \tag{D-6}$$

$$\left.\frac{\partial \Delta p_{mi}}{\partial z}\right|_{z=0} = 0 \tag{D-7}$$

Presenting the above equations in dimensionless form leads to:

$$\frac{\partial^2 p_{mDi}}{\partial z_D^2} = \frac{3(\alpha_i - \omega_i)}{\lambda_i}\frac{\partial p_{mDi}}{\partial t_D} \tag{D-8}$$

$$p_{mDi}(z,0) = 0 \tag{D-9}$$

$$p_{mDi}(1,0) = p_{fDi} \tag{D-10}$$

$$\left.\frac{\partial p_{mDi}}{\partial z_D}\right|_{z_D=0} = 0 \tag{D-11}$$

De Swaan[11] presented the solution in dimensionless form for the case of a single-layer reservoir. For a multi-layer system the solution can be modified and presented as:

$$p_{mDi} = 1 - \frac{4}{\pi}\sum_{n=1}^{\infty}\frac{(-1)^n}{2n+1}\sin\left(\frac{(2n+1)\pi z_D}{2}\right)e^{-\frac{n^2\pi^2 3(\alpha_i-\omega_i)}{\lambda_i}t_D} \tag{D-12}$$

The flux at the interface is determined by Darcy's law, which requires an expression for the pressure distribution within the matrix. Therefore, the pressure gradient at the slab boundary can be obtained from Equation (D-12) as:

$$\left.\frac{\partial p_{mDi}}{\partial z_D}\right|_{z_D=1} = 2\sum_{n=1}^{\infty}(-1)^n\sin\left(\frac{(2n+1)\pi}{2}\right)e^{-\frac{n^2\pi^2 3(\alpha_i-\omega_i)}{\lambda_i}t_D} \tag{D-13}$$

Taking the Laplace transform to the above equation gives:

$$\left.\frac{\partial \bar{p}_{mDi}}{\partial z_D}\right|_{z_D=1} = \sqrt{\frac{\lambda_i}{3(\alpha_i - \omega_i)s}}\tanh\sqrt{\frac{3(\alpha_i - \omega_i)s}{\lambda_i}} \tag{D-14}$$

Substituting Equation (D-14) into Equation (D-3) yields:

$$\bar{q}_{mDi} = s\bar{p}_{fDi}\beta_i\sqrt{\frac{\lambda_i(\alpha_i - \omega_i)}{3s}}\tanh\sqrt{\frac{3(\alpha_i - \omega_i)s}{\lambda_i}} \tag{D-15}$$

Then, the f_i function required to simulate the double porosity behavior under transient matrix flow of a slab geometry assumption between matrix and fracture can be obtained by substituting the dimensionless source equation into Equation (B-23):

$$f(s)_i = \omega_i\beta_i + \beta_i\sqrt{\frac{\lambda_i(\alpha_i - \omega_i)}{3s}}\tanh\sqrt{\frac{3(\alpha_i - \omega_i)s}{\lambda_i}} \tag{D-16}$$

The above derived equation agreed with the one presented by Mavor and Walkup Jr.[47].

APPENDIX E

TRANSIENT MATRIX FLOW OF A SUGAR-CUBE GEOMETRY

As mentioned earlier, De Swaan[11] developed the analytical equations for the asymptotes (two parallel straight lines) considering transient matrix flow and both slab (layer) and sugar-cube geometries. Therefore, the derivation for transient matrix flow in a sugar-cube matrix is similar to that given in Appendix D for slab system. A sphere of equal volume approximates the sugar-cube matrix. Therefore, the following spherical equation describes the flow in the sugar-cube matrix:

$$\frac{1}{r^2}\frac{\partial}{\partial r}\left(r^2\frac{\partial \Delta p_{mi}}{\partial r}\right)=\frac{1}{\eta_{mi}}\frac{\partial \Delta p_{mi}}{\partial t} \qquad \text{(E-1)}$$

and the initial and boundary conditions are:

$$\Delta p_{mi}(r,0)=0 \qquad \text{(E-2))}$$

$$\Delta p_{mi}(R,0)=\Delta p_{fi} \qquad \text{(E-3)}$$

$$\Delta p_{mi}(0,t)=0 \qquad \text{(E-4)}$$

Presenting the above equations in dimensionless form gives:

$$\frac{\partial^2 p_{mDi}}{\partial r_D^2}+\frac{2}{r_D}\frac{\partial p_{mDi}}{\partial r_D}=\frac{15(\alpha_i-\omega_i)}{\lambda_i}\frac{\partial p_{mDi}}{\partial t_D} \qquad \text{(E-5)}$$

$$p_{mDi}(r_D,0)=0 \qquad \text{(E-6)}$$

$$p_{mDi}(1,0)=p_{fDi} \qquad \text{(E-7)}$$

$$\Delta p_{mi}(0,t_D)=0 \qquad \text{(E-8)}$$

De Swaan[11] presented the solution in dimensionless form for the case of a single-layer reservoir. For a multi-layer system the solution can be modified and presented as:

$$p_{mDi} = 1 + \frac{2}{\pi r_D} \sum_{n=1}^{\infty} \frac{(-1)^n}{n} \sin(n\pi r_D) e^{-\frac{n^2\pi^2 15(\alpha_i - \omega_i)}{\lambda_i} t_D} \tag{E-9}$$

The flux at the interface is determined by Darcy's law, which requires an expression for the pressure distribution within the matrix. Therefore, the pressure gradient at sugar-cube boundary can be obtained from Equation (E-9) as:

$$\left. \frac{\partial p_{mDi}}{\partial r_D} \right|_{r_D = 1} = 2 \sum_{n=1}^{\infty} e^{-\frac{n^2\pi^2 15(\alpha_i - \omega_i)}{\lambda_i} t_D} \tag{E-10}$$

The above equation can be transformed into Laplace space:

$$\left. \frac{\partial \overline{p}_{mDi}}{\partial r_D} \right|_{r_D = 1} = \sqrt{\frac{3\lambda_i}{5s}} \coth \sqrt{\frac{15(\alpha_i - \omega_i)s}{\lambda_i}} - \frac{\lambda_i}{5s(\alpha_i - \omega_i)} \tag{E-11}$$

Substituting Equation (E-11) into Equation (D-3) yields:

$$\overline{q}_{mDi} = s\overline{p}_{fDi} \frac{\lambda_i \beta_i}{5s} \left\{ \sqrt{\frac{15(\alpha_i - \omega_i)s}{\lambda_i}} \coth \sqrt{\frac{15(\alpha_i - \omega_i)s}{\lambda_i}} - 1 \right\} \tag{E-12}$$

Then, a new f_i function is derived to simulate the double porosity multi-layer behavior under transient matrix flow of a sugar-cube geometry assumption between matrix and fracture by substituting the dimensionless source equation into Equation (B-23):

$$f(s)_i = \omega_i \beta_i + \frac{\lambda_i \beta_i}{5s} \left\{ \sqrt{\frac{15(\alpha_i - \omega_i)s}{\lambda_i}} \coth \sqrt{\frac{15(\alpha_i - \omega_i)s}{\lambda_i}} - 1 \right\} \tag{E-13}$$

The above equation is new and was not derived by Mavor and Walkup Jr.[47].

APPENDIX F

ESTIMATING SKIN FROM DRILLING DATA

After drilling a well, the in-situ stresses that originally were supported by the drilled material concentrate near the bore-hole wall compressing and sometimes crushing the rock. As a consequence, there is a localized permeability change that is termed mechanical skin damage. Hydraulic fracturing is one of the stimulation methods which is used to eliminate the damage zone caused by mud-filtration and redistribution of stresses during drilling around the wellbore. The fractured wells remove the stress concentrations by redistributing them into the fracture wells.

Morales et al.[84] described and quantified the mechanical skin damage resulting from the redistribution of stresses caused by drilling the well. He concluded that a hydraulic fracture, with fracture lengths greater than the damaged zone, can overcome the damage by dispersing the stresses into the fracture walls.

Based on the above discussion, the positive skin can be removed by creating a short high conductivity fracture with wing length extending beyond the damage zone, as shown in Figure F.1. Thus, knowledge of the extension of formation damaged region is considered essential for the preparation of an appropriate fracture stimulation design. Interpreting hydraulic fractured reservoirs was discussed in the previous chapters. In these chapters, Tiab's Direct Synthesis technique was used to calculate the half-fracture length, x_f. Hence, the main objective in this section is to quantify the changing in skin factor and damage radius along the well depth using drilling data. Therefore, a simplified model is developed illustrating the variability of the damage zone along the depth of a vertical well. Below, a brief discussion about the mechanical damage due to drilling fluids is shown. The development of the damaged radius model is further presented.

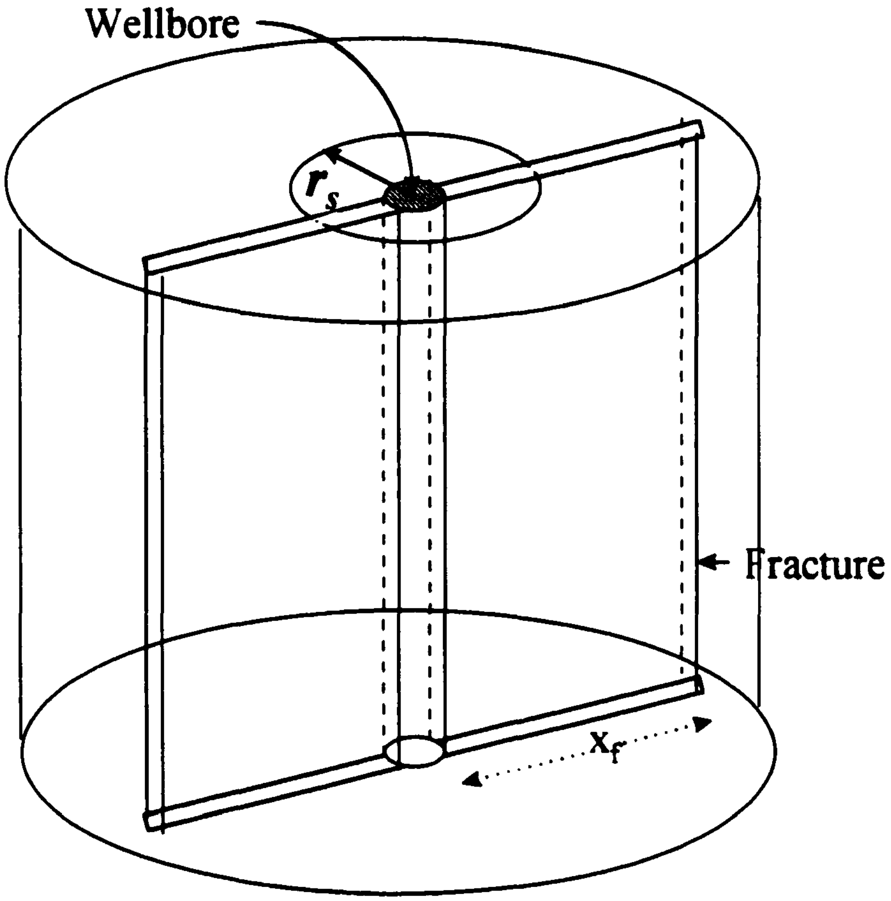

Figure F.1 Fracture extending beyond the skin damaged zone.

F.1 Damage During Drilling

The selection of well site as well as the drilling technique depends on the following factors: reservoir geometry, reservoir characteristics (heterogeneities), drilling technique, productive length, type of well completion, risk, and cost. Drilling through a producing formation should be considered a completion operation as well as a drilling operation. In order to maximize hydrocarbon production rates and recoveries, the interaction of drilling fluids, various formation damage mechanisms, and reservoir heterogeneities must be considered.

Formation permeability damage can be caused during drilling operations. This damage can be estimated in terms of the skin factor using well testing techniques. A positive skin indicates damage or restriction to flow and a negative skin indicates stimulation. The skin factor will be positive for a damaged well and has a larger value if the damage extends deeper into the formation. During drilling, changes in stress affect the permeability of the formation inducing a skin near the wellbore. Increased effective stresses near a wellbore reduce the reservoir permeability. This behavior can cause permanent formation damage and reduce production rates significantly. As petroleum engineers, we try to have as lower skin factor as possible because the higher the skin, the less the production. Therefore, our target is to avoid this problem by designing preventative methods.

As it is known to negatively impact formation productivity at the wellbore, damage should be minimized during both drilling and completion operations. This damage can usually be estimated from well test interpretation and is referred to as a skin value. However, in a multi-permeability layered reservoir, the amount of formation damage in each layer will be proportional to its permeability. During well testing, this may result in significantly lowering the contribution of the highly damaged zone, and hence cause a miss-estimation of the effective permeability and skin. Identifying the high fluid loss zones will impact completion efforts to remove the damage and mud formulation to minimize the invasion and reduce the damage. Subsequently, a proper stimulation program can be developed. That will also lead to engineering understanding of the reservoir and is very helpful in infill drilling.

Hawkins[85] introduced a simple formula for calculating the effective infinitesimal skin effect or van Everdingen[86] and Hurst[87] skin which results from a zone of altered permeability about the wellbore. The permeability change may be the result of mud filtrate invasion during drilling, fines migration, accumulation after production, etc.

Skin factor is actually a composite effect of several phenomena which characterize the actual flow to a well.

1. formation damage or mechanical damage,
2. partial penetration effects,
3. perforation effects,
4. high velocity flow effects,
5. saturation blockage near the wellbore, and
6. sand control.

In this work emphasis is on identifying and characterizing the mechanical damage due to drilling fluids.

F.2 Estimating Skin and Damage Radius from Drilling Data

Drilling, like many other field operations, can cause formation damage. This damage comes about because the process itself can reduce the ability of fluids to flow through the formation toward the wellbore. Formation permeability damage minimizes production performance; therefore, any well must have a good reservoir permeability to have a good production.

Engler et al.[88] developed a model illustrating the variability of the damage zone along the length of a horizontal well. The changing skin factor along the horizontal well is considered. The work of Engler et al[88] describes the damaged region as a combination cylindrical-conical shape. They used the experimental model developed by Ferguson and Klotz[89] to relate the formation damage to mud filtrate invasion. Then, they developed expressions for mud filtrate invasion and drilling penetration rate to calculate the maximum damage radius. Their results showed that at the furthest end, the formation damage is the least. Therefore, they concluded that the productivity of a horizontal well should be best at the furthest end.

The filtration process can be divided into three classes: (1) dynamic filtration; (2) static filtration; and (3) filtration from beneath the bit. The formation damage due to mud filtrate invasion is time dependent as indicated by Ferguson and Klotz[89]. They conducted experimental work on filtration from drilling muds, radially through porous media, during mud circulation, and drilling rotation. Their data indicate that the mud filtration rate per unit area can be modeled for the dynamic and static periods as an exponential function of time:

$$q_m = ae^{-bt} \tag{F.1}$$

where q_m is defined as the mud filtration rate per unit length, and a and b are filtration constants which are experimentally derived values. For example, the constant a=0.08 and $b=1.67X10^{-5}$ were estimated by Donaldson[92] for five sand-stones. The above equation is an approximation for water-based-mud systems; therefore, only a water-based-mud system is considered for the mud filtrate invasion model.

A relationship between the radius of formation damage and the rate of mud invasion can be developed based on Equation F.1. A cylindrical shaped damaged region is assumed in a vertical well. As shown in Figure F.2, the cross sectional area of the damage region is assumed to be a circle. The general equation for the volume of a cylinder is:

$$V_{cyl} = \pi r_s^2 h \tag{F.2}$$

The volume invaded by the mud filtrate is the pore volume, thus:

$$V_{cyl} = \pi \phi r^2 h \tag{F.3}$$

The rate of change of the invasion volume per unit length with time is given by:

$$\frac{\partial \left(V_{cyl} / h \right)}{\partial t} = \pi \phi \frac{\partial r^2}{\partial t} \tag{F.4}$$

This time is drilling time to penetrate a given foot of formation. By integrating, the following general equation can be developed:

$$\int_0^t \frac{\partial \left(V_{cyl} / h \right)}{\partial t} \partial t = \pi \phi \int_0^{r_s^2} \partial r^2 \tag{F.5}$$

The R.H.S. is:

$$\pi\phi\int_0^{r_s^2} \partial r^2 = \pi\phi r_s^2 \tag{F.6}$$

The L.H.S. is:

$$\int_0^t \frac{\partial\left(V_{cyl} / h\right)}{\partial t}\partial t = \int_0^t ae^{-bt}dt = \frac{a}{b}\left[1 - e^{-bt}\right] \tag{F.7}$$

Ferguson and Klotz[89] indicated the mud filtration rate per unit area is an exponential function of time. Thus, the solution of Equation F.4 is:

$$\frac{a}{b}\left[1 - e^{-bt}\right] = \pi\phi r_s^2 \tag{F.8}$$

The following equation has been developed to solve for the damage radius in a vertical well:

$$r_s^2 = \frac{1}{\pi\ \phi}\frac{a}{b}\left(1 - e^{-bt}\right) \tag{F.9}$$

The rate of penetration can be assumed constant and defined as:

$$ROP = \frac{\Delta h}{\Delta t} \tag{F.10}$$

where Δt is the time needed to penetrate a given reservoir height of Δh. Now a relationship can be developed using ROP by substituting Equation F.10 into Equation F.9:

$$r_s^2 = \frac{1}{\pi\ \phi}\frac{a}{b}\left(1 - e^{-b\frac{\Delta h}{ROP}}\right) \tag{F.11}$$

To verify the above equation, an example is made to estimate the damage radius r_s along a vertical well. The rate of penetration ROP is assumed constant at 10 ft/hr. Table

F.1 lists the input parameters necessary for the model and the results. Skin factor is determined using Hawkins[85] relationship. Figure F.3 illustrates the damage shape region around the vertical well which has been drilled. As expected, a cylinder damage region is obtained, i.e. the formation damage along the vertical well depth is shaped like a cylinder.

Because of drilling, completion, and work-over, the permeability around a wellbore is different from the formation permeability. The zone from altered permeability is called "skin" and its effect on the wellbore pressure or sand-face flow behavior is called "skin effect"[7]. The van Everdingen and Hurst skin factor is defined as a dimensionless constant which relates the pressure drop in the skin to the dimensionless rate of flow. The relationship is defined in Equation 2.10 and it is independent of time.

The skin factor can be determined by the Hawkins[85] relationship as:

$$S = \left(\frac{k}{k_s} - 1\right) \ln\left(\frac{r_s}{r_w}\right) \tag{F.12}$$

The above equation related the skin factor to a zone of altered permeability, k_s, which extends to the distance r_s into the formation. Table F.2 shows a simple calculation of skin factor using Equations F.11 for r_s and F.12 for skin, other parameters obtained from another source of data[88].

The length of time is a function of rate of penetration and mud invasion models. Therefore, the effect of different penetration rate models on skin factor and damage radius is presented in Figures F.4 and F.5. These figures show that the extension of skin damage is dependent on the contact time of the mud with the formation. As a consequence, a faster rate of penetration will decrease the damage region. Figure F.6 shows that for isotropic formation different values of ROP lie on a single curve. Table F.1 lists the input data for Figures F.4 through F.6.

As a conclusion, results show the extension of damaged zone can be calculated using drilling data. Subsequently, a proper stimulation program can be prepared. All in all, due to the requirement of the knowledge of damaged region extension is considered essential for the preparation of an appropriate fracture stimulation design, reliable information (such as drilling data, stimulation, completion, etc.) is definitely of help in analyzing pressure data. The new model results in a uniform, cylindrical damage region along the entire well depth. It is believed that while the proposed model is a result of theoretical development, it still can be used for practical purposes as a first approximation.

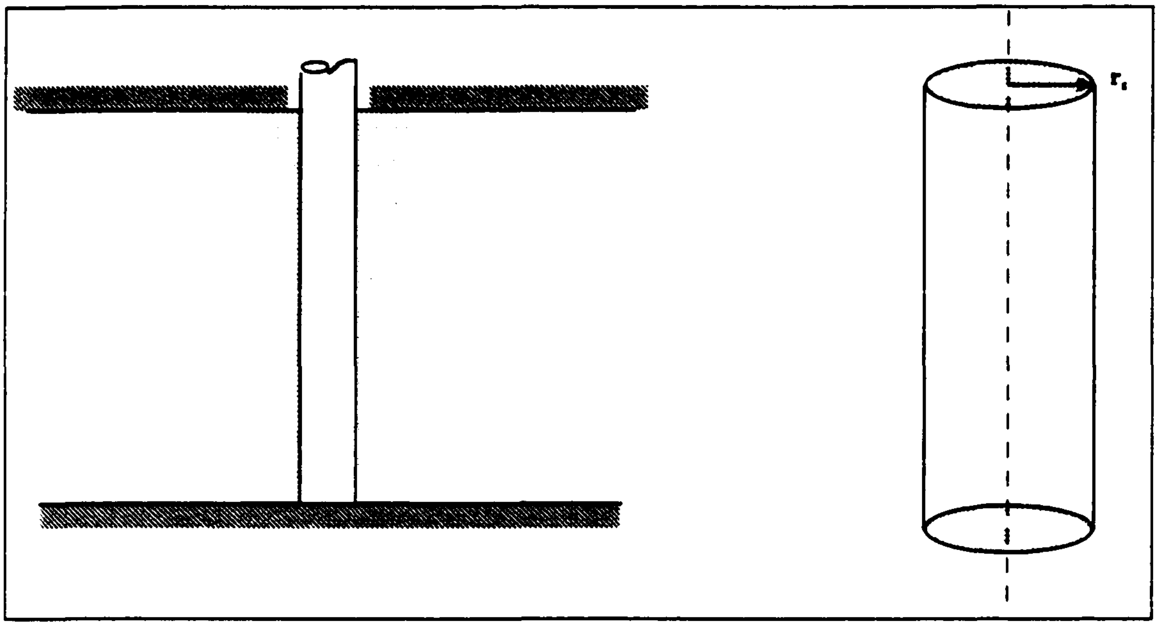

Figure F.2 Ideal cylindrical-shaped damaged region.

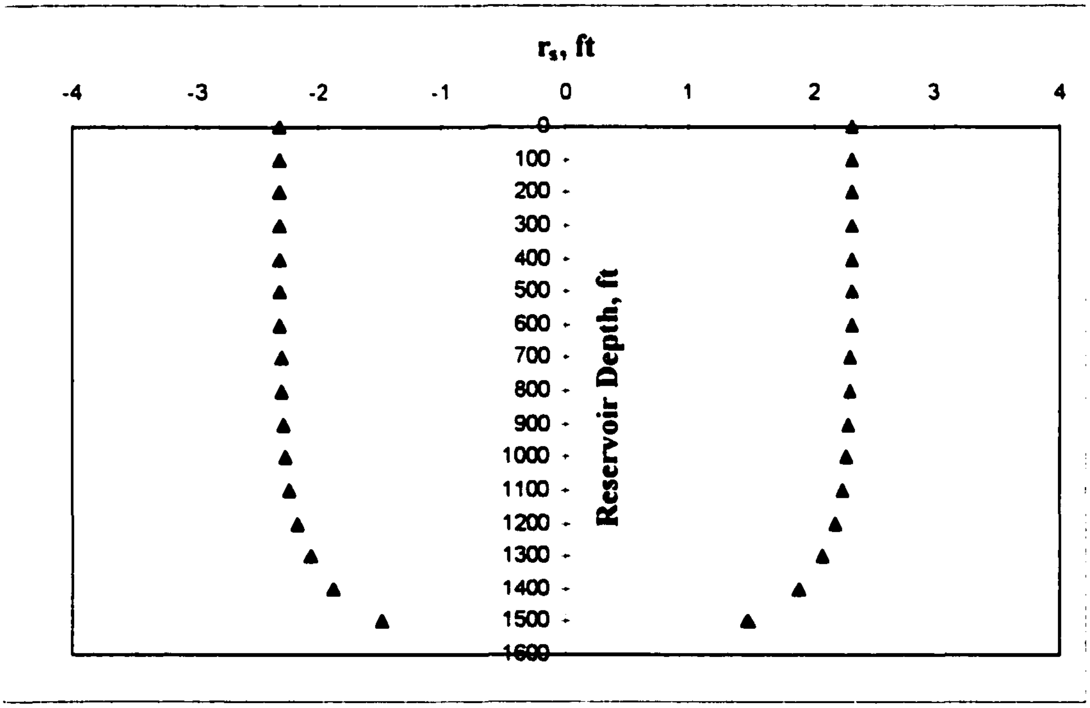

Figure F.3 Damage shape region around a vertical well, ROP=10 ft/hr.

Porosity = 0.10
r_w, *ft* = 0.229
a, ft^3*/ft-hr* = 0.088
b, *1/hr* = 0.052
k/k_s = 5.0

L_c, ft	ROP, ft/hr	t_c, hr	r_s, ft	*Skin*
100	10	150.00	2.3205	9.263
200	10	140.00	2.3201	9.263
300	10	130.00	2.3196	9.262
400	10	120.00	2.3187	9.260
500	10	110.00	2.3171	9.257
600	10	100.00	2.3145	9.253
700	10	90.00	2.3102	9.245
800	10	80.00	2.3028	9.233
900	10	70.00	2.2903	9.211
1000	10	60.00	2.2691	9.174
1100	10	50.00	2.2331	9.110
1200	10	40.00	2.1711	8.997
1300	10	30.00	2.0627	8.792
1400	10	20.00	1.8662	8.392
1500	10	10.00	1.4779	7.459

Table F.1 Comparison of Results

Porosity = 0.10
r_w, *ft* = 0.229
a, ft^3/*ft-hr* = 0.088
b, 1/*hr* = 0.052
k/k_s = 5.0

L_c, ft	ROP, ft/hr	t_c, hr	r_s, ft	*Skin*
100	1	100.00	2.3145	9.253
100	5	20.00	1.8662	8.392
100	10	10.00	1.4779	7.459
100	15	6.67	1.2562	6.809
100	20	5.00	1.1105	6.316
100	25	4.00	1.0058	5.919
100	30	3.33	0.9259	5.588
200	1	100.00	2.3145	9.253
200	5	40.00	2.1711	8.997
200	10	20.00	1.8662	8.392
200	15	13.33	1.6413	7.878
200	20	10.00	1.4779	7.459
200	25	8.00	1.3540	7.108
200	30	6.67	1.2562	6.809
300	10	30.00	2.0627	8.792

Table F.2 Comparison of Results

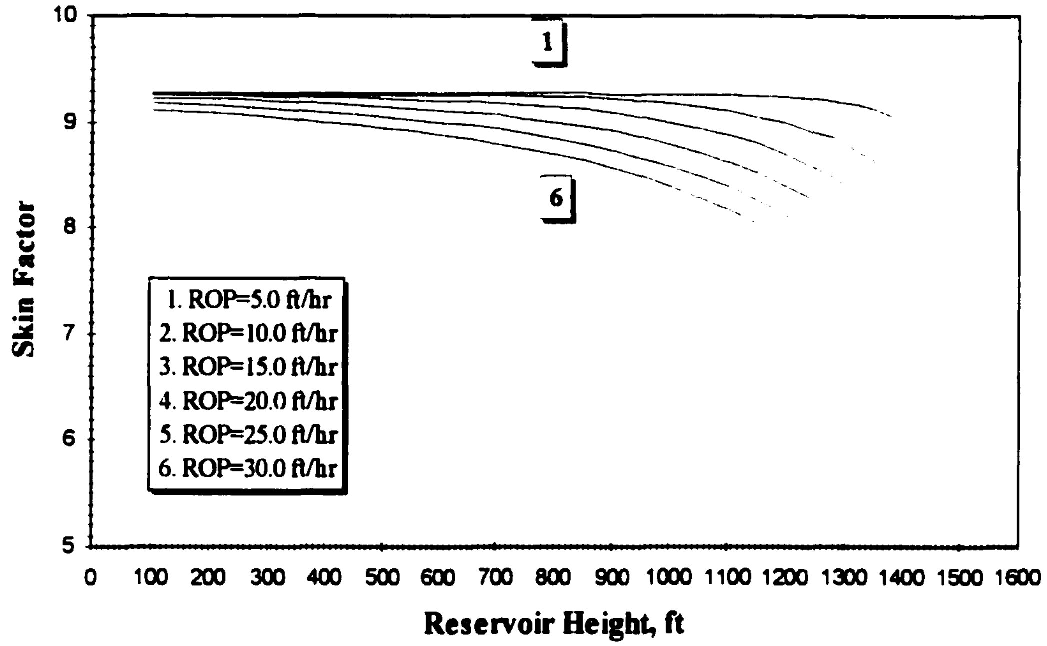

Figure F.4 Variation in skin factor along the well depth.

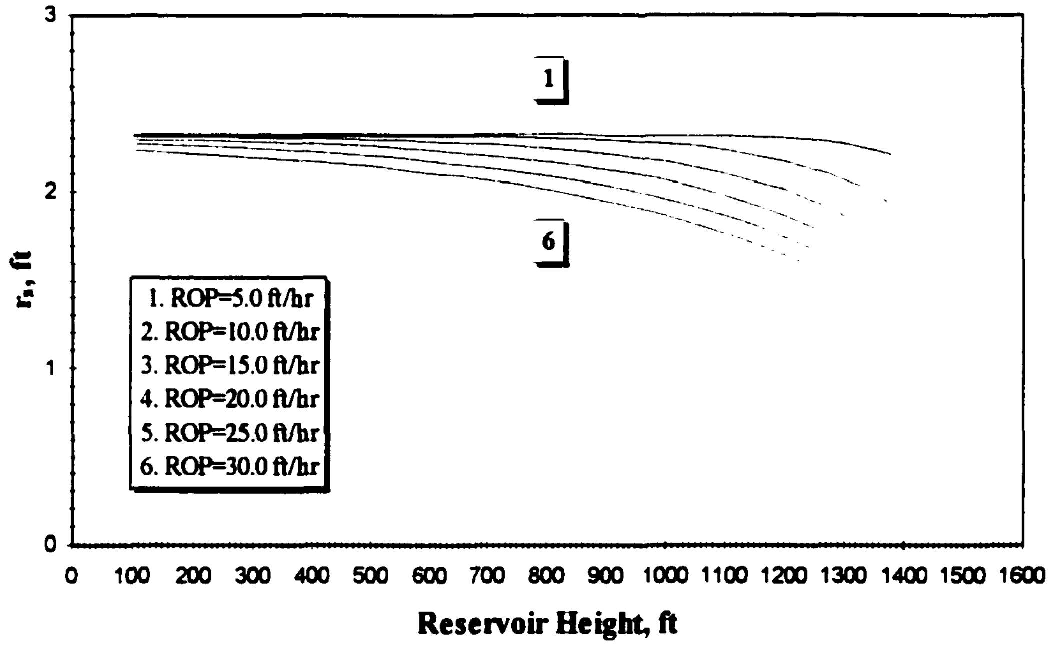

Figure F.5 Variation in damage radius along the well depth.

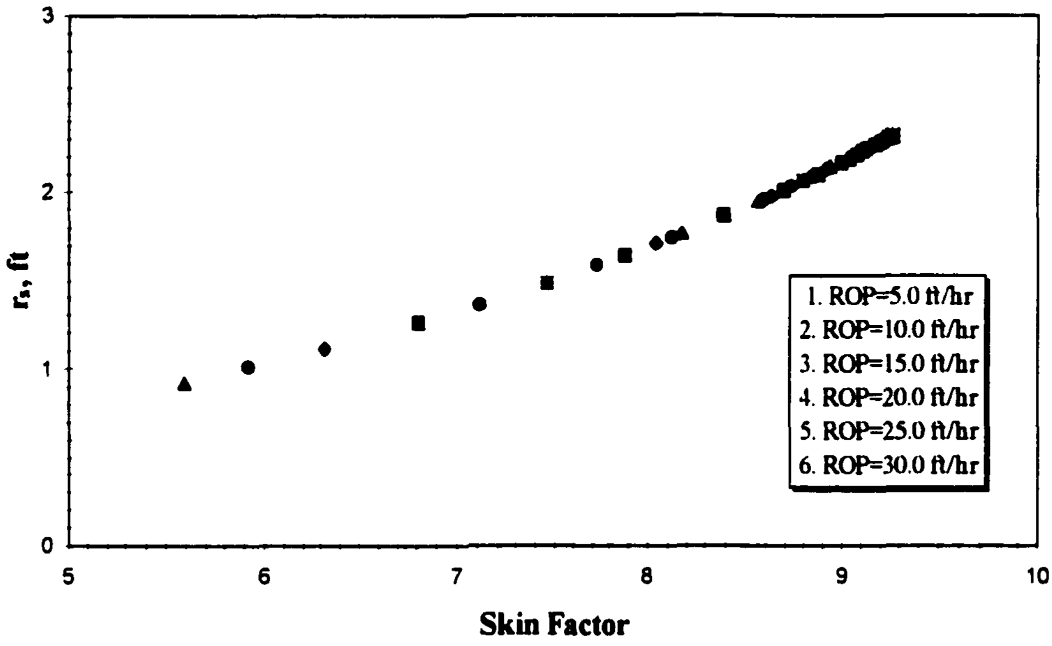

Figure F.6 Variation in skin factor with damage radius.

APPENDIX G

VERTICAL FRACTURED WELL IN CLOSED RECTANGULAR RESERVOIR WITH DOUBLE POROSITY

Liu and Yang[80] presented the solutions in Laplace domain for fractured well in closed rectangular reservoir with double porosity. The defining partial differential equations in dimensionless form are:

$$\frac{\partial^2 p_{fD}}{\partial x_D^2} + \frac{\partial^2 p_{fD}}{\partial y_D^2} = \omega \frac{\partial p_{fD}}{\partial t_D} + (1-\omega)\frac{\partial p_{mD}}{\partial t_D} \tag{G.1}$$

$$(1-\omega)\frac{\partial p_{mD}}{\partial t_D} = \lambda(p_{fD} - p_{mD}) \tag{G.2}$$

Wellbore conditions for storage and skin effects are:

$$q_{fD} = 1 \tag{G.3}$$

$$p_{wD} = \tilde{p}_{fD} \tag{G.4}$$

where $\tilde{p}_{fD}$ is the average pressure for fractured plane, defined by:

$$\tilde{p}_{fD} = \frac{1}{x_{fD}} \int_0^{x_{fD}} p_{fD}(x_D, 0, t_D)\,dx_D \tag{G.5}$$

The flux conditions for the constant rate of vertically fractured well are given by:

$$\left.\frac{\partial p_{fD}}{\partial y_D}\right|_{y_D=0} = \begin{cases} -\dfrac{\pi}{2}\dfrac{1}{x_{fD}} q_{fD}, & 0 \le x_D \le x_{fD} \\ 0, & x_{fD} < x_D < 1 \end{cases} \tag{G.6}$$

The initial and outer boundary conditions for closed rectangular reservoir are:

$$p_{iD}(x_D, y_D, 0) = 0, \qquad i = f, m \tag{G.7}$$

$$\frac{\partial p_{fD}(\pm 1, y_D, t_D)}{\partial x_D} = 0 \qquad (G.8)$$

$$\frac{\partial p_{fD}(x_D, \pm y_{eD}, t_D)}{\partial y_D} = 0 \qquad (G.9)$$

where the following dimensionless variables were used:

$$p_{fD} = \frac{2\pi k_f h(p_{init} - p_f)}{q_t B\mu} \qquad (G.10)$$

$$p_{mD} = \frac{2\pi k_m h(p_{init} - p_m)}{q_t B\mu} \qquad (G.11)$$

$$p_{wD} = \frac{2\pi k_f h(p_{init} - p_w)}{q_t B\mu} \qquad (G.12)$$

$$t_D = \frac{k_f t}{(\phi_f c_{tf} + \phi_m c_{tm})\mu x_f^2} \qquad (G.13)$$

and the dimensionless coordinates are:

$$x_D = \frac{x}{x_e} \qquad (G.14)$$

$$y_D = \frac{y}{x_e} \qquad (G.15)$$

$$x_{fD} = \frac{x_f}{x_e} \qquad (G.16)$$

$$y_{eD} = \frac{y_e}{x_e} \qquad (G.17)$$

The dimensionless flow rate of well at sand-face to the surface flow rate is:

$$q_{fD} = \frac{q}{q_t} \qquad (G.18)$$

Interporosity flow parameter, λ, is:

$$\lambda = \alpha' x_f^2 \left(\frac{k_m}{k_f} \right) \qquad (G.19)$$

where, for slab geometry:

$$\alpha = \frac{12}{h_m^2} \tag{G.20}$$

and for spherical matrix blocks:

$$\alpha = \frac{15}{r_m^2} \tag{G.21}$$

where h_m is the slab-matrix thickness and r_m is the matrix-sphere radius. The dimensionless storage coefficient, ω:

$$\omega = \left[\frac{\phi_f c_{tf}}{\phi_f c_{tf} + \phi_m c_{tm}}\right] \tag{G.22}$$

The above equations are solved by transformation to Laplace Space. Equations G.1-9 become in Laplace space:

$$\frac{\partial^2 \bar{p}_{fD}}{\partial x_D^2} + \frac{\partial^2 \bar{p}_{fD}}{\partial y_D^2} = \omega s \frac{\partial \bar{p}_{fD}}{\partial t_D} + (1-\omega) s \bar{p}_{mD} \tag{G.23}$$

$$(1-\omega) s \bar{p}_{mD} = \lambda(\bar{p}_{fD} - \bar{p}_{mD}) \tag{G.24}$$

$$\bar{q}_{fD} = \frac{1}{s} \tag{G.25}$$

$$\bar{p}_{wD} = \bar{\bar{p}}_{fD} \tag{G.26}$$

$$\bar{\bar{p}}_{fD}(s) = \frac{1}{x_{fD}} \int_0^{x_{fD}} \bar{p}_{fD}(x_D, 0, s)\,dx_D \tag{G.27}$$

$$\left.\frac{\partial \bar{p}_{fD}}{\partial y_D}\right|_{y_D=0} = \begin{cases} -\dfrac{\pi}{2}\dfrac{1}{x_{fD}}\bar{q}_{fD}, & 0 \le x_D \le x_{fD} \\ 0, & x_{fD} < x_D < 1 \end{cases} \tag{G.28}$$

$$\frac{\partial \bar{p}_{fD}(\pm 1, y_D, s)}{\partial x_D} = 0 \tag{G.29}$$

$$\frac{\partial \overline{p}_{fD}(x_D, \pm y_{eD}, s)}{\partial y_D} = 0 \tag{G.30}$$

where,

$$\overline{p}_{iD} = \int_0^\infty p_{iD} e^{-st_D} dt_D, \qquad i = f, m, w. \tag{G.31}$$

$$\overline{q}_{fD} = \int_0^\infty q_{fD}(t_D) e^{-st_D} dt_D \tag{G.32}$$

Rearranging Equation G.24 gives:

$$\overline{p}_{mD} = \frac{\overline{p}_{fD}\lambda}{(1-\omega)s+\lambda} \tag{G.33}$$

Combining Equation G.23 with the above equation yields:

$$\frac{\partial^2 \overline{p}_{fD}}{\partial x_D^2} + \frac{\partial^2 \overline{p}_{fD}}{\partial y_D^2} = s f(s) \overline{p}_{fD} \tag{G.34}$$

where the $f(s)$ function required to simulate the double porosity behavior under pseudosteady-state flow assumption between matrix and fracture. Under the assumption of pseudosteady state for interporosity flow between the matrix and fracture system, the $f(s)$ function is given by:

$$f(s) = \frac{\omega(1-\omega)s+\lambda}{(1-\omega)s+\lambda} \tag{G.35}$$

Considering the boundary conditions G.29 and G.30 of closed rectangular reservoir and using the method of variable separation, the elementary solution of equation G.34 yields:

$$\cosh[F_n(y_{eD} - y_D)]\cos(n\pi x_D) \tag{G.36}$$

where,

$$F_n = \left[sf(s) + (n\pi)^2 \right]^{1/2} \tag{G.37}$$

Expanding the boundary condition G.28 into Fourier series gives:

$$\frac{\partial \bar{p}_{fD}(x_D,0,s)}{\partial y_D} = \frac{\pi}{2}\bar{q}_{fD}\left[2\sum_{n=1}^{\infty} \frac{1}{(n\pi x_{fD})} \sin(n\pi x_{fD})\cos(n\pi x_D) \right] \tag{G.38}$$

The Laplace space for pressure of vertically fractured well in a double porosity reservoir is:

$$\begin{aligned} \bar{p}_{fD}(x_D,y_D,s) = \frac{\pi}{2}\bar{q}_{fD}\Bigg\{ & \frac{\cosh[F_o(y_{eD}-y_D)]}{F_o \sinh(F_o y_{eD})} \\ & + 2\sum_{n=1}^{\infty}\frac{1}{(n\pi x_{fD})}\sin(n\pi x_{fD})\cos(n\pi x_D)\frac{\cosh[F_n(y_{eD}-y_D)]}{F_n \sinh(F_n y_{eD})}\Bigg\} \end{aligned} \tag{G.39}$$

The dimensionless pressure of a well intersected by a vertical fracture of uniform-flux can be obtained from the above equation at $x_D = 0$. Substituting Equation G39 into G.27 yields:

$$\bar{\bar{p}}_{fD} = \frac{\pi}{2}\bar{q}_{fD}\left\{ \frac{\coth(F_o y_{eD})}{F_o} + 2\sum_{n=1}^{\infty}\frac{1}{(n\pi x_{fD})^2}\sin^2(n\pi x_{fD})\frac{\coth(F_n y_{eD})}{F_n} \right\} \tag{G.40}$$

Applying the conditions G.25 and G.26 into the above Equation gives the Laplace transform for pressure of vertically fractured well in a double porosity reservoir ignoring wellbore storage and skin:

$$\bar{p}_{wD} = \frac{B}{s} \tag{G.41}$$

where,

$$B = \frac{\pi}{2}\left\{\frac{\coth(F_o y_{eD})}{F_o} + 2\sum_{n=1}^{\infty}\frac{1}{(n\pi x_{fD})^2}\sin^2(n\pi x_{fD})\cos(n\pi x_D)\frac{\coth(F_n y_{eD})}{F_n}\right\} \quad (G.42)$$

The dimensionless pressure of a well intersected by a vertical fracture of infinite conductivity can be obtained from Equation G.39 at $x_D = 0.732$.

The Laplace transform solution including skin was given by Liu and Yang[80] as:

$$\bar{p}_{wD} = \frac{B+S}{s} \quad (G.43)$$

where, S refers to skin factor.